NBSIR 77-854

LIQUEFIED NATURAL GAS RESEARCH *at the* NATIONAL BUREAU OF STANDARDS

PROGRESS REPORT FOR THE PERIOD
1 JULY – 31 DECEMBER 1976

D.E. Diller, Editor

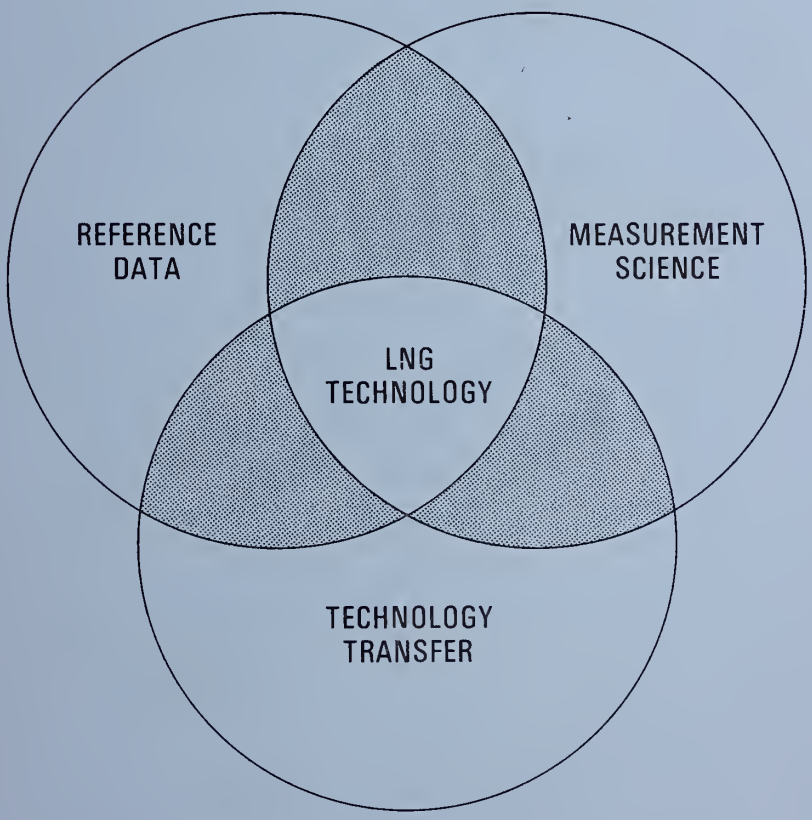

CRYOGENICS DIVISION • NBS–INSTITUTE FOR BASIC STANDARDS • BOULDER, COLORADO

NBSIR 77-854

LIQUEFIED NATURAL GAS RESEARCH
at the
NATIONAL BUREAU OF STANDARDS

D.E. Diller, Editor

Cryogenics Division
Institute for Basic Standards
National Bureau of Standards
Boulder, Colorado 80302

Progress Report for the Period
1 July—31 December, 1976

U.S. DEPARTMENT OF COMMERCE, Juanita M. Kreps, Secretary

Dr. Betsy Ancker-Johnson, Assistant Secretary for Science and Technology

NATIONAL BUREAU OF STANDARDS, Ernest Ambler, Acting Director

Prepared for:

American Gas Association, Inc.
1515 Wilson Boulevard
Arlington, Virginia 22209

LNG Density Project Steering Committee
(in cooperation with the American Gas Association, Inc.)

Pipeline Research Committee
(American Gas Association, Inc.)

Federal Power Commission
Bureau of Natural Gas
Washington, DC 20426

U. S. Department of Commerce
Maritime Administration
Washington, DC 20235

U. S. Department of Commerce
National Bureau of Standards
Institute for Basic Standards
Boulder, Colorado 80302

U. S. Department of Commerce
National Bureau of Standards
Office of Standard Reference Data
Washington, DC 20234

U. S. Department of Commerce
National Bureau of Standards
Office of International Standards
Washington, DC 20234

LNG Sampling Measurements Supervisory Committee

National Aeronautics and Space Administration
Lewis Research Center
Cleveland, Ohio 44135

American Bureau of Shipping
45 Broad Street
New York, NY 10004

ABSTRACT

Twenty-five cost centers, supported by six other agency sponsors in addition to NBS, provide the basis for liquefied natural gas (LNG) research at NBS. During this six-month reporting period the level of effort was 20 man-years/year with funding expenditures of over $500,000. This integrated progress report to be issued in January and July is designed to:

1) Provide all sponsoring agencies with a semi-annual and an annual report on the activities of their individual programs.

2) Inform all sponsoring agencies on related research being conducted at the Cryogenics Division of NBS-IBS.

3) Provide a uniform reporting procedure which should maintain and improve communication while minimizing the time, effort and paperwork at the cost center level.

The contents of this report will augment the quarterly progress meetings of some sponsors, but will not necessarily replace such meetings. Distribution of this document is limited and intended primarily for the supporting agencies. Data or other information must be considered preliminary, subject to change and unpublished; and therefore not for citation in the open literature.

Key words: Cryogenics; liquefied natural gas; measurement; methane; properties; research.

CONTENTS

1. Title. THERMOPHYSICAL PROPERTIES DATA FOR PURE COMPONENTS AND MIXTURES OF LNG COMPONENTS

Principal Investigators. R. D. Goodwin, H. M. Roder, G. C. Straty, R. Tsumura*, W. M. Haynes, and R. D. McCarty

2. Cost Center Number. 2750574, 2750548

3. Sponsor Project Identification. American Gas Association, Inc., Project BR-50-10. National Aeronautics and Space Administration, Lewis Research Center, Purchase Order C-78014-C.

4. Introduction. Accurate phase equilibrium, equation of state (PVT), and thermodynamic properties data are needed to design and optimize gas separation and liquefaction processes and equipment as well as heat transfer calculations. Accurate data for the pure components and selected mixtures of hydrocarbon systems will permit developing comprehensive accurate predictive calculation methods which take into account the dependence of the thermophysical properties of mixtures on the composition, temperature, and density.

   This project will provide comprehensive accurate thermophysical properties data and predictive calculation methods for compressed and liquefied hydrocarbon gases and their mixtures to support the development of LNG technology at NBS and throughout the fuel gas industry. It will also serve as the base for a comprehensive mixtures prediction methodology.

5. Objectives or Goals. The objectives of our work are the determination of comprehensive accurate thermophysical properties data and predictive calculation methods for the major pure components and selected mixtures (methane, ethane, propane, butanes, and nitrogen) of liquefied natural gas and hydrocarbon mixtures at temperatures between 90 K and 300 K and at pressures up to 350 MPa (5000 psi). Our goal is to provide a range and quality of data that will be recognized as definitive or standard for all foreseeable low temperature engineering calculations.

6. Background. Liquefied natural gas is expected to supply an increasing percentage of the United States' future energy requirements. It is likely that massive quantities of liquefied natural gas will be imported during the years 1976 - 1990. Ships and importation terminals are being built for transporting, storing, and vaporizing liquefied natural gas for distribution. Accurate physical and thermodynamic properties data for compressed and liquefied natural gas and hydrocarbon mixtures are needed to support these projects. For example, accurate compressibility and thermodynamic properties data are needed to design and optimize liquefaction and transport processes; accurate data for the heating value, which for liquefied natural gas mixtures depends on the total volume, the density, and the composition, are needed to provide a basis for equitable custody transfer. Accurate mixtures prediction methods are needed for use in automated heat transfer calculations.

   Accurate thermodynamic properties data for liquefied gas mixtures must be based on precise compressibility and calorimetric measurements; compressibility data give the dependence of thermodynamic properties on pressure and density (at fixed temperatures); calorimetric data give

---

*Consejo Nacional de Ciencia y Tecnologia (CONACYT) Mexico City. Currently a guest worker with the Cryogenics Division, National Bureau of Standards, Institute for Basic Standards in Boulder, Colorado.

the dependence of thermodynamic properties on temperature (at fixed pressures and densities). It is impossible, however, to perform enough compressibility and calorimetric measurements directly on multicomponent mixtures to permit accurate interpolation of the data to arbitrary composition, temperatures and pressure. Instead, thermodynamic properties data for multicomponent mixtures usually must be predicted (extrapolated) from a limited number of measurements on the pure components and their binary mixtures. This project was initiated to provide the natural gas and aerospace industry with comprehensive accurate data for pure compressed and liquefied methane, the most abundant component in LNG mixtures. We have published National Bureau of Standards Technical Note 653, "Thermophysical Properties of Methane, From 90 to 500 K at Pressures to 700 Bar," by Robert D. Goodwin (April 1974), and National Bureau of Standards Technical Note 684, "Thermophysical Properties of Ethane, From 90 to 600 K at Pressures to 700 Bar," by Robert D. Goodwin, H. M. Roder, and G. C. Straty (August 1976). These reports contain the most comprehensive and accurate tables available for the thermophysical properties of pure gaseous and liquid methane and ethane, and provide accurate basis for calculating thermophysical properties data for LNG and hydrocarbon mixtures.

7. Program and Results.

7.1 Ethane, Specific Heat Data -- H. M. Roder

This phase of the program is complete. Two manuscripts describing the results of the research have been published:

H. M. Roder, Measurements of the Specific Heats, C_σ and C_v of Dense Gaseous and Liquid Ethane, J. Res. Nat. Bur. Stand. (U.S.), Vol 80A, No. 5, 739-59 (Sep-Oct 1976).

H. M. Roder, The Heats of Transition of Solid Ethane, J. Chem. Phys. Vol 65, No. 4, 1371-3 (Aug 1976).

7.2 Ethane, Sound Velocity Data -- R. Tsumura, G. C. Straty

Sound speed measurements on ethane have been completed. Measurements were made on both the saturated and compressed fluid in a temperature range from near the triple point ($\sim$ 91 K) to 320 K and to pressures of 35 MPa. A systematically increasing disagreement between data for the saturated liquid obtained at 1 MHz and 10 MHz as the triple point temperature is approached has been explained as a wave-guide effect due to experimental geometry.

A manuscript entitled "Speed of Sound in Saturated and Compressed Fluid Ethane," by R. Tsumura and G. C. Straty has been prepared and submitted to CRYOGENICS for publication.

7.3 Ethane, Thermophysical Properties Data -- R. D. Goodwin

The manuscript, National Bureau of Standards Technical Note 684, "Thermophysical Properties of Ethane, From 90 to 600 K at Pressures to 700 Bar," by R. D. Goodwin, H. M. Roder, and G. C. Straty (August 1976) has been published and distributed.

7.4 Propane, Thermophysical Properties Data -- R. D. Goodwin

Available, published physical properties data, acquired through our Cryogenic Data Center, have been evaluated and formulated as required for thermal computations. These numerous properties now have been used to compute a complete set of Provisional tables of thermodynamic functions.

The manuscript, "Provisional Thermodynamic Functions of Propane, From 85 to 700 K at Pressures to 700 Bar," is 50% complete. Present plans are to publish these provisional tables as a National Bureau of Standards Internal Report by mid-1977.

7.5 Propane, Experimental Measurements -- W. M. Haynes

A magnetic suspension densimeter, which has been used previously (Rev. Sci. Instr. 47, 1237 (1976)) for measurements on liquids (including mixtures) at temperatures between 95 and 300 K and at pressures to 3.5 MPa (500 psi), is being modified for PVT measurements on liquid propane at pressures to 35 MPa (5000 psi). Significant differences between the two apparatus are noted here. A capacitor with slotted concentric cylinders will be located just above the density sensor in the high pressure cell for simultaneous dielectric constant measurements on liquid propane. Major modifications have been carried out on an existing cryostat so that it is compatible with the high-pressure magnetic suspension densimeter.

A copper equilibrium cell with a prototype window assembly for use at pressures to 35 MPa (5000 psi) has been fabricated. This type of window assembly has been tested at pressures to 6,250 psi at room temperature and liquid nitrogen temperature. The assembly was cycled between these temperature limits four times and no leaks were detected.

A new differential capacitance sensor, designed to be minimally sensitive to changes in the dielectric constant of the test fluid, is being evaluated as a detector of the motion of the magnetic buoy that serves as the density sensor. It has at least the sensitivity to changes in the position of the buoy as the linear differential transformer used in the previous work.

The auxiliary systems for handling of the test fluids including those for pressure measurements have been assembled and tested. An oil dead weight gauge will be used for most pressure measurements. Two spiral quartz Bourdon gauges and a double revolution Bourdon gauge have been calibrated against an air dead weight gauge and will be used to measure the vapor pressure of the liquid propane in the cell and the vapor pressure of liquids in vapor bulbs that are used to monitor temperature gradients along the length of the cell.

Major tasks to be completed before PVT data for propane are obtained are as follows:

a) Performance tests on magnetic suspension densimeter circuitry including servo system, differential capacitance sensor, support coil, etc.

b) Final assembly of capacitor and differential capacitor sensor inside the sample holder.

c) Installation of sample cell and associated components (guard ring, shields, capillary tubes, vapor bulbs, thermocouples, platinum resistance thermometer, etc.) inside cryostat.

d) Wiring of cryostat, sample cell, and sensors for measuring density, dielectric constant, and temperature.

e) Alignment of cryostat, sample cell, support coil, microscope, and buoy for control and determination of buoy-coil separation distance.

f) Capabilities for simultaneous measurements of density, temperature, pressure, and dielectric constant. These tests will include measurements on well-characterized fluids.

7.6 Calculational Methods -- R. D. McCarty

Four available calculation methods have been evaluated and optimized under another project (2752574) from the standpoint of predicting orthobaric liquid densities of LNG-like mixtures at pressures below about 2 MPa (290 psi). These methods are now being examined for predicting the thermophysical properties of mixtures over a wide range of temperatures and pressures. Available data in the literature for the methane-nitrogen system have been compiled for use in evaluating the extended corresponding states method. Thus far, efforts have concentrated on mapping PVT properties as a logical first step prior to examining the utility of the method in calculating other thermodynamic properties.

8. Problem Areas. None.

9. Funding. July 1 - December 31, 1976.

Man-years expended	1.8
Equipment and/or Services Purchased	14.3K$
Total Reporting Period Cost	109.8K$
Balance Remaining	75.2K$

10. Future Plans.

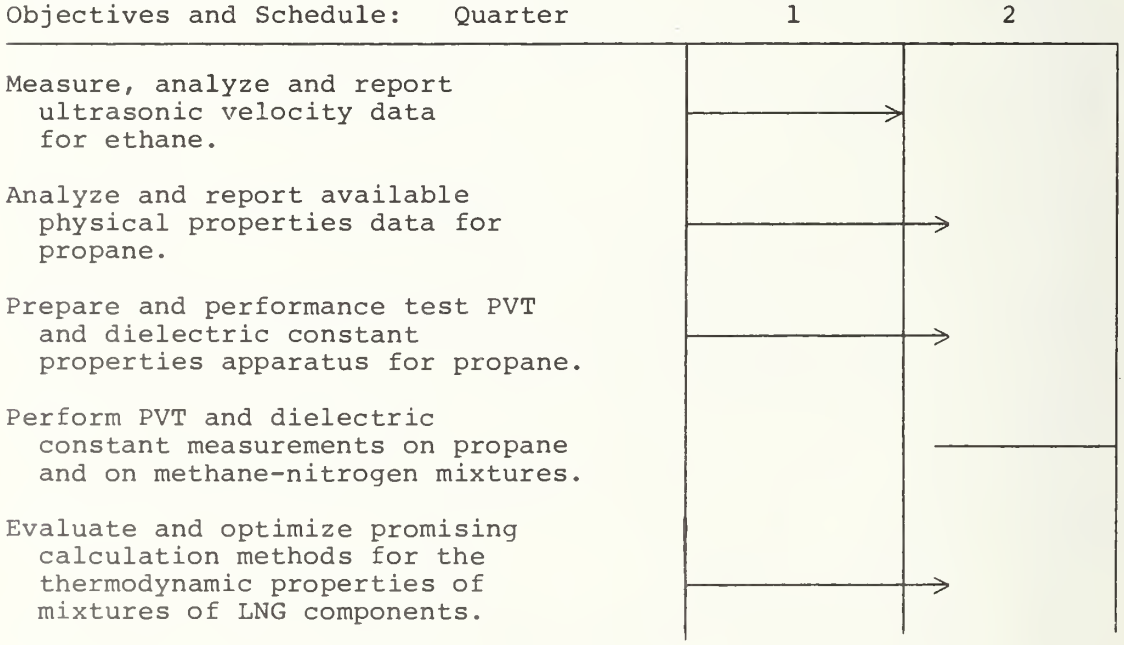

1. Title. FLUID TRANSPORT PROPERTIES

Principal Investigator. Howard J. M. Hanley

2. Cost Center Number. 2750124

3. Sponsor Project Identification. NBS-Office of Standard Reference Data

4. Introduction. Methods for predicting the transport properties of fluid mixtures are unreliable and data are scarce. Prediction methods are needed, however, to supply the necessary design data needed to increase efficiency and reduce costs.

5. Objectives or Goals. The long range or continuing goal of the program is to perform a systematic study of the theories and experimental measurements relating to transport properties, specifically the viscosity and thermal conductivity coefficients, of simple mixtures over a wide range of experimental conditions. The specific objectives of the program include: 1) the systematic correlation of the transport properties of simple binary mixtures and the development of prediction techniques, 2) development of a mixture theory for the dilute gas region and the dense gas and liquid regions, 3) extension of the theory and prediction techniques to multicomponent systems, and 4) suggested guidelines for future areas of experimental work.

6. Background. A continuing program has successfully expanded the state-of-the-art of transport phenomena for pure fluids. Information for pure fluids is required as a prerequisite for mixture studies. The theory of transport phenomena has been developed and applied to produce practical numerical tables of the viscosity, thermal conductivity and diffusion coefficients of simple fluids: Ar, Kr, Xe, N_2, O_2, F_2, He, H_2, CH_4.

Recent work has extended this approach to ethane. It has been shown that a successful mixture program can emerge from combining the results for pure fluids with equation of state studies. The equation of state work is being carried out by other investigators in this laboratory.

7. Program and Results. A procedure to predict the transport properties of mixtures has been developed via corresponding states.[1] The method has been shown to be satisfactory. The program has been expanded by the addition of James C. Rainwater, a NBS/NRC Postdoctoral Research Fellow who will investigate the theoretical background. Progress has already been made in this direction. A paper reporting the transport properties of ethane has been submitted to the Journal of Physical and Chemical Reference Data for publication.

8. Problem Areas. The lack of suitable experimental mixture transport properties data for comparison purposes is the main problem. Also equation of state (PVT) data for mixtures are needed.

9. Funding. July 1 - December 31, 1976.

Allocation	60.0K$	OSRD
Labor	0.4 MY	22.8K$
Other Costs		7.3K$
Total		30.1K$

10. Future Plans. The transport properties of propane and ethylene will be investigated. The corresponding states predictive procedure for mixtures will be expanded in line with the concurrent equation of state studies.

References

1. H. J. M. Hanley, Cryogenics 16, 643 (1976).

1. Title. PROPERTIES OF CRYOGENIC FLUIDS

Principal Investigators. G. C. Straty, B. J. Ackerson, and D. E. Diller

2. Cost Center Number. 2750141

3. Sponsor Project Identification. NBS

4. Introduction. Accurate thermophysical properties data and predictive calculation methods for cryogenic fluids are needed to support advanced cryogenic technology projects. For example, liquefied natural gas is expected to supply an increasing percentage of the United States' energy requirements through 1990. Liquefaction plants, ships and receiving terminals are being constructed to transport and store natural gas in the liquid state (LNG). Accurate thermophysical properties data for LNG are needed to design low temperature processes and equipment. Accurate data will benefit the energy industries and the consumer by providing for safe and efficient operations and reduced costs.

5. Objectives or Goals. The objectives of this project are to provide comprehensive accurate thermodynamic, electromagnetic and transport properties data and calculation methods for technically important compressed and liquefied gases (helium, hydrogen, oxygen, nitrogen, methane, ethane, etc.) at low temperatures. Precise compressibility, calorimetric and other physical property measurements will be performed to fill gaps and reconcile inconsistencies. Definitive interpolation functions, computer programs and tables will be prepared for engineering calculations. The immediate goals of this work are to obtain accurate sound velocity and thermal diffusivity data for compressed and liquefied gases by using laser light scattering spectroscopy techniques. Sound velocity data are useful for testing the consistency of volumetric, calorimetric and thermodynamic properties data, and are potentially useful for density gauging applications. Thermal diffusivity data are required for performing thermodynamic and heat transfer calculations.

6. Background. When light is incident on a perfectly homogeneous fluid, the reradiated (scattered) light field sums to zero in all but the exact forward direction. For a "real" fluid, however, fluctuations, arising through various mechanism, destroy the perfect homogeneity and results in the scattering of light in other directions as well. For example, thermally activated density fluctuations (phonons), propagating with the characteristic velocity of sound, give rise to scattered light which is Doppler shifted in frequency from the incident light frequency and whose spectrum contains information on the sound velocity and attenuation. Local non-propagating temperature fluctuations, which decay diffusively, give rise to scattered light in a narrow frequency band about the incident light frequency and whose spectrum contains information on the lifetime of the fluctuations (thermal diffusivity). Since the frequency shifts are generally very small, it was not until the advent of the lasers with their extremely well defined frequency, that practical experiments using these phenomena were possible.

The application of laser light scattering techniques to obtaining thermophysical properties data was initiated to complement and check other measurement methods and to solve measurement problems inherent in more conventional methods. For example, laser light scattering techniques permit measurements of sound velocities for fluids under conditions for which sound absorption is too large to perform ultrasonic measurements; laser light scattering techniques permit measurements of thermal diffusivities under conditions for which convection interferes with measurements of thermal conduction. The feasibility of light scattering experiments to obtain data on binary diffusion coefficients has also been demonstrated.

7. Program and Results. An apparatus has been assembled for laser light scattering spectroscopy measurements on compressed and liquefied gases (76-300 K, 35 MPa). The apparatus consists of a high pressure optical cell, a cryostat refrigerated by means of liquid nitrogen, an argon ion laser and low-level light detection equipment.

The light scattered from fluctuations in the fluid can be analyzed with either digital autocorrelation techniques for the examination of the very narrow lines associated with scattering from temperature fluctuations (Rayleigh scattering) or with a scanned Fabry Perot interferometer for the measurement of the Doppler frequency shifts associated with the scattering from propagating density (pressure) fluctuations (Brillouin scattering).

Apparatus for photon-counting and digital autocorrelation has been assembled, interfaced with computer facilities and programmed to enable on-line data accumulation and analysis. Initial problems associated with signal modulations from excessive building vibrations have been solved by levitating the apparatus on an air suspension system. A small, highly stable capacitor has also been designed, constructed and installed inside the scattering cell to permit the dielectric constant of the scattering fluid to be determined, which should allow more accurate fluid densities to be obtained for use in the data analysis. Apparatus tests on well characterized, strongly scattering, test fluids have been made to verify data analysis programs.

Extensive thermal diffusivity data have been obtained for methane, primarily along the critical isochore, over the temperature interval of 190 K to 220 K. Replicate measurements indicating accuracies approaching about 5 percent are now being achieved in this region. The range of measurements in the critical region is expected to be substantially increased with the use of the aforementioned capacitor method of density determination which will negate the necessity for measurements along an isochore (i.e., the critical isochore). Some measurements in regions more removed from the critical point have also been made.

8. Problem Areas. Light scattering has proven to be a valuable tool for obtaining thermal diffusivity data on fluids. This is particularly true in a broad temperature and density range around the critical point, where more conventional experimental methods fail or are severely limited. The intensity of the scattered light however decreases drastically as one moves away from the critical region. Data accuracy in this region becomes limited by the statistical nature of the scattering process and the ability to maintain stability and precise experimental parameters over the extended periods of time necessary for data accumlation.

We are currently investigating other experimental techniques, which could be used to complement the light scattering measurements, in order to provide sufficiently accurate data in regions where light scattering methods are expected to be unsatisfactory, and which could be used for mutual confirmation of data in the regions of overlap. Preliminary investigations have suggested that the recently refined[1] transient hot wire measurement method of thermal conductivity determinations may be well suited for measurements on fluids in the liquid state at low temperatures. This possibility is being investigated and considered further.

9. Funding. July 1 - December 31, 1976

Man-years expended	0.5
Equipment and/or Services Purchased	10.8K$
Total Reporting Period Cost	47.8K$
Balance Remaining	61.7K$

10. Future Plans.

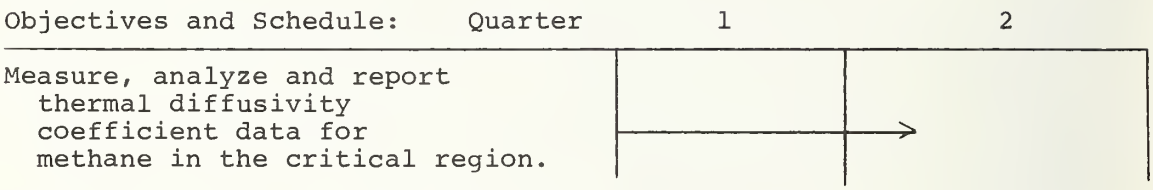

References

1. J. J. De Groot, J. Kestin and H. Sookiazian, Physica 75, 454 (1974).

1. Title. PROPERTIES OF CRYOGENIC FLUID MIXTURES

Principal Investigators. M. J. Hiza, W. M. Haynes, A. J. Kidnay (part-time), and R. C. Miller (part-time).

2. Cost Center Numbers. 2750142, 2750145 and 2754574

3. Sponsor Project Identification. NBS, NBS (OSRD), AGA

4. Introduction. Accurate thermodynamic properties data and predictive calculation methods for mixtures of cryogenic fluids are needed to design and optimize low temperature processes and equipment. This project provides new experimental measurements on equilibrium properties and compilations of evaluated equilibrium properties data which are suitable for direct technological use or for the evaluation of predictive calculation methods.

5. Objectives or Goals. The overall objectives of this project are to provide critically evaluated data, original and from other sources, on the phase equilibria and thermodynamic properties of cryogenic fluid mixtures. The program has been divided into the following elements:

   a) Preparation of a comprehensive bibliography on experimental measurements of equilibrium properties for mixtures of selected molecular species of principal interest in cryogenic technology.

   b) Selection and/or development of methods for correlation, evaluation and prediction of equilibrium properties data.

   c) Retrieval and evaluation of experimental data for specific mixture systems selected on the basis of theoretical and/or technological importance.

   d) Preparation of guidelines for future research based on the deficiencies noted in (a), (b), and (c).

   e) Performing experimental research to alleviate deficiencies and provide a basis for improvement of prediction methods.

6. Background. A physical equilibria of mixtures research project was established in the Cryogenics Division in 1959. The initial effort, based on a bibliographic search and other considerations, was directed toward the acquisition of new experimental data on the solid-vapor and liquid-vapor equilibria and physical adsorption properties for a limited number of binary and ternary mixtures of components with widely separated critical temperatures. Most of the systems studied included one of the light hydrocarbon species -- methane, ethane, or ethylene (ethene) -- with one of the quantum gases -- helium, hydrogen, or neon. The data for these systems led to significant improvements in the predictions of physical adsorption equilibrium and a correlation for the prediction of deviations from the geometric mean rule for combining characteristic energy parameters. In addition, significant new information was obtained for interaction third virial coefficients which was used in a correlation by one of our consultants, J. M. Prausnitz. The approach taken in this work has been as fundamental as possible with the intention of having an impact on a broad range of mixture problems.

   Recent efforts have been directed toward problems associated with systems containing components with overlapping liquid temperature ranges, such as the nitrogen + methane system.

7. Program and Results. The recent progress is summarized as follows:

   a) A paper reporting new liquid-vapor equilibria measurements for the methane + ethane and the methane + ethylene systems is in press in the Journal of Chemical Thermodynamics.

   b) Data on the liquid-vapor equilibria, Henry's constants, excess Gibbs functions, liquid phase heats of mixing and excess volumes have been compiled, evaluated, and correlated for the methane + ethane system. A paper discussing this work is now in editorial review. When released, this paper will be submitted to the Journal of Physical and Chemical Reference Data.

   c) An equation of state, recently proposed by Peng and Robinson, has been optimized to represent the phase equilibria data for the nitrogen + methane and methane + ethane systems. The optimized equation has now been used to generate the nitrogen + methane K-values and liquid and vapor equilibrium compositions for inclusion in the LNG Materials and Fluids Data Handbook.

   d) An empirical excess volume model has been developed based on orthobaric liquid density measurements for the pure components and binary mixtures completed in the LNG density project. This model has been tested on multicomponent LNG mixtures data and appears to be a simple and reliable method for predicting LNG densities from 105 to 120 K. A short paper discussing the development of this model is in preparation.

8. Problem Areas. None.

9. Funding. July 1 - December 31, 1976

Man-years expended	0.7
Equipment and/or Services Purchased	1.2K$
Total Reporting Period Cost	55.6K$
Balance Remaining	83.0K$

10. Future Plans.

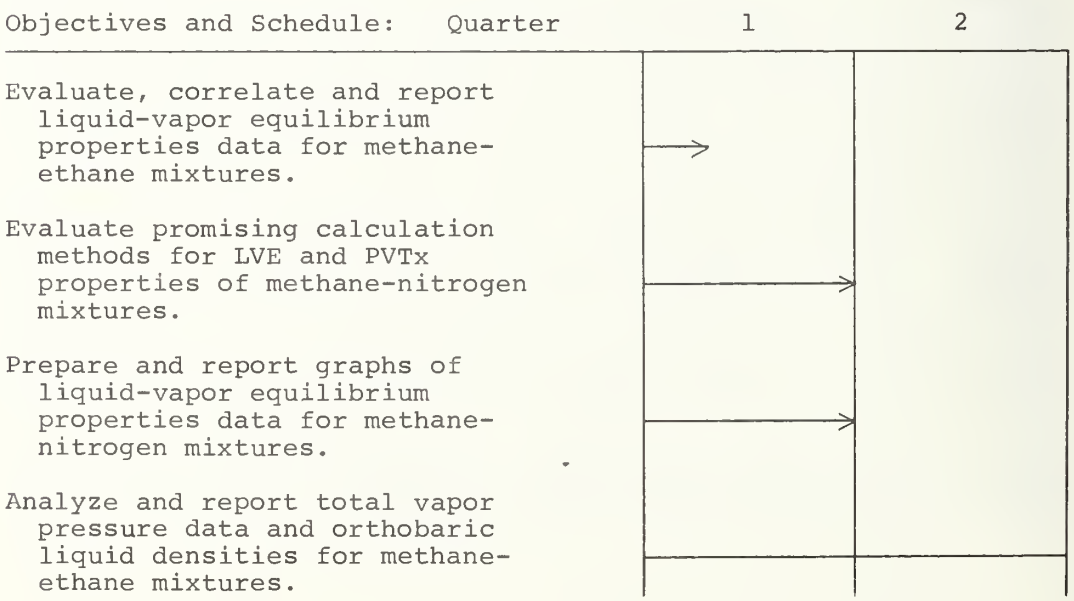

Objectives and Schedule: Quarter	1	2
Prepare and performance test phase equilibria apparatus for total vapor pressure measurements of methane-isobutane mixtures.		

1. Title. DENSITIES OF LIQUEFIED NATURAL GAS MIXTURES

Principal Investigators. M. J. Hiza, W. M. Haynes, R. D. McCarty and W. R. Parrish

2. Cost Center Numbers. 2751574

3. Sponsor Project Identification. LNG Density Project Steering Committee; American Gas Association, Inc., Project BR-50-11.

4. Introduction. Accurate density measurements and calculation methods for liquefied natural gas mixtures are needed to provide a basis for custody transfer agreements and for mass, density, and heating value gauging throughout the fuel gas industry.

The basis for the custody transfer of natural gas is its heating value. It is difficult to determine and agree on the heating value of extremely large volumes of natural gas in the liquid state. For example, methods for calculating the heating value of a liquefied natural gas mixture require knowing its density, which in turn depends on its composition, temperature, and pressure. As the compositions of LNG mixtures vary considerably, depending on the sources of the gas and the processing conditions, accurate methods are needed for calculating liquid densities at arbitrary compositions, temperatures and pressures. The accuracy is important because of the extremely large volumes of liquid involved.

5. Objectives or Goals. The objectives of this work are to perform accurate (0.1%) and precise (0.02%) measurements of the densities of saturated liquid methane, ethane, propane, butanes, nitrogen and their mixtures mainly in the temperature range 105-140 K, and to test and optimize methods for calculating the densities of LNG mixtures at arbitrary compositions and temperatures.

6. Background. This project is being carried out at NBS because of the realization that equitable custody transfer agreements could be reached more readily if the density measurements and the evaluation and development of calculation methods were performed by independent professionals of established reputation.

An apparatus incorporating a magnetic suspension technique has been developed for absolute density measurements on liquids and liquid mixtures, particularly at saturation, for temperatures between 90 and 300 K. The estimated imprecision of measurement is less than 0.02% and the estimated inaccuracy is less than 0.1%.

7. Program and Results.

7.1 Measurements. All measurements on pure fluids as well as binary and multicomponent mixtures have now been completed. Three papers have been prepared reporting the results of the pure component measurements.[1,2,4] A paper on the binary mixture results is in the final stages of review.[3]

A paper on the multicomponent mixture results is in the final stages of preparation. In addition, two papers on the magnetic suspension densimeter have been published.[4,5]

7.2 Calculational Methods. Four promising methods of calculating the densities of liquid mixtures have been tested, modified and optimized utilizing the pure component and binary mixture data reported above. The four methods are a corresponding states method, a cell model, a hard-sphere model and a graphical method. Computer programs have been written for all four methods and these have been used to calculate densities for comparison with the data for the mixtures measured. The calculated results agree with the experimental data to within 0.1% for

all multicomponent mixtures except those containing methane and butanes but no nitrogen. If nitrogen is present the inaccuracies reduce to 0.1% or less.

A report has been prepared on the calculational methods work and is currently in the review process. A summary report of the entire project is also in preparation and a two-part paper has been submitted to the LNG-5 Conference in Dusseldorf, Germany, August 1977.

8. Problem Areas. At this time, a definite answer cannot be given as to why there is an inconsistency between calculated and measured data for multicomponent mixtures containing butanes. Further work is being done on the calculational methods under another project (2750548). In addition, it is hoped that new measurements can be made at a later date on the butane-containing mixtures.

9. Funding. July 1 - December 31, 1976

2751574 (measurements)

Man-years expended	0.3
Equipment and/or Services Purchased	1.1K$
Total Reporting Period Cost	21.4K$
Balance Remaining	0.2K$

2752574 (calculation methods)

Man-years expended	0.1
Equipment and/or Services Purchased	0.8K$
Total Reporting Period Cost	3.2K$
Balance Remaining	0.0K$

10. Future Plans.

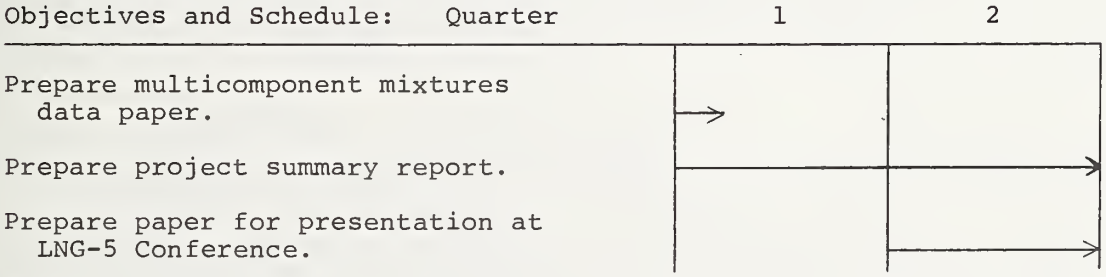

References

1. W. M. Haynes and M. J. Hiza, Orthobaric Liquid Densities of Normal Butane from 135 to 300 K as Determined with a Magnetic Suspension Densimeter, Advan. Cryog. Eng. 21, 516-21 (Plenum Press, New York, 1976).

2. W. M. Haynes and M. J. Hiza, Measurements of the Orthobaric Liquid Densities of Methane, Ethane, Propane, Isobutane, and Normal Butane, J. Chem. Thermodynamics (Feb 1977).

3. M. J. Hiza, W. M. Haynes and W. R. Parrish, Orthobaric Liquid Densities and Excess Volumes for Binary Mixtures of Low Molecular Weight Alkanes and Nitrogen Between 105 and 140 K, J. Chem. Thermodynamics (to be submitted).

4. W. M. Haynes, M. J. Hiza and N. V. Frederick, Magnetic Suspension Densimeter for Measurements on Fluids of Cryogenic Interest, Rev. Sci. Instrum. 47, No. 10, 1237-50 (Oct 1976).

5. W. M. Haynes, A Simplified Magnetic Suspension Densimeter for Absolute Density Measurements, Rev. Sci. Instrum. 48, 39 (1977).

1. Title. PROGRAM FOR REDUCING THE COST OF LNG SHIP HULL CONSTRUCTION -- PHASE II SHIP STEEL IMPROVEMENT PROGRAM

Principal Investigators. H. I. McHenry, M. B. Kasen, and R. P. Reed

2. Cost Center Number.
2753430 - LNG Ship Hull Materials (Shipyard Contracts)
2751430 - LNG Ship Construction Materials (Metallurgical Evaluation)
2752430 - LNG Ship Hull Materials (Fracture Properties)

3. Sponsor Project Identification. Maritime Administration Misc. P. O. 400-58073.

4. Introduction. Construction of LNG tankers requires the use of fine grain normalized steels for the part of the hull structure that is cooled by the cargo to temperatures in the range of 0 to -50°F. Several ABS steels have satisfactory base plate properties but extreme care must be exercised during welding to avoid degradation of the steel adjacent to weld (the heat affected zone) to a level of toughness below U. S. Coast Guard requirements. Significant cost problems are being encountered by U. S. shipyards due to the resulting inefficient low-heat-input welding procedures that must be employed to meet the fracture requirements in the heat affected zone.

The feasibility of reducing the cost of LNG ship hull construction was investigated in Phase I of this project, leading to the Phase II program described below.

5. Objective. The objectives of the Phase II program are 1) to have the four major plate producers supply three LNG shipyards with production heats of ABS steels modified to possess improved transverse fracture properties at low temperatures, 2) to have the LNG shipyards evaluate these plates by qualifying optimum welding procedures in accordance with the USCG requirements, and 3) to provide a metallurgical evaluation of factors that influence heat affected zone toughness in the improved steels.

6. Background. Early in 1974, the Welding Panel of MarAd's Ship Production Committee recommended that a program be conducted to reduce the cost of ship hull construction. NBS was requested by MarAd to propose such a program to the LNG subcommittee of the Welding Panel at a meeting in Boulder in August. In mid-October, MarAd approved the initial phase of NBS's recommended program, i.e., to survey the problem and the technology available for its solution. On the basis of this survey and as the result of a meeting of the Welding Panel in March, 1975, a coordinated program involving the LNG shipyards, the steel suppliers, and NBS was recommended to MarAd and to the Welding Panel. This program was approved and work started in May 1975. Cost-sharing contracts for the evaluation of the improved steels were awarded in 1975 to the three participating shipyards: Avondale Shipyards, Inc., Newport News Shipbuilding and Drydock Co. and General Dynamics-Quincy Shipbuilding Division.

7. Program and Results. Steel deliveries to the three LNG shipyards were completed in August 1976. The properties of the steels delivered in this reporting period are summarized below:

Steel Grade	Steel Co.	Plate	Transverse Charpy Energy (ft-lb)
V-062 (low sulfur)	Armco	1/2-in-thick	62 ft lb @ -80°F
		1-in-thick	43 ft lb @ -80°F
V-062 (SSC)	Armco	1/2-in-thick	66 ft lb @ -80°F
		1-in-thick	129 ft lb @ -80°F
ASTM A537A-Mod (SSC)	Bethlehem	1/2-in-thick	76 ft lb @ -60°F
		1-in-thick	61 ft lb @ -60°F

Each of the shipyards started the weld evaluation test program during this reporting period. A status meeting was held at Newport News Shipyard on November 3, 1976. The 17 attendees included representatives of four shipyards (Newport News, General Dynamics/Quincy, Avondale and Bethlehem Sparrows Point), four steel producers (Bethlehem, Armco, Lukens and U.S. Steel), ABS, MarAd and NBS. The initial results indicate that ABS grades V-051, V-062 and CS are significantly improved by sulfide shape control and that this improvement is reflected in the Charpy-impact toughness of the heat affected zone (HAZ). In the case of ASTM A537A-Mod steel, the base plate properties are significantly improved, but the HAZ toughness at -60°F is worse than the HAZ toughness in conventional A537A-Mod.

A contract was signed with Lukens Steel Company to evaluate Cb-treated V-051 steel with and without sulfide shape control. Lukens will provide the steel and perform the weld evaluation. It was originally intended that a shipyard would conduct the weld evaluation, but the shipyards contacted did not want to participate on a cost-sharing basis.

8. Problem Areas. The A537A-Mod steel procured by General Dynamics for this program does not meet the requirements for -60°F applications. It may be necessary to downgrade this steel to grade CS for use to -30°F. The cost of downgrading is a potential program expense of nearly $6000.

9. Funding. July 1 - December 31, 1976.

Cost Center	Cost to 12/31/76	Balance
2753430	144 K$	1 K$
2751430	61 K$	19 K$
2752430	43 K$	17 K$

10. Future Plans. The shipyard evaluation should be completed by June 30, 1977 and work should start on the comparative testing program (Phase II of the Ship Steel Improvement Program).

1. Title. CUSTODY TRANSFER - LNG SHIPS
Principal Investigators. R. S. Collier and J. D. Siegwarth

2. Cost Center Number. 2750460

3. Sponsor Project Identification. Maritime Administration, Misc. P.O. #400-58074, #400-69012.

4. Introduction. In response to a request from the U.S. shipbuilding industry, NBS is conducting an independent design review of the shipboard custody transfer systems under the sponsorship of the Maritime Administration and in cooperation with the major U.S. shipbuilding companies.

5. Objectives. The objectives of this program are to 1) Identify the major technical areas relating to uncertainties in the measurement of total mass and total heating value, 2) Estimate uncertainties in the total mass and total heating value due to these identified factors, 3) Develop a proposed testing program for custody transfer system components, and 4) Investigate improved gauging techniques.

6. Background. Calendar year 1974 funding provided for the initial review of ships designated by MA Design LG8-S-102a MA Hulls 289, 290, 291. The current funding provides for an extension of this program to include ships of other designs which are being built by the major U.S. shipbuilding companies and also to verify tank survey and gauging methods for LNG custody transfer.

7. Program and Results. A. Working relationships with four major U. S. shipbuilders have been initiated. Most of the problem areas which are common to custody transfer systems of all types have been identified and are listed as follows:

   1. Density
      a) accuracy
      b) rangeability
      c) stability
   2. Tank Strapping (Tank Surveys)
      a) thermal effects
      b) loading factors
      c) measurement techniques
   3. Convection (Non-Uniform Density)
      a) density or composition stratification
      b) possible isolation of measurement stillwells
   4. Tank Weathering
      a) time changes in composition, stratification, etc.
      b) composition measurement
      c) sampling
   5. Liquid Level/Total Volume Measurement
   6. Pressure and Temperature Measurements (gradients included).
   7. Electronic Signal Conditioning, Data Reduction, Analysis and Readout

B. Progress - The procedures for NBS involvement in evaluating the multiple station photogrammetry were established with representatives of the ship owners, the shipyard and tank fabrication facility, and the survey contractors. Considerations of production schedules and physical accessability to the inner tank surfaces have been reasonable constraints to NBS activity at the tank construction site.

Gauge rods were manufactured and two prototype rods were tested during an actual photogrammetric survey. As a result of this test only minor problems were encountered and it is felt the entire complement of ten gauge rods may be deployed during one of the next two surveys without interference with the survey procedure. Nominal length measurements were taken between targets on the ends of these rods and arrangements were made with the NBS Dimensional Metrology Section in Gaithersburg, MD for more precise measurements at the conclusion of the program.

At NBS' request, twelve extra targets were painted on the inner tank surface for use as redundant surface coordinate data. This is part of a program to determine whether as many as 100 extra targets per tank will be necessary or whether the present number of targets is sufficient. The extra targets will be used to evaluate the closeness of fit to a tank surface calculated from the original set of targets.

Surveys were obtained between targets located in the mid, and upper regions of the tank using a solid aluminum rod held to the tank surface with positive vacuum suction cups. These measurements were taken with the use of construction scaffolding in the later stages of tank construction. Surface temperatures were recorded.

Photographic plates were examined with an x-y plotting microscope using equipment of the NBS Dimensional Metrology Section. It was determined that the 3σ uncertainty for an inexperienced operator to find the center of the target was approximately 2 μm; and with care could be improved by a factor of 2 to the order of 1 μm. This corresponds in actual coordinate dimensions to well within the $\pm$ 1.2 mm for specifying the coordinate location. Of course, this is just one aspect of the coordinate determinations but probably the most important one.

Arrangements were made for obtaining the target coordinate data on computer cards in a form where programs for calculating the model for the tank surface may be utilized.

The program of RF gauging was continued with measurement on a 35 ft diameter aluminum LNG container in cooperation with the Cincinnati Gas and Electric Company. This is part of a program to establish scaling laws between the resonance modes for extremely large tanks and their laboratory size models. (If these laws are obtained, calibration curves for the large tanks can be obtained from data taken on the models). The primary frequencies of the 35 ft diameter tank were, within experimental error, exactly those calculated from measurements of the tank size. Extra modes were obtained which were thought to be due to guy wires stretched across the tank diameter; this was confirmed by similar rigging of the laboratory model. It appears now, at least for aluminum tanks, that the scaling laws for the empty tanks are completely predictable.

It also appears that RF resonance measurement may be useful in measuring some of the major dimensions of a large tank independently of other measurement methods.

8. Problem Areas. A long baseline measurement in a horizontal direction is deemed necessary in order to minimize the estimated uncertainties in coordinate location. This may be difficult to do within the desired accuracy. Tape or wire measurements and microwave methods have been considered along with RF resonance methods.

9. Funding. July 1 - December 31, 1976

Man-years expended	0.5
Total Cost	36.7K$
Balance Remaining	4.0K$

10. Future Plans.

1. NBS will install a sufficient number of gauge rods on one of the next two photogrammetric surveys in order to complete the assessment of the photogrammetric technique to measure coordinate differences in the lower and upper portions of the tank.

2. We will continue to assess the ability of RF resonance measurements to give major dimensions of the empty tank and also to evaluate its potential as a method of gauging LNG.

3. We will continue to work with the shipbuilders to assess the effects of loading and stresses due to thermal contractions on the projected tank capacity.

4. Depending on the continued funding of this program, we will analyze the coordinate data as it comes from the photogrammetric procedure and evaluate results using independent data from the gauge rods and the redundant coordinates in order to complete the assessment of the empty tank survey accuracy.

1. Title. HEATING VALUE OF FLOWING LNG
Principal Investigators. J. A. Brennan and J. M. Arvidson

2. Cost Center Number. 2756579

3. Sponsor Project Identification. Pipeline Research Committee (American Gas Association) PR-50-48.

4. Introduction. This project will test instrumentation for making heating value measurements in actual applications of flowing LNG. Information from projects currently underway by Younglove (cost center 2757574) on densimeters and by Haynes and Hiza (cost center 2751574) on mixture densities will be utilized where appropriate to provide state of the art information.

5. Objectives. The objective of this program is to measure total heating value of LNG flowing in a pipeline by the integration of individual measurements of flow, density and specific heating value. Flow measurement requires determination of flowmeter performance in line sizes larger than presently available calibration facilities. Therefore, a secondary objective is to establish appropriate flowmeter scaling laws.

6. Background. The LNG flow facility at NBS will be utilized to evaluate the response of the individual elements in the heating value measurement. Different compositions of LNG will be prepared to provide a range of densities and temperatures sufficient to determine any dependencies. A limited amount of sampling work is included to determine the relative importance of this parameter to the overall measurement.

   Flowmeter scaling is being done utilizing the cryogenic and the water flow facilities at NBS and private LNG peak shaving facilities. This portion of the program is behind schedule because of scheduling problems at the private LNG facilities.

7. Results. A. Tests at NBS.

   Three separate densitometer tests were run in liquid nitrogen on the NBS liquid nitrogen flow facility. The shift in performance referred to in the last report continued to occur each time the densitometer was thermally cycled between room temperature and liquid nitrogen temperature. There were seven such cycles during these nitrogen tests but the densitometer had been cycled many more times during tests on other instrumentation.

   The magnitude of the densitometer performance shifts did decrease during the last series of tests and the shifts were bi-directional. This probably indicates the performance is stabilizing but not yet stable. No similar performance characteristics were detected in the first densitometer so nothing can be said about how typical this performance might be. The performance will continue to be closely monitored and additional data on other densitometers obtained whenever possible.

   The densitometer was reinstalled in the LNG facility so that tests could be run on the integrated system. System integration was done by monitoring the individual elements of the measurement station with a mini-computer system and appropriate computations made to indicate heating value on a rate basis. Some problems were experienced in obtaining a suitable signal from the calorimeter but subsequent discussions with the manufacturer have indicated possible solutions. These solutions will be tried during the next test. In the interim, heating value measurements were entered into the computer manually. Since the heating value cannot change rapidly this procedure was not difficult to do for these tests, but it is not a satisfactory solution to the problem.

Shortly after starting the tests some of the computer peripheral equipment started to malfunction. This problem finally resulted in the loss of the computer altogether, so the major purpose of the test could not be completed. The test was not terminated, however, since there was other information that could be obtained that would be useful in future tests.

Of significant importance was the ability to get additional data on the densitometer. This was done by extending the test over several days and allowing the composition to change due to boil off from one day to the next. Density changes within the day were obtained primarily by changes in the LNG temperature. LNG density was calculated from an analysis of a sample withdrawn from the LNG. A check on the analysis was also made by calculating the heating value based on the analysis and comparing it with the heating value measured with the calorimeter.

Initially the comparisons between the two heating values were pretty good -- usually within the experimental error. As the LNG weathered, the comparisons became worse. The weathering observed in these tests was much worse than in any normal LNG facility because we were looking for wide variations in the compositions and density. Therefore, the discrepancies observed in the heating value may never occur in a normal LNG installation but are of sufficient importance to warrant further investigation.

Additional testing on the NBS LNG flow facility will be done in conjunction with some testing required on a LNG sampling project (cost center 2750575). In that way more timely control can be exercised since the gas analysis will be conducted on a more timely basis. During this series of tests the computer will also be used to integrate the signals from the individual components of the measurement system. The turbine flowmeter will be removed from the flow loop during these tests to facilitate the installation of the sampling probes required for the other project. This change will not affect the test on the measurement station since the turbine flowmeter is not used for that purpose.

Results of all the tests will be published in a separate report after the tests are completed.

B. Tests at Transco.

The new instrumentation on the gas phase flow measurements was installed at the Transco peak shaving facility in Carlstadt, NJ in October. This instrumentation includes measurements on orifice ΔP, line pressure, gas temperature, ambient temperature and elapsed time. Both a 16 inch and the 12 inch meter runs were instrumented. Recordings of these data will be on magnetic tape which will be returned to NBS for processing.

Recording of the data from the liquid flow measurements was expanded to include the data from the sonic flowmeter as well as the second sensor on the vortex shedding flowmeter. These data plus the output from the first sensor on the vortex shedding flowmeter, the liquid temperature and pressure and the elapsed time are also recorded on magnetic tape for processing at NBS.

Recording of the liquid and gas phase measurements are on separate recorders but they are synchronized so that each recording is started at the same time. Data is recorded on all measurements every ten seconds.

The system was checked out during vaporizer tests on December 1 and 2, 1976. Everything appeared to work normally during these tests and the preliminary data reduction looks good. Data will continue to be recorded during any send out for the remainder of the season and the results should be available for the next report.

C. Installation at Southern Energy.

A twelve inch vortex shedding flowmeter has been ordered for installation at the Southern Energy Company's Elba Island import terminal. This flowmeter will be installed between the storage tanks and the vaporizers and

will measure the flow of LNG to the vaporizers. This measurement will be compared to the vaporized gas measurement in the same way that the measurements are compared at the Transco facility.

At the import terminal not only will data on a larger flowmeter be available but, in addition, much more data will be available. Since the import terminal will operate continuously, data will be available as required for as long as desired.

In addition to the flowmeter the installation at Southern will include a densitometer and temperature and pressure instrumentation. All of the instrumentation will be installed during the construction phase of the terminal and ready for use when the terminal becomes operational.

8. Problem Areas. None.

9. Funding. July 1 - December 31, 1976.

Man-years Expended	1.0
Total Reporting Period Costs	86.0K$
Balance Remaining	40.0K$

10. Future Plans. Additional component integration tests on the NBS LNG facility will be run in conjunction with tests on another LNG project. Flowmeter field tests at the peak shaving facility will continue whenever possible for the remainder of this send out season. Flowmeter installation at Southern Energy will be completed as soon as possible.

1. Title. LNG DENSITY REFERENCE SYSTEM
Principal Investigators. Ben Younglove, John Arvidson and J. D. Siegwarth.

2. Cost Center Number. 2757574, 2750161

3. Sponsor Project Identification. American Gas Association, Inc., Project BR-50-10; National Bureau of Standards

4. Introduction. A density reference system has been developed to evaluate the ability of commercially available instruments to measure densities of LNG directly. Density is an essential measurement in determining the total energy content of natural gas reservoirs. This effort is oriented towards metrology, whereas the output from cost center 2751574 will provide basic reference data on pure liquids and mixtures, to evaluate methods for calculating the density indirectly.

5. Objectives. The objective of this research is to provide a system for evaluating the density measurement capability of commercially available meters. From the commercial meters we will attempt to select one or two capable of performance as transfer standards, in order to provide traceability of accuracy to field density measurement systems.

6. Background. The density reference system project was initiated in 1973. Since that time the reference system has been designed, constructed, and is now in operation, evaluating commercial density metering systems.

7. Program and Results. Additional methane density data were acquired and the provisional accuracy report for the LNG density reference system has been completed, reviewed and approved for publication as an NBSIR report. The accuracy of a future density measurement has been established as $\pm$ 0.21%. A second densimeter test has been planned for the same set of densimeters and most of the densimeters have been remounted, recalibrated by the vendor, readjusted or whatever else was required to obtain the best results. Modifications to the density reference system include: the crystal disconnect is now in the liquid so no mass and bouyancy corrections are required for the suspension, and the stirrer speed has been increased and the stirrer converted to turbine pump to shorten sample equilibrium time. The balance will be monitored in the future to ascertain that the measured weights lie within the balance range.

8. Problem Areas. The cause of the small occasion-to-occasion shift in density measurement has not been located yet. Perhaps the change in the crystal suspension arrangement will have eliminated this problem. Monitoring the absolute weight may help locate it.

9. Funding. July 1 - December 31, 1976

Man-years Expended	0.2
Total Project Cost	11.0K$

10. Future Plans. The four commercial densimeters previously tested will be retested after the Archimedes type has been recalibrated and the vibrating plate type has been remounted to the cryostat. The readout parameter has been changed in the capacitance type. The results of this retest will be reported in the next period.

1. Title. LNG SAMPLING MEASUREMENT STUDY
Principal Investigator. W. R. Parrish

2. Cost Center Number. 2750575

3. Sponsor Project Identification. LNG-Sampling Measurements Supervisory Committee.

4. Introduction. Composition is used to determine both the heating value and the quantity (through density) of LNG shipments. Thus, any error in composition doubles when calculating the total heating value and dollar value of a LNG tanker cargo. Compositions are determined by sampling LNG, on either a batch or continuous basis, and analyzing the vaporized mixture. Although several sampling techniques exist, none have received widespread acceptance in the LNG industry. Also, a standard technique has not been established for analyzing the vaporized sample.

5. Objectives or Goals. The objectives of this work are to evaluate existing sampling techniques appropriate to LNG systems and to recommend the most accurate analytical technique. Only sampling devices applicable to pipelines are being considered. The sampling techniques are judged on:

   a) representativeness of sample,

   b) insensitivity of results to composition, temperature, pressure, degree of liquid subcooling, flow rate and operator, and

   c) simplicity.

   Initial evaluations will be made in a laboratory-scale apparatus; final evaluation of the most promising sampling techniques will be performed in the LNG flow facility.

6. Background. This work is being performed at NBS because there is a need to determine the best means for obtaining the composition of LNG shipments. Current LNG buying contracts include specifications on when and how many liquid samples are to be taken but omit the sampling technique to be used. The evaluation of sampling techniques by impartial professionals will lead to the acceptance of the most accurate composition determination method by all parties involved in LNG custody transfer.

7. Program and Results. An evaluation of techniques for analyzing LNG type mixtures has been completed. Gas mixtures, prepared gravimetrically in this laboratory were analyzed by mass spectrometry (MS) and by gas chromatography (GC). The standard deviation in the heating values computed from the compositions obtained by MS ranged between 1.5 to 2 percent. By comparison the standard deviation in the heating values calculated from the GC analysis was 0.06 percent; the average error in computed heating values was 0.03 percent. The evaluation of the GC technique failed to show any composition, operator or day-to-day biases for mixtures comparable to Algerian LNG.

   Construction of the laboratory apparatus was completed and two sampling probes, a pitot tube and a side tap, have been evaluated. Although the data have not been thoroughly evaluated, it appears that both probes can be used to collect a representative sample from a flowing LNG stream.

   The apparatus is being modified to accommodate several different kinds of sample collecting and conditioning devices. Evaluation of these devices will begin shortly. We expect to begin evaluating the most promising sampling systems in the LNG flow facility in February 1977.

8. Problem Areas. None.

9. Funding. July 1 - December 31, 1976.

Man-years expended	0.8
Total reporting period cost	60.0K$
Balance remaining	27.0K$

10. Future Plans.

Objectives and Schedule:	Quarter 1	2
Evaluate sampling techniques in laboratory scale apparatus	→	
Evaluate most promising sampling techniques in the LNG flow facility	→	

1. Title. SURVEY OF CURRENT LITERATURE ON LNG AND METHANE
Principal Investigator. Neil A. Olien

2. Cost Center Number. 2759574

3. Sponsor Project Identification. American Gas Association, Inc., Project BR-50-10.

4. Introduction. It is important that all NBS personnel working in LNG, as well as the AGA and others, keep up with what is going on throughout the world in the LNG field. This project is designed to provide the Current Awareness and other information services to allow workers to keep abreast of new research and other developments.

5. Objectives or Goals. We will publish and distribute each April, July, October, and January a listing of all significant papers, reports, and patents relating to methane and LNG properties and technology. The references will be listed under convenient subject headings. The Quarterly will be distributed to all interested AGA member companies and be made available to the general public on a subscription basis. In addition, LNG related information will be entered into the Cryogenic Data Center's Information System for quick retrieval. A continuing awareness of the current publication scene is maintained for any new periodicals to be reviewed cover-to-cover. Finally we will update and make available comprehensive bibliographies on the properties and technology of LNG. There are three bibliographies involved: methane properties, methane mixtures properties, and processes and equipment involving methane and LNG. These three will be updated annually.

6. Background. In 1969 we made a thorough review of the world's publications to determine which periodicals and abstracting services should be scanned cover-to-cover to adequately encompass the LNG field. The result is that we now scan over 330 primary publications and nearly 25 secondary publications. Of these, approximately one-third are directly related to LNG. In addition, we have increased our coverage of the energy field to include hydrogen as a future fuel. Much of this information is also pertinent to LNG and as such is listed in our LNG-related publications. Our Current Awareness Service has been published weekly since 1964 (beginning in 1975 the publication became biweekly) and the Liquefied Natural Gas Survey has been published quarterly since 1970.

7. Program and Results. Four issues of the LNG Quarterly are prepared each year and distributed. There are now 126 subscriptions going to AGA Member Companies and 163 to other subscribers.

The three comprehensive bibliographies mentioned in section 5 have been reviewed and shortened, and more selective bibliographies have resulted. The latest versions were completed as of January 1, 1976.

B-1371 THE THERMOPHYSICAL PROPERTIES OF METHANE AND DEUTERO-METHANE IN THE SOLID, LIQUID AND GASEOUS PHASES - A SELECTED BIBLIOGRAPHY. Indexed by property, phase and author, 80 pages (Jan 1976). ($8.00).

B-1372 THE THERMOPHYSICAL PROPERTIES OF METHANE MIXTURES - A SELECTED BIBLIOGRAPHY. Indexed by property, system and author, 140 pages (Jan 1976). ($10.00).

B-1264 PROCESSES AND EQUIPMENT INVOLVING LIQUEFIED NATURAL GAS AND METHANE - A SELECTED BIBLIOGRAPHY. Indexed by subject and author, 76 pages (Feb 1975). ($8.00).

B-1367 Supplement to B-1264, indexed by subject and author, 40 pages (Jan 1976). ($5.00).

Over the past five years we have distributed over 430 copies of these and the comprehensive bibliographies. A bibliography on LNG Patents was supplied to AGA in May, 1975. Two supplements to this were also completed, one in July 1975 and one in January 1976.

8. Problem Areas. None.

9. Funding. July 1 - December 31, 1976.

Labor	5.5K$
Other Costs	1.4K$
Total	6.9K$
Remaining	1.2K$

10. Future Plans. Issue 76-4 was delivered to the printer on January 7, 1977. In January 1977 we will update the three LNG bibliographies mentioned above (B-1371, B-1372, B-1367). In addition we will prepare a new bibliography on LNG related patents which will replace the one prepared in May 1976 as well as the two supplements.

1. Title. LIQUEFIED NATURAL GAS TECHNOLOGY TRANSFER
Principal Investigator. D. B. Mann

2. Cost Centers. 2750403, 2751403, 2752403, 2750570, 2754574 and 2758574.

3. Sponsor Project Identification. Maritime Administration Miscellaneous Purchase Order No. 400-69012; American Gas Association, Inc. Project BR 50-10; American Bureau of Shipping, letter dated 21 November 1975.

4. Introduction. The liquefied natural gas program at the Cryogenics Division of NBS-IBS/Boulder represents an investment by industry and Government agencies of over $5 million over the past six years. This investment was designed to develop reference quality properties data for both fluids and materials, instrumentation and measurement technology for the use of the LNG and related industries. Information developed under this program must be transmitted to the ultimate user in a timely and useful format. The classical publication methods of NBS most certainly provide the scientist and research engineer information in a form most useful to the academic or near academic community. However, as a result of extensive assessments of user requirements, it was found that an additional effective mode for technology transfer would be an LNG Materials and Fluids Data Book. A complete outline and planned table of contents has appeared in previous semi-annual reports. The Maritime Administration of the Department of Commerce and the American Bureau of Shipping have agreed to sponsor the first year's efforts on the materials section and the American Gas Association, Inc. has agreed to sponsor the section on fluids and fluid mixtures. The project was begun on April 1, 1976.

5. Objectives. The Liquefied Natural Gas Materials and Fluids Data Book will provide a method of quick dissemination of property data and related information for the effective generation, utilization and transportation of LNG. The object is to improve technology transfer from the current NBS Cryogenics Division LNG physical measurements program to the users, including federal agencies, the states and industry. For the purpose of this data book, liquefied natural gas is defined as a cryogenic mixture (at less than approximately 150 K) of hydrocarbons, predominantly methane, with less than a total of 20% of the minor components ethane, propane, iso and normal butane, and nitrogen as an inert contaminant. LNG materials will be those associated with the liquefaction, transport and storage of liquefied natural gas.

6. Background. The Data Book is only one of a number of information dissemination methods used to provide workers in the liquefied natural gas (LNG) industry with properties data of known quality in a format consistent with the requirements of the intended user. In the case of the LNG Data Book, the intended audience is the field engineer, plant manager, ship designer or process engineer interested in a ready reference of assessed quality for data to be used in conceptual design, process monitoring, process analysis, and intercomparisons where precision and accuracy are secondary to specific problem solutions. The hierarchy of accuracy and precision will be defined and traceable through reference to scientific and engineering literature.

Data is classified into three groups by the NBS Cryogenics Division.

Group 1. Data which has been generated experimentally by NBS or has been assessed, evaluated or experimentally verified by NBS.

Group 2. Data which has been assessed and evaluated by NBS.

Group 3. Data available in the scientific engineering literature through the NBS Cryogenic Data Center or elsewhere. No NBS evaluation or assessment has been made at this date.

In general, all data included in the LNG Data Book will be from groups 1 and 2. No new assessments or correlations are anticipated or required for this work.

Data will be presented primarily in graphical form. Tables and analytical expressions will be used only where absolutely necessary. Graphs and charts will be in loose-leaf form for ease of updating and additions. This form will also allow immediate implementation for data already available under the NBS LNG program and will provide a convenient form for the output of data from existing projects. The data book will not be a substitute for traditional publications in the scientific literature where measurement science, technique, precision and accuracy are paramount, but will provide the data and references for the necessary assessment by the user.

The publication of both graphical and tabular data will be in a dual system of physical units. These units will be the traditional LNG industry British System of BTU, pound, degree Fahrenheit and the SI system of joule, kilogram and kelvin. It is the intent to give equal weight to each system of units.

Nine structural metals have been selected with additions possible upon consultation with the sponsors. Primary emphasis in the liquid section will be data on pure methane, pure nitrogen, and methane-nitrogen mixtures.

7. Program and Results. A three-post expandable post binder and special graphics have been selected, purchased and delivered. Over 80% of the graphic material has been completed, which includes three of the six wall size multi-property diagrams on nitrogen and methane.

8. Problem Areas. None.

9. Funding. July 1 - December 31, 1976.

Labor - Man years expended	1.0
Funds expended	77.0K$
Balance remaining	43.0K$

10. Future Plans. The first edition of the Data Book should be completed and distributed by April with the first printing of 750 copies. A second edition of the Data Book or an extended supplement seems to be assured by the anticipated continuing support of existing sponsors and the addition in sponsorship by the NBS Office of Standard Reference Data. Supplementary data will include properties on non-structural materials, insulations, pure ethane and mixtures of methane, nitrogen and ethane.

1. Title. OIML JOINT SECRETARIAT ON LNG MEASUREMENTS
Principal Investigator. Douglas Mann

2. Cost Center Number. 2750104

3. Sponsor Project Identification. American Gas Association, Inc.; NBS-Office of International Standards; and NBS-Cryogenics Division.

4. Introduction. The liquefied natural gas program of the National Bureau of Standards Cryogenics Division has, over the past five years, provided the gas industry and interested Government agencies with properties data on materials and fluids, instrumentation, and measurement assistance in the support of commerce in this significant and growing segment of the supplementary fossil energy supply. Support of this program by the American Gas Association, Inc. and Federal Government agencies such as the Maritime Administration (MarAd), NASA, GSA, Federal Power Commission and the NBS-Office of Standard Reference Data has provided a basis for the national acceptance of the results of the NBS LNG program. Through the U.S. membership in the International Organization of Legal Metrology there exists, at the present time, an opportunity to extend, internationally, the utility of data and measurement practice developed under our joint Government/industry program. We have been requested (by OIML membership) to establish an LNG Measurement Secretariat within OIML which, if implemented, would provide a significant international forum for the results of our joint work. It is believed that a joint Secretariat with the LNG industry would provide the most effective means of accomplishing these objectives.

5. Objectives or Goals. Our objective is to accomplish the following goals within the next three years.

a) To establish U.S. (NBS) thermophysical properties data for LNG as the standard data in international usage.

b) To establish U.S. (NBS) materials property data used in fabrication and construction of LNG facilities (liquefiers, storage, transport) as the standard data in international usage.

c) To establish U.S. (NBS) approved measurement technology and instrumentation as related to LNG (pressure, temperature, density, liquid level, flow) as the standard in international LNG trade. The precedent has been established with the successful completion of the joint NBS-CGA cryogenic flow measurement program which has resulted in the adoption of a cryogenic flow measurement code by the National Conference on Weights and Measures. We wish to extend this code on an international basis.

d) To establish and maintain the leadership of U.S. science, engineering, and industry in the research, technology, manufacture and marketing of instruments and measurement systems for liquefied natural gas.

6. Background. OIML was founded in 1955 to promote intergovernmental cooperation in the field of legal metrology which relates to the compatibility of standards of measurement and the legislation and government regulations which may affect such standards of measurement. OIML recommends uniform international requirements for scientific and measurement instruments used in industry and commerce and works out model laws and regulations for consideration by member nations; and, in addition, serves as a center of documentation and information exchange in legal metrology. At present 43 nations are members of this intergovernmental organization.

The United States joined OIML in 1972 (the Senate by resolution of August 11, 1972 gave its advice and consent to the accession of the U.S. to the convention establishing OIML). The responsibility for managing U.S. participation in OIML was assigned to the Department of Commerce

and has since been delegated by the Department to the National Bureau of Standards (NBS). Under the general guidance of the Department of State and the Secretary of Commerce, NBS is directly responsible for formulating and implementing U.S. policy towards OIML. U. S. participation in the organization is deemed important for two reasons: First, to protect and enhance some $1 billion worth of scientific and measurement instruments exported each year by U. S. firms and to insure equity in the trade of commodities measured by these instruments; and second, to maintain the U.S. as the world leader in the field of metrology.

In the spring of 1975 at a meeting in Paris of the International Committee of Legal Metrology, the French and U.S. representatives discussed the possibility of creating a new Reporting Secretariat No. 13 on "Liquefied Natural Gas (LNG) Measurement." The U. S. representative, W. E. Andrus, Jr. of NBS, agreed to explore the possibility with U. S. industry and interested government agencies. These discussions resulted in a decision to propose a joint Secretariat with the American Gas Association and NBS-Cryogenics Division in order to best accomplish the tasks. These conclusions were reached during several meetings extending through the latter part of 1975 and early 1976.

7. Program and Results. The final organizational meeting was held at NBS Boulder in August 1976 attended by representatives of the American Gas Association, the American Petroleum Institute and the NBS Office of International Standards Program. At this meeting Mr. Lee Hillburn, an employee of the Phillips Petroleum Company was selected as the A.G.A. co-technical advisor for the Secretariat on LNG Measurements. Mr. Douglas Mann has been designated as the NBS co-technical advisor.

   Mr. D. E. Edgerly, NBS Special Assistant for International Standards Program, indicated that the Secretariat for LNG Measurements will be proposed to the International Committee in October and will be assigned to the Pilot Secretariat No. 5 "Measurements of Volumes of Liquids." The Pilot Secretariat has not been assigned to a country but currently the U.S., West Germany and France are involved in assuming this Secretariat.

   The first task of the Working Secretariat on LNG Measurements will be to provide a definition of the scope of the Secretariat on LNG Measurements. Consideration will be given to both static and dynamic measurement methods.

8. Problem Areas. None.

9. Funding. July 1 - December 31, 1976.

Labor - Man years expended	0.1
Funds expended	11.0K$
Balance remaining	22.0K$

10. Future Plans. A draft scope for the LNG Measurements Secretariat will be generated and circulated to interested industry and government agencies prior to submission to the NBS Office of International Standards.

1. Title. FEDERAL POWER COMMISSION CONSULTATION

   Principal Investigators. D. B. Chelton, T. R. Strobridge and A. F. Schmidt.

2. Cost Center Number. 2750404

3. Sponsor. Federal Power Commission - Bureau of Natural Gas -- letter agreement dated 4 June 1973.

4. Goals. The Cryogenics Division will provide consultation and advisory services to the Federal Power Commission on the cryogenic safety and the design aspects of current applications before the FPC for authorization of LNG terminal and storage facilities. These services cover properties of cryogenic environments, insulation systems, cryogenic safety, thermodynamics, heat transfer, instrumentation, and cryogenic processes such as refrigeration and liquefaction.

5. Background. Cost Center initiated July 7, 1973.

6. Program and Results. The status of those facilities presently under the jurisdiction of the Federal Power Commission and subject to our review are outlined in the following table.

   Elements of the facilities that are subject to review are the land-based cryogenic storage tank components, bounded by the tanker or barge, the inlet and distribution pipelines. These include, but are not limited to the transfer lines, the storage tanks, the vaporizers and the process piping as it interacts with the storage tanks. It is essential that the reviews cover the operation, maintenance and emergency procedural philosophies for each terminal. Based upon these studies, reports are submitted to the staff of the FPC setting forth the technical evaluations and conclusions on each proposal.

   Emphasis is placed on the safety aspects of the facilities including their possible interactions with the surrounding areas. The impact of engineering design such as appropriate use of existing technology and material selection for structural integrity must be assessed. The basis of review includes various codes and standards, prior experience, precedent and engineering knowledge. Vapor cloud generation and plume dispersion is considered a subject beyond our area of expertise.

7. Funding.

June 30 - December 31, 1976	40K$
Anticipated Man-years of Effort FY 77	0.8
FY 77	50K$

8. Future Plans. At the present time there are several pending applications, but detailed information is not yet available. It is anticipated that additional facilities will be reviewed as applications are made to the Federal Power Commission.

FPC CONSULTATION - LNG FACILITY REVIEW

Applicant	Location	Type Facility	Storage Facility	Status		
				Site Inspection	Technical Meeting	Review
Distrigas - New York Terminal	Staten Island, NY	Import Terminal	2-900,000 barrel	8/21/73	8/21/73	Complete
Distrigas - Everett Marine Terminal	Everett, MA	Import Terminal	1-600,000 barrel 1-374,000 barrel	8/23/73 4/02/76	8/23/73	Complete
Algonquin LNG, Inc.	Providence, RI	Import Terminal	1-600,000 barrel	8/24/73	8/24/73	Complete
Northern Natural Gas Co.	Carlton, MN	Peak Shaving	1-630,000 barrel 10.8 MMCFD liquefier	10/30/73 7/29/75	10/30/73	Complete
Northwest Pipeline Corp.	Plymouth, WA	Peak Shaving	1-348,000 barrel 6.0 MMCFD liquefier	10/31/73 7/31/75	10/31/73	Complete
East Tennessee Natural Gas Co.	Kingsport, TN	Peak Shaving	1-348,000 barrel 5.0 MMCFD liquefier	6/24/75	11/29/73	Complete
Transco Terminal Co.	Bridgeport, NJ	Import Terminal	3-600,000 barrel	1/23/74	1/23/74	Complete
Southern Energy Co.	Savannah, GA	Import Terminal	4-400,000 barrel	1/24/74	2/06/74	Complete
Alabama-Tennessee Natural Gas Co.	Greenbrier, AL	Peak Shaving	1-117,000 barrel 2.0 MMCFD liquefier	**	2/05/74	Complete
Trunkline LNG, Inc.	Lake Charles, LA	Import Terminal	3-600,000 barrel	2/07/74	5/14/74	Complete
Chattanooga Gas Co.	Chattanooga, TN	Peak Shaving	1-348,000 barrel 10.0 MMCFD liquefier	2/28/74	2/28/74	Complete
Tennessee Natural Gas Co.	Nashville, TN	Peak Shaving	1-290,000 barrel 5.0 MMCFD liquefier	2/27/74	2/27/74	Complete
Northern Natural Gas Co.	Hancock Co., IA	Peak Shaving	1-630,000 barrel 10.8 MMCFD liquefier	*	*	In process
Texas Eastern Transmission Company	Staten Island, NY	Peak Shaving/ Import	* 9.0 MMCFD liquefier	*	*	In process
El Paso Alaska Co.	Gravina Pt., Alaska	Export Terminal	4-550,000 barrel	8/19/74	*	Pending

* to be determined
** NBS visit not scheduled

FPC CONSULTATION - LNG FACILITY REVIEW (Continued)

Applicant	Location	Type Facility	Storage Facility	Status		
				Site Inspection	Technical Meeting	Review
Pacific Alaska LNG Co.	Nikiski, Alaska	Export Terminal	2-550,000 barrel 400 MMCFD liquefier	*	3/02/76	Complete†
Western LNG Terminal Co.	L. A. Harbor, CA	Import Terminal	2-550,000 barrel	*	10/21/76	Complete†
	Oxnard, CA	Import Terminal	2-550,000 barrel	12/09/75	12/09/75	Complete†
	Pt. Conception, CA	Import Terminal	2-550,000 barrel	12/10/75	*	Pending
Northern States Power Co.	Eau Claire, WI	Peak Shaving	1- 78,000 barrel 2.0 MMCFD liquefier	3/30/76	3/30/76	In process
Northern States Power Co.	Wescott, MN	Peak Shaving	1-580,000 barrel 1- 38,000 barrel 10 MMCFD liquefier	3/31/76 8/04/76	8/04/76	Complete
Northwest Pipeline Corp. LNG-II	Plymouth, WA	Peak Shaving	1-522,000 barrel 10.0 MMCFD liquefier	*	*	In process
Peoples Natural Gas	Hancock Co., IA	Peak Shaving	1-630,000 barrel 14.5 MMCFD liquefier	*	*	In process
Tenneco LNG, Inc.	W. Deptford, NJ	Import Terminal	4-550,000 barrel	*	*	Pending

* to be determined
** NBS visit not scheduled
† additional review/site inspection is pending final design.

BIBLIOGRAPHY

NBS Reports and Publications Related to LNG Technology

1. Goodwin, R.D., "An equation of state for thermodynamic properties of fluids," Proceedings, Fifth International CODATA Conference, University of Colorado, June 28-July 1, 1976.

2. Goodwin, R.D., Roder, H.M., and Straty, G.C., "Thermophysical properties of ethane from 90 to 600 K at pressures to 700 bar," NBS Technical Note 684 (August 1976).

3. *Straty, G.C., and Tsumura, R., "Phase transition and melting pressures of solid ethane," J. Chem. Phys. 64, 859 (1976).

4. *Straty, G.C., and Tsumura, R., "PVT and vapor pressure measurements on ethane," J. Res. Natl. Bur. Stds. 80A, 35 (1976).

5. Tsumura, R., and Straty G.C., "Speed of sound in saturated and compressed fluid ethane," Cryogenics (in press, 1977).

6. *Weber, L.A., "Dielectric constant and the derived Clausius-Mossotti function for compressed gaseous and liquid ethane," J. Chem. Phys. 65, 446 (1976).

7. *Roder, H.M., "The heats of transition of solid ethane," J. Chem. Phys. 65, 1371 (1976).

8. *Roder, H.M., "Measurements of the specific heats, C_σ and C_v, of dense gaseous and liquid ethane," J. Res. Natl. Bur. Stds. 80A, 739 (1976).

9. Roder, H.M., "The PVT surface of simple liquids at densities near melting," Proceedings of the Fifth International CODATA Conference, University of Colorado, June 28-July 1, 1976.

10. Diller, D.E., "Thermophysical properties data research on compressed and liquefied gases at the NBS Cryogenics Division," Advan. Cryog. Eng. 21, 522 (1976).

11. *Diller, D.E., "LNG densities for custody transfer," Proceedings, International School for Hydrocarbon Measurement, University of Oklahoma, April 12-14, 1977.

12. Haynes, W.M., and Hiza, M.J., "Orthobaric liquid densities of normal butane from 135 to 300 K as determined with a magnetic suspension densimeter," Advan. Cryog. Eng. 21, 516 (1976).

13. *Haynes, W.M., Hiza, M.J., and Frederick, N.V., "Magnetic suspension densimeter for measurements on fluids of cryogenic interest," Rev. Sci. Instrum. 47, 1237 (1976).

14. *Haynes, W.M., "A simplified magnetic suspension densimeter for absolute density measurements," Rev. Sci. Instrum. 48, 39 (1977).

15. *Haynes, W.M., and Hiza, M.J., "Measurements of the orthobaric liquid densities of methane, ethane, propane, isobutane and normal butane," J. Chem. Thermodynamics (in press, 1977).

*See attached reprints or preprints in appendices.

16. Hiza, M.J., Haynes, W.M., and Parrish, W.R., "Orthobaric liquid densities and excess volumes for binary mixtures of low molecular weight alkanes and nitrogen between 105 and 140 K," J. Chem. Thermodynamics (submitted 1977).

17. Parrish, W.R., and Hiza, M.J., "On the consistency of liquid-vapor equilibria data for binary mixtures of methane with the light paraffin hydrocarbons," Adv. Cryog. Eng. 21, 485 (1976).

18. Miller, R.C., Kidnay, A.J., and Hiza, M.J., "Liquid + vapor equilibria in the methane + ethene and methane + ethane systems from 150 to 190 K," J. Chem. Thermodynamics (in press, 1977).

19. *Hanley, H.J.M., Haynes, W.M., and McCarty, R.D., "The viscosity and thermal conductivity coefficients for dense gaseous and liquid methane," J. Phys. Chem. Ref. Data (in press, 1977).

20. Hanley, H.J.M., Gubbins, K.E., and Murad, S., " A correlation of the existing viscosity and thermal conductivity coefficients of gaseous and liquid ethane," J. Phys. Chem. Ref. Data (in press, 1977).

21. Hanley, H.J.M., and Cohen, E.G.D., "Analysis of the transport coefficients of simple dense fluids: the diffusion and bulk viscosity coefficients," Physica 83A, 215 (1976).

22. Hanley, H.J.M., Sengers, J.V., and Ely, J.F., "On estimating thermal conductivity coefficients in the critical region of gases," Thermal Conductivity 14, Proc. 14th Int. Conf., Storrs, Conn. June 2-4, 1975, (Plenum Press, New York, 1976).

23. *Hanley, H.J.M., "Prediction of the viscosity and thermal conductivity coefficients of mixtures," Cryogenics 16, 643 (1976).

24. *Tobler, R.L., and Reed, R.P., "Fracture mechanics parameters for a 5083-0 aluminum alloy at low temperatures," Journal of Materials for Engineering and Technology (submitted, 1977).

25. *McHenry, H.I., "Ship steel weldments for low temperature service," Welding Journal 55, 387 (1976).

26. McHenry, H.I., and Reed, R.P., "Fracture behavior of the heat affected zone in 5% Ni steel weldments," Welding Journal (in press, 1977).

27. McHenry, R.I., "Fracture mechanics and its application to cryogenic structures," Advances in Cryogenic Engineering, 22, (in press, 1977).

28. Clark, A.F., Haynes, W.M., Deason, V.A., and Trapani, R.J., "Low temperature thermal expansion of barium ferrite." Cryogenics 16, 267 (1976).

29. *Younglove, B.A., and Siegwarth, J.D., "Cryogenic fluids density reference system: provisional accuracy statement," NBSIR 77-852 (January 1977).

30. *Mann, D. B., "What's new in LNG measurement and instrumentation" Pipeline Industry 45, 21 (1976).

APPENDICES

A through O

Phase transition and melting pressures of solid ethane*

G. C. Straty and R. Tsumura†

National Bureau of Standards, Institute for Basic Standards, Cryogenics Division, Boulder, Colorado 80302
(Received 29 September 1975)

The melting pressures of ethane at 14 temperatures from near the triple point to 95.50 K and pressures to 32.0 MPa are reported. A triple point temperature of 90.348±0.005 K is obtained from the data which is in agreement with the determination of Clusius and Weigand (1940) but in substantial disagreement with other determinations. Qualitative evidence has been obtained which indicates the existence of a previously unrecognized solid phase transition along a boundary roughly parallel to the melting line at a temperature about 0.5 K below the melting temperature, suggesting that some previous melting point determinations may have been influenced by a misinterpretation of the effects of this transition.

INTRODUCTION

Although a number of melting point determinations have been reported for ethane,[1–4] there still exists considerable disagreement on the correct triple-point temperature. Furthermore, no accurate data for the melting pressures above about 4.3 MPa exist. Clusius and Weigand[1] in 1940 reported the measurement of the melting line of ethane to a maximum pressure of 4.27 MPa and obtained a triple-point temperature of 90.35 K. Other determinations of the melting temperature,[2–4] however, yielded values in the vicinity of 89.9 K.

In this paper we report new measurements of the melting pressures of ethane at 14 different temperatures to a maximum pressure of 32.8 MPa at 95.5 K. The data have been represented by a Simon equation which has been used to obtain the triple-point temperature of 90.348±0.005 K in excellent agreement with the earlier data of Clusius and Weigand.[1] Qualitative evidence has been obtained which indicates the existence of a solid-phase transition along a (P, T) boundary roughly parallel to the melting line at a temperature about 0.5 K below the melting temperature, suggesting that some previous determinations of the melting point may have been influenced by a misinterpretation of the effects of this transition.

EXPERIMENTAL PROCEDURES

The ethane used in these experiments was commercially available research grade with minimum purity certified by the supplier at 99.98%. This purity was verified by chromatographic analysis. Temperatures were measured with a platinum resistance thermometer calibrated by the National Bureau of Standards on the IPTS-1968. Pressures were determined by referencing, through differential pressure transducers, to oil pressures derived from a precision oil dead-weight gauge accurate to within the greater of 500 Pa or 0.015%. The apparatus and instrumentation was similar to that used previously in this laboratory[5] with small modifications to be discussed.

Measurements of the pressure as a function of temperature along the melting line of other fluids such as H_2, O_2, F_2, and CH_4[6–9] have been performed routinely in this laboratory as part of programs to accurately characterize technically important cryogenic fluids. For such measurements, it has only been necessary to fill the cell with compressed liquid to the maximum pressure, at a temperature slightly above the freezing temperature corresponding to that pressure, and to then measure the pressure as the temperature is reduced. The slope of the pressure–temperature locus changes dramatically as the liquid begins to freeze indicating that the two-phase condition exists in the cell. Measurements along the freezing line can then be made. The normal temperature gradient along the filling capillary and the small solid fraction in the cell during these measurements have been sufficient to prevent solid from plugging the capillary. Furthermore, upon solidification there is usually a sufficient change in density so that the solid-liquid boundary can be traversed over a considerable pressure range from near the filling pressure to low pressures near the triple point.

Initial attempts to use these procedures for ethane were unsuccessful because of experimental difficulties associated with the somewhat unusual properties of ethane. In attempting to obtain samples in the two-phase region by filling at higher pressures and cooling to the melting line, considerable subcooling was observed before the onset of freezing. When freezing began, a solid plug would apparently form in the filling capillary, isolating the pressure measurement system from the cell. To remedy this, the capillary was brought into the cell through a reentrant cavity machined into the stainless steel cell closure and was provided with a heater. In this configuration, a considerable temperature difference could be maintained between the massive copper cell body and the filling capillary.

Several attempts were made to obtain data with this modification. The samples were prepared by filling at moderate pressure, cooling to well below the expected triple point to ensure solidification and then taking data while warming. Data obtained in this way clustered about a line as indicated by • in Fig. 1. These data suggested a triple point temperature of about 89.9 K, consistent with some earlier determinations,[2–4] and were initially interpreted incorrectly as representing the melting line. Attempts to make measurements above about 4 MPa by warming were found to be impossible, however, since this pressure corresponds to the vapor pressure of ethane at the ambient laboratory temperature and when this pressure was exceeded, considerable mass transfer out of the cell was associated with the condensation of liquid into the external portions

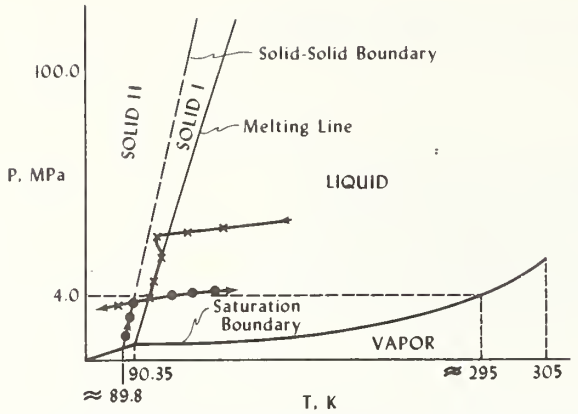

FIG. 1. Schematic phase diagram in the PT plane for ethane. The solid–solid boundary above 100.0 MPa was observed by Webster and Hoch (Ref. 11). The solid–solid boundary below 4.0 MPa from this work. Path of typical data before apparatus modifications: ● data obtained by warming, X data obtained by cooling. For a more complete explanation, see text.

of the system. Attempts to obtain data by cooling from high pressure and temperature were also unsatisfactory since the data then clustered about a second curve indicated in Fig. 1 by X. In either case, it was impossible to cross the pressure of about 4.0 MPa because of the mass transfer problem. Both sets of measurements were also unsatisfactory because of large scatter and lack of adequate reproducibility. The indications of what appeared to be segments of two separate melting curves were also difficult to explain at first.

The behavior was, however, understood upon closer examination. For measurements below the pressure of 4.0 MPa, almost all of the ethane in the system resided in the cell, resulting in a sample almost entirely in the solid phase. Heat applied to the capillary was sufficient to ensure that pressure communication with the cell was always maintained, and the data obtained were, in fact, a manifestation of a solid transition along a boundary (•Fig. 1) roughly parallel to the true melting curve but about 0.5 K lower. The higher pressure line (X, Fig. 1) traversed a portion of the true melting line. The lack of reproducibility and large scatter were found to be associated with large cell temperature gradients imposed by an unnecessarily high power input to the capillary heater.

To verify this interpretation of the results, additional modification to the apparatus was made. The cell volume was increased to over 50 cm^3 while the volume of the external portions of the system were minimized to less than 1 cm^3. In addition, these external portions were heated to about 330 K, well above the ethane critical temperatures of 305 K.

With these modifications it was then found possible to fill the cell with liquid at the highest pressure of interest, to cool sufficiently to initiate solidification, and to then traverse the melting line in either direction without encountering the difficulty at 4 MPa as found previously. Under these conditions, the solid fraction in the cell was always small. The heat input to the capillary necessary to prevent plugging was also found to be very small or zero, consistent with the experience with other fluids. Data were highly reproducible with minimum scatter, and were found to coincide roughly with the high pressure portion of the curve observed previously and its extension to lower pressures.

THE MELTING LINE

The results of the melting line measurements were fitted to the Simon melting pressure equation,

$$P = P_t + P_0[(T/T_t)^{\epsilon} - 1] \ , \qquad (1)$$

where the subscript t refers to the triple point, and P and T are the pressure and temperature. The value of $P_t = 1.2$ Pa was taken from a vapor pressure correlation for ethane by Goodwin[10] at the triple point temperature of 90.35 K. The parameters yielding the best fit were the following:

$P_t = 1.2$ Pa (Ref. 10) ,

$P_0 = 255.97$ MPa ,

$T_t = 90.348$ K ,

$\epsilon = 2.179$.

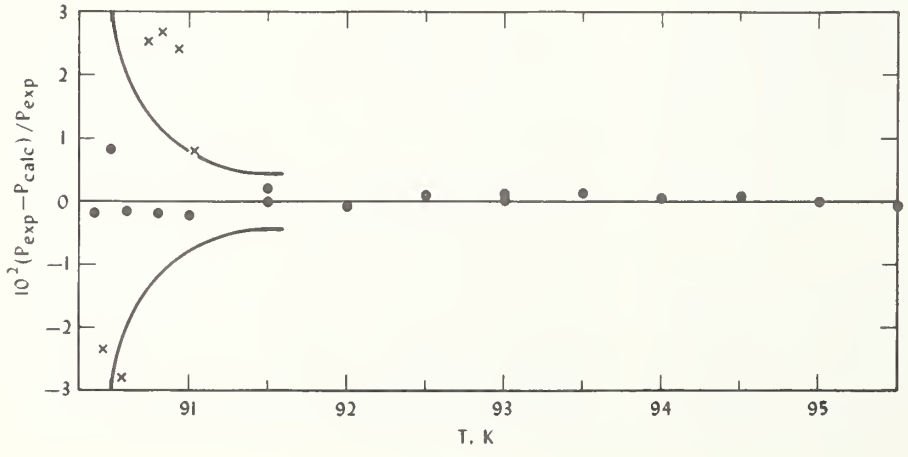

FIG. 2. Deviations of experimental melting pressures from the Simon equation, ●, this work, X, Ref. 1. The solid line corresponds to the range of pressure resulting from a difference of ±0.005 K in temperature.

TABLE I. Ethane melting pressures and deviations from Eq. (1).

T (K)	P (MPa)	$\frac{P_{exp}-P_{calc}}{P_{exp}} \times 10^2$
90.40	0.3231	−0.189
90.45[a]	0.6181	−2.345
90.50	0.9496	+0.810
90.57[a]	1.338	−2.804
90.60	1.558	−0.182
90.64[a]	1.895	4.549
90.74[a]	2.493	2.551
90.80	2.795	−0.219
90.83[a]	3.070	2.690
90.93[a]	3.698	2.411
91.00	4.035	−0.247
91.03[a]	4.266	0.801
91.50	7.182	0.196
91.50	7.145	−0.317
92.00	10.30	−0.095
92.50	13.49	0.081
93.00	16.66	0.008
93.00	16.67	0.091
93.50	19.89	0.117
94.00	23.09	0.024
94.50	26.35	0.064
95.00	29.59	−0.026
95.50	32.85	−0.107

[a]Reference 1.

The experimental results and their deviations from the equation are given in Table I. These deviations are plotted in Fig. 2 along with the data of Clusius and Weigand[1] for comparison. The derived triple point temperature of 90.348±0.005 K is in excellent agreement with 90.35±0.03 K obtained by Clusius and Weigand.[1]

It is interesting to note that experiments performed by completely freezing a solid sample and then warming through the melting transition resulted in values for the triple point of about 89.9 K[2-4] while those of Clusius and Weigand,[1] made by cooling the liquid until freezing, resulted in a higher melting temperature. This suggests that the measurements performed by warming the solid from low temperature may have been misinterpreted and that the effect of the solid transition has been responsible for obtaining such low melting points. This would, of course, be the situation for specific heat type experiments if the heat of transition was incorrectly interpreted as a large pre-melting effect or as the heat of fusion.

SOLID-SOLID TRANSITION

When measurements were made with a small solid fraction in the cell and with very low heater power to the capillary, as was necessary for the melting line measurements, it was, of course, impossible to observe the solid transition due to the unavoidable plugging of the capillary. However, if the cell were filled to a large solid fraction, and by using fairly large heater power to the capillary, pressure communication with the cell could be maintained and the solid transition could be detected. The necessary large gradients imposed on the cell, however, introduces considerable uncertainty in the temperature determinations and the observations can only be considered qualitative.

An additional check on the existence of the solid transition was made by observing the temperature as a function of time as the cell, filled with solid, was slowly warmed. A number of runs using various constant input powers to the cell were made and in each case distinct changes in the warming rate were observed at about 89.8 K associated with the solid transformation and at about 90.3 K corresponding to melting. Based on these qualitative results, it appears that the solid–solid boundary is roughly parallel to the melting line at a temperature about 0.5 K lower. This is not inconsistent with the measurements of Webster and Hoch[11] who detected a definite solid transformation above about 100.0 MPa. Experimental difficulties prevented them from making measurements below 100.0 MPa but from their data and from certain theoretical considerations, they predicted a solid–solid–liquid triple point for ethane at lower pressure. No evidence for such a triple point below our maximum pressure of 32.8 MPa was observed in this work, and the solid–solid boundary, in fact, appears to continue to low pressure.

Note: After the completion of this work, we learned of some visual observations and dilatometric measurements on solid ethane by Professor D. Eggers[12] who confirms the existence of a plastic-crystalline phase in a temperature range extending to about 0.45 K below the melting temperature. He has found this isotropic phase to be thermodynamically stable and not a metastable phase formed only under certain special conditions.[13] We thank Dr. Eggers for discussing his work with us prior to publication.

*This work was carried out at the National Bureau of Standards under the sponsorship of the American Gas Association, Inc.

†Consejo Nacional De Ciencia Y Tecnologia (CONACYT) Mexico City. Currently a guest worker with the Cryogenics Division, National Bureau of Standards, Institute for Basic Standards.

[1]K. Clusius and K. Weigand, Z. Phys. Chem. B 46, 1 (1940).
[2]R. Wiebe, K. H. Hubbard, and M. J. Brevoort, J. Am. Chem. Soc. 52, 611 (1930).
[3]R. K. Witt and J. D. Kemp, J. Am. Chem. Soc. 59, 273 (1937).
[4]L. J. Burnett and B. H. Muller, J. Chem. Eng. Data 15, 154 (1970).
[5]See for example G. C. Straty, and R. Prydz, Rev. Sci. Instrum. 41, 1223 (1970).
[6]R. D. Goodwin, J. Res. Nat. Bur. Stand. C 65, 231 (1961).
[7]L. A. Weber, J. Res. Nat. Bur. Stand. A 74, 1 (1970).
[8]R. Prydz and G. C. Straty, Nat. Bur. Stand. (U.S.) Tech. Note 392 (Revised 1973).
[9]R. D. Goodwin, Nat. Bur. Stand. (U.S.) Tech. Note 653 (1974).
[10]R. D. Goodwin, Natl. Bur. Stand. (U.S.) Interim Report, NBSIR 74–398 (1974).
[11]D. S. Webster and M. J. R. Hoch, J. Phys. Chem Solids 32, 2663 (1971).
[12]D. F. Eggers, Jr., J. Phys. Chem. 79, 2116 (1975).
[13]For an example of metastable behavior, see for example, W. F. Giauque and J. B. Ott, J. Am. Chem. Soc. 82, 2689 (1960).

JOURNAL OF RESEARCH of the National Bureau of Standards—A. Physics and Chemistry
Vol. 80A, No. 1, January–February 1976

PVT and Vapor Pressure Measurements on Ethane*

G. C. Straty and R. Tsumura**

Institute for Basic Standards, National Bureau of Standards, Boulder, Colorado 80302

(October 15, 1975)

New measurements of the vapor pressures and *PVT* properties of ethane are reported. *PVT* determinations have been made from near the triple point to 320 K at pressures to 33 MPa. The density range investigated extends to more than three times the critical density. The new measurements of the vapor pressures of ethane extend from 160 K to near the critical point.

Key words: Density: ethane: vapor pressure: *PVT*.

1. Introduction

Liquefied fuel gases, such as LNG, are expected to play an increasing role in satisfying future energy requirements. Accurate thermophysical properties data for these liquefied gas mixtures are necessary for the design of liquefaction plants, transport equipment, shipping and receiving terminals, and for custody transfer. The near infinite variations in mixture compositions encountered with these fuel gases rule out completely experimental or strictly computational approaches for determining these properties. Calculation methods, based on accurate, wide range pure component data and selected mixtures data are being developed in a number of laboratories, and appear to offer the only reliable and economical approach for the generation of the necessary thermophysical properties.

This paper reports new measurements of vapor pressures and *PVT* properties of pure ethane. The measurements have been made as part of a comprehensive program to provide the required experimental data and to develop suitable calculation techniques for mixture properties determinations. *PVT* measurements have been made from near the triple point (90.348 K) [1][1] to 320 K at pressures up to 33 MPa. The density range extends to more than three times the critical density. The new measurements of the vapor pressures extend from 160 K to near the critical temperature (305 K).

2. Experimental Detail

To measure single-phase densities, the gas expansion technique was used. A series of pressure-temperature observations are made on a nearly constant density sample of fluid confined in a cell of accurately calibrated volume. When either the maximum pressure or maximum temperature is reached, the fluid is expanded, to low pressure, into large calibrated volumes maintained at an accurately known temperature above room temperature. The density can then be determined from the cell volume and the compressibility factor (PV/RT) of the ethane at the conditions of the expansion volumes.

The ethane used was commercially available research grade with specified minimum purity of 99.98 percent. This purity was verified by chromatographic analysis. Temperatures were measured on the IPTS (1968) with a platinum resistance thermometer calibrated by the National Bureau of Standards. Pressures above about 3 MPa were measured by referencing to oil pressures derived from an oil dead weight gauge accurate to within 0.015 percent. Lower pressures were measured with a precision fused quartz bourdon tube gauge which had been previously calibrated against an air dead weight gauge accurate to within 0.01 percent. The apparatus and procedures were similar to those used previously in this laboratory for measurements on several other cryogenic fluids [2–5] and have been described in detail [6–8]. Slight modification to existing apparatus was necessary because of the higher critical temperature of ethane. Those external parts of the system which contained fluid during a measurement were heated to well above the critical temperature (typically 330 K) in order to reduce the relative density of the fluid residing in these parts, permitting a more accurate adjusted density to be computed.

*This work was carried out at the National Bureau of Standards under the sponsorship of the American Gas Association, Inc.

**Consejo Nacional De Ciencia Y Tecnologia (CONACYT) Mexico City. Currently a guest worker with the Cryogenics Division, National Bureau of Standards, Institute for Basic Standards.

[1] Figures in brackets indicate the literature references at the end of this paper.

3. Results

With the techniques used here, each experimental *PVT* "run" consists of a number of pressure-temperature observations lying along a near-isochoric path. About 50 such runs were made covering a density range of from about 1.5 to over 21.5 mol/l. Each run consisted of from 5 to 16 *PVT* points, depending on the density. Measurements were always made at fixed temperatures to permit direct analysis in terms of isotherms. A total of over 450 *PVT* data points was determined. These data are tabulated along isotherms in table 1.

TABLE 1. PVT *data for ethane*

P (MPa)	ρ (mol/l)
$T=92.00$ K	
0.7928	21.629
$T=93.00$ K	
8.7870	21.682
$T=94.00$ K	
3.5870	21.599
10.4980	21.664
$T=96.00$ K	
6.3091	21.555
14.6217	21.641
$T=98.00$ K	
8.1853	21.503
19.1732	21.625
$T=100.00$ K	
1.7991	21.348
11.3755	21.468
23.8694	21.613
$T=102.00$ K	
4.7964	21.315
15.4890	21.448
28.5382	21.603
$T=104.00$ K	
1.1828	21.198
6.9584	21.269
19.9098	21.434
33.1959	21.594
$T=106.00$ K	
9.0567	21.221
24.4329	21.422
$T=108.00$ K	
1.8227	21.065
6.4514	21.125
12.4806	21.193
29.0045	21.412
$T=110.00$ K	
4.7101	21.034
16.4766	21.176
33.5810	21.403
$T=112.00$ K	
1.1911	20.911
6.8417	20.990
11.2851	21.041
20.6898	21.163
$T=114.00$ K	
3.8739	20.882
8.8149	20.942
24.9715	21.152
$T=116.00$ K	
1.9636	20.776
6.3156	20.841
12.0035	20.913
19.0660	21.009
29.2820	21.143
$T=118.00$ K	
8.0478	20.791
15.7492	20.896
23.2017	20.997
$T=120.00$ K	
1.2747	20.621
6.8130	20.702
10.8020	20.757
19.6919	20.883
27.3594	20.988
$T=122.00$ K	
3.8664	20.592
14.2998	20.737
23.7193	20.873
31.5310	20.979
$T=124.00$ K	
6.2436	20.553
11.6827	20.627
18.0492	20.724
27.7606	20.863
$T=126.00$ K	
7.9236	20.505
21.9553	20.712
31.8410	20.855
$T=128.00$ K	
0.6715	20.312
10.4787	20.470
18.8911	20.597
25.8617	20.703
35.9026	20.847
$T=130.00$ K	
2.9285	20.287
13.7499	20.450
29.7809	20.694
$T=132.00$K	
5.4980	20.254
17.2765	20.436
26.4639	20.577
33.6963	20.687
$T=134.00$ K	
7.2368	20.209
20.8906	20.425
$T=136.00$ K	
1.3689	20.030
9.2490	20.167
24.5518	20.416
34.0682	20.561
$T=138.00$ K	
3.7831	20.008
12.1243	20.144
28.2309	20.407
$T=140.00$ K	
6.0574	19.972
15.3375	20.129
31.9091	20.400
$T=142.00$ K	
7.6559	19.926
18.7024	20.117
35.5822	20.392
$T=144.00$ K	
0.9387	19.722
9.8460	19.890
22.1094	20.107
$T=148.00$ K	
5.4489	19.667
15.7717	19.856
28.9678	20.091
$T=152.00$ K	
1.2079	19.424
8.9240	19.584
22.1746	19.836
35.8308	20.077
$T=156.00$ K	
5.5978	19.369
14.2846	19.545
28.6589	19.820
$T=160.00$ K	
0.4675	19.091
8.9636	19.288
20.2324	19.524
35.1468	19.806
$T=164.00$ K	
4.2580	19.043
14.0474	19.250
26.2885	19.508
$T=168.00$ K	
1.7297	18.817
7.6437	18.969
19.6507	19.230
32.3436	19.495
$T=172.00$ K	
1.2449	18.650
5.7607	18.768
11.8776	18.916
25.3400	19.214
38.3722	19.482
$T=176.00$ K	
1.1073	18.488
5.2091	18.602
8.8759	18.691
16.9907	18.892
31.0365	19.201
$T=180.00$ K	
0.5247	18.295
4.9583	18.442
8.2782	18.525
13.3001	18.655
22.2633	18.876
36.7092	19.189
$T=184.00$ K	
3.9725	18.253
7.9795	18.368
12.4806	18.483
18.2646	18.635
27.5482	18.862

TABLE 1. PVT *data for ethane*—Continued

P (MPa)	ρ (mol/l)
$T = 188.00$ K	
1.9817	18.021
7.2058	18.186
11.9718	18.323
17.2059	18.463
23.3273	18.620
32.8340	18.850
$T = 192.00$ K	
0.9865	17.815
5.5964	17.977
10.6669	18.128
16.5186	18.302
22.0330	18.447
28.3464	18.607
$T = 196.00$ K	
0.4943	17.619
4.4533	17.775
8.4330	17.903
14.9662	18.104
21.1586	18.286
26.8669	18.434
33.3677	18.595
$T = 200.00$ K	
0.6801	17.445
3.5738	17.581
7.3933	17.709
12.2367	17.866
19.4175	18.087
25.8517	18.273
31.6945	18.423
$T = 204.00$ K	
3.7760	17.411
6.7420	17.524
10.6983	17.658
16.4076	17.846
23.9051	18.074
30.2305	18.262
36.4896	18.412
$T = 208.00$ K	
0.5897	17.079
6.8033	17.354
9.6616	17.461
14.6253	17.634
20.6552	17.831
28.3791	18.062
35.0871	18.251
$T = 212.00$ K	
3.4269	17.048
9.6570	17.293
13.3583	17.434
18.6673	17.619
24.9088	17.819
32.8419	18.051

P (MPa)	ρ (mol/l)
$T = 216.00$ K	
2.1043	16.798
6.4050	16.998
13.2349	17.267
17.2225	17.417
22.7370	17.606
29.1542	17.808
$T = 220.00$ K	
1.4301	16.567
5.1249	16.761
8.9985	16.934
16.9669	17.250
21.1113	17.404
26.8053	17.594
33.3471	17.798
$T = 224.00$ K	
4.3322	16.536
7.6124	16.699
12.2714	16.904
20.7255	17.237
25.0127	17.392
30.8565	17.584
$T = 228.00$ K	
1.8552	16.198
6.9228	16.483
10.4762	16.654
15.7164	16.887
24.4895	17.225
28.8946	17.382
34.8859	17.574
$T = 232.00$ K	
1.2667	15.950
4.5825	16.167
9.4583	16.428
13.6904	16.633
19.2025	16.874
28.2402	17.215
32.7523	17.372
$T = 236.00$ K	
3.8508	15.920
7.0049	16.114
12.4747	16.403
16.9765	16.618
22.6904	16.862
31.9811	17.205
$T = 240.00$ K	
1.2548	15.515
2.2021	15.586
6.3368	15.877
9.4209	16.062
15.5972	16.387
20.2787	16.606
26.1772	16.852
35.7046	17.196

P (MPa)	ρ (mol/l)
$T = 244.00$ K	
3.6366	15.487
4.6703	15.556
8.5355	15.817
12.2246	16.039
18.7424	16.375
23.5869	16.595
29.6476	16.842
$T = 248.00$ K	
1.7380	15.078
5.9925	15.449
6.8908	15.508
11.1353	15.788
15.1129	16.023
21.8905	16.364
26.8798	16.586
33.1044	16.833
$T = 252.00$ K	
1.5930	14.811
3.9746	15.056
8.0325	15.392
9.0553	15.457
13.8649	15.771
18.0296	16.011
25.0394	16.354
30.1617	16.577
$T = 256.00$ K	
3.7062	14.790
6.1397	15.018
10.3740	15.358
11.5324	15.433
16.6249	15.758
20.9491	16.000
28.1716	16.345
33.4255	16.568
$T = 260.00$ K	
2.6858	14.414
5.7990	14.757
8.0637	14.963
12.8526	15.340
14.0783	15.417
19.3947	15.747
23.8662	15.990
31.2936	16.336
$T = 264.00$ K	
2.4038	14.085
4.6766	14.389
7.6561	14.705
10.2294	14.931
15.3689	15.327
16.6466	15.405
22.1619	15.737
26.7721	15.981
34.3986	16.328

P (MPa)	ρ (mol/l)
$T = 268.00$ K	
3.0548	13.884
4.2654	14.062
6.5471	14.352
9.6680	14.669
12.5033	14.914
17.8943	15.316
19.2306	15.395
24.9268	15.728
29.6684	15.973
$T = 272.00$ K	
2.0844	1.243
3.6257	13.670
4.8506	13.859
6.0679	14.032
8.2942	14.302
11.8077	14.650
14.8065	14.901
20.4232	15.306
21.8042	15.385
27.6780	15.719
32.5542	15.964
$T = 276.00$ K	
2.1376	1.242
3.2684	13.256
5.3267	13.644
6.5457	13.824
7.7197	13.983
10.2212	14.275
13.9836	14.636
17.1196	14.890
22.9462	15.297
24.3837	15.377
30.4166	15.711
35.4306	15.957
$T = 280.00$ K	
2.1904	1.241
2.9758	12.787
4.8428	13.234
6.9195	13.604
8.1526	13.778
9.4890	13.951
12.2137	14.259
16.1653	14.625
19.4376	14.880
25.4635	15.288
26.9473	15.368
33.1520	15.703
$T = 284.00$ K	
2.2428	1.240
4.3982	12.768
6.3596	13.203
8.4885	13.563
9.8840	13.751
11.3395	13.933
14.2261	14.247
18.3557	14.615
21.7505	14.872
27.9731	15.280
29.4971	15.360
35.8724	15.696

TABLE 1. PVT *data for ethane*—Continued

P (MPa)	ρ (mol/l)
$T=288.00$ K	
2.2951	1.239
3.0547	1.955
3.9706	12.194
5.8026	12.745
7.7971	13.160
10.1657	13.540
11.6682	13.735
13.2063	13.920
16.2439	14.237
20.5477	14.607
24.0580	14.863
30.4719	15.273
32.0446	15.353
$T=292.00$ K	
2.3466	1.239
3.8113	11.522
5.2158	12.173
7.1396	12.707
9.3105	13.131
11.8771	13.525
13.4688	13.723
15.0863	13.910
18.2640	14.228
22.7394	14.598
26.3645	14.855
32.9673	15.265
$T=296.00$ K	
2.3987	1.238
3.2373	1.952
3.8806	2.880
4.3963	11.212
4.8686	11.505
6.4389	12.146
8.4817	12.672
10.8697	13.115
13.6040	13.514
15.2773	13.713
16.9735	13.900
20.2846	14.219
24.8761	14.591
28.6475	14.848
35.4484	15.258

P (MPa)	ρ (mol/l)
$T=300.00$ K	
2.4492	1.237
4.0309	2.875
4.6932	10.611
5.3970	11.196
5.9485	11.485
7.6275	12.109
9.8845	12.652
12.4490	13.102
12.4489	13.102
15.3377	13.504
17.0906	13.704
18.8621	13.892
22.3018	14.211
27.0931	14.583
30.9501	14.841
$T=304.00$ K	
2.4997	1.237
3.4158	1.950
4.1784	2.873
4.6828	4.325
4.7721	9.097
4.9674	9.788
5.3930	10.298
5.5668	10.596
6.3948	11.173
6.9986	11.455
8.8474	12.082
11.3086	12.638
14.0362	13.092
17.0942	13.495
18.9013	13.696
20.7454	13.884
24.3137	14.204
29.2629	14.576
33.2309	14.833
$T=306.00$ K	
4.8094	4.323
4.9441	6.533
5.0757	9.092
5.8014	10.290

P (MPa)	ρ (mol/l)
$T=308.00$ K	
2.5499	1.236
4.3236	2.871
4.9341	4.321
5.1434	6.530
5.3872	9.086
5.6969	9.775
6.2111	10.280
6.4452	10.574
7.3779	11.142
8.0352	11.424
10.0940	12.066
12.7418	12.628
15.6258	13.083
18.6310	13.487
20.7132	13.688
22.6296	13.876
26.3246	14.196
31.4261	14.569
35.5024	14.826
$T=312.00$ K	
2.5996	1.235
3.5908	1.947
4.4668	2.869
5.1793	4.316
5.5401	6.522
6.0206	9.072
6.4330	9.756
7.0307	10.254
7.3179	10.546
8.3744	11.116
9.1114	11.404
11.3574	12.054
14.1819	12.618
17.2177	13.075
20.5666	13.480
22.5240	13.681
24.5119	13.869
28.3286	14.189
33.5824	14.562

P (MPa)	ρ (mol/l)
$T=316.00$ K	
2.6491	1.235
4.6083	2.866
5.4200	4.312
5.9358	6.513
6.6610	9.054
7.1729	9.732
7.8532	10.229
8.1986	10.522
9.3878	11.099
10.1982	11.390
12.6240	12.044
18.8045	13.068
22.3004	13.472
24.3313	13.673
26.3890	13.862
30.3236	14.183
$T=320.00$ K	
2.6983	1.234
3.7629	1.945
4.7483	2.864
5.6574	4.307
6.3309	6.503
7.3064	9.032
7.9172	9.710
8.6869	10.211
9.0937	10.506
10.4137	11.087
11.2486	11.380
13.9007	12.036
17.0663	12.602
20.4014	13.060
24.0318	13.466
26.1304	13.667
28.2588	13.855
32.3174	14.176

Although comparison with data from other sources is, in general, impossible without multiple interpolations, the agreement has been deduced by examining the density deviations of the various data sets [9, 10] from densities calculated from an equation of state for ethane due to Goodwin [11]. The agreement is found to be, in general, within the combined experimental error. Maximum difference occur in the critical region where the equation of state representation is expected to be less satisfactory and where the experimental densities are subject to increasing uncertainty. Estimated uncertainty in the experimental densities in this work is typically ± 0.1 percent at the lowest temperatures, increasing to ± 0.2 percent at higher temperatures and lower densities, becoming as much as ± 1.0 percent in the critical region.

New vapor pressure measurements also have been made at 5 K intervals from 160 to 300 K and are given in table 2. At each temperature, the pressure was measured at least twice with some ethane being removed from the cell between measurements. Identical pressure observations indicated that the two-phase condition existed in the cell.

A vapor pressure equation of the form

$$ln(P/P_t) = A\chi + B\chi^2 + C\chi^3 + D\chi^4 + E\chi(1-\chi)^{3/2} \quad (1)$$

was fit to all available data for ethane [12]. Here, $\chi = (1-T_t/T)/(1-T_t/T_c)$, and P and T are the pressure and temperature and t and c refer to the triple and critical points. Coefficients giving the best fit were found to be the following:

$A = 10.67324$
$B = 8.33782$
$C = -3.08489$
$D = -0.65857$
$E = 6.04955$
$P_t = 1.14 \times 10^{-5}$ bar
$T_t = 90.348$ K [Ref 1]
$T_c = 305.330$ K [Ref 10]

TABLE 2

T (K)	P kPa	T (K)	P kPa
160.00	21.502	230.00	700.48
165.00	30.670	235.00	825.96
170.00	42.870	240.00	966.60
175.00	58.636	245.00	1124.4
180.00	78.734	245.00	1124.8
180.00	78.706	250.00	1300.0
185.00	103.84	250.00	1301.9
190.00	134.63	250.00	1302.1
190.00	134.72	250.00	1301.8
195.00	172.21	255.00	1495.0
195.00	172.26	260.00	1670.3
200.00	217.26	265.00	1947.9
200.00	217.32	270.00	2208.0
205.00	270.93	275.00	2493.1
205.00	271.00	275.00	2493.2
210.00	334.13	280.00	2804.6
210.00	334.17	280.00	2806.2
210.00	333.98	285.00	3144.3
210.00	333.99	290.00	3513.5
215.00	407.34	298.15	4190.9
220.00	492.16	298.15	4188.9
225.00	589.73	300.00	4353.5

Deviations of the experimental vapor pressures from those calculated from this equation for the various data sets [9, 10, 13] are shown in figure 1.

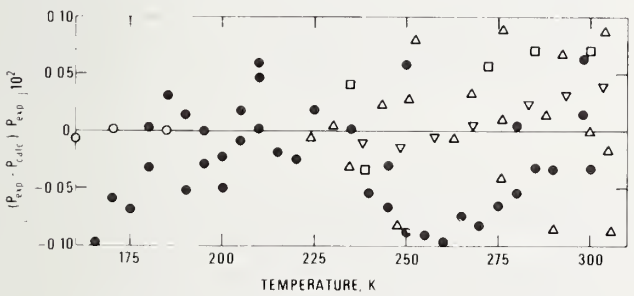

FIGURE 1. *Deviations of vapor pressures from* eq. 1.

● This work; Ziegler et al. (Ref. [13]); Pal (Ref. [9]); . . Pope (Ref. [9]); ▽ Douslin and Harrison (Ref. [10]).

4. Summary

We have made new wide-range measurements of the vapor pressures and *PVT* properties of ethane. These are the only data currently available which cover the entire temperature range from the triple point to 320 K. In addition, these data are the only accurate *PVT* data available for the compressed liquid below about 190 K. The data are being used along with other available data to refine the calculation of thermodynamic functions for ethane and as input to, and as a check upon, new calculation methods for predicting liquefied natural (fuel) gas properties being studied in this and other laboratories.

5. References and Notes

[1] Straty, G. C., and Tsumura, R., J. Chem. Phys., **64**, 859 (1976).
[2] Weber, L. A., J. Res. Nat. Bur. Stand. (U.S.), **74A** (Phys. and Chem.), No. 1, 93–129 (Jan.–Feb. 1970).
[3] Prydz R., and Straty, G. C. Nat. Bur. Stand. (U.S.), Tech. Note 392, 197 pages (Revised 1973).
[4] Goodwin, R. D., Nat. Bur. Stand. (U.S.) Tech. Note 653, 280 pages (April 1974).
[5] Weber, L. A., NASA SP-3088/NBSIR 74–374 (1975).
[6] Goodwin, R. D., J. Res. Nat. Bur. Stand. (U.S.), **65C**, (Eng. and Instr.), No. 4, 231–243, (Oct.–Dec. 1961).
[7] Straty, G. C., and Prydz, R., Rev. Sci. Inst. **41**, 1223 (1970).
[8] Goodwin and Prydz, R., J. Res. Nat. Bur. Stand. (U.S.), **76A** (Phys. and Chem.), No. 2, 81–101 (Mar.–Apr. 1972).
[9] Pope G. A., (also reports vapor pressure and *PVT* data of A. K. Pal). Ph.D. Thesis, Dept. of Chemical Engineering, Rice University, Houston, Texas (July 1971).
[10] Douslin, D. R., and Harrison, R. H., J. Chem. Thermo **5**, 491 (1973).
[11] Goodwin, R. D., NBSIR 74–398 (1974). Goodwin has used a nonanalytic equation of state to correlate previously available data on ethane and to calculate provisional thermodynamic functions. Experimental data from this work are being used to fill in gaps in previously published data and to refine the equation of state to permit more accurate calculations of thermodynamic properties to be made. We defer extensive comparisons between data sets and a more elaborate analysis for inclusion in a final report in preparation.
[12] Further refinements in the correlation are expected which will probably alter slightly the final values of the constants. The deviation plot, however, is representative of the agreement among data sets. Coefficients for this equation will be included in the final report. See also reference [8].
[13] Ziegler, W. T., Kirk, B. S., Mullins, J. C., and Berquest, A. R., Tech. Rept. No. 2, Project A–764, Eng. Expt. Sta. Georgia Inst. Tech.: Atlanta, Georgia, December 1964.

(Paper 80A1–878)

Dielectric constant data and the derived Clausius–Mossotti function for compressed gaseous and liquid ethane*

L. A. Weber

National Bureau of Standards, Institute for Basic Standards, Cryogenics Division, Boulder, Colorado 80302
(Received 25 March 1976)

Measurements are presented for the dielectric constant of ethane in the saturated liquid and compressed fluid states at temperatures between 95 and 323 K. Pressures ranged up to 390 bar. The data, which have an estimated uncertainty of 0.01%, are combined with accurate density data from several sources to produce the Clausius–Mossotti function over a wide range of temperature and density. An analytical expression of the Clausius–Mossotti function is given, and the consistency of the available density data is discussed.

I. INTRODUCTION

This paper presents dielectric constant measurements and the derived Clausius–Mossotti function for ethane. Measurements were made on the saturated liquid from the triple point to near the critical point and on seven compressed fluid isotherms in the range 95–323.15 K. The data range in pressure up to 390 bar and in density from 0.036 to 3.16 times the critical density. This work is part of a series which previously has included data on hydrogen,[1] oxygen,[2] fluorine,[3] nitrogen,[4] and methane.[5]

Measurements of the dielectric constant, combined with accurate density data for gases and liquids, provide useful information about molecular polarizabilities and molecular interactions.[6] Such measurements are generally combined to form the Clausius–Mossotti (CM) function, $(1/\rho)(\epsilon-1)/(\epsilon+2)$, where ϵ is the dielectric constant and ρ is the density. The CM function has the property of being nearly a constant, generally varying only about one percent over a wide range of density and temperature for nonpolar molecules. A knowledge of the CM function provides a convenient and sensitive way of determining density from accurate dielectric constant measurements.[7] In addition, dielectric constant data can provide a convenient and sensitive intercomparison between independent PVT measurements, even in situations where the PVT data are widely separated in temperature.

II. EXPERIMENTAL

The dielectric constant measurements were made with the highly stable cylindrical capacitor developed by Younglove and Straty,[8] which has a vacuum capacitance of about 33 pF. The curve of its vacuum capacitance versus temperature has proven to be stable to within one part in 10^5. The dielectric constant ϵ is given by the ratio C/C_0, where C is the capacitance with fluid between the plates and C_0 is the vacuum capacitance at the same temperature. The capacitance was measured with a three-terminal ac bridge. Uncertainty in the determination of the dielectric constant is estimated to be less than 0.01%. Temperatures were measured with a platinum resistance thermometer calibrated on the IPTS 1968 scale and were reproducible to 0.001 K. The overall accuracy varied from 0.005 at the lowest temperatures to 0.03 K for the room temperature measurements. Pressures were measured with an oil dead weight gauge having an accuracy of about 0.01 percent. The sample holder and cryostat are described elsewhere.[5,9] The sample used was 99.99% pure ethane which was passed through a molecular sieve trap to remove any water.

III. RESULTS

The dielectric constant of the saturated liquid was measured at 34 temperatures between 95 and 295 K.

TABLE I. Dielectric constant and calculated Clausius–Mossotti values of saturated liquid ethane.

T (K)	$\rho\times10^3$ (mol/cm^3)	ϵ	CM (cm^3/mol)
95.00	21.520[a]	1.93563	11.047
100.00	21.341	1.92576	11.050
105.00	21.159	1.91590	11.054
110.00	20.975	1.90606	11.059
115.00	20.793	1.89612	11.062
120.00	20.602	1.88952	11.101
125.00	20.419	1.87661	11.074
130.00	20.232	1.86687	11.080
135.00	20.046	1.85700	11.084
140.00	19.857	1.84713	11.089
145.00	19.667	1.83721	11.094
150.00	19.475	1.82729	11.099
155.00	19.281	1.81729	11.104
160.00	19.086	1.80725	11.109
165.00	18.887	1.79714	11.115
170.00	18.687	1.78696	11.121
175.00	18.484	1.77669	11.126
180.00	18.279	1.76628	11.131
185.00	18.070	1.75576	11.136
190.00	17.861	1.74516	11.140
200.00	17.429	1.72349	11.148
210.00	16.971	1.70104	11.161
220.00	16.499	1.67786	11.171
230.00	15.997	1.65352	11.181
240.00	15.464	1.62780	11.191
250.00	14.890	1.60036	11.199
260.00	14.261	1.57076	11.208
270.00	13.549	1.53778	11.220
275.00	13.186[b]	1.51962	11.196
280.00	12.747	1.49994	11.206
285.00	12.258	1.47809	11.214
290.00	11.699	1.45318	11.218
295.00	11.024	1.42343	11.220

[a]Densities from Ref. 10. [b]Densities from Ref. 11.

TABLE II. Dielectric constant and calculated Clausius–Mossotti values of compressed liquid and gaseous ethane.

T (K)	P (bar)	ϵ	$\rho\times10^3$ (mol/cm^3)	CM (cm^3/mol)
120.00	304.927	1.90928	21.026[a]	11.062
120.00	171.351	1.89966	20.848	11.066
120.00	66.985	1.89165	20.705	11.066
160.00	360.454	1.84490	19.827	11.083
160.00	358.376	1.84471	19.824	11.083
160.00	36.520	1.81160	19.171	11.107
160.00	36.628	1.81161	19.171	11.107
200.00	377.816	1.78020	18.564	11.118
200.00	256.633	1.76482	18.266	11.122
200.00	151.137	1.74954	17.965	11.127
200.00	69.172	1.73601	17.689	11.137
200.00	13.071	1.72560	17.472	11.147
240.00	392.029	1.71687	17.305	11.145
240.00	294.735	1.70044	16.975	11.151
240.00	211.148	1.68411	16.645	11.156
240.00	115.755	1.66165	16.186	11.164
240.00	62.930	1.64649	15.869	11.172
240.00	30.356	1.63563	15.637	11.181
280.00	376.142	1.64857	15.919	11.166
280.00	253.274	1.61794	15.274	11.182
280.00	165.058	1.58855	14.653	11.193
280.00	100.002	1.55858	14.016	11.199
280.00	54.692	1.52795	13.355	11.205
320.00	380.835	1.58441	14.579	11.183
320.00	196.092	1.51088	12.962	11.226
320.00	113.562	1.44096	11.402	11.239
320.00	79.146	1.36772	9.711	11.244
320.00	67.649	1.29621	7.894	11.256
320.00	62.595	1.22571	6.220	11.249
320.00	56.260	1.15041	4.235	11.274
320.00	40.699	1.07576	2.194	11.227
323.15	318.351	1.55939	14.051[b]	11.185
323.15	243.358	1.52894	13.389	11.195
323.15	204.702	1.50940	12.959	11.201
323.15	184.435	1.49630	12.668	11.205
323.15	163.787	1.48155	12.339	11.210
323.15	132.020	1.45243	11.684	11.216
323.15	109.032	1.42223	10.993	11.223
323.15	94.055	1.39319	10.321	11.227
323.15	84.177	1.36464	9.650	11.230
323.15	77.255	1.33429	8.924	11.235
323.15	72.719	1.30433	8.195	11.238
323.15	69.510	1.27426	7.455	11.236
323.15	66.909	1.24358	6.686	11.231
323.15	64.448	1.21258	5.893	11.229
323.15	61.725	1.18186	5.089	11.231
323.15	58.073	1.15018	4.246	11.227
323.15	52.652	1.11762	3.362	11.221
323.15	44.559	1.08526	2.466	11.207
323.15	34.222	1.05686	1.662	11.191
323.15	62.010	1.18469	5.166	11.225
323.15	54.090	1.12503	3.566	11.220
323.15	38.024	1.06621	1.929	11.196
323.15	24.604	1.03699	1.089	11.185
323.15	16.106	1.02249	0.6660	11.174
323.15	10.202	1.01362	0.4046	11.170
323.15	6.027	1.00782	0.2326	11.171

[a]Densities from Ref. 15.
[b]Densities from Ref. 11.

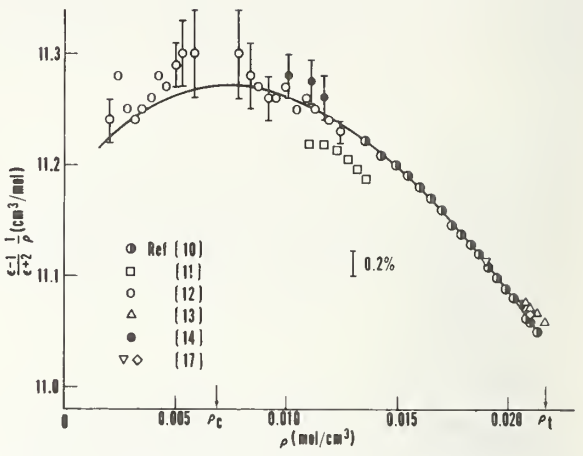

FIG. 1. Clausius–Mossotti function for the saturated liquid and vapor derived from our ϵ measurements combined with densities from the references cited. References 12 and 13 are independent $\epsilon-\rho$ measurements. The curve represents the fit of Eq. (2).

The results are given in Table I. Measurements were also made along seven isotherms between 120 and 323.15 K at pressures up to 390 bar. The results are shown in Table II. Because the cylindrical capacitor was mounted vertically, measurements in the vicinity of the critical point (approximately 305.3 K) were not attempted. Due to the configuration of the sample holder it was also not possible to make measurements in the saturated vapor.

The dielectric constant data for the saturated liquid were combined with available densities to produce the Clausius–Mossotti function, shown in Fig. 1. For temperatures up to 270 K the densities of Haynes and Hiza[10] and of Canfield *et al.*[17] were used. At temperatures above 270 K the density data of Douslin and Harrison,[11] represented by their smooth curve, were used. Also shown in the figure are the independent density–dielectric constant data of Sliwinski[12] for the saturated liquid and vapor near the critical point and the liquid CM data of Pan, Mady, and Miller[13] near the triple point. Three points derived from the saturated liquid density curve given by Burton and Balzarini[14] are shown. The error bars on these points indicate the uncertainty involved in estimating densities from the figure given in their publication.

The single phase isothermal CM function data are plotted in Fig. 2. The isotherms at temperatures from 120 to 320 K made use of the PVT data of Straty and Tsumura,[15] and the CM data at 323.15 K made use of the densities of Douslin and Harrison[11] at that temperature. Also shown is the single CM datum of Watson, Rao, and Ramaswamy[16] at a pressure of one atmosphere at 298 K. The isothermal density data were fitted with polynomials of the form,

$$P = RT\rho + \sum_i A_i \rho^i, \tag{1}$$

for the purpose of smoothing and interpolation. At temperatures below the critical, the polynomials were

constrained at the saturation boundary to the densities from Ref. 10 and 12. The density was then calculated by an iterative procedure for a given pressure.

IV. ACCURACY AND COMPARISONS

The calculated CM function is extremely useful for intercomparing sets of PVT data. In Fig. 1 the saturated liquid densities of Sliwinski are seen to be highly consistent with those of Haynes and Hiza. Sliwinski's estimated uncertainty in CM of 0.1% increasing to 0.4% nearest the critical point is shown in the figure. In the range 270–295 K Douslin's densities are seen to be 0.2%–0.3% higher than the others. The Burton and Balzarini results agree with those of Sliwinski within the uncertainty with which we could estimate the former. The Miller *et al.* densities are in agreement with those of Haynes and Hiza near the triple point to within about 0.1%. The data of Canfield *et al.*[17] lie between those of Miller *et al.* and those of Haynes and Hiza at 108 and 115 K and agree very well with those of Haynes and Hiza at 161 K.

In Fig. 2 the isothermal CM data are compared with the best estimate of the saturation curve from Fig. 1. The isotherms between 120 and 280 K, using the densities of Straty and Tsumura, are seen to be in good agreement with the saturation curve. The small variation with temperature at a given density has been observed for other fluids and is believed to be real. Their density data at 320 K may be compared directly with the density data given by Douslin and Harrison at 323.15 K (assuming negligible dependence of CM on temperature over this small range), and it is seen that the latter's densities are again systematically higher by about 0.2%. The error bars indicate the deviations which would be introduced by a 0.01% uncertainty to the dielectric constant. All of the newer data are in good agreement with the datum of Watson, Rao, and Ramaswamy,[16] reported in 1934.

Our dielectric constants are consistently smaller than those of Sliwinski by about 0.014%, which is about equivalent to the precision of his data. Our measurements are also smaller by about 0.018% than those of Miller *et al.*, who used a capacitor similar to ours. Since, in each case, the agreement is within the combined uncertainty of the authors, these differences are not considered significant.

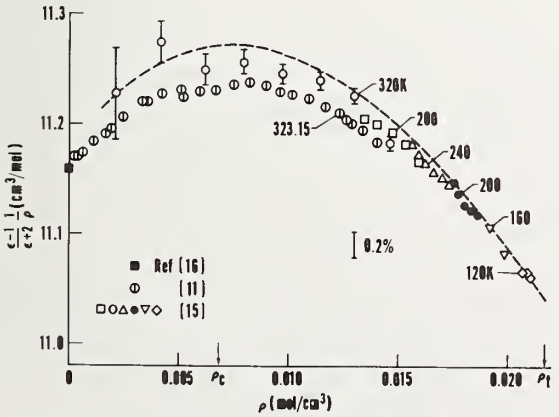

FIG. 2. Clausius–Mossotti function for the single phase fluid making use of densities from the references cited. The curve is for saturation conditions, from Fig. 1.

TABLE III. Parameters for Eq. (2); density in mol/cm^3, temperature in kelvin.

A	11.180 ± 0.005
B	30.7 ± 2.1
C	−1627 ± 77
D	−0.021 ± 0.003

The dielectric constant measurements presented here, in combination with the saturated liquid densities recorded by Haynes and Hiza and the PVT data recorded by Straty and Tsumura, along with the independent measurements recorded by Sliwinski have been fitted with the equation,

$$CM = \frac{\epsilon - 1}{\epsilon + 2}\frac{1}{\rho} = A + B\rho + C\rho^2 + DT\rho \qquad (2)$$

to provide an analytical expression for the results. The very precise PVT data recorded by Douslin and Harrison were not included because of their large systematic deviation from the others. The coefficients given in Table III are estimated to reproduce the Clausius–Mossotti function of ethane to within 0.1%.

In Table III, the parameter A, which is related to the molecular polarizability, is much larger than the corresponding parameter for methane and for the diatomic gases previously measured in this laboratory. This is to be expected based on considerations of molecular size. The molecular polarizability is calculated to be 4.43×10^{-24} cm^3. The dielectric second virial coefficient, B, is also considerably larger than the coefficient found for the smaller molecules. Sliwinski found 11.22, 20, and −1460 for the values of A, B, and C from an analysis of his data alone. His value for B should be compared with the quantity $(B+DT)$ from Table III. At room temperature this quantity has a value of about 24. However, little reliance should be placed on the significance of the value of B given here as it is based upon only one supercritical isotherm.

V. CONCLUSIONS

We have used a highly stable cylindrical capacitor to measure the dielectric constant of ethane over a wide range of density and temperature. The derived CM function has been used to intercompare the available PVT data for ethane, and an analytical expression has been given to relate density, temperature, and the dielectric constant.

*This work was carried out at the National Bureau of Standards under the sponsorship of the American Gas Association, Inc.

[1]J. W. Stewart, J. Chem. Phys. 40, 3297 (1964).
[2]B. A. Younglove, J. Res. Natl. Bur. Stand. Sec. A 76, 37 (1972).
[3]G. C. Straty and B. A. Younglove, J. Chem. Phys. 57, 2255

(1972).
[4]J. F. Ely and G. C. Straty, J. Chem. Phys. **61**, 1480 (1974).
[5]G. C. Straty and R. D. Goodwin, Cryogenics **13**, 712 (1973).
[6]C. J. F. Böttcher, *Theory of Electric Polarization* (Elsevier, New York, 1973), Vol. 1, and references cited therein.
[7]L. A. Weber, Phys. Rev. A **2**, 2379 (1970).
[8]B. A. Younglove and G. C. Straty, Rev. Sci. Instrum. **41**, 1087 (1970).
[9]D. E. Diller, J. Chem. Phys. **47**, 3096 (1968).
[10]W. M. Haynes and M. J. Hiza (unpublished data).
[11]D. R. Douslin and R. H. Harrison, J. Chem. Thermodyn. **5**, 491 (1973).
[12]P. Sliwinski, Z. Phys. Chem. **68**, 91 (1969).
[13]W. P. Pan, M. H. Mady, and R. C. Miller, AIChE J. **21**, 283 (1975).
[14]M. Burton and D. Balzarini, Can. J. Phys. **52**, 2011 (1974).
[15]G. C. Straty and R. Tsumura (to be published).
[16]H. E. Watson, G. G. Rao, and K. L. Ramaswamy, Proc. R. Soc. London Ser. A **143**, 558 (1934).
[17]C. Chui and F. B. Canfield, Trans. Faraday Soc. **67**, 2933 (1971); M. J. Shanaa and F. B. Canfield, Trans. Faraday Soc. **64**, 2281 (1968).

R-971

The heats of transition of solid ethane*

Hans M. Roder

Cryogenics Division, National Bureau of Standards, Institute for Basic Standards, Boulder, Colorado 80302
(Received 3 May 1976)

The existence of a solid–solid transition in ethane is now generally accepted. A value for the heat of transition, 2437 ± 35 J/mol at 89.774 K, together with a new value for the heat of fusion, 279 ± 6 J/mol at 90.337 K, is reported in this work. The sum of the new values is in excellent agreement with the earlier measurements, provided that the heat required to raise the temperature of the solid between transitions is included. The transition temperatures are in agreement with the most recent determinations of other authors.

I. INTRODUCTION

Several recent papers address the question of a solid–solid phase transition in ethane at temperatures close to the triple point. Webster and Hoch[1] detected a definite transition at high pressures, above about 100 MPa. However, these authors predicted that a solid–solid transition does not occur at zero pressure. Eggers[2] showed that two different solid phases existed down to zero pressure and identified the new phase as a plastic-crystalline form. At the same time Straty and Tsumura,[3] while attempting to remeasure the melting pressures of ethane, found evidence of a solid phase transition along a pressure–temperature boundary roughly parallel to the ordinary melting curve but approximately 0.5 K lower.

In connection with ongoing measurements of the specific heats of liquid ethane,[4] it appeared possible and worthwhile to measure the heats of transition of ethane. We have determined new enthalpy differences for the solid–solid transition and for the heat of fusion. In addition, values for the specific heat of solid and liquid ethane were obtained from the experiment, as well as an estimate for the specific heat of the solid at temperatures between the two transitions. The sum of enthalpy for the solid–solid transition, the new heat of fusion, and the heat required to change temperatures between the two solid phases is in excellent agreement with earlier measurements by Witt and Kemp[5] who apparently identified the total as the "heat of fusion."

II. APPARATUS

The apparatus used is a constant volume adiabatic calorimeter fully described by Goodwin.[6] The essential features are a spherical sample holder, a filling capillary, a heating/cooling interceptor ring, an adiabatic shield, and a platinum resistance thermometer mounted externally on the sample holder. The instrument has been used to measure the specific heats of hydrogen,[7,8] oxygen,[9,10] fluorine,[11,12] and methane.[13] Measurements of C_v and C_{sat} for liquid ethane are in progress.[4] While not specifically designed for solidified gases the system has been used to intercompare the heat capacity of solid argon[7] with excellent results. Minor modifications to the original system have been described by Goodwin and Weber.[9] The only change made for the present experiment was to connect the heater voltage leads to the same potentiometer as the heater current leads. This left the other potentiometer available for a continuous display of temperature. The new connection degrades the accuracy of the power measurement to about 0.2%. However, in view of other effects the inaccuracy in the power measurement is not a limiting restriction.

III. PROCEDURE

The experiment consisted of running a cooling curve from several K above the triple point to several K below on one day, and a heating curve covering the same temperature range on the following day. A continuous display of temperature vs time was obtained on a recorder for each run. Temperatures were measured with a platinum resistance thermometer calibrated by the National Bureau of Standards on the IPTS-1968. The sample holder had been filled during a regular specific heat run with 1.432 moles of ethane. The ethane used in these experiments was commercially available research grade with minimum purity certified by the supplier at 99.98%. This purity was verified by chromatographic analysis. Nominal volume of the sample holder is about 73 cm^3. Thus, near the triple point the sample holder was about 90% full. With the very low vapor pressure of ethane, a negligible amount of sample resides in the filling capillary. Using liquid nitrogen as refrigerant, cooling was applied by placing helium gas in the space around the sample holder. This space is normally under vacuum. Using the known specific heat of saturated liquid ethane[4] the cooling applied to sample and holder was estimated to be somewhat over 1.1 W. Of course, as the temperature difference between sample holder and nitrogen bath decreased, the applied refrigeration decreased also. Total cooling time was about $1\frac{1}{2}$ h.

For the heating curve the pertinent events taken from the recorder charts are summarized in Table I. The applied power was chosen to be approximately $\frac{1}{4}$ that of the cooling, namely 0.2764 W, in order to reduce thermometer offsets as much as possible. Total heating time was 5 h with power readings taken every 10 min. For a period of 30 min in the middle of the run the power was turned off to observe thermometer equilibration. A similar observation was made at the end of heating after all of the sample had melted. The final drift of the thermometer is quite in keeping with the normal specific heat runs on the liquid where equilibration times of up to 30 min are common. During the heating period both the interceptor ring heater and the

TABLE I. Events during heating.

Time (min)	Events	Comments
137.	Power on	86.466 K at start
174.75	Onset of solid–solid transition	
347.	Power off } Check thermometer equilibration	Temperature lower by 0.315 K
377.	Power on }	
415.3 ± 3	End of solid–solid transition	
427.12	Onset of melting	
451.25	End of melting	
475.	Power off } Check thermometer equilibration	Final thermometer drift 0.46 K
491.	End of run }	Final temperature 94.505 K

adiabatic shield heater were under automatic control, as they normally are during a specific heat run.

IV. RESULTS

The initial portion of the cooling curve is shown in Fig. 1. Any lingering doubts about one vs two transitions are resolved. The two transitions, liquid to solid and solid to solid, are clearly in evidence. A schematic representation of what would be expected under ideal conditions is shown in the upper portion of Fig. 1. It is obvious that the thermometer is not in equilibrium with the sample in this portion of the experiment. At the onset of each transition the thermometer recovers to a value quite close to the transition temperature but still offset from it. Maximum amount of thermometer offset in the cooling experiment is about 100 μV, or approximately 0.5 K. Most of the results are, therefore calculated from the heating curve with information from the cooling curve being used to estimate errors in the measurements.

The temperature and heats of transition are given in Table II. The temperatures are taken from the heating curve at the point where the slope changes at the onset

TABLE II. Temperatures and heats of transition of ethane.

Transition	Transition temperatures (K)	Heats of transition (J/mol)	
Liquid–solid	This experiment	90.333 ± 0.05	279 ± 6
	Eggers	90.27	
	Straty and Tsumura	90.348	
Solid–solid	This experiment	89.774 ± 0.13	2437.5 ± 35
	Eggers	89.82	
	Straty and Tsumura	89.8	

of each transition. This is also the point where the temperature curve stays flat for the longest period of time. The heats of transition are calculated from the elapsed time between phase changes, the applied power, and the amount of sample. The only time which cannot be established with any degree of precision is the end of the solid–solid transition, as indicated in Table I. It is the uncertainty in the end of this transition which leads directly to the rather large uncertainty in the heat of the solid–solid transition. The uncertainty in the new heat of fusion 279 ± 6 J/mol is estimated from the uncertainty in the power measurement 0.2% and a maximum uncertainty of 0.5 min in the time that this power is applied. The uncertainty can be confirmed from the cooling curve. We had estimated the amount of cooling applied to be 1.1 W from the known heat capacity of saturated liquid ethane and the heat capacity of the empty calorimeter. This value together with the elapsed time yields a value of 285 J/mol for the heat of fusion on cooling.

To calculate values of specific heat one needs, in addition to the elements above, the heat capacity of the empty calorimeter. These values are available.[4] Values for the specific heat of solid and liquid ethane calculated from the heating curve are given in Table III. The agreement between this experiment and others[4,5] for liquid ethane is excellent, 0.3%. The specific heat of solid ethane below the lower transition is in very good agreement with the earlier measurements by Witt and Kemp.[5] The agreement found here, and the fact

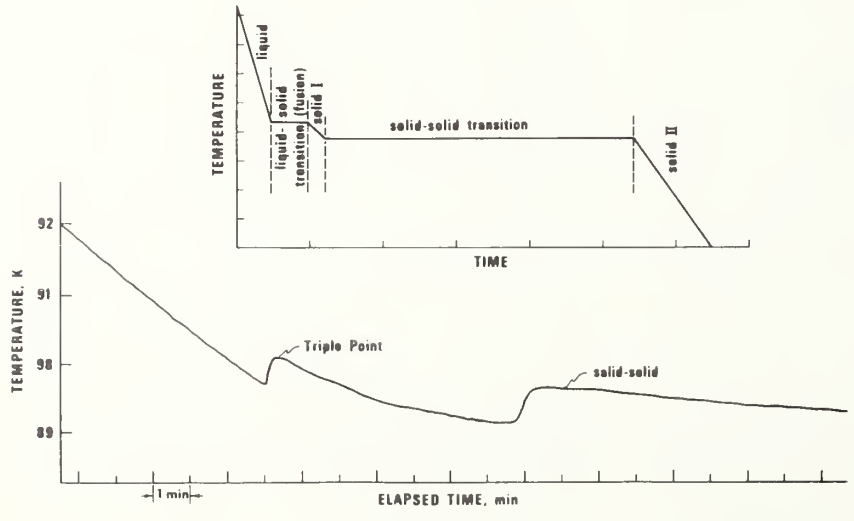

FIG. 1. The initial portion of the cooling curve.

TABLE III. Specific heats of ethane.

Phase	Temperature range (K)	Specific heats (J/mol-K) This experiment	Others	Ref.
Liquid	90.3–94	68.5 ± 1	68.3	4
			68.3	5
Solid	89.7–90.3	214 ± 70[a]		
Solid	86.4–89.7	91.5 ± 7	87.1[b]	5

[a]The heat capacity of the empty calorimeter is 43.95 J/K for this interval.
[b]At 86.73 K.

that a highly purified sample was used, suggests that the rise in heat capacity is an intrinsic property of pure ethane. It also suggests that the impurity content of Witt and Kemp[5] was probably much lower than the 0.5% that they estimated from "premelting." The uncertainty of the specific heat of the solid between the two transitions is quite large. There is a definite indication of the end of the solid–solid transition on the heating trace, however; the time associated with the end of the transition is smeared out over an interval of about 6 min.

V. DISCUSSION

We note that our system is not especially appropriate for these measurements. An instrument specifically designed to measure heats of fusion should be thin walled, should provide an isothermal sample space, i.e., have internal vanes and the thermometer should be mounted inside the sample holder in intimate contact with the sample being tested. As a result, the lack of precise knowledge of the sample temperature was disconcerting, but not unexpected. In both cooling and heating experiments the thermometer indication is running ahead of the true sample temperature. In Fig. 1 the thermometer recovers toward the proper temperature at the onset of each phase change but does not quite reach the actual values of the sample temperature. With the much lower power used for the heating experiment, the offset experienced at the onset of a phase change is expected to be the minimum possible, hence the transition temperatures were taken at the very beginning of each phase change. To provide an estimate of the temperature error we averaged the temperatures from both heating and cooling curves at the fixed points obtaining 90.29 K for the triple point and 89.65 K for the lower transition. The difference between these values and the ones given in Table II are taken as an indication of the temperature errors at the fixed points, namely 0.05 and 0.13 K.

The imprecision in sample temperature, however, does not carry over into the heat measurements. The indications of a phase change given by the thermometer trace are very sharp, and with the exception noted in Table I, the phase changes can be determined to better than 0.5 min. Earlier measurements of the heat of fusion of ethane[5,14] were made before the existence of two solid phases was known. We can compare the earlier measurements to the sum of the heat of solid–solid transition, the heat required to raise the temperature of the solid between transitions, and the new heat of fusion. The values are 2858[5] and 2854 J/mol for the present experiment. The agreement 0.14% is excellent.

The higher temperature solid has been identified as a plastic crystal[1,2] and is thus associated with a change in positional order only. The solid–solid transition is associated with a change in the long-range orientational order. The entropy or enthalpy change for the melting transition is, therefore, expected to be much less than that of the solid–solid transition. Our experiment confirms this, the ratio of the heat of fusion to the heat of transition being nearly 1 to 9.

*This work was carried out at the National Bureau of Standards under the sponsorship of the American Gas Association, Inc.

[1]D. S. Webster and M. J. R. Hoch, J. Phys. Chem. Solids 32, 2663 (1971).
[2]D. F. Eggers, Jr., J. Phys. Chem. 79, 2116 (1975).
[3]G. C. Straty and R. Tsumura, J. Chem. Phys. 64, 859 (1976).
[4]H. M. Roder, J. Res. Natl. Bur. Stand. U.S. (to be published).
[5]R. K. Witt and J. D. Kemp, J. Am. Chem. Soc. 59, 273 (1937).
[6]R. D. Goodwin, J. Res. Natl. Bur. Stand. U.S. Sect. C 65, 231 (1961).
[7]B. A. Younglove and D. E. Diller, Cryogenics 2, 283 (1962).
[8]B. A. Younglove and D. E. Diller, Cryogenics 2, 348 (1962).
[9]R. D. Goodwin and L. A. Weber, J. Res. Natl. Bur. Stand. U.S. Sect. A 73, 1 (1969).
[10]R. D. Goodwin and L. A. Weber, J. Res. Natl. Bur. Stand. U. S. Sec. A 73, 15 (1969).
[11]R. D. Goodwin and R. Prydz, J. Res. Natl. Bur. Stand U.S. Sect. A 74, 499 (1970).
[12]R. Prydz and R. D. Goodwin, J. Res. Natl. Bur. Stand. (U.S.) Sect. A 74, 661 (1970).
[13]B. A. Younglove, J. Res. Natl. Bur. Stand. (U.S.) Sect. A 78, 401 (1974).
[14]R. Wiebe, K. H. Hubbard, and M. J. Brevoort, J. Am. Chem. Soc. 52, 611 (1930).

JOURNAL OF RESEARCH of the National Bureau of Standards—A. Physics and Chemistry
Vol. 80A, Nos. 5 and 6, September–December 1976

Measurements of the Specific Heats, C_σ, and C_v, of Dense Gaseous and Liquid Ethane*

Hans M. Roder

Institute for Basic Standards, National Bureau of Standards, Boulder, Colorado 80302

(August 20, 1976)

The specific heats of saturated liquid ethane, C_σ, have been measured at 106 temperatures in the temperature range 93 to 301 K. The specific heats at constant volume, C_v, have been measured at 19 densities ranging from 0.2 to 3.1 times the critical density, at temperatures between 91 and 330 K, with pressures to 33 MPa, at 200 PVT states in all. The uncertainty of most of the measurements is estimated to be less than 2.0 percent. As the critical point is approached the uncertainty rises to about 5.0 percent. The measurements were performed to provide input data for accurate calculations of the thermodynamic properties for ethane. They are believed to be the most comprehensive specific heat measurements available for the liquid and vapor states of ethane.

Key words: Constant volume; ethane; heat capacity; liquid; saturated liquid; specific heat; vapor.

1. Introduction

For the calculation of the thermodynamic properties of a fluid, properties such as internal energy, enthalpy, entropy, and velocity of sound, especially at temperatures less than critical, one needs either the latent heat of vaporization or a specific heat along a path traversing the temperatures of interest. Heat capacity measurements are much easier to make than latent heat measurements, and they are not restricted to the liquid-vapor curve but can be made at temperatures and densities in the single phase fluid region as well.

For ethane, the specific heat of the saturated liquid, C_σ, was measured from 93 to 301 K, and specific heats at constant volume, C_v, were measured on 19 isochores with densities ranging from 1.5 mol/l to 21 mol l with temperatures from 91 to 330 K and pressures up to 33 MPa [1].[1]

In a forthcoming publication Goodwin [2] uses the present results together with extensive PVT data to construct a complete thermodynamic network for ethane from the triple point to 600 K with pressures up to 70 MPa.

2. Experimental Method

The basics of the specific heat experiment are deceptively simple. The heat capacity of a sample of fluid is determined in principle as follows. A sample holder is filled with a known amount of sample, N, and is placed in an adiabatic environment. If we now apply a carefully measured amount of heat, Q, to the sample holder, then the temperature of sample and holder will rise to a new value, from an initial temperature, T_1, to a final temperature, T_2, the change in temperature being ΔT. To obtain the heat capacity of the sample we must account for the heat absorbed by the container. This is accomplished by conducting a second experiment with the sample holder empty to find the heat capacity of the empty container, C_0. With

$$C_0=\frac{Q_{\mathrm{MT}}}{\Delta T_{\mathrm{MT}}} \tag{1}$$

the desired specific heat of the sample can be calculated from

$$C=\frac{Q-C_0\cdot\Delta T}{\Delta T\cdot N}. \tag{2}$$

Thus, the parameters we must measure in the experiment are C_0, Q, ΔT, and N.

3. Apparatus and Procedures

The apparatus used is a constant volume adiabatic calorimeter fully described by Goodwin [3]. The essential features are a spherical sample holder, a filling capillary, a heating/cooling interceptor guard ring, an adiabatic shield, and a platinum resistance thermometer mounted on the sample holder. Calorimeter and cryostat are shown in figure 1. The refrigerants used were liquid nitrogen, ice, and cold

*This work was carried out at the National Bureau of Standards under the sponsorship of the American Gas Association.

[1] Figures in brackets indicate the literature references at the end of this paper.

water. The instrument has been used to measure the specific heats, C_σ and C_v, of hydrogen [4, 5], oxygen [6, 7], fluorine [8, 9], and methane [10]. Measurements of the heat of fusion and of the solid-solid transition in ethane with this apparatus have been reported elsewhere [11]. Minor modifications to the system have been described by Goodwin and Weber [6].

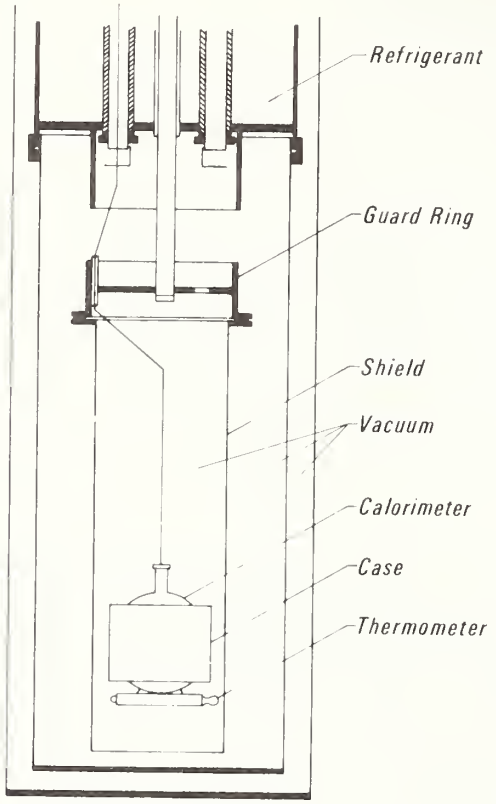

FIGURE 1. *Calorimeter and cryostat.*

The major experimental parameters are Q, ΔT, and N. These are measured as follows. We obtain the calorimetric heating rate from nearly simultaneous readings of the potential and current applied to the calorimeter heater. The time of the heating interval is measured by an electronic counter triggered by the potential across the calorimeter heater. Temperatures are measured with the platinum resistance thermometer. The thermometer was calibrated by the NBS Temperature Section. Temperatures are on the IPTS–68 scale. The temperature of the adiabatic shield and guard ring are controlled to the sample temperature with difference thermocouples and automatic power regulation. The amount of sample is determined from an observed temperature T and pressure P in the single-phase domain, from the bomb volume at this T, P, and from the fluid density derived from an equation of state [2].

The ethane used in these experiments was commercially available research grade with minimum purity certified by the supplier at 99.98 percent. This purity was verified by chromatographic analysis.

The procedures used for measurement of the empty calorimeter, for loading of the sample, and for the specific heat measurements are the same as those used previously [4–10] except for filling the sample holder at low densities, and in the sequence of measurements. Differences in the filling of the calorimeter arise because the critical temperature of ethane is above room temperature. The ethane supply tank is normally at room temperature, about 296 K and the corresponding supply pressure, vapor pressure, is about 4 MPa. Fillings with liquid densities down to 12 mol/l are determined by selecting the temperature of the calorimeter, as before. However, different techniques had to be used to achieve densities below 12 mol/l. One was to raise the filling pressure by placing the ethane supply tank in a hot water bath, up to 40 °C. The other was to fill the sample holder around 12 mol/l, heat it to a temperature above critical, and then bleed it in small increments down to the desired density.

The sequence of measurements adopted was to conduct the C_σ and C_v measurements with a single filling rather than with different fillings as was the practice before. In this scheme the sample holder is filled to a known density in the single phase region and is then cooled to a temperature where both liquid and vapor are present in the calorimeter. Heating intervals are applied to the two phase sample, the data reduction yields values of C_σ. During these measurements both liquid and vapor densities are changing, gradually filling the sample holder. From that point on the data reduction is carried out to yield values of C_v. The heating interval in which the sample holder contains both two phase and single phase fluid is called the "breakthrough" point. A sharp change in rate of temperature rise can be seen on a recorder trace of calorimeter temperature, and both guard ring and shield heaters show a slight "bump" on the recorder traces of the differential thermocouples corresponding to a change in power requirement.

4. Calculations and Adjustments

The data reduction applicable to this experiment has been described in detail by Goodwin and Weber [6, 7]. However, for ethane the separate programs of C_σ and C_v were combined and a phasefinder developed that would pinpoint the "breakthrough" point of each filling. The phasefinder, the filling conditions, and the PVT conditions at which each point was measured are based on the equation of state by Goodwin [2].

One of the primary experimental parameters is the total amount of sample in the system, N. The pressure and temperature at filling are measured, the corresponding density is calculated from the PVT surface, and N is evaluated from a knowledge of the calorimeter volume, and the various ancillary volumes such as capillary, connector, and valve volumes. As mentioned before, the critical point of ethane, at 305.33 K, is above room temperature. A number of fillings and experimental measurements

were made between 305 and 330 K. For these runs the portion of the sample in the capillary is not negligible, and has to be accounted for accurately. All of the "nuisance" volumes were revised, in particular the valve volume which, nominally at room temperature, was larger than previously estimated. To partially alleviate the problem the valve was thermostated at 40 °C, and a variable valve temperature was included in the data reduction routines. The amount in the capillary is determined by assuming a temperature distribution along the capillary. This distribution was changed to accommodate a variable temperature at the valve end.

Several other corrections made in the programs are reviewed briefly. The calorimeter volume depends both on temperature, thermal expansion, and on pressure [4, 6]. Since the sample holder is a thin stainless steel sphere it stretches as the pressure increases. Thus, in a C_v measurement work is done by the sample due to the increase in sample volume. This correction developed by Walker [12] ranges from 0.5 to 5 percent of the resulting C_v value. However, it can be made accurately. The density for each C_v measurement is calculated from the filling density after correcting for sample holder expansion and the amount compressed into the filling capillary [7]. In the case of a C_σ measurement the effects of the latent heat of vaporization and heat absorbed by the vapor must be subtracted [4, 6, 8]. This type of correction has been derived by Hoge [13].

It is worthwhile to mention that of the three state variables, pressure, temperature, and density, only temperature is measured during the measurement of a specific heat point. The amount of sample in the calorimeter is used to establish the density and pressure at the mean temperature of the experiment. While the total amount of sample remains constant, the distribution between calorimeter and capillary changes from point to point because the calorimeter volume changes with temperature and pressure. Thus, while the results for C_v are corrected to be a true C_v, the measurements of a given run are made at slightly changing mean densities.

Curvature adjustments have been made for the C_σ values at temperatures above 101.5 K. Adjustments to the experimental gross heat capacity-liquid and vapor-range from 0.002 J/mol-K to 0.366 J mol-K, or up to 0.16 percent of the total value of C_σ. Curvature adjustments for the values of C_v were not significant, and were, therefore, omitted.

5. Heat Capacity of the Empty Calorimeter

Early estimates revealed that under the best of circumstances 50 percent of the applied heat is required for the calorimeter; for the very low densities at the highest temperatures up to 93 percent of the heating goes to raise the temperature of the calorimeter. Since the critical temperature of ethane is 305.33 K it appeared desirable to make at least some of the C_v measurements at temperatures above critical. An upper limit of 338 K is imposed by the fact that the platinum resistance thermometer is mounted with Wood's metal, which melts at 65 °C. Measurements on the other fluids had been carried out to only 300 K, therefore, an extension of the measurements on the empty calorimeter were indicated.

Remeasuring the heat capacity of the calorimeter C_0 provided an opportunity to conduct additional checks of the system with regard to systematic errors, and to see if the precision of the measurements could be improved. The measurements of the heat capacity of the empty calorimeter included large and small ΔT's from 8 to 0.5 K; large and small applied powers, from 1.0 to 0.23 W; runs with deliberate temperature offsets in both guard ring and shield temperatures, 3 K (100 μV) hot and cold; as well as different coolants in the refrigerant tank, runs 2, 3, 4, with ice and runs 5, 6, 7 with liquid nitrogen. The results of these measurements, some 92 points, are shown in table 1. The applied temperature differences are small enough so that a curvature correction is not required. Intercomparison of the data is achieved by using the functional representation developed by Goodwin and Weber [6].

$$\mathrm{Log}_e\,(C_0/50) = \sum_{i=1}^{8} C_i \cdot (100/T)^{i-1}. \qquad (3)$$

Values of the coefficients, C_i, are given in the heading of table 1.

Points 208 through 304 are included in table 1 to show the most extreme variation in ΔT. They were not used to obtain the coefficients, C_i, because during these runs one of the d.c. amplifiers had a large bias which was not corrected until the start of run 4. The analytical curve represents the heat capacities of the empty calorimeter with an imprecision of 0.07 percent. To the level of 0.1 percent in C_0 there are no discernible systematic errors that can be related to the size of the ΔT, the size or rate of the applied heating, the temperature gradient of the capillary, or to temperature errors in shield or guard ring systems. The agreement of the present values with those measured by Goodwin and Weber [6] is well within the imprecision of the separate measurements. In the temperature range 87 to 320 K the uncertainty in the quantity $(Q - C_0\Delta T)/\Delta T$ will range from 0.04 to 0.08 J/K due to the uncertainties in C_0 alone.

6. Results

The results to be presented include values for the specific heat of saturated liquid ethane, values for the specific heat of single phase ethane, both in compressed liquid and in gaseous states, and a limited set of measurements on methane, made for purposes of comparison. As mentioned above, both C_σ and C_v measurements were made during a single filling. Table 2 gives the loading conditions for all experimental runs; the runs are shown in density-temperature coordinates in figure 2. Temperature and pres-

TABLE 1. *Heat capacity of the empty calorimeter*

Coefficients, eq [3]:
C1= 1.352617652, C2= −7.469809247, C3=30.953781888, C4=−76.348710878
C5=110.748213166, C6=−94.987724059, C7=44.485629941, C8= −8.756298569

Run No. — Point	Temperature	Power	Time	Heat, Q	ΔT	C_0	C_0 Calc.	Dev.	Remarks
No.	K	W	s	J	K	J/K	J/K	0/0	
208	300. 294	0. 23661	723. 20	171. 11	2. 066	82. 810	83. 088	−0. 34	Not used in fit
209	302. 419	. 23724	721. 35	171. 13	2. 061	83. 040	83. 230	−. 23	Not used in fit
210	303. 809	. 23720	185. 20	43. 93	. 528	83. 142	83. 322	−. 22	Not used in fit
302	275. 050	. 24587	181. 92	44. 73	. 549	81. 523	81. 311	. 26	Not used in fit
303	275. 881	. 24655	360. 18	88. 80	1. 091	81. 389	81. 373	. 02	Not used in fit
304	278. 500	. 93146	361. 54	336. 76	4. 129	81. 559	81. 566	−. 01	Not used in fit
401	279. 032	1. 00446	360. 92	362. 53	4. 446	81. 543	81. 605	−. 08	
402	283. 489	1. 00375	360. 25	361. 60	4. 416	81. 892	81. 927	−. 04	
403	287. 955	1. 00340	361. 62	362. 85	4. 414	82. 213	82. 243	−. 04	
404	292. 433	1. 00341	360. 78	362. 01	4. 387	82. 526	82. 555	−. 04	
405	296. 923	1. 00302	361. 68	362. 77	4. 385	82. 733	82. 862	−. 15	
406	295. 532	1. 00384	362. 13	363. 52	4. 397	82. 683	82. 767	−. 10	
407	300. 004	1. 00318	360. 49	361. 64	4. 357	83. 010	83. 069	−. 07	
408	304. 486	1. 00292	361. 54	362. 60	4. 357	83. 232	83. 367	−. 16	
409	309. 774	1. 00062	361. 05	361. 27	4. 320	83. 636	83. 712	−. 09	Guard ring 3 K cold
410	314. 120	1. 00050	360. 63	360. 81	4. 301	83. 884	83. 992	−. 13	Guard ring 3 K cold
411	318. 482	1. 00075	360. 05	360. 32	4. 278	84. 235	84. 269	−. 04	Guard ring 3 K cold
412	309. 649	1. 00114	358. 38	358. 79	4. 291	83. 620	83. 704	−. 10	Guard ring 3 K hot
413	314. 300	1. 00111	360. 84	361. 24	4. 298	84. 044	84. 004	. 05	Guard ring 3 K hot
414	319. 013	1. 00083	361. 65	361. 95	4. 286	84. 442	84. 303	. 16	Guard ring 3 K hot
501	273. 211	1. 01274	363. 70	368. 33	4. 535	81. 219	81. 173	. 06	
502	277. 724	1. 01203	360. 42	364. 76	4. 472	81. 572	81. 509	. 08	
503	282. 215	1. 01194	361. 01	365. 31	4. 462	81. 871	81. 835	. 04	
504	286. 704	1. 01106	361. 10	365. 09	4. 442	82. 199	82. 155	. 05	
505	291. 192	1. 01099	361. 06	365. 02	4. 423	82. 520	82. 469	. 06	
506	295. 681	1. 01067	361. 04	364. 89	4. 406	82. 814	82. 777	. 04	
507	300. 167	1. 01023	360. 65	364. 34	4. 383	83. 132	83. 080	. 06	
508	304. 708	1. 00964	361. 07	364. 55	4. 369	83. 447	83. 381	. 08	
509	309. 206	1. 00927	360. 48	363. 82	4. 346	83. 711	83. 675	. 04	
510	314. 458	1. 00864	483. 74	487. 91	5. 802	84. 100	84. 014	. 10	
511	319. 745	1. 00766	360. 77	363. 53	4. 306	84. 418	84. 349	. 08	
601	127. 080	. 57391	482. 10	276. 68	4. 659	59. 390	59. 270	. 20	
602	131. 608	. 57368	482. 80	276. 97	4. 566	60. 662	60. 644	. 03	
603	136. 098	. 57391	482. 56	276. 91	4. 470	61. 945	61. 920	. 04	
604	142. 318	. 57390	899. 00	515. 94	8. 114	63. 588	63. 562	. 04	
605	150. 056	1. 00467	485. 05	487. 31	7. 443	65. 474	65. 422	. 08	
606	131. 622	. 58565	174. 94	102. 45	1. 690	60. 607	60. 648	−. 07	
607	134. 090	. 58574	347. 99	203. 83	3. 322	61. 354	61. 360	−. 01	
608	137. 347	. 58516	347. 34	203. 25	3. 266	62. 225	62. 261	−. 06	
609	139. 657	. 58460	174. 57	102. 05	1. 623	62. 897	62. 877	. 03	
610	142. 810	. 58371	518. 78	302. 82	4. 755	63. 686	63. 686	. 00	

611	147. 463	. 58495	514. 99	301. 24	4. 647	64. 827	64. 819	. 01	
612	152. 806	. 58497	693. 56	405. 71	6. 141	66. 064	66. 039	. 04	
613	161. 128	. 57559	605. 25	348. 38	5. 143	67. 734	67. 782	—. 07	
614	167. 386	. 57535	897. 63	516. 45	7. 490	68. 948	68. 983	—. 05	
615	174. 725	. 57518	899. 07	517. 13	7. 355	70. 309	70. 284	. 04	
616	175. 502	1. 01504	263. 20	267. 16	3. 793	70. 431	70. 415	. 02	
617	179. 197	1. 01430	262. 02	265. 77	3. 742	71. 022	71. 025	—. 00	
618	182. 608	1. 01317	261. 33	264. 77	3. 703	71. 509	71. 567	—. 08	
619	186. 241	1. 01301	262. 22	265. 63	3. 686	72. 065	72. 122	—. 08	
620	188. 966	1. 01269	136. 12	137. 84	1. 899	72. 580	72. 525	. 08	
621	190. 803	1. 01218	135. 19	136. 84	1. 878	72. 861	72. 790	. 10	
622	194. 400	1. 01244	392. 67	397. 55	5. 425	73. 275	73. 295	—. 03	
623	199. 723	1. 01223	392. 50	397. 30	5. 372	73. 962	74. 009	—. 06	
624	202. 396	1. 01658	516. 29	524. 84	7. 062	74. 323	74. 353	—. 04	
625	206. 831	. 28352	516. 44	146. 42	1. 954	74. 940	74. 906	. 04	
626	208. 722	. 28345	519. 22	147. 17	1. 960	75. 102	75. 134	—. 04	
627	212. 843	. 97721	517. 07	505. 29	6. 685	75. 583	75. 619	—. 05	
628	220. 458	1. 01519	654. 30	664. 24	8. 686	76. 476	76. 469	. 01	
629	226. 417	. 28269	920. 69	260. 27	3. 377	77. 059	77. 096	—. 05	
630	229. 716	. 28266	922. 57	260. 77	3. 365	77. 501	77. 430	. 09	
631	235. 624	1. 01464	658. 73	668. 38	8. 567	78. 014	78. 006	. 01	
632	232. 939	. 58665	783. 62	459. 71	5. 909	77. 793	77. 748	. 06	
633	238. 781	. 58629	784. 29	459. 82	5. 872	78. 313	78. 304	. 01	
634	244. 575	. 58619	780. 71	457. 64	5. 807	78. 810	78. 833	—. 03	
635	250. 293	. 58579	786. 49	460. 72	5. 808	79. 320	79. 334	—. 02	
636	256. 055	. 58558	784. 73	459. 52	5. 756	79. 836	79. 821	. 02	
637	261. 790	. 58544	785. 31	459. 75	5. 723	80. 339	80. 287	. 06	
638	267. 500	. 58482	782. 99	457. 91	5. 665	80. 832	80. 737	. 12	
639	273. 202	. 58484	785. 46	459. 37	5. 657	81. 207	81. 172	. 04	
640	277. 804	. 58479	786. 09	459. 70	5. 639	81. 520	81. 515	. 01	
641	283. 507	. 58451	784. 38	458. 47	5. 594	81. 956	81. 928	. 03	
642	289. 440	. 58427	785. 21	458. 77	5. 567	82. 403	82. 347	. 07	
643	295. 144	. 58405	784. 02	457. 90	5. 529	82. 822	82. 741	. 10	
644	87. 956	. 58825	329. 66	193. 92	4. 522	42. 888	42. 881	. 01	
645	92. 450	. 58814	346. 38	203. 72	4. 502	45. 250	45. 272	—. 05	
646	96. 923	. 58758	361. 11	212. 18	4. 469	47. 476	47. 464	. 02	
647	101. 371	. 58799	375. 32	220. 68	4. 456	49. 524	49. 519	. 01	
648	105. 801	. 58779	388. 99	228. 64	4. 442	51. 476	51. 454	. 04	
649	110. 252	. 58769	407. 99	239. 77	4. 499	53. 297	53. 290	. 01	
650	114. 693	. 58742	421. 62	247. 67	4. 503	54. 999	55. 013	—. 02	
651	119. 179	. 58700	435. 77	255. 80	4. 519	56. 604	56. 645	—. 07	
652	123. 684	. 58733	450. 21	264. 42	4. 549	58. 134	58. 179	—. 08	
653	128. 143	. 58676	450. 00	264. 04	4. 435	59. 538	59. 601	—. 10	
701	276. 822	. 58535	781. 32	457. 34	5. 616	81. 429	81. 442	—. 02	Guard ring 3 K cold
702	282. 678	. 58521	785. 71	459. 80	5. 617	81. 865	81. 869	—. 00	Guard ring 3 K cold
703	276. 345	. 58488	784. 87	459. 05	5. 642	81. 369	81. 407	—. 05	Guard ring 3 K hot
704	281. 862	. 58439	784. 15	458. 25	5. 606	81. 749	81. 810	—. 07	Guard ring 3 K hot
705	276. 552	. 58419	781. 97	456. 82	5. 612	81. 400	81. 422	—. 03	Shield 3 K cold
706	282. 382	. 58464	783. 58	458. 11	5. 598	81. 834	81. 847	—. 02	Shield 3 K cold
707	275. 701	. 58248	782. 35	455. 70	5. 604	81. 320	81. 359	—. 05	Shield 3 K hot
708	281. 212	. 58417	784. 63	458. 36	5. 610	81. 706	81. 763	—. 07	Shield 3 K hot

TABLE 2. *Calorimeter loading conditions for the measurement runs*

Run No.	Pressure	Density	Temperature	Calorimeter volume	Total sample	Valve temperature	Breakthrough conditions	
							Density	Temperature
	MPa	mol/l	K	cm^3	mol	K	mol/l	K
1	4. 0982	14. 641	258. 899	73. 238	1. 0730	296. 45	14. 659	254. 048
2	3. 8329	20. 998	110. 512	72. 794	1. 5289	296. 45	21. 013	108. 627
3	4. 0753	16. 135	231. 874	73. 150	1. 1811	296. 45	16. 157	227. 207
4	3. 8996	19. 648	147. 427	72. 892	1. 4326	296. 45	19. 664	144. 870
5	2. 3023	18. 923	165. 524	72. 928	1. 3802	314. 65	18. 932	163. 802
6	3. 8980	17. 985	190. 218	73. 018	1. 3135	314. 55	18. 001	186. 776
7	3. 4113	16. 912	214. 723	73. 089	1. 2363	314. 27	16. 925	211. 275
8	4. 0396	15. 059	251. 910	73. 215	1. 1028	314. 19	15. 071	247. 239
9	3. 9223	14. 001	268. 047	73. 267	1. 0261	314. 16	14. 010	263. 866
10	3. 9178	12. 950	280. 749	73. 308	. 9495	314. 00	12. 956	277. 448
11	3. 9875	11. 978	289. 559	73. 339	. 8786	313. 42	11. 981	287. 411
12	5. 3477	5. 886	310. 707	73. 425	. 4325	314. 15	5. 889	305. 158
13	5. 0159	4. 610	308. 612	73. 414	3387	313. 15	4. 612	303. 177
14	4. 9503	9. 179	304. 928	73. 401	. 6740	313. 59	9. 181	303. 179
15	5. 4586	3. 269	329. 810	73. 491	. 2406	313. 25	3. 277	296. 609
16	5. 2186	11. 045	299. 922	73. 387	. 8109	313. 25	11. 053	294. 671
17	6. 0158	7. 884	313. 979	73. 444	. 5796	313. 17	7. 894	305. 106
18	4. 0370	20. 298	129. 892	72. 845	1. 4790	296. 45	20. 314	127. 574
19	3. 2471	1. 583	319. 878	73. 431	. 1163	313. 78	1. 587	274. 258

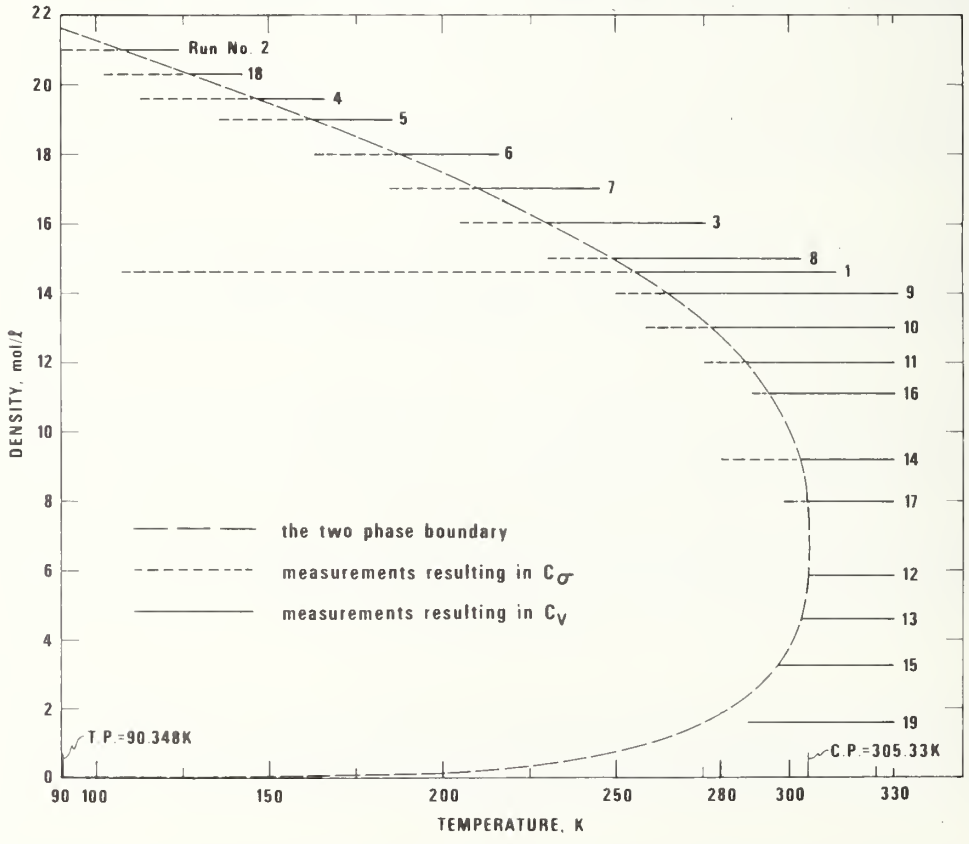

FIGURE 2. *The locus of experimental runs in the density-temperature plane.*

——— ——— ——— the two phase boundary
..... measurements resulting in C_σ
——————— measurements resulting in C_v

sure, obtained by computation from laboratory observations, are in effect direct measurements. The volume of the calorimeter is computed, the density is obtained from the equation of state [2]. The total number of moles, N, includes the amount in capillary and valve with the upper stem temperature equal to the indicated valve temperature. Breakthrough density and temperature define the point on the saturation boundary applicable to the run in question. The values are calculated from the equation of state, the loading conditions and the vapor pressure by considering the variation of calorimeter volume with temperature and pressure.

6.1. Performance Tests: The Specific Heats C_σ and C_v of Methane

Prior to making measurements on ethane we made a limited set of measurements on methane. The purpose was to check on the operation of the instrument by comparison to the values previously measured by Younglove [10]. Several values of C_σ and 29 values of C_v were measured at three different filling densities and at widely differing temperatures. Results and comparisons are shown in table 3. Two conclusions can be drawn from the measurements on methane. One is rather surprising, namely that the values of the specific heats calculated from the raw data will differ, if slightly different PVT surfaces are used in the data reduction process. The other is expected, namely that the values of the specific heats depend directly on the values measured for the heat capacity of the empty calorimeter.

To calculate the present results, which are shown in column 5 of table 3, we used Goodwin's most recent formulation of the PVT surface of methane [14]. Since Younglove used a different, earlier formulation [15], a second calculation of our results using the earlier PVT surface is shown in column 6 of table 3. One of the most important differences between these two PVT surfaces is the assignment of critical density, 10.0 mol/l for reference [14], and 10.15 mol/l for reference [15]. The intercomparison of the two calculations is given in column 7. Clearly, both C_σ and C_v are sensitive to the PVT surface used in the data reduction process. Furthermore, the differences vary from point to point on the PVT surface. Recomputing all of Younglove's results with the two different PVT surfaces leads to maximum differences of .08 percent in both C_σ and C_v. Accordingly, the most consistent way to compare the present results with those of Younglove [10] is to use the same PVT surface. This comparison involves columns 6 and 10 of table 3, with differences given in column 11. The disagreement between the two experiments runs from −1 to +1 percent. Several explanations were considered, only one of which is displayed in table 3. There exists a consistent offset, 0.4 percent, between the C_0 measured in the course of this experiment and that measured by Younglove [10]. In column 8 we have calculated our present results on methane using Younglove's [10] values for C_0 and Goodwin's earlier formulation of the PVT surface [15]. Column 9 shows the departure of the values in column 8 from those in column 6. Finally, a comparison of columns 9 and 11 suggests if not quantitatively, then at least qualitatively, that indeed the difference in the values of the C_0's is the explanation for the difference between the present measurements and those of Younglove [10].

6.2. The Specific Heats, C_σ, of Saturated Liquid Ethane

The specific heat of saturated liquid ethane was measured for 106 temperatures. The lowest was 93.7 K, the triple point is 90.348 K, the highest temperature was 301.5 K, the critical point is 305.33 K. Values of C_σ along with the experimental conditions, experimental parameters, and the various correction terms are given in table 4. A plot of C_σ is shown in figure 3. The measurements for C_σ were made with ΔT between 3 and 5 kelvin, and with loadings such that at each temperature C_σ is defined by at least two different fillings (see column 11, table 4). Curvature corrections were necessary only at temperatures above 101 K. The results for C_σ are represented with an analytical equation as follows:

$$C_\sigma = C_1 + C_2 T + C_3 T/(T_c - T)^{0.6} + C_4/T + C_5/T^2 \quad (4)$$

where T_c is the critical temperature, 305.33 K and values of the coefficients are given in the heading of table 4. Values calculated from eq. (4) and differences between experimental and calculated values expressed in percent are also given in table 4. The standard deviation of the entire fit is 0.3 J/mol-K. For temperatures below 260 K the imprecision in the experiment is ±0.1 percent, not much larger than that experienced for measurements of the empty calorimeter. Considering all sources the estimated uncertainty in the measured value of C_σ is about 0.5 percent generally, increasing to about 5 percent within a few kelvin of the critical point.

Comparison with the earlier measurements of Wiebe et al. [16], and Witt and Kemp [17] is made using eq (4) for interpolation. Differences in C_σ are shown in table 5. They are negligible at low temperatures but increase gradually to 5 percent at the highest temperatures of comparison. The explanation of the differences lies in the different PVT surfaces used to evaluate the experimental data and correction terms, in particular the rather large difference in assignment of the critical density, 6.80 mol/l this experiment and 6.99 mol/l for the other authors.

6.3. The Specific Heats, C_v, of Dense Gaseous and Liquid Ethane

The specific heats at constant volume were measured at 19 densities ranging from 0.2 to 3.1 times the critical density, at temperatures between 91 and 330 K, and with pressures to 33 MPa. As shown in figure 2, a given density is limited either by the maximum allowable system pressure, about

TABLE 3. *Results and intercomparison of the specific heats of methane*

Run No. —point No.	Saturation conditions based on reference [14]			The specific heat, C_σ, of saturated liquid methane						
				Results this paper calculated with C_0 and PVT sources below					Interpolated from ref. [10]	
				C_0: This paper PVT: Ref. [14]	This paper ref. [15]		Ref. [10] Ref. [15]			
	Vapor pressure MPa	Liquid density mol/l	Temperature K	J/mol-K	J/mol-K	Dev. col 5 to 6 0/0	J/mol-K	Dev. col 6 to 8 0/0	J/mol-K	Dev. col 6 to 10 0/0
118	0.1436	25.939	116.044	56.58	56.74	−0.27	56.97	−0.42	56.52	0.39
119	.1721	25.710	118.479	56.76	56.91	−.27	57.16	−.43	56.75	.29
120	.2219	25.365	122.089	57.29	57.44	−.27	57.70	−.44	57.19	.45

Run No. —point No.	*PVT* conditions based on reference [14]			The specific heat, C_v, of singlephase fluid methane						
				Results this paper calculated with C_0 and PVT sources below					Interpolated from ref. [10]	
				C_0: This paper PVT: Ref. [14]	This paper ref. [15]		Ref. [10] Ref. [15]			
	Pressure MPa	Density mol/l	Temperature K	J/mol-K	J/mol-K	Dev. col 5 to 6 0/0	J/mol-K	Dev. col 6 to 8 0/0	J/mol-K	Dev. col 6 to 10 0/0
101	6.4874	11.802	200.945	34.01	34.21	−0.60	34.62	−1.20	34.42	−0.61
102	6.7965	11.801	202.608	33.47	33.67	−.60	34.08	−1.21	33.88	−.63
103	7.2646	11.798	205.115	32.77	32.96	−.60	33.37	−1.23	33.04	−.23
104	7.8939	11.795	208.469	32.16	32.36	−.60	32.75	−1.22	32.45	−.29
105	8.6908	11.791	212.697	31.56	31.75	−.60	32.13	−1.20	31.69	.18
106	9.6540	11.786	217.783	31.12	31.31	−.60	31.67	−1.16	31.00	.98
107	4.6707	11.811	190.959	51.72	52.03	−.59	52.45	−.81		
108	4.9409	11.809	192.489	40.10	40.34	−.60	40.76	−1.05		
109	5.2290	11.808	194.092	37.79	38.02	−.60	38.44	−1.11		
110	5.5236	11.807	195.713	36.47	36.69	−.60	37.11	−1.15	37.09	−1.09
111	5.8105	11.805	197.280	35.39	35.60	−.60	36.02	−1.18	35.79	−.54
112	6.1116	11.804	198.915	34.65	34.85	−.60	35.27	−1.19	35.24	−1.11
113	6.4166	11.802	200.564	34.09	34.30	−.60	34.71	−1.20	34.59	−.86
114	6.7237	11.801	202.217	33.41	33.61	−.60	34.03	−1.22	33.92	−.92
115	7.1915	11.798	204.724	32.87	33.06	−.60	33.47	−1.22	33.10	−.11
116	7.8235	11.795	208.095	32.24	32.43	−.60	32.83	−1.22	32.49	−.18
117	8.6216	11.791	212.330	31.63	31.82	−.60	32.20	−1.20	31.75	.21
201	6.5423	20.504	170.403	30.30	30.21	.27	30.44	−.74	30.63	−1.38
202	7.6896	20.499	172.193	30.33	30.26	.22	30.49	−.75	30.57	−1.03
203	9.4196	20.489	174.898	30.22	30.17	.16	30.40	−.77	30.51	−1.12
204	11.7168	20.479	178.506	30.16	30.11	.17	20.35	−.79	30.42	−1.01
205	13.9877	20.470	182.089	30.09	30.04	.17	20.28	−.80	30.33	−.98
301	6.8455	23.445	146.608	31.16	31.15	.04	31.20	−.48	31.50	−1.13
302	8.5366	23.438	148.358	31.13	31.12	.04	31.28	−.49	31.46	−1.07
303	10.1996	23.431	150.090	31.14	31.13	.04	31.29	−.50	31.42	−.92
304	12.6822	23.417	152.695	31.10	31.08	.05	31.25	−.52	31.35	−.85
305	15.9591	23.403	156.170	31.05	31.03	.07	31.20	−.54	31.27	−.76
306	19.5801	23.385	160.058	31.01	31.01	.03	31.18	−.57	31.18	−.56
307	23.5208	23.368	164.346	30.93	30.92	.05	31.11	−.60	31.11	−.60

TABLE 4. *The specific heat, C_σ, of saturated liquid ethane*

Coefficients, eq[4]: C1=0.22648226 83E+02, C2=0.8796160711E−01, C3=0.1090610627E+01, C4=0.5871201054E+04, C5=−0.2123389940E+06

Run No. —point No.	Saturation conditions			C_σ J/mol-K	C_σ Calc. J/mol-K	Dev. θ/θ	Heat, Q J	ΔT K	C_0 J/K	Sample mol	Calorimeter Volume cm³	Expansion + capillary correction J/mol-K	Vaporization + vapor correction J/mol-K	Curvature correction J/mol-K
	Vapor pressure MPa	Liquid density mol/l	Temperature K											
202	0.0000	21.558	93.712	68.27	68.14	0.18	504.66	3.358	45.910	1.5289	72.726	0.000	−0.000	
203	.0000	21.436	97.045	68.30	68.29	.02	504.23	3.318	47.520	1.5289	72.733	.000	−.000	
1801	.0000	21.398	98.095	68.44	68.32	.17	508.65	3.408	48.020	1.4790	72.735	.000	−.000	
204	.0000	21.317	100.322	68.45	68.40	.08	499.81	3.252	49.040	1.5289	72.740	.000	−.000	
1802	.0000	21.274	101.482	68.44	68.44	.01	507.43	3.365	49.570	1.4790	72.742	.000	−.000	
205	.0000	21.198	103.565	68.46	68.50	−.06	503.65	3.246	50.490	1.5289	72.747	.000	.000	
1803	.0000	21.152	104.828	68.53	68.54	−.01	508.13	3.334	51.040	1.4790	72.750	.000	−.000	
206	.0000	21.080	106.788	68.35	68.59	−.34	502.83	3.215	51.870	1.5289	72.754	.000	.000	
1804	.0001	21.031	108.142	68.60	68.62	−.04	507.45	3.298	52.430	1.4790	72.757	.000	−.000	
127	.0001	21.026	108.287	68.60	68.63	−.04	622.67	4.938	52.490	1.0730	72.757	.000	−.000	
1805	.0001	20.943	110.531	68.66	68.68	−.04	698.13	4.506	53.400	1.4790	72.762	.000	−.000	
401	.0001	20.931	110.862	68.72	68.59	.04	751.16	4.943	53.530	1.4326	72.763	.000	−.000	
128	.0001	20.846	113.180	68.73	68.75	−.03	624.36	4.870	54.440	1.0730	72.769	.000	−.010	
1806	.0002	20.779	115.018	68.71	68.79	−.12	701.10	4.473	55.130	1.4790	72.773	.000	−.000	
402	.0002	20.751	115.760	68.82	68.81	.02	750.67	4.874	55.410	1.4326	72.775	.000	−.000	
129	.0003	20.669	118.003	68.84	68.87	−.04	624.10	4.797	56.230	1.0730	72.780	.000	−.010	
1807	.0003	20.615	119.454	68.81	68.91	−.13	698.71	4.408	56.740	1.4790	72.784	.000	−.000	
403	.0004	20.573	120.599	68.93	68.94	−.01	753.25	4.832	57.140	1.4326	72.786	.000	−.000	
130	.0005	20.493	122.751	68.97	69.00	−.04	623.42	4.727	57.870	1.0730	72.792	.000	−.020	
1808	.0006	20.455	123.782	68.95	69.03	−.11	681.47	4.254	58.210	1.4790	72.794	.000	.000	
404	.0006	20.438	124.252	68.99	69.04	−.07	755.80	4.808	58.370	1.4326	72.795	.000	−.000	
131	.0009	20.320	127.423	69.06	69.14	−.11	620.83	4.650	59.380	1.0730	72.803	.000	−.030	
405	.0011	20.261	129.007	69.22	69.19	.04	754.44	4.744	59.870	1.4326	72.807	.000	−.000	
132	.0016	20.148	132.037	69.29	69.30	−.01	624.02	4.617	60.770	1.0730	72.815	.000	−.040	
406	.0020	20.085	133.712	69.39	69.36	.05	754.17	4.694	61.250	1.4326	72.819	.000	−.000	
133	.0026	19.985	136.389	69.50	69.46	.05	686.43	5.024	62.000	1.0730	72.826	.000	−.060	
407	.0032	19.911	138.362	69.62	69.55	.11	753.09	4.641	62.530	1.4326	72.832	.000	.000	
134	.0044	19.797	141.365	69.64	69.68	−.06	686.18	4.967	63.320	1.0730	72.840	.000	−.080	
412	.0049	19.757	142.426	69.79	69.73	.07	747.04	4.567	63.590	1.4326	72.842	.000	.010	
421	.0049	19.750	142.604	69.78	69.74	.05	690.48	4.221	63.630	1.4325	72.843	.000	.010	
135	.0070	19.611	146.274	69.98	69.93	.07	685.20	4.903	64.540	1.0730	72.853	.001	−.110	
501	.0090	19.499	149.205	70.13	70.09	.06	749.49	4.626	65.230	1.3802	72.861	.000	−.000	
136	.0106	19.425	151.131	70.22	70.21	.02	685.67	4.857	65.670	1.0730	72.866	.001	−.140	
502	.0133	19.323	153.786	70.37	70.37	.01	749.13	4.585	66.250	1.3802	72.873	.001	.010	
137	.0157	19.240	155.932	70.57	70.51	.08	684.57	4.800	66.710	1.0730	72.879	.001	−.180	
503	.0189	19.147	158.321	70.76	70.68	.11	748.66	4.541	67.210	1.3802	72.886	.001	.020	
138	.0226	19.055	160.684	70.84	70.85	−.01	684.78	4.757	67.690	1.0730	72.893	.001	−.220	
601	.0228	19.049	160.830	70.87	70.86	.01	751.08	4.670	67.720	1.3135	72.893	.001	−.020	
504	.0244	19.012	161.771	71.03	70.93	.15	398.68	2.403	67.910	1.3802	72.896	.001	.030	
518	.0254	18.992	162.290	70.95	70.97	−.03	463.12	2.792	68.010	1.3802	72.897	.001	.030	
505	.0259	18.981	162.575	70.96	70.99	−.05	307.56	1.853	68.070	1.3802	72.898	.001	.030	
139	.0315	18.870	165.384	71.22	71.21	.01	684.22	4.709	68.610	1.0730	72.906	.002	−.260	
602	.0317	18.867	165.464	71.23	71.22	.02	755.36	4.657	68.620	1.3135	72.907	.001	−.010	

TABLE 4. *The specific, C_σ, of saturated liquid ethane*—Continued

Run No. —point No.	Saturation conditions			C_σ J/mol-K	C_σ Calc. J/mol-K	Dev. 0/0	Heat, Q J	ΔT K	C_0 J/K	Sample mol	Calorimeter Volume cm³	Expansion + capillary correction J/mol-K	Vaporization + vapor correction J/mol-K	Curvature correction J/mol-K
	Vapor pressure MPa	Liquid density mol/l	Temperature K											
140	0. 0430	18. 685	170. 038	71. 72	71. 61	0. 15	683. 91	4. 660	69. 470	1. 0730	72. 920	0. 002	−0. 300	
603	. 0431	18. 684	170. 061	71. 69	71. 61	. 10	752. 92	4. 602	69. 470	1. 3135	72. 920	. 002	. 010	
141	. 0501	18. 589	172. 446	71. 91	71. 83	. 11	758. 69	5. 147	69. 890	1. 0730	72. 927	. 003	−. 320	
604	. 0573	18. 501	174. 613	72. 08	72. 04	. 06	752. 45	4. 563	70. 260	1. 3135	72. 933	. 002	. 030	
142	. 0683	18. 382	177. 535	72. 34	72. 33	. 02	758. 05	5. 096	70. 750	1. 0730	72. 942	. 004	−. 360	
605	. 0749	18. 317	179. 126	72. 52	72. 49	. 03	751. 80	4. 524	71. 010	1. 3135	72. 947	. 003	. 060	
143	. 0909	18. 176	182. 564	72. 90	72. 87	. 04	756. 20	5. 034	71. 560	1. 0730	72. 957	. 005	−. 400	
606	. 0963	18. 133	183. 603	73. 00	72. 98	. 03	753. 08	4. 497	71. 720	1. 3135	72. 960	. 004	. 110	
701	. 1119	18. 016	186. 415	73. 42	73. 31	. 15	755. 67	4. 638	72. 150	1. 2363	72. 969	. 005	−. 020	
144	. 1187	17. 968	187. 540	73. 46	73. 45	. 02	756. 57	4. 990	72. 320	1. 0730	72. 972	. 006	−. 430	
101	. 1200	17. 960	187. 745	73. 37	73. 47	−. 13	739. 12	4. 877	72. 350	1. 0730	72. 973	. 006	−. 430	
702	. 1416	17. 822	190. 995	73. 94	73. 88	. 08	754. 21	4. 593	72. 820	1. 2363	72. 982	. 006	. 030	
102	. 1530	17. 756	192. 556	74. 06	74. 08	−. 02	738. 00	4. 824	73. 040	1. 0730	72. 987	. 007	−. 440	
703	. 1767	17. 628	195. 533	74. 49	74. 49	. 00	753. 06	4. 552	73. 450	1. 2363	72. 997	. 007	. 090	
103	. 1923	17. 550	197. 332	74. 75	74. 74	. 01	740. 70	4. 798	73. 690	1. 0730	73. 002	. 009	−. 450	
704	. 2177	17. 432	200. 029	75. 14	75. 13	. 01	753. 12	4. 517	74. 050	1. 2363	73. 011	. 008	. 170	
104	. 2383	17. 342	202. 057	75. 40	75. 44	−. 05	735. 51	4. 724	74. 310	1. 0730	73. 017	. 010	−. 430	
301	. 2391	17. 339	202. 127	75. 45	75. 45	. 00	746. 93	4. 571	74. 320	1. 1811	73. 017	. 009	. 020	
705	. 2651	17. 234	204. 490	75. 90	75. 83	. 09	752. 84	4. 478	74. 620	1. 2363	73. 025	. 010	. 270	
302	. 2694	17. 217	204. 866	75. 76	75. 89	−. 17	748. 89	4. 565	74. 660	1. 1811	73. 026	. 010	. 070	
105	. 2915	17. 133	206. 723	76. 15	76. 19	−. 05	735. 14	4. 681	74. 890	1. 0730	73. 032	. 012	−. 390	
706	. 3186	17. 036	208. 850	76. 43	76. 55	−. 16	728. 54	4. 307	75. 150	1. 2363	73. 039	. 011	. 400	
303	. 3255	17. 012	209. 372	76. 56	76. 64	−. 11	748. 35	4. 523	75. 210	1. 1811	73. 040	. 012	. 180	
106	. 3529	16. 921	211. 363	76. 97	77. 00	−. 04	740. 46	4. 675	75. 450	1. 0730	73. 047	. 014	−. 330	
304	. 3893	16. 806	213. 835	77. 41	77. 45	−. 06	747. 19	4. 480	75. 730	1. 1811	73. 055	. 014	. 320	
107	. 4230	16. 705	215. 978	77. 87	77. 86	. 01	739. 54	4. 628	75. 980	1. 0730	73. 062	. 017	−. 230	
305	. 4613	16. 596	218. 259	78. 37	78. 32	. 07	746. 39	4. 437	76. 230	1. 1811	73. 069	. 016	. 490	

108	. 5020	16. 487	220. 536	78. 87	78. 79	. 09	735. 37	4. 561	76. 480	1. 0730	73. 077	. 019	−. 100	
306	. 5421	16. 384	222. 647	79. 13	79. 25	−. 14	745. 84	4. 404	76. 700	1. 1811	73. 084	. 019	. 700	
109	. 5907	16. 264	225. 058	79. 79	79. 79	−. 00	738. 77	4. 546	76. 960	1. 0730	73. 092	. 022	. 070	
110	. 6896	16. 038	229. 541	80. 79	80. 86	−. 09	734. 29	4. 483	77. 410	1. 0730	73. 107	. 025	. 300	
801	. 7366	15. 937	231. 507	81. 41	81. 36	. 05	769. 10	4. 614	77. 610	1. 1028	73. 114	. 026	. 670	
111	. 7992	15. 807	233. 988	81. 97	82. 03	−. 07	739. 19	4. 474	77. 850	1. 0730	73. 122	. 029	. 580	
802	. 8553	15. 695	236. 091	82. 60	82. 61	−. 01	773. 02	4. 600	78. 050	1. 1028	73. 129	. 029	1. 010	
112	. 9344	15. 543	238. 894	83. 41	83. 44	−. 03	810. 00	4. 856	78. 310	1. 0730	73. 139	. 033	. 970	
803	. 9863	15. 447	240. 641	84. 06	83. 97	. 10	772. 07	4. 551	78. 480	1. 1028	73. 145	. 033	1. 430	
113	1. 0825	15. 275	243. 704	84. 90	84. 97	−. 09	809. 41	4. 809	78. 750	1. 0730	73. 156	. 038	1. 460	
804	1. 1189	15. 212	244. 814	85. 26	85. 35	−. 11	655. 14	3. 836	78. 850	1. 1028	73. 160	. 037	1. 910	
901	1. 2188	15. 043	247. 726	86. 41	86. 40	. 02	786. 22	4. 725	79. 110	1. 0260	73. 171	. 043	1. 380	
114	1. 2453	14. 999	248. 469	86. 56	86. 67	−. 13	808. 37	4. 758	79. 180	1. 0730	73. 173	. 043	2. 070	
902	1. 3930	14. 761	252. 414	88. 29	88. 24	. 05	786. 10	4. 678	79. 520	1. 0260	73. 188	. 048	2. 060	
903	1. 5827	14. 468	257. 059	90. 39	90. 33	. 07	784. 89	4. 625	79. 900	1. 0260	73. 205	. 054	2. 910	
1001	1. 7130	14. 274	260. 020	91. 87	91. 81	. 06	785. 82	4. 755	80. 150	. 9495	73. 216	. 063	2. 270	
905	1. 7461	14. 225	260. 744	92. 04	92. 19	−. 17	787. 80	4. 611	80. 200	1. 0260	73. 218	. 060	3. 740	
904	1. 7756	14. 182	261. 383	92. 32	92. 54	−. 24	687. 69	4. 021	80. 250	1. 0260	73. 221	. 061	3. 910	
1002	1. 9373	13. 948	264. 754	94. 60	94. 50	. 11	785. 32	4. 699	80. 520	. 9495	73. 234	. 071	3. 450	
1003	2. 1805	13. 603	269. 456	97. 75	97. 66	. 09	790. 15	4. 675	80. 890	. 9495	73. 252	. 080	5. 000	
1004	2. 4435	13. 236	274. 128	101. 37	101. 47	−. 10	789. 86	4. 622	81. 240	. 9494	73. 270	. 089	7. 050	
1101	2. 4671	13. 203	274. 528	101. 81	101. 84	−. 03	784. 34	4. 725	81. 270	. 8786	73. 272	. 097	5. 490	0. 002
1102	2. 7585	12. 795	279. 261	106. 68	106. 78	−. 09	783. 94	4. 661	81. 620	. 8786	73. 290	. 108	8. 260	. 005
1401	3. 0487	12. 381	283. 620	112. 75	112. 69	. 05	753. 66	4. 841	81. 940	. 6739	73. 308	. 156	3. 470	. 013
1103	3. 0713	12. 348	283. 946	112. 85	113. 21	−. 32	784. 57	4. 602	81. 960	. 8785	73. 309	. 121	12. 230	. 012
1402	3. 3806	11. 888	288. 238	121. 72	121. 33	. 32	659. 46	4. 154	82. 260	. 6739	73. 327	. 174	8. 440	. 022
1601	3. 6532	11. 456	291. 779	130. 47	130. 84	−. 29	749. 65	4. 389	82. 510	. 8108	73. 342	. 158	21. 760	. 048
1403	3. 7091	11. 364	292. 479	133. 41	133. 19	. 16	662. 09	4. 093	82. 560	. 6739	73. 345	. 193	16. 110	. 048
1414	3. 7139	11. 355	292. 539	133. 54	133. 40	. 11	651. 15	4. 025	82. 560	. 6739	73. 345	. 193	16. 250	. 047
1701	3. 9357	10. 967	295. 236	146. 32	144. 80	1. 04	496. 69	3. 142	82. 750	. 5795	73. 357	. 240	16. 650	. 062
1415	4. 0476	10. 756	296. 550	151. 71	152. 27	−. 37	651. 54	3. 944	82. 840	. 6738	73. 363	. 213	29. 830	. 143
1404	4. 0571	10. 737	296. 661	152. 77	152. 98	−. 14	661. 25	3. 994	82. 840	. 6738	73. 363	. 213	30. 370	. 146
1702	4. 2086	10. 426	298. 389	167. 24	166. 28	. 57	499. 15	3. 091	82. 960	. 5795	73. 371	. 259	32. 170	. 153
1416	4. 3812	10. 025	300. 295	187. 54	188. 77	−. 66	589. 30	3. 467	83. 090	. 6738	73. 379	. 232	59. 180	. 331
1405	4. 4048	9. 965	300. 550	191. 34	192. 82	−. 77	590. 93	3. 471	83. 110	. 6738	73. 380	. 234	62. 640	. 366
1703	4. 4911	9. 729	301. 473	212. 29	210. 92	. 64	499. 06	2. 990	83. 170	. 5794	73. 384	. 278	68. 370	. 358

35 MPa, which in turn leads to a maximum pressure of 33 MPa at the mean temperature of the experiment, or by the upper limit in temperature, 330 K. Values of C_v along with the experimental conditions, the major experimental parameters, and the correction term are given in table 6. The temperature and density dependence of C_v is illustrated in figure 4. For a wide range of densities to either side of the critical density the specific heat increases sharply as the coexistence envelope is approached. At liquid densities far removed from critical the temperature dependence is relatively weak.

TABLE 5. *Comparison of the calculated C_σ with results of others*

Temperature K	C_σ-calculated this paper J/mol-K	C_0 from the literature J/mol-K	Difference in 0/0
	Reference [16]		
96. 77	68. 27	68. 46	−0. 3
96. 82	68. 28	68. 76	−. 7
98. 06	68. 32	68. 55	−. 3
101. 54	68. 44	68. 71	−. 4
107. 08	68. 60	68. 63	−. 0
108. 65	68. 64	68. 55	. 1
115. 74	68. 81	68. 67	. 2
116. 19	68. 82	68. 45	. 5
122. 70	69. 00	69. 13	−. 2
123. 60	69. 02	69. 17	−. 2
128. 08	69. 16	69. 55	−. 6
128. 49	69. 17	69. 51	−. 5
132. 65	69. 32	69. 84	−. 8
138. 00	69. 53	69. 89	−. 5
138. 18	69. 54	70. 01	−. 7
138. 31	69. 55	69. 84	−. 4
142. 43	69. 73	70. 10	−. 5
143. 36	69. 78	70. 05	−. 4
151. 75	70. 24	69. 97	. 4
152. 60	70. 30	70. 14	. 2
154. 99	70. 45	70. 26	. 3
156. 98	70. 58	70. 26	. 5
157. 42	70. 61	70. 10	. 7
160. 10	70. 80	71. 10	−. 4
162. 65	70. 99	71. 18	−. 3
164. 49	71. 14	71. 73	−. 8
165. 93	71. 26	71. 31	−. 1
168. 09	71. 44	71. 60	−. 2
170. 18	71. 62	71. 77	−. 2
172. 05	71. 79	71. 77	. 0
172. 69	71. 85	72. 15	−. 4
178. 17	72. 39	72. 82	−. 6
181. 50	72. 75	73. 07	−. 4
182. 03	72. 81	73. 32	−. 7
190. 00	73. 75	73. 53	. 3
199. 86	75. 11	74. 37	1. 0
208. 88	76. 56	75. 66	1. 2
212. 80	77. 26	75. 96	1. 7
220. 48	78. 78	77. 80	1. 2
228. 76	80. 67	80. 61	. 1
236. 21	82. 65	82. 32	. 4
244. 61	85. 28	83. 96	1. 6
252. 53	88. 29	87. 14	1. 3
258. 22	90. 89	88. 44	2. 7
265. 25	94. 80	92. 33	2. 6
273. 06	100. 53	98. 11	2. 4
278. 07	105. 41	101. 33	3. 9
284. 07	113. 41	109. 12	3. 8
291. 27	129. 25	122. 69	5. 1
294. 85	142. 89	135. 79	5. 0

TABLE 5. *Comparison of the calculated C_σ with results of others*—Continued

Temperature K	C_σ-calculated this paper J/mol-K	C_0 from the literature J/mol-K	Difference in 0/0
	Reference [17]		
91. 59	68. 03	68. 30	−0. 4
92. 97	68. 10	68. 46	−. 5
94. 94	68. 20	68. 38	−. 3
96. 60	68. 27	68. 25	. 0
98. 23	68. 33	68. 88	−. 8
98. 89	68. 35	68. 38	−. 0
100. 49	68. 41	68. 34	. 1
104. 05	68. 51	68. 59	−. 1
106. 67	68. 59	68. 88	−. 4
109. 24	68. 65	68. 92	−. 4
111. 67	68. 71	69. 13	−. 6
114. 20	68. 77	69. 01	−. 3
116. 24	68. 82	69. 17	−. 5
119. 33	69. 90	69. 30	−. 6
122. 72	69. 00	69. 43	−. 6
125. 96	69. 09	69. 59	−. 7
129. 47	69. 20	69. 55	−. 5
134. 49	69. 39	69. 64	−. 4
138. 72	69. 56	69. 76	−. 3
142. 83	69. 75	69. 89	−. 2
145. 97	69. 91	70. 05	−. 2
149. 80	70. 13	70. 31	−. 3
153. 58	70. 36	70. 77	−. 6
157. 95	70. 65	70. 77	−. 2
162. 82	71. 01	71. 02	−. 0
167. 43	71. 38	71. 52	−. 2
172. 02	71. 79	71. 56	. 3
176. 54	72. 23	72. 06	. 2
180. 88	72. 68	72. 11	. 8

Representation of the specific heats has been achieved by Goodwin [2] who correlates the available PVT data, the specific heats of the ideal gas, the specific heat of the saturated liquid from this experiment, and selected values of C_v from runs 1, 8, and 9. Values of C_v calculated from his equation of state and differences between experimental and calculated values expressed in percent are given in table 6. A scan of column 7 in table 6 reveals that the agreement between experimental and calculated values is excellent over much of the PVT surface, i.e., a nominal 2 percent or less. It is only in the region near the critical point where the experimental heat capacities increase drastically that the representation is not able to match the experimental surface of C_v, departures reach values of up to 18 percent. The agreement for the very lowest density, run 19, is particularly gratifying since for this run the experimental uncertainty in C_v is about 2 percent, whereas the calculation of C_v from ideal gas and a very small PVT contribution should have very little error attached to it.

Experimental measurements of specific heats have been made by other authors [18,19], however these measurements are measurements of the specific heat at constant pressure, C_p. The values can be compared only indirectly to the present measure-

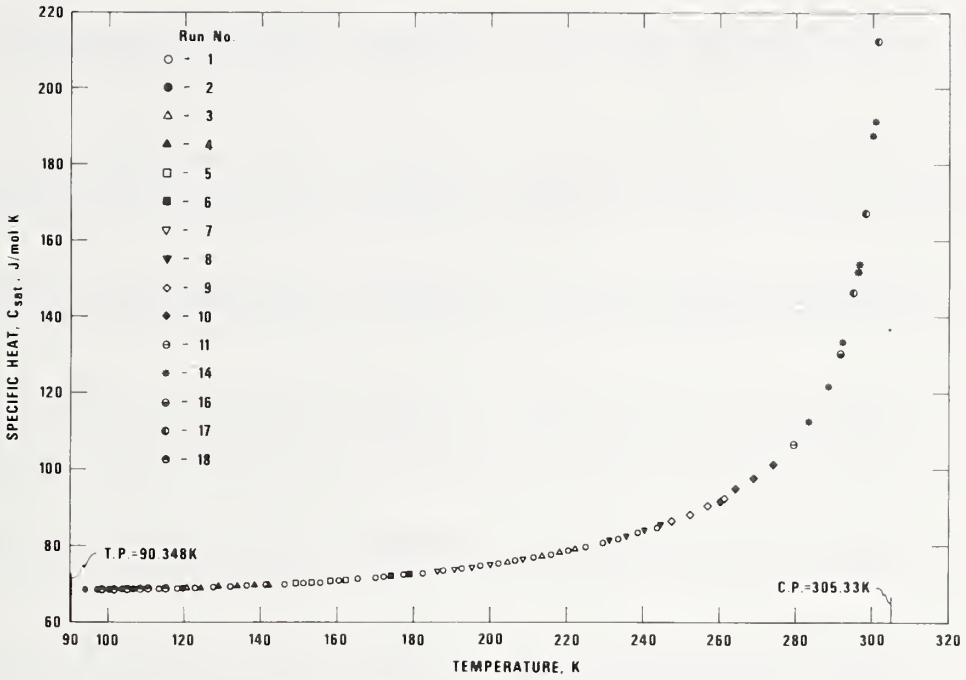

FIGURE 3. *The specific heats,* C_σ, *of saturated liquid ethane.*

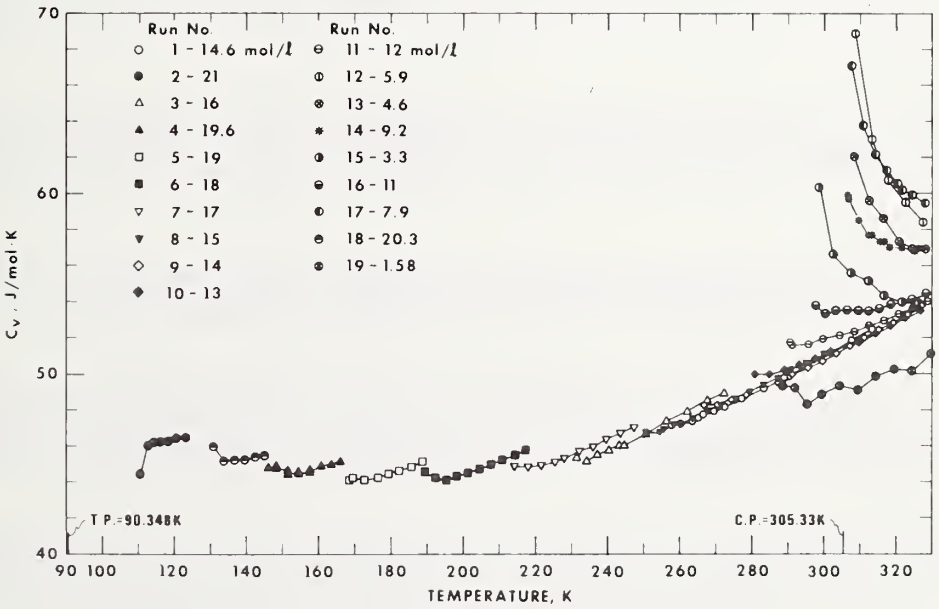

FIGURE 4. *The specific heats,* C_v, *of dense gaseous and liquid ethane.*

ments through the use of a PVT surface. Since C_p measurements are normally made along isobars while C_v measurements are made along isochores, the most appropriate PVT states for comparisons are at those values of pressure and density common to both sets of data. For the results of Furtado [18] and the present measurements this intercomparison is given in table 7. The pressures are taken

220-208 O - 77 - 4

TABLE 6. *The specific heat, Cv, of singlephase fluid ethane*

Run No. point No.	PVT conditions			C_v J/mol–K	C_v calc. from Goodwin [2] J/mol–K	Dev. 0/0	Heat, Q J	ΔT K	C_0 J/K	Sample mol	Calorimeter volume cm^3	Volume change correction J/mol–K
	Pressure MPa	Density mol l	Temperature K									
116	4. 1720	14. 644	258. 973	47. 20	47. 10	0. 20	806. 66	6. 065	80. 060	1. 0725	73. 240	2. 173
117	7. 5074	14. 628	265. 038	47. 57	47. 58	−. 03	805. 26	6. 054	80. 550	1. 0722	73. 297	1. 372
118	10. 8447	14. 616	271. 085	48. 17	48. 10	. 14	806. 72	6. 015	81. 010	1. 0721	73. 354	1. 371
119	14. 1443	14. 604	277. 105	48. 61	48. 64	−. 07	805. 29	5. 962	81. 450	1. 0721	73. 412	1. 386
120	17. 4012	14. 592	283. 089	49. 12	49. 21	−. 18	805. 78	5. 922	81. 900	1. 0721	73. 470	1. 407
121	20. 6171	14. 580	289. 038	49. 76	49. 79	−. 06	804. 40	5. 863	82. 320	1. 0721	73. 528	1. 429
122	21. 1487	14. 578	290. 026	49. 84	49. 89	−. 09	806. 75	5. 873	82. 390	1. 0721	73. 538	1. 433
123	24. 3353	14. 567	295. 968	50. 48	50. 48	−. 01	806. 34	5. 823	82. 800	1. 0720	73. 596	1. 456
124	27. 4843	14. 555	301. 879	51. 13	51. 09	. 06	805. 76	5. 772	83. 190	1. 0720	73. 654	1. 480
125	30. 6035	14. 543	307. 773	51. 82	51. 71	. 22	806. 49	5. 730	83. 580	1. 0720	73. 712	1. 503
126	33. 6956	14. 532	313. 655	52. 46	52. 32	. 25	805. 85	5. 682	83. 960	1. 0720	73. 770	1. 527
146	3. 3933	14. 647	257. 577	47. 20	47. 00	. 42	404. 93	3. 029	79. 950	1. 0726	73. 226	2. 898
147	5. 0544	14. 637	260. 618	47. 30	47. 23	. 16	404. 05	3. 050	80. 190	1. 0722	73. 255	1. 438
148	6. 7546	14. 631	263. 680	47. 38	47. 47	−. 19	405. 73	3. 057	80. 440	1. 0722	73. 284	1. 384
149	8. 4463	14. 624	266. 736	47. 74	47. 73	. 02	404. 93	3. 037	80. 680	1. 0722	73. 313	1. 375
150	10. 1277	14. 618	269. 783	47. 92	47. 99	−. 13	404. 36	3. 023	80. 910	1. 0721	73. 342	1. 376
151	11. 7992	14. 612	272. 823	48. 20	48. 25	−. 10	404. 37	3. 011	81. 140	1. 0721	73. 371	1. 382
152	13. 4607	14. 606	275. 855	48. 48	48. 53	−. 10	403. 76	2. 994	81. 370	1. 0721	73. 400	1. 390
208	3. 6415	20. 996	110. 494	44. 79	45. 02	−. 52	249. 72	1. 938	53. 390	1. 5284	72. 793	4. 605
209	7. 4628	20. 981	112. 401	46. 07	45. 06	2. 18	245. 90	1. 896	54. 140	1. 5280	72. 829	3. 385
210	11. 4471	20. 969	114. 288	46. 20	45. 10	2. 39	247. 71	1. 897	54. 860	1. 5279	72. 868	3. 332
211	15. 3828	20. 957	116. 167	46. 21	45. 13	2. 33	246. 42	1. 878	55. 560	1. 5279	72. 906	3. 325
212	19. 8576	20. 944	118. 324	46. 28	45. 17	2. 41	315. 54	2. 464	56. 340	1. 5279	72. 950	3. 323
213	24. 8511	20. 930	120. 762	46. 41	45. 20	2. 62	324. 08	2. 433	57. 200	1. 5279	73. 000	3. 338
214	29. 7379	20. 915	123. 178	46. 43	45. 22	2. 60	324. 68	2. 422	58. 010	1. 5278	73. 050	3. 356
308	3. 6029	16. 140	231. 182	45. 31	44. 84	1. 03	402. 58	2. 983	77. 580	1. 1806	73. 143	3. 292
309	5. 8108	16. 129	234. 160	45. 16	45. 07	. 21	404. 39	3. 032	77. 870	1. 1802	73. 176	1. 870
310	8. 0795	16. 121	237. 158	45. 53	45. 30	. 50	405. 00	3. 022	78. 150	1. 1802	73. 211	1. 823
311	10. 3326	16. 113	240. 148	45. 79	45. 53	. 56	404. 52	3. 005	78. 430	1. 1802	73. 245	1. 815
312	12. 5647	16. 105	243. 126	46. 06	45. 77	. 63	404. 88	2. 995	78. 700	1. 1801	73. 279	1. 818
313	13. 6122	16. 101	244. 528	46. 08	45. 88	. 44	806. 74	5. 961	78. 830	1. 1801	73. 295	1. 811
314	17. 9966	16. 086	250. 439	46. 68	46. 35	. 71	806. 99	5. 908	79. 350	1. 1801	73. 363	1. 830
315	22. 3017	16. 071	256. 303	47. 34	46. 84	1. 06	806. 20	5. 847	79. 840	1. 1801	73. 431	1. 854
316	26. 5329	16. 056	262. 126	47. 92	47. 91	. 01	806. 48	5. 799	80. 310	1. 1801	73. 499	1. 880
317	30. 7076	16. 041	267. 928	48. 53	48. 36	. 35	806. 20	5. 747	80. 770	1. 1800	73. 566	1. 907
318	33. 7881	16. 029	272. 246	48. 91	48. 72	. 39	402. 54	2. 853	81. 100	1. 1800	73. 617	1. 937
409	1. 6032	19. 657	145. 929	44. 78	43. 67	2. 49	161. 75	1. 212	64. 450	1. 4324	72. 866	3. 424
414	4. 7513	19. 643	148. 039	44. 89	43. 73	2. 57	421. 18	3. 121	64. 950	1. 4320	72. 901	4. 002
410	4. 7903	19. 643	148. 064	44. 98	43. 74	2. 76	415. 86	3. 078	64. 960	1. 4320	72. 902	4. 013
411	9. 4211	19. 624	151. 130	44. 41	43. 83	1. 20	415. 62	3. 113	65. 670	1. 4316	72. 953	2. 975
415	9. 4536	19. 624	151. 151	44. 39	43. 83	1. 25	420. 32	3. 149	65. 670	1. 4316	72. 954	2. 974
416	14. 2813	19. 609	154. 270	44. 48	43. 93	1. 24	421. 01	3. 135	66. 360	1. 4316	73. 008	2. 957
417	19. 0188	19. 594	157. 366	44. 66	44. 03	1. 41	420. 11	3. 107	67. 020	1. 4316	73. 062	2. 965
418	23. 6646	19. 579	160. 437	44. 84	44. 13	1. 58	419. 85	3. 085	67. 640	1. 4315	73. 115	2. 980
419	28. 2240	19. 565	163. 485	44. 93	44. 23	1. 57	420. 06	3. 069	68. 250	1. 4315	73. 169	2. 999
420	31. 7899	19. 553	165. 894	45. 10	44. 30	1. 76	248. 70	1. 807	68. 700	1. 4315	73. 211	3. 026
423	4. 7430	19. 643	148. 027	44. 78	43. 73	2. 33	424. 39	3. 155	64. 950	1. 4320	72. 901	3. 802

424	9.4819	19.624	151.152	44.52	43.83	1.54	421.19	3.147	65.670	1.4317	72.954	3.103
425	14.2777	19.609	154.267	44.55	43.93	1.39	420.94	3.132	66.350	1.4316	73.008	2.989
426	19.0103	19.594	157.364	44.65	44.03	1.40	420.28	3.108	67.020	1.4315	73.062	2.981
509	14.2771	18.877	174.677	44.83	43.83	2.23	434.68	3.198	70.280	1.3793	73.072	2.761
511	3.8855	18.916	166.750	44.64	43.48	2.59	443.61	3.280	68.860	1.3798	72.947	3.460
512	8.1541	18.898	170.023	44.52	43.62	2.02	444.61	3.289	69.460	1.3795	72.998	3.104
513	12.4645	18.883	173.301	44.48	43.77	1.60	444.40	3.287	70.040	1.3794	73.050	2.774
514	16.7633	18.868	176.572	44.50	43.91	1.32	444.52	3.274	70.590	1.3793	73.102	2.754
515	20.9940	18.855	179.822	44.71	44.06	1.47	443.92	3.250	71.130	1.3793	73.154	2.759
516	25.1643	18.841	183.059	44.81	44.20	1.35	444.90	3.214	71.640	1.3793	73.206	2.771
517	29.2726	18.827	186.280	45.01	44.35	1.47	444.92	3.223	72.130	1.3792	73.257	2.788
520	3.2642	18.919	166.260	44.15	43.46	1.57	445.77	3.323	68.770	1.3799	72.940	3.219
507	5.8435	18.908	168.242	44.19	43.55	1.45	435.73	3.226	69.140	1.3797	92.970	3.594
521	7.5377	18.901	169.533	44.21	43.60	1.37	442.92	3.280	69.370	1.3796	72.990	3.382
522	11.7968	18.885	172.795	44.17	43.74	.96	444.97	3.303	69.950	1.3794	73.042	2.783
523	16.0901	18.871	176.058	44.27	43.89	.86	444.69	3.285	70.510	1.3793	73.094	2.755
524	20.3225	18.857	179.304	44.43	44.03	.90	445.20	3.270	71.040	1.3793	73.145	2.757
525	24.4871	18.843	182.531	44.63	44.18	1.00	444.17	3.244	71.550	1.3793	73.197	2.769
526	28.5822	18.830	185.736	44.83	44.32	1.12	445.21	3.233	72.050	1.3792	73.249	2.785
527	32.6165	18.816	188.925	45.12	44.47	1.45	444.58	3.207	72.520	1.3792	73.300	2.802
608	2.6873	17.990	189.118	44.55	43.56	2.22	442.40	3.284	72.550	1,3133	73.002	2.800
609	6.1932	17,974	192.360	44.21	43.74	1.06	444.14	3.281	73.010	1.3130	73.047	3.285
610	9.6987	17.959	195.613	44.09	43.93	.37	444.20	3.299	73.460	1.3127	73.093	2.520
611	12.3412	17.950	198.035	44.27	44.07	.47	444.48	3.289	73.790	1.3127	73.127	2.463
612	15.8638	17.938	201.281	44.50	44.25	.55	446.15	3.285	74.210	1.3126	73.174	2.448
613	19.3395	17.927	204.510	44.71	44.44	.59	442.66	3.242	74.620	1.3126	73.220	2.452
614	22.7639	17.915	207.717	44.94	44.63	.69	444.78	3.241	75.010	1.3126	73.266	2.462
615	26.1418	17.903	210.907	45.21	44.81	.87	442.70	3.208	75.390	1.3125	73.312	2.476
616	29.4745	17.892	214.081	45.46	45.00	1.01	444.44	3.204	75.760	1.3125	73.358	2.481
617	32.7619	17.881	217.237	45.74	45.19	1.21	442.86	3.176	76.120	1.3125	73.403	2.508
708	2.9578	16.914	214.213	44.89	44.16	1.63	526.64	3.923	75.780	1.2361	73.083	2.402
709	6.3377	16.898	218.081	44.88	44.42	1.02	524.81	3.882	76.120	1.2358	73.130	2.834
710	9.6894	16.884	221.935	44.97	44.69	.62	524.91	3.893	76.630	1.2355	73.178	2.141
711	13.0632	16.872	225.787	45.16	44.96	.44	525.14	3.878	77.030	1.2355	73.226	2.092
712	15.3575	16.864	228.421	45.31	45.15	.36	526.13	3.873	77.300	1.2354	73.259	2.088
713	18.6724	16.852	232.253	45.70	45.42	.62	525.64	3.844	77.680	1.2354	73.308	2.095
714	21.9409	16.841	236.060	45.98	45.69	.63	525.92	3.826	78.050	1.2354	73.356	2.107
715	25.1669	16.830	239.848	46.36	45.96	.86	525.73	3.801	78.400	1.2354	73.404	2.122
716	28.3479	16.818	243.612	46.75	46.24	1.09	524.19	3.767	78.750	1.2353	73.452	2.139
717	31.4873	16.807	247.355	47.07	46.52	1.17	525.11	3.754	79.080	1.2353	73.500	2.156
806	3.1815	15.063	250.496	46.73	45.87	1.84	530.46	3.995	79.350	1.1026	73.201	1.747
807	5.5686	15.051	254.472	46.78	46.21	1.22	533.28	3.987	79.690	1.1023	73.240	2.252
808	7.9440	15.039	258.449	47.15	47.19	−.09	532.66	3.982	80.020	1.1021	73.280	1.623
809	10.3307	15.030	262.425	47.46	47.50	−.08	532.93	3.968	80.340	1.1020	73.319	1.531
810	6.5052	15.046	256.633	46.91	46.35	1.19	534.05	3.989	79.820	1.1022	73.256	2.135
811	8.8884	15.035	260.021	47.20	47.31	−.24	533.40	3.984	80.150	1.1020	73.295	1.562
812	11.2775	15.027	264.005	47.52	47.62	−.22	533.80	3.969	80.460	1.1020	73.335	1.523
813	13.6450	15.018	267.971	47.97	47.95	.05	533.07	3.940	80.770	1.1019	73.375	1.519
814	15.9881	15.009	271.915	48.29	48.29	.01	532.91	3.919	81.080	1.1019	73.415	1.526
815	18.3110	15.001	275.845	48.66	48.64	.03	532.27	3.894	81.370	1.1019	73.455	1.536
816	20.6178	14.993	279.768	49.05	49.00	.10	532.98	3.879	81.660	1.1019	73.495	1.549
817	22.9060	14.984	283.679	49.41	49.37	.08	532.59	3.856	81.940	1.1019	73.535	1.563
818	25.1761	14.976	287.579	49.75	49.75	−0	532.33	3.836	82.220	1.1019	73.575	1.578
819	27.4251	14.968	291.462	50.27	50.13	.28	532.26	3.812	82.490	1.1018	73.615	1.593
820	29.6660	14.959	295.349	50.62	50.52	.20	531.12	3.785	82.750	1.1018	73.655	1.609
821	32.3464	14.949	300.025	51.18	51.00	.36	760.20	5.382	83.070	1.1018	73.703	1.624

TABLE 6. *The specific heat, Cv, of singlephase fluid ethane*—Continued

Run No. point No.	PVT conditions			C_v J/mol–K	C_v calc. from Goodwin [2] J/mol–K	Dev. 0/0	Heat, Q J	ΔT K	C_0 J/K	Sample mol	Calorimeter volume cm³	Volume change correction J/mol–K
	Pressure MPa	Density mol/l	Temperature K									
907	3. 3507	14. 004	266. 868	48. 30	47. 62	1. 42	533. 44	4. 050	80. 690	1. 0259	73. 256	1. 430
908	5. 2994	13. 994	270. 918	48. 29	47. 97	. 66	532. 42	4. 019	81. 000	1. 0256	73. 292	1. 893
909	7. 2349	13. 983	274. 958	48. 61	48. 33	. 56	532. 78	4. 019	81. 360	1. 0454	73. 327	1. 401
910	9. 1760	13. 976	278. 996	48. 89	48. 71	. 38	532. 34	4. 002	81. 600	1. 0253	73. 362	1. 259
911	11. 1122	13. 968	283. 030	49. 18	49. 09	. 18	532. 86	3. 989	81. 890	1. 0252	73. 398	1. 242
912	13. 0368	13. 961	287. 053	49. 57	49. 49	. 17	532. 29	3. 964	82. 180	1. 0252	73. 434	1. 232
913	14. 9508	13. 954	291. 068	49. 99	49. 88	. 22	532. 31	3. 943	82. 460	1. 0252	73. 470	1. 250
914	16. 8538	13. 947	295. 074	50. 34	50. 29	. 10	532. 39	3. 925	82. 740	1. 0252	73. 506	1. 260
915	18. 7466	13. 940	299. 072	50. 72	50. 70	. 04	532. 40	3. 906	83. 010	1. 0252	73. 542	1. 272
916	20. 6314	13. 933	303. 068	51. 12	51. 11	. 02	532. 51	3. 887	83. 270	1. 0251	73. 578	1. 285
917	22. 5043	13. 926	307. 053	51. 58	51. 53	. 10	530. 25	3. 850	83. 540	1. 0251	73. 614	1. 299
919	24. 5909	13. 918	311. 509	52. 00	52. 00	0	530. 82	3. 833	83. 820	1. 0251	73. 655	1. 315
920	26. 4506	13. 911	315. 497	52. 44	52. 42	. 05	530. 30	3. 810	84. 080	1. 0251	73. 691	1. 329
921	28. 3059	13. 904	319. 489	52. 84	52. 84	. 01	531. 84	3. 802	84. 330	1. 0251	73. 728	1. 343
922	30. 1546	13. 897	323. 481	53. 30	53. 26	. 07	529. 10	3. 763	84. 580	1. 0251	73. 764	1. 358
923	31. 9987	13. 890	327. 478	53. 80	53. 68	. 21	530. 45	3. 752	84. 830	1. 0251	73. 801	1. 372
1006	3. 8940	12. 950	280. 688	49. 94	48. 89	2. 11	532. 04	4. 084	81. 730	0. 9493	73. 308	1. 183
1007	5. 4845	12. 941	284. 835	49. 93	49. 29	1. 29	531. 99	4. 063	82. 020	. 9491	73. 340	1. 602
1008	7. 0695	12. 932	288. 976	50. 22	49. 69	1. 06	534. 04	4. 075	82. 310	. 9488	73. 372	1. 136
1009	8. 6596	12. 925	293. 117	50. 47	50. 09	. 75	532. 16	4. 048	82. 600	. 9488	73. 404	1. 024
1010	8. 7885	12. 925	293. 453	50. 60	50. 13	. 94	534. 37	4. 061	82. 620	. 9488	73. 407	1. 021
1011	10. 3808	12. 918	297. 602	50. 83	50. 54	. 57	533. 14	4. 036	82. 910	. 9487	73. 440	1. 008
1012	11. 9663	12. 912	301. 740	51. 20	50. 96	. 46	532. 61	4. 013	83. 180	. 9487	73. 472	1. 009
1014	15. 1274	12. 900	310. 014	51. 71	51. 81	−. 20	533. 64	3. 990	83. 730	. 9487	73. 538	1. 026
1015	16. 7073	12. 894	314. 163	52. 22	52. 25	−. 05	531. 89	3. 954	83. 990	. 9486	73. 571	1. 037
1016	18. 2826	12. 888	318. 308	52. 68	52. 68	0	531. 33	3. 929	84. 260	. 9486	73. 605	1. 049
1017	19. 8541	12. 882	322. 453	53. 17	53. 11	. 11	532. 03	3. 913	84. 520	. 9486	73. 638	1. 061
1018	21. 4289	12. 876	326. 617	53. 56	53. 55	. 03	532. 16	3. 896	84. 780	. 9486	73. 672	1. 074
1105	4. 3795	11. 976	290. 820	51. 74	50. 15	3. 07	536. 23	4. 164	82. 440	. 8784	73. 347	1. 012
1106	5. 6995	11. 968	295. 076	51. 64	50. 54	2. 13	336. 58	4. 150	82. 740	. 8782	73. 377	1. 372
1107	4. 5546	11. 975	291. 384	51. 62	50. 20	2. 75	538. 51	4. 183	82. 480	. 8784	73. 351	1. 038
1108	5. 8805	11. 967	295. 658	51. 73	50. 60	2. 19	537. 49	4. 154	82. 780	. 8781	73. 381	1. 346
1109	7. 2048	11. 959	299. 925	51. 98	51. 00	1. 88	532. 89	4. 116	83. 060	. 8779	73. 411	0. 890
1110	8. 5348	11. 954	304. 195	52. 14	51. 42	1. 39	537. 27	4. 137	83. 350	. 8779	73. 441	. 838
1111	9. 8732	11. 948	308. 490	52. 37	51. 84	1. 02	537. 32	4. 123	83. 630	. 8779	73. 471	. 829
1112	11. 1743	11. 943	312. 666	52. 65	52. 26	. 76	504. 24	3. 854	83. 900	. 8778	73. 501	. 832
1113	12. 4352	11. 938	316. 715	52. 99	52. 66	. 62	502. 63	3. 825	84. 160	. 8778	73. 530	. 839
1114	13. 6959	11. 933	320. 765	53. 33	53. 07	. 49	501. 18	3. 798	84. 410	. 8778	73. 559	. 847
1115	14. 9594	11. 928	324. 828	53. 62	53. 48	. 27	503. 47	3. 800	84. 670	. 8778	73. 588	. 857
1116	16. 2269	11. 923	328. 907	54. 03	53. 89	. 26	502. 60	3. 776	84. 920	. 8778	73. 618	. 867

1201	5. 1530	5. 887	308. 511	68. 85	61. 64	10. 47	501. 98	4. 420	83. 630	. 4322	73. 416	. 435
1202	5. 5670	5. 884	313. 190	62. 98	59. 72	5. 17	503. 22	4. 518	83. 930	. 4321	73. 436	. 572
1203	5. 9863	5. 881	317. 960	60. 78	58. 79	3. 27	503. 13	4. 544	84. 240	. 4320	73. 457	. 538
1204	6. 4088	5. 878	322. 792	59. 47	58. 27	2. 02	502. 67	4. 553	84. 540	. 4319	73. 479	. 412
1205	6. 8341	5. 876	327. 675	58. 71	57. 97	1. 26	502. 69	4. 555	84. 840	. 4319	73. 501	. 366
1301	4. 9833	4. 611	308. 116	62. 03	58. 83	5. 16	426. 37	4. 071	83. 600	. 3385	73. 412	. 365
1302	5. 2602	4. 609	312. 344	59. 59	57. 95	2. 76	410. 37	3. 939	83. 880	. 3384	73. 430	. 427
1303	5. 5228	4. 607	316. 397	58. 61	57. 45	1. 97	380. 37	3. 652	84. 140	. 3383	73. 447	. 545
1304	5. 7766	4. 604	320. 349	57. 30	57. 15	. 27	375. 90	3. 616	84. 390	. 3383	73. 463	. 533
1305	6. 0260	4. 603	324. 259	56. 95	56. 97	−. 02	377. 80	3. 631	84. 630	. 3382	73. 479	. 428
1306	6. 2766	4. 601	328. 210	56. 92	56. 88	. 08	378. 42	3. 630	84. 880	. 3381	73. 496	. 363
1407	5. 2172	9. 177	306. 501	59. 73	53. 88	9. 79	377. 40	3. 038	83. 500	. 6737	73. 410	. 728
1408	5. 7778	9. 173	309. 793	58. 44	53. 88	7. 80	375. 80	3. 038	83. 710	. 6735	73. 427	. 899
1409	6. 3472	9. 169	313. 122	57. 70	53. 99	6. 44	375. 87	3. 051	83. 930	. 6734	73. 445	. 623
1410	6. 9235	9. 166	316. 478	57. 34	54. 15	5. 57	376. 10	3. 055	84. 140	. 6733	73. 464	. 539
1413	8. 6765	9. 158	326. 629	56. 92	54. 81	3. 70	373. 93	3. 029	84. 780	. 6733	73. 519	. 505
1418	5. 1849	9. 177	306. 311	59. 88	53. 88	10. 01	373. 34	3. 003	83. 490	. 6737	73. 409	. 714
1419	5. 7106	9. 173	309. 399	58. 49	53. 87	7. 89	371. 75	3. 005	83. 690	. 6735	73. 425	. 915
1420	6. 2429	9. 169	312. 513	57. 77	53. 96	6. 59	371. 21	3. 012	83. 890	. 6734	73. 442	. 659
1421	6. 7799	9. 166	315. 643	57. 36	54. 11	5. 67	372. 18	3. 024	84. 090	. 6733	73. 459	. 550
1422	7. 3256	9. 164	318. 812	57. 04	54. 28	4. 82	372. 31	3. 026	84. 290	. 6733	73. 476	. 520
1423	7. 8739	9. 161	321. 990	56. 95	54. 49	4. 33	372. 44	3. 024	84. 490	. 6733	73. 494	. 509
1424	8. 4266	9. 159	325. 186	56. 77	54. 71	3. 62	371. 33	3. 013	84. 690	. 6733	73. 511	. 506
1425	8. 9849	9. 156	328. 408	56. 85	54. 94	3. 34	372. 69	3. 018	84. 890	. 6733	73. 529	. 506
1501	4. 1439	3. 276	298. 669	60. 31	55. 73	7. 58	372. 96	3. 824	82. 980	0. 2404	73. 371	0. 260
1502	4. 3292	3. 276	302. 904	56. 64	55. 19	2. 56	435. 15	4. 489	83. 260	. 2404	73. 387	. 264
1503	4. 5274	3. 275	307. 501	55. 60	54. 85	1. 36	436. 31	4. 498	83. 560	. 2404	73. 405	. 271
1504	4. 7242	3. 274	312. 122	55. 11	54. 66	. 81	435. 24	4. 479	83. 860	. 2404	73. 423	. 281
1505	4. 9200	3. 272	316. 773	54. 33	54. 59	−. 48	437. 11	4. 493	84. 160	. 2403	73. 441	. 296
1506	5. 1138	3. 271	321. 425	53. 93	54. 62	−1. 28	434. 99	4. 462	84. 450	. 2403	73. 459	. 321
1507	5. 3073	3. 270	326. 113	53. 91	54. 71	−1. 48	436. 78	4. 467	84. 750	. 2403	73. 477	. 366
1603	4. 6182	11. 049	297. 554	53. 79	51. 31	4. 60	375. 57	2. 952	82. 900	. 8107	73. 373	. 860
1604	5. 3719	11. 044	300. 530	53. 36	51. 55	3. 39	372. 72	2. 927	83. 100	. 8105	73. 391	1. 186
1605	6. 1267	11. 039	303. 509	53. 51	51. 80	3. 20	374. 13	2. 935	83. 300	. 8104	73. 410	1. 007
1606	6. 8874	11. 035	306. 501	53. 59	52. 06	2. 85	373. 14	2. 926	83. 500	. 8103	73. 429	. 757
1607	7. 6523	11. 031	309. 501	53. 58	52. 33	2. 34	372. 69	2. 919	83. 690	. 8102	73. 448	. 712
1608	8. 4210	11. 028	312. 511	53. 55	52. 60	1. 76	372. 65	2. 915	83. 890	. 8102	73. 468	. 699
1609	9. 1928	11. 025	315. 531	53. 68	52. 88	1. 49	373. 04	2. 911	84. 080	. 8102	73. 487	. 695
1610	9. 9703	11. 021	318. 570	53. 85	53. 16	1. 27	373. 46	2. 907	84. 270	. 8102	73. 507	. 696
1611	10. 7480	11. 018	321. 607	54. 04	53. 45	1. 09	371. 74	2. 886	84. 470	. 8101	73. 527	. 699
1612	11. 5291	11. 015	324. 656	54. 14	53. 74	. 74	373. 12	2. 890	84. 660	. 8101	73. 546	. 704
1613	12. 4082	11. 012	328. 087	54. 44	54. 06	. 70	464. 76	3. 588	84. 870	. 8101	73. 569	. 709
1705	5. 2078	7. 891	307. 853	67. 13	55. 71	17. 02	374. 85	3. 052	83. 590	. 5793	73. 414	. 600
1706	5. 6238	7. 888	311. 011	63. 75	55. 19	13. 43	372. 84	3. 077	83. 790	. 5792	73. 430	. 788
1707	6. 0466	7. 884	314. 211	62. 20	55. 05	11. 49	373. 21	3. 101	84. 000	. 5791	73. 445	. 605
1708	6. 4742	7. 882	317. 440	61. 26	55. 06	10. 11	372. 18	3. 103	84. 200	. 5790	73. 461	. 481
1709	6. 9054	7. 880	320. 690	60. 54	55. 15	8. 91	372. 05	3. 108	84. 410	. 5790	73. 478	. 444
1710	6. 9598	7. 879	321. 099	60. 20	55. 16	8. 37	374. 42	3. 132	84. 430	. 5790	73. 480	. 442
1711	7. 4171	7. 877	324. 541	59. 88	55. 31	7. 63	409. 73	3. 427	84. 650	. 5789	73. 497	. 428
1712	7. 8992	7. 875	328. 165	59. 49	55. 50	6. 70	412. 12	3. 447	84. 870	. 5789	73. 515	. 423

TABLE 6. *The specific heat, Cv, of singlephase fluid ethane*—Continued

Run No. point No.	PVT conditions			C_v J/mol-K	C_v calc. from Goodwin [2] J/mol-K	Dev. 0/0	Heat, Q J	ΔT K	C_0 J/K	Sample mol	Calorimeter volume cm^3	Volume change correction J/mol-K
	Pressure MPa	Density mol/l	Temperature K									
1810	6. 0623	20. 289	131. 088	45. 99	44. 25	3. 77	381. 55	2. 837	60. 490	1. 4783	72. 866	4. 067
1811	11. 0190	20. 270	133. 939	45. 15	44. 31	1. 85	381. 37	2. 874	61. 320	1. 4780	72. 918	3. 151
1812	16. 1127	20. 254	136. 801	45. 23	44. 37	1. 89	382. 21	2. 861	62. 110	1. 4780	72. 972	3. 144
1813	21. 1154	20. 239	139. 647	45. 25	44. 43	1. 80	381. 25	2. 836	62. 870	1. 4780	73. 025	3. 155
1814	26. 0147	20. 224	142. 469	45. 40	44. 49	2. 01	381. 83	2. 820	63. 600	1. 4779	73. 079	3. 172
1815	30. 8178	20. 209	145. 270	45. 46	44. 54	2. 03	380. 71	2. 795	64. 290	1. 4779	73. 132	3. 192
1901	2. 7144	1. 585	288. 868	49. 30	48. 60	1. 43	280. 23	3. 182	82. 310	. 1162	73. 322	. 173
1902	2. 7708	1. 585	292. 068	49. 21	48. 71	1. 02	281. 45	3. 189	82. 530	. 1162	73. 333	. 174
1903	2. 8271	1. 585	295. 282	48. 28	48. 84	−1. 16	281. 02	3. 180	82. 750	. 1162	73. 344	. 175
1904	2. 8980	1. 585	299. 364	48. 87	49. 04	−. 34	435. 51	4. 908	83. 030	. 1162	73. 359	. 176
1905	2. 9836	1. 584	304. 333	49. 32	49. 32	−0	436. 70	4. 901	83. 360	. 1162	73. 376	. 178
1906	3. 0687	1. 584	309. 311	49. 10	49. 65	−1. 10	435. 44	4. 870	83. 680	. 1162	73. 394	. 180
1907	3. 1531	1. 583	314. 289	49. 85	50. 00	−. 31	436. 06	4. 855	84. 000	. 1162	73. 412	. 182
1908	3. 2372	1. 583	319. 287	50. 21	50. 39	−. 37	435. 39	4. 828	84. 320	. 1162	73. 429	. 184
1909	3. 3213	1. 582	324. 315	50. 18	50. 81	−1. 26	435. 80	4. 816	84. 630	. 1162	73. 447	. 187
1910	3. 4004	1. 582	329. 076	51. 11	51. 22	−. 22	383. 50	4. 219	84. 930	. 1162	73. 464	. 189

TABLE 7. *Intercomparison of C_v and C_p*

Pressure MPa ref. [18]	Density mol/l This paper	Temperature K from eq. ref. [2]	C_v J/mol-K interpol. this paper	PVT Contr. J/mol-K calc. ref. [2]	C_p J/mol-K calc. col. 4,5	C_p J/mol-K interpol. ref [18]	Diff pct
3. 4474	14. 647	257. 677	47. 19	44. 44	91. 64	90. 43	−1. 3
6. 8948	14. 630	263. 928	47. 41	41. 87	89. 28	88. 29	−1. 1
10. 3421	14. 617	270. 176	48. 00	39. 64	87. 64	87. 15	−. 6
13. 7895	14. 605	276. 459	48. 55	37. 72	86. 27	86. 01	. 3
6. 8948	20. 983	112. 105	45. 94	23. 41	69. 35	68. 58	1. 1
13. 7895	20. 962	115. 407	46. 19	23. 17	69. 36	68. 34	−1. 5
6. 8948	16. 125	235. 582	45. 31	34. 72	80. 03	79. 59	−. 6
13. 7895	16. 100	244. 770	46. 08	32. 80	78. 88	79. 09	. 3
1. 7237	19. 656	146. 015	44. 79	26. 12	70. 91	69. 97	−1. 4
6. 8948	19. 634	149. 450	44. 69	25. 80	70. 49	70. 06	−. 6
13. 7895	19. 611	153. 944	44. 46	25. 39	69. 85	70. 00	. 2
6. 8948	18. 904	169. 041	44. 22	27. 18	71. 40	71. 43	0
13. 7895	18. 879	174. 296	44. 80	26. 63	71. 44	70. 92	−. 7
6. 8948	17. 971	193. 014	44. 16	29. 20	73. 36	74. 08	1. 0
13. 7895	17. 945	199. 373	44. 38	28. 38	72. 76	72. 67	−. 1
6. 8948	16. 896	218. 724	44. 89	32. 10	76. 99	76. 45	−. 7
13. 7895	16. 869	226. 616	45. 20	30. 77	75. 97	76. 03	. 1
3. 4474	15. 062	250. 932	46. 72	41. 53	88. 26	87. 42	−1. 0
6. 8948	15. 044	256. 692	46. 98	39. 54	86. 53	85. 99	−. 6
10. 3421	15. 030	262. 445	47. 46	37. 78	85. 24	84. 71	−. 6
13. 7895	15. 017	268. 213	48. 00	36. 22	84. 22	83. 83	−. 5
3. 4474	14. 004	267. 065	48. 30	50. 15	98. 44	97. 38	−1. 1
6. 8948	13. 985	274. 251	48. 54	46. 23	94. 77	93. 93	−. 9
10. 3421	13. 971	281. 423	49. 06	43. 00	92. 06	91. 31	−. 8
13. 7895	13. 958	288. 629	49. 74	40. 33	90. 07	89. 67	−. 4
4. 9160	12. 944	283. 347	49. 88	60. 62	110. 51	106. 99	−3. 3
6. 8948	12. 933	288. 518	50. 22	56. 10	106. 31	104. 85	1. 4
8. 6184	12. 925	293. 012	50. 44	52. 78	103. 21	102. 07	−1. 1
10. 3421	12. 918	297. 507	50. 83	49. 93	100. 76	100. 07	−. 7
13. 7895	12. 905	306. 513	51. 49	45. 28	96. 77	95. 46	−1. 4
4. 9160	11. 973	292. 548	51. 49	80. 27	131. 76	129. 01	−2. 1
6. 8948	11. 961	298. 929	51. 96	70. 21	122. 17	*109. 17	*−11. 9
8. 6184	11. 954	304. 461	52. 15	63. 61	115. 76	113. 57	−1. 9
10. 3421	11. 946	309. 999	52. 47	58. 39	110. 86	109. 53	−1. 2
13. 7895	11. 933	321. 071	53. 35	50. 62	103. 97	103. 25	−. 7
5. 6468	5. 883	314. 096	62. 30	404. 02	466. 31	501. 97	7. 1
6. 8948	9. 166	316. 310	57. 35	171. 78	229. 12	*197. 27	*−16. 1
8. 6184	9. 158	326. 292	56. 89	116. 33	173. 22	164. 57	−5. 3
4. 6678	3. 274	310. 787	55. 29	94. 73	150. 03	149. 97	−0
4. 9160	3. 272	316. 685	54. 35	80. 07	134. 42	134. 19	−. 2
5. 1711	3. 271	322. 812	53. 89	69. 26	123. 15	123. 24	. 1
4. 9160	11. 047	298. 730	53. 57	116. 03	169. 59	162. 31	−4. 5
6. 8948	11. 035	306. 527	53. 59	91. 41	145. 00	142. 31	−1. 9
8. 6184	11. 027	313. 282	53. 56	78. 02	131. 58	127. 85	−2. 9
10. 3421	11. 020	320. 026	53. 94	68. 58	122. 53	119. 45	−2. 6
12. 0658	11. 013	326. 749	54. 30	61. 55	115. 85	115. 11	−. 6
5. 6468	7. 888	311. 185	63. 62	509. 77	573. 39	527. 29	−8. 7
6. 8948	7. 880	320. 609	60. 60	217. 16	277. 77	273. 85	−1. 4
6. 8948	20. 286	131. 554	45. 81	24. 64	70. 45	69. 02	−2. 1
13. 7895	20. 261	135. 496	45. 14	24. 33	69. 47	69. 04	−. 6

*Some of Furtado's values [18] may be in error by as much as 10 percent, see text.

from reference [18], the densities from the present measurements. A temperature corresponding to the P and ρ of an intersection is obtained from the equation of state [Goodwin, 2], and experimental values of C_v and C_p are interpolated from the two sets of data. The comparison is completed by calculating a value of C_p from

$$C_p = C_v + \frac{T\left(\frac{\partial P}{\partial T}\right)_\rho^2}{\rho^2\left(\frac{\partial P}{\partial \rho}\right)_T}. \quad (5)$$

The second term in equation 5 is the contribution from the PVT surface. It is clear from table 7 that in almost all cases the PVT contribution to C_p-calculated is as large or larger than the value of C_v. The mean deviation between calculated and experimental C_p for the 50 intersections is just under 2 percent. This implies that the thermodynamic consistency between experimental C_v and C_ρ measurements is indeed excellent, i.e., at least as good as 2 percent, but quite probably much better than that for two reasons. First, a large part of the total discrepancy must be assigned to errors in the PVT surface derivatives. Second, some of the values presented by Furtado [18] may be in error by as much as 10 percent. A detailed example is as follows.

In our table 7 a comparison is made at 6.8948 MPa (1000 psia) and 298.929 K (78.40°F). Furtado's closest smoothed value of C_p taken from his table VIII–5 at 6.8948 MPa (1000 psia) and 299.817 K (80°F) is 111.84 J/mol-K (0.889 BTU/lb-°F). This value changes to 124.06 J/mol-K if interpolated from his table VIII–3, a table of smoothed enthalpies, or to 122.4 J/mol-K if interpolated from his figure VIII–6, a plot of C_p versus temperature for the 1000 psia isobar. Thus the inconsistencies in Furtado's values, depending on how they are obtained, are at times as large at 10 percent.

7. Discussion

It is readily apparent that accurate values of C_0 are essential if we wish to obtain accurate values of either C_σ or C_v. A change of 0.1 percent in C_0, for example, will result in a change of 1 percent in the values of C_v calculated for run 19. The temperature increment, ΔT, is evaluated at the middle of the heating interval by extrapolating the temperature drift rates just before heating and after an equilibrating time has elapsed. Since the drift is linear the statistics of the extrapolation can be used to estimate an uncertainty in the ΔT. For the first 14 points of C_0 the average slope uncertainty was 0.19×10^{-3} K/min, since the average elapsed time to the center of the measurement interval is about 20 min, the average uncertainty in ΔT turns out to be ±0.004 K. This in turn implies that if we seek 0.1 percent precision in the specific heats the ΔT must be 4 K or larger. The choice of ΔT, as shown in tables 4 and 6, was based on this consideration and on the idea that there ought to be at least 5 points per experimental run. The imprecision in the temperature time data is attributed to the exact setting or resetting of the platinum thermometer current rather than potentiometer inaccuracy. Potentiometer inaccuracy was actually reduced from values given by Goodwin and Weber [6] to a maximum of 0.003 K by consideration of a potentiometer calibration. Heat leak to and from the sample is estimated to be less than 0.1 percent by considering the difference in drift rates before heating and after equilibration has been reached. Shield temperatures lag at the start of the heating interval by about 0.02 K. They lag again at the end of the heating interval after the power is turned off. The two lags compensate to produce a nearly adiabatic environment during the entire heating interval. Deliberate changes of temperature along the capillary were introduced to see if the applied heat, and therefore the results could be changed. In run 14 points 1401–1413 were obtained with liquid nitrogen in the refrigerant tank. These points were duplicated for 1414–1425 using cold water as coolant. The results, as shown in tables 4 and 6, are virtually identical. However, when we applied deliberate heating to the capillary, actually quite drastic heating 100 ma to a 140 Ω heater, the results changed. Points 508–517 differ from those obtained in a duplicate run 520–527 without heating the capillary by 1 percent at the lowest temperature. The difference disappears entirely at the highest temperature of the run. However, rather than changing the applied heat, heating the capillary apparently changes the distribution of sample between calorimeter and stem.

The same problem, distribution of sample between calorimeter and stem, is thought to give rise to the curvature of the runs. Runs 18, 4, 5, 6, and 7 show a definite curvature as to two phase boundary is approached, see figure 4, if compared to the values calculated by Goodwin [2]. The curvature seems to abate at pressures above the critical pressure, or at a point where mass change between calorimeter and stem has stabilized. It is possible that a heat of vaporization correction to Q should be included for the C_v calculation as long as sample is being transferred from calorimeter to stem. It should be noted that the correction term, column 13 of table 6, is irregular for the first few points of the runs in question.

Sample distribution is also thought to explain the departure of point 208 from the rest of run 2. The possibiity exists that for run 208 the capillary was frozen, because if point 208 is recalculated with zero stem volume the value of C_v is increased by about 2.5 percent.

We had hoped to employ the breakthrough points to resolve the problem of sample distribution. Experimental breakthrough temperatures agree well with calculated values; densities and total sample agree to a point where we are confident that the calorimeter volume has not changed. However, to calculate C_σ and C_v values from a breakthrough point requires that we know the time of breakthrough

exactly in order to proportion the applied heat Q. There is simply too much lag in the response of the recorders to permit an accurate determination of the breakthrough time.

The imprecision in the experiment depends primarily on the imprecision of C_0 and on the amount of sample since in most cases the ΔT is around 4 K. For liquid densities the imprecision from point to point along an isochore is about 0.1 percent with occasional differences as large as 0.3 percent. For densities less than critical the imprecision, the variation of C_v point to point from a smooth curve, increases to about 1 percent. The inaccuracy or uncertainty of the present measurements is estimated from the comparison to the experiments of others and from the comparison to values calculated from the PVT correlation. We consider the excellent agreement between the present results and the experiments of others [10, 16, 17, 18], in particular the agreement with experimental values of C_p, and we consider the results of deliberately introducing changes in the present experiment. It is difficult to see how systematic errors larger than about 2 percent for liquid densities or larger than 5 percent for vapor densities close to critical could remain undetected in the present experiment.

8. References

[1] The S. I. (international system) unit of pressure is the Pascal (1 Pa=1 N/m²). The bar is 10^5 Pa, also 1 atm=1.01325×10^5 Pa, 1 lb/in²=6894.757 Pa, 1 dyne/cm²=10^{-1} Pa: see Page, C. H. and Vigoureux, P., Nat. Bur. Stand. (U.S.), Spec. Publ. 330, (Jan. 1971). Also one mole ethane=30.07 g, based on the ^{12}C scale and the natural isotopic abundance averages: see Remy, H., Chem. Berichte **101**, 1 (1968).

[2] Goodwin, R. D., Roder, H. M., and Straty, G. C., Nat. Bur. Stand. (U.S.), Tech. Note 684 (in press), for provisional data see Goodwin, R. D., Nat. Bur. Stand. (U.S.), NBSIR 74-398 (1 June 1974). (Available as COM 74-11717 from the National Technical Information Services, Springfield, VA 22161.)

[3] Goodwin, R. D., J. Res. Nat. Bur. Stand. (U.S.) **65C** (Eng. and Instr.), No. 4, 231-243 (Oct.-Dec. 1961).

[4] Younglove, B. A., and Diller, D. E., Cryogenics **2**, 283 (1962).

[5] Younglove, B. A., and Diller, D. E., Cryogenics **2**, 348 (1962).

[6] Goodwin, R. D., and Weber, L. A., J. Res. Nat. Bur. Stand, (U.S.) **73A**, (Phys. and Chem.), No. 1, 1-13 (Jan.-Feb. 1969).

[7] Goodwin, R. D., and Weber, L. A., J. Res. Nat. Bur. Stand. (U.S.) **73A**, (Phys. and Chem.), No. 1, 15-24 (Jan.-Feb. 1969).

[8] Goodwin, R. D., and Prydz, R., J. Res. Bur. Stand. (U.S.) **74A**, (Phys. and Chem.), No. 4, 499-505 (July-Aug. 1970).

[9] Prydz, R., and Goodwin, R. D., J. Res. Nat. Bur. Stand. (U.S.) **74A**, (Phys. and Chem.), No. 5, 661-665 (Sept.-Oct. 1970).

[10] Younglove, B. A., J. Res. Nat. Bur. Stand. (U.S.) **78A**, (Phys. and Chem.) No. 3, 401-420 (May-June 1974).

[11] Roder, H. M., J. Chem. Phys. **65**, 1371 (1976).

[12] Walker, P. A., Dissertation (University of London, 1956).

[13] Hoge, H. J., J. Res. Nat. Bur. Stand. (U.S.) **36**, 111-118, (1946) RP1693.

[14] Goodwin, R. D., Nat. Bur. Stand. (U.S.), Tech. Note 653 208 pages (April 1974).

[15] Goodwin, R. D., and Prydz, R., J. Res. Nat. Bur. Stand. (U.S.) **76A**, (Phys. and Chem.), No. 2, 81-102 (Mar.-Apr. 1972).

[16] Wiebe, R., Hubbard, K. H., and Brevoort, M. J., J. Am. Chem. Soc. **52**, 611 (1930).

[17] Witt, R. K., and Kemp, J. D., J. Am. Chem. Soc. **59**, 273 (1937).

[18] Furtado, A., Ph.D. Thesis, Department of Chem. Engineering, University of Michigan (Dec. 1973).

[19] Bier, K., Kunze, J., and Maurer, G., to be published, J. Chem. Thermodynamics **8**, 857 (1976).

(Paper 80A5-915)

LNG DENSITIES FOR CUSTODY TRANSFER*†

Dwain E. Diller
Cryogenics Division
Institute for Basic Standards
National Bureau of Standards
Boulder, Colorado 80302

ABSTRACT

Accurate LNG densities are required for equitable custody transfer contracts and operations. Mathematical models and direct reading densimeters for use on LNG type mixtures are being evaluated at the National Bureau of Standards. Accurate (0.1%) orthobaric liquid density data have been obtained for LNG components and their mixtures and are being used to optimize and evaluate four published mathematical models. A density reference system has been constructed and is being used to evaluate commercially available densimeters. Recent progress on these tasks is summarized and discussed.

Key words: Custody transfer; densimeter; density; liquefied natural gas; mathematical model.

* This work was carried out at the National Bureau of Standards under the sponsorship of British Gas Corp., Chicago Bridge and Iron Co., Columbia Gas Service Corp., Distrigas Corp., Easco Gas LNG, Inc., El Paso Natural Gas., Gaz de France, Marathon Oil Co., Mobil R&D Corp., Natural Gas Pipeline Co., Phillips Petroleum Co., Shell International Gas, Ltd., Sonatrach, Southern California Gas Co., Tennessee Gas Pipeline, Texas Eastern Transmission Co., Tokyo Gas Co., Ltd., and Transcontinental Gas Pipe Line Corp., through a grant administered by the American Gas Association, Inc.

† This work was carried out at the National Bureau of Standards under the sponsorship of the American Gas Association, Inc.

LNG DENSITIES FOR CUSTODY TRANSFER

Dwain E. Diller

INTRODUCTION

LNG is typically bought and sold on the basis of its heating value. Important elements in calculations of the heating value of LNG in tanks and pipelines include tank volume and liquid level, flow rate, density, composition, temperature, pressure and specific heating value of the vaporized liquid. The density of the liquid is required in all heating value calculations. The basis for determining the density is usually agreed to in custody transfer contracts, which may involve several companies and countries. LNG densities can be either calculated from a mathematical model, as a function of composition and temperature (or pressure), or measured directly in a tank or pipeline. During the course of a typical contract the density will be determined many times with systematic errors benefiting one of the contractual parties. An inaccuracy of 1% in the density of a 125,000 m^3 LNG cargo is currently worth approximately $40,000. An inaccuracy of less than 0.1% in the density has been selected as a reasonable goal for this calculation or measurement.

CALCULATION OF THE DENSITIES OF LNG TYPE MIXTURES*

Calculation of the densities of LNG with a mathematical model has several advantages and disadvantages. An advantage is that the model can be based on the most accurate available density measurements performed under ideal laboratory conditions. A disadvantage is that use of the model depends on knowledge of the mixture composition, which may be difficult or inconvenient to obtain with sufficient accuracy. Another disadvantage is that accurate mathematical models, which cover a large range of mixture compositions, temperatures and pressures, are fairly difficult to use.

The molar volume V_{mix} of a fluid mixture can be written

$$V_{mix} = \Sigma x_i V_i + V^E \qquad (1)$$

where x_i, V_i and V^E are conventionally the mole fractions, molar volumes of the constituents, and the excess volume respectively, all at the temperature and pressure of the mixture. For LNG type mixtures V^E is typically negative and 1-2% of V_{mix}. Therefore an accurate mathematical model for V_{mix} (or V^E) is required to achieve an inaccuracy of less than 0.1% in the density. Several promising models for calculating accurate densities of LNG type mixtures have been published. They include the Klosek and McKinley excess volume correlation [1], the modified cell model [2], the modified corresponding states model [3], and the modified hard sphere equation of state model [4]. The details of these models are given in the references. The mathematical models must be based on and tested against accurate density measurements for LNG components and their mixtures. For contractual purposes it is desirable that the measurements and evaluation be carried out by an independent third party.

Until recently there have been few accurate (0.1%) density measurements available for liquefied LNG components and their mixtures in the normal boiling temperature range (110-115 K) of LNG type mixtures. To obtain the additional data needed a magnetic suspension densimeter has been constructed and performance tested for measurements in the temperature range 90-300 K at pressures to 5 MPa (725 psi) [5], and a comprehensive program of orthobaric liquid density measurements has been carried out on six LNG components (methane, ethane, propane, isobutane, normal butane and nitrogen) [5,6], on 29 compositions of 13 binary mixtures [7], and on 13 multicomponent mixture compositions [8], including several LNG type mixtures. This work has been carried out by W. M. Haynes, M. J. Hiza, and others at the National Bureau of Standards. The measurements

on the pure components, at temperatures mainly between 95 and 160 K, have an estimated imprecision less than 0.02% and an estimated inaccuracy of approximately 0.1%. The estimated imprecision is primarily based on the standard deviation obtained for 123 measurements on liquid methane. The estimated inaccuracy of a single density measurement on liquid methane was taken as the square root of the sum of the squares of the systematic error plus an allowance of three times the standard deviation for random error. The measurements on the binary and multicomponent mixtures, at temperatures mainly between 105 and 140 K, have a typical estimated inaccuracy of approximately 0.1% and a maximum estimated inaccuracy of 0.16%. The derived excess volumes V^E of the binary mixtures can be classified into several quantitatively distinguishable groups: in the temperature range of these measurements the alkane mixtures without methane have excess volumes which are less than 0.1% of V_{mix}, the alkane mixtures containing methane have excess volumes up to 3% of V_{mix}, and the nitrogen-alkane mixtures have excess volumes up to 10% of V_{mix}.

The modified Klosek and McKinley correlation, the modified corresponding states model and the modified hard sphere equation of state model are being optimized and evaluated by R. D. McCarty at the National Bureau of Standards. The modified cell model is being optimized and evaluated by M. A. Albright at the Phillips Petroleum Company. Within various composition range limitations these models have correlated most of the NBS data within their estimated inaccuracies. The results are now being prepared for publication.

DIRECT READING DENSIMETERS FOR LNG TYPE MIXTURES†

Direct reading densimeters for use on LNG type mixtures also have several advantages and disadvantages. Advantages include the relative simplicity of use (knowledge of the mixture composition is not required) and the possibility of continuously monitoring the density. Disadvantages include the need for calibration of densimeters now commercially available and the difficulty of obtaining sufficient information on the calibration and performance of a

particular densimeter. For contractual purposes it is desirable that the performance of types of available densimeters be evaluated by an independent third party. Accordingly, an apparatus [9] for evaluating the performance of types of commercially available densimeters on LNG components and their mixtures has been constructed and tested at the National Bureau of Standards. This work has been carried out by B. A. Younglove and others. The direct reading densimeters to be evaluated are placed in a density reference system (DRS) containing carefully characterized liquefied gases and are compared against an accurate absolute densimeter based on Archimedes' principle. The accessible temperature range of the DRS is 80 to 300 K and the pressure limit is 7 bars ($\sim$ 100 psi). The estimated inaccuracy of the reference densimeter is less than 0.21%. The estimated inaccuracy was based on the sum of the known sources of systematic error, $\pm$ 0.026%, plus three times the standard deviation, $\pm$ 0.062%, based on 71 independent measurements using eight different samples of liquid methane (99.97% pure). The direct reading densimeters can also be compared with densities calculated from measurements of the composition and temperature and a mathematical density model. Tests have been performed on commercially available densimeters based on Archimedes' principle, on dielectric property measurements, and on the frequency response of several vibrating elements. The results are now being prepared for publication.

SUMMARY AND CONCLUSIONS

Comprehensive accurate orthobaric liquid density data have been obtained for six LNG components and their mixtures and are being used to optimize and evaluate four promising calculation methods. Within various composition limitations these models have correlated most of the data within their estimated inaccuracies. Several significant differences between the measured and calculated densities still remain, and efforts to resolve these differences are continuing.

A density reference system has been constructed and is being used to evaluate the performance of commercially available densimeters for use on LNG type mixtures. Several types of densimeters look promising for obtaining direct density measurements on LNG in tanks and pipelines within the estimated inaccuracy of the reference densimeter.

REFERENCES

1. J. Klosek and C. McKinley, Densities of Liquefied Natural Gas and of Low Molecular Weight Hydrocarbons, Proc. First Int. Conf. on LNG, IGT, Chicago (1968), Session 5, paper 22.

2. M. A. Albright, A Model for the Precise Calculation of Liquefied Natural Gas Densities, NGPA Technical Publication TP-3 (1973).

3. J. Mollerup and J. S. Rowlinson, The Prediction of Densities of Liquefied Natural Gas and of Lower Molecular Weight Hydrocarbons, Chem. Eng. Sci. 29, 1373 (1974).

4. J. B. Rodosevich and R. C. Miller, Calculation of LNG Excess Volumes by a Modified Hard-Sphere Model, Adv. Cryog. Eng. 19, 339 (1974).

5. W. M. Haynes, M. J. Hiza and N. V. Frederick, A Magnetic Suspension Densimeter for Measurements on Fluids of Cryogenic Interest, Rev. Sci. Instr. 47, 1237 (1976).

6. W. M. Haynes and M. J. Hiza, Measurements of the Orthobaric Liquid Densities of Methane, Ethane, Propane, Isobutane and Normal Butane, J. Chem. Thermo. (in press) (1976).

7. M. J. Hiza, W. M. Haynes and W. R. Parrish, Orthobaric Liquid Densities and Excess Volumes for Binary Mixtures of Low Molecular Weight Alkanes and Nitrogen Between 105 and 140 K, to be submitted to J. Chem. Thermo.

8. M. J. Hiza and W. M. Haynes, unpublished data.

9. B. A. Younglove and J. D. Siegwarth, Cryogenic Fluids Density Reference System Provisional Accuracy Statement, unpublished data.

Magnetic suspension densimeter for measurements on fluids of cryogenic interest*

W. M. Haynes, M. J. Hiza, and N. V. Frederick

National Bureau of Standards, Institute for Basic Standards, Cryogenics Division, Boulder, Colorado 80302

(Received 24 June 1976)

An apparatus incorporating a magnetic suspension technique has been developed for density measurements on liquids and liquid mixtures, particularly at saturation, at temperatures between 90 and 300 K and at pressures to 5 MPa (approximately 50 atm). The feasibility of adapting this method, previously used at room temperature, for low temperature use had been demonstrated in an earlier study with a density measurement on saturated liquid nitrogen near its normal boiling point. The present apparatus, which is significantly improved, and in most respects different from the earlier model, is described in detail. It includes a cryostat for continuous wide-range temperature control, a windowed equilibrium cell particularly suited for studies of liquid mixtures, and a new electronic servocircuit with a linear differential transformer for position control of the magnetic buoy. Extensive tests and density measurements have been carried out to evaluate the performance of this apparatus. Densities of saturated liquid nitrogen between 95 and 120 K and saturated liquid methane between 105 and 160 K are reported. The estimated standard deviation of a single density measurement is less than 0.02%. The total systematic error in the measurement process from known sources is approximately 0.05%. The total uncertainty of a single density measurement, which is taken as three times the standard deviation plus the systematic error, is approximately 0.1%. Comprehensive comparisons of the present results with previous experimental data are presented.

I. INTRODUCTION

With the advent of large-scale liquefaction and global transport of natural gas, accurate equilibrium liquid-phase densities have become important for custody transfer. The density data for liquefied natural gas mixtures and their components have been generally characterized by the existence of large discrepancies (approximately 0.5%) between different sets of data for the pure components and by a limited amount of mixture data. Hence, an apparatus has been developed to provide accurate, consistent, and comprehensive density data for liquefied natural gas mixtures and their predominant pure components at saturation conditions. These measurements will serve as a data base for testing and optimizing selected mathematical models (correlations) useful in predicting the densities of liquefied natural gas. In the present paper the apparatus and experimental procedures are described in detail and representative measurements for two components of liquefied natural gas are presented.

A magnetic suspension densimeter, which is based on an application of Archimedes' principle, has been selected for the present measurements primarily because this instrument is suitable for an independent, direct determination of the density of a saturated liquid over wide ranges of temperature and pressure within the precision and accuracy required for anticipated technical applications. In an earlier study,[1] the feasibility of adapting the magnetic suspension technique for density measurements at low temperature was demonstrated with a measurement on saturated liquid nitrogen near its normal boiling point. The present apparatus (see Fig. 1 for a scaled assembly drawing), which is a much improved version of the earlier model, incorporates a three-coil support system,[2] a cryostat for temperature control at any temperature between 90 and 300 K, a windowed equilibrium cell suitable for projected studies on liquid mixtures at pressures to 5 MPa, and a new electronic servocircuit with a linear differential transformer that serves as a position sensor for a barium ferrite magnetic buoy.

The present work has included an extensive evaluation of the use of a magnetic suspension densimeter for absolute density measurements. (Here the term "absolute density" is used to indicate that cryogenic fluids were not used to calibrate the instrument.) Results of performance tests along with densities for saturated liquid nitrogen between 95 and 120 K and saturated liquid methane between 105 and 160 K are presented in this paper to demonstrate the low temperature performance of this new apparatus. The estimated standard deviation of a single density measurement is less than 0.02%. The total uncertainty of a single measurement, which is taken as the sum of the systematic error and three times the standard deviation, is approximately 0.1%.

In Sec. II the general principles of a magnetic

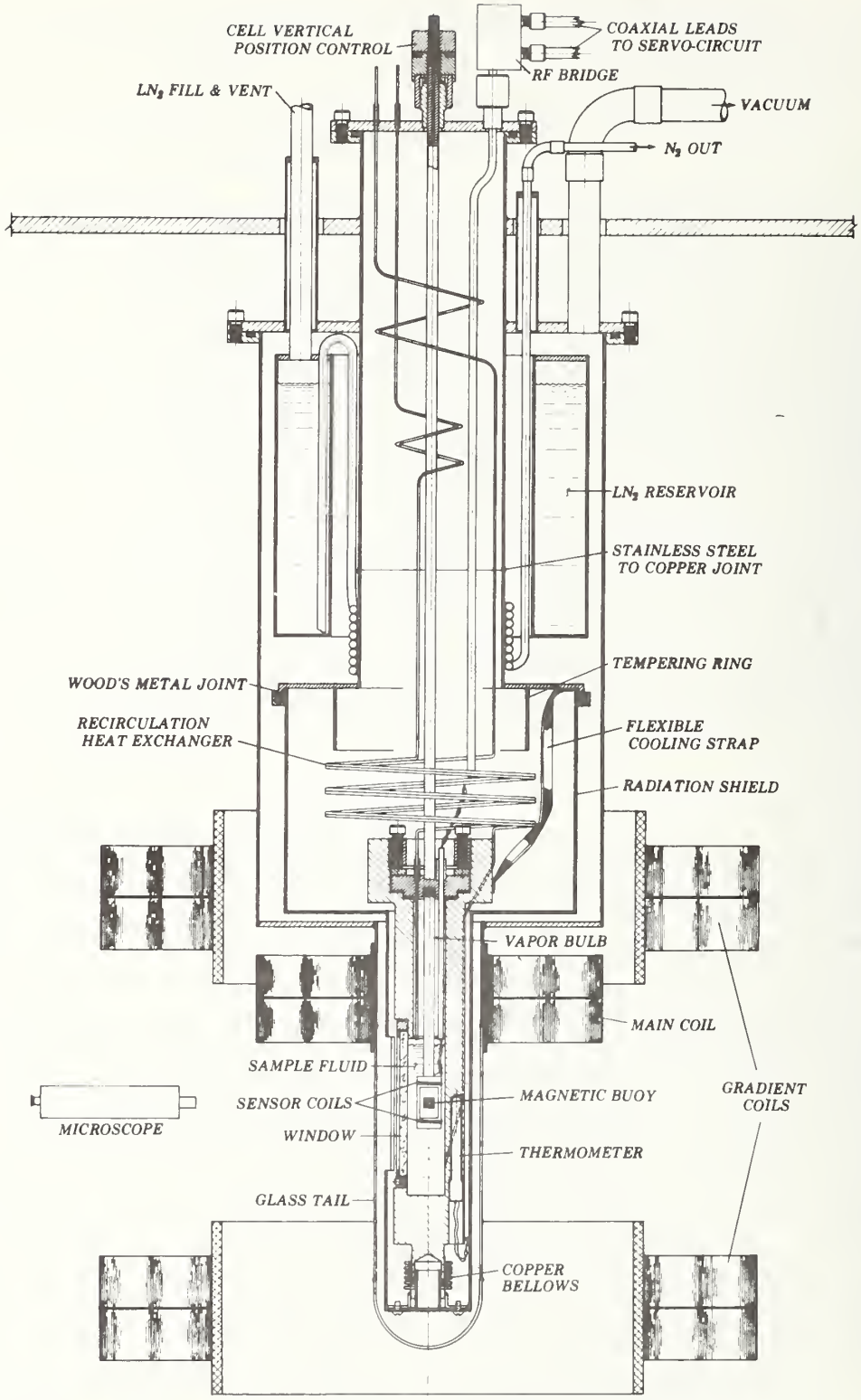

FIG. 1. Assembly drawing (approximately to scale) of a magnetic suspension densimeter for cryogenic fluids.

suspension densimeter are outlined. Section III is devoted to a detailed description of the experimental apparatus. A comprehensive discussion of the experimental procedures and measurements is given in Sec. IV. In Sec. V a summary of performance tests carried out in evaluating the instrument is presented. This sec-

tion also deals with the uncertainties in the density measurements. Finally, the experimental data for saturated liquid nitrogen and methane, along with comparisons with independent measurements, are reported in Sec. VI.

II. PRINCIPLES OF OPERATION

A piece of magnetic material is magnetically suspended in a fluid at a stable equilibrium position through the use of a closed-loop servosystem. When the float (or buoy) is in free support, there are three forces acting on it. In the present system the magnetic float is more dense than the fluid in which it is suspended; thus, an upward magnetic force is added to the buoyancy force to balance the downward gravitational force.

In the present work a three-coil (air-core) system[2] is used to supply the magnetic force. The three coils are aligned coaxially. Each coil is symmetric about an axis in common with the cylindrical axis of the magnetic buoy. The three coils consist of a main coil, which supplies the major part of the field necessary to lift the float, and a pair of gradient coils. The horizontal position of the float, which is in the shape of a right circular cylinder (length/diameter > 1) magnetized along its cylindrical axis, is maintained by the axially symmetrical, diverging field of the main coil. The magnetic force on the ferromagnetic buoy is given by

$$F_{\text{mag}} = M \frac{dH}{dZ}, \tag{1}$$

where M is the total magnetic moment of the buoy and dH/dZ is the variation of the external field intensity along the common cylindrical axis of the coils. For the present system the float is a permanent magnet for which the total magnetic moment (excluding temperature dependence) can be represented by

$$M = M_0 + M_I(H), \tag{2}$$

where M_0 is the permanent moment, and $M_I(H)$ is the induced moment resulting from an applied field.

At a fixed position along the cylindrical axis of an air-core solenoid,

$$H = kI \tag{3}$$

and

$$\frac{dH}{dZ} = k'I, \tag{4}$$

where I is the solenoid current and k and k' are constants dependent upon the number of turns and dimensions of the coil.

As mentioned earlier, the float is supported at a position relative to the main coil such that its horizontal position is fixed. This results in the float being supported at a distance below the main coil slightly larger than the inside radius of this coil. The float is supported approximately midway between the gradient coils. These coils are connected in series such that their magnetic field intensity contributions cancel at the float position. (For a Helmholtz coil arrangement the magnetic fields would add at the midpoint.) Thus, the magnetic field intensity at the float position is due solely to the main coil contribution. Similarly, the magnetic field gradients of the gradient coils add at the float position.

For this three-coil arrangement and with a constant main coil current (I_M) (and subsequently the magnetic moment of the float does not change), the density of the fluid (ρ) is related to the gradient coil current (I_G) by the following relation:

$$\rho = A + BI_G, \tag{5}$$

where A and B are constants to be determined by calibration with fluids of known density. This relationship is valid whether the float is magnetically hard or soft. Knowledge of the mass and volume of the float is not required to obtain relative density results using Eq. (5). However, since the magnetic moment of the float is temperature dependent, the constants A and B would have to be determined at each temperature of interest.

At low temperatures at least two fluids of known density, one of which may be "vacuum," are needed for calibrating the instrument for use in performing relative density measurements. However, the densities of low temperature fluids are not known to sufficient accuracy to permit them to be used as calibration fluids and, in fact, this had been one of the major motivations for developing an independent technique for density measurements on cryogenic fluids.

In the previous work by Haynes and Stewart,[1] a new method was demonstrated for determining absolute densities using the same three-coil arrangement, but which is dependent upon the magnetic properties of the buoy material. If one uses a permanent magnetic material for the float and its induced moment is zero or, at least, very small compared to the permanent moment, then the magnetic force on the float is given by the relation,

$$F_{\text{mag}} = C'I_M + D'I_G, \tag{6}$$

where C' and D' are constants depending on the relative position of the coils and float, the magnetic moment of the float, and the dimensions and number of turns of the support coils. One should note that for Eq. (6) the main coil current (I_M) is not held constant. Now the density of the fluid is given by the expression,

$$\rho = (m - CI_M - DI_G)/V, \tag{7}$$

where m and V are the mass and volume of the float. The acceleration of gravity has been included in the constants C and D. (The mass and volume of the float must be determined by independent measurements.) The validity of this equation can be tested experimentally. For measurements in a vacuum, Eq. (7) reduces to the following relation:

$$m = CI_M + DI_G. \quad (8)$$

It should be emphasized that the critical assumption in deriving Eq. (7) is that there is no induced moment in the buoy resulting from changes in the magnetic field intensity over the range of magnetic fields needed for the density measurements. (For the present measurements this includes fields between 0.006 and 0.016 T.)

The current in the gradient coils has been measured as a function of the current in the main coil while the float was suspended at a constant height in a given fluid, usually vacuum, at constant temperature. The currents were fitted by the method of least squares to either Eq. (6) or Eq. (8). The quality of this fit indicated the validity of the assumption concerning the dependence of the magnetic moment upon the magnetic field. (Results will be presented in a later section.) For the present measurements the main coil current, and thus the magnetic field, could be varied over a range amounting to 25% of its maximum value. The minimum ratio of I_M/I_G was determined by the loss of horizontal stability of the float.

From the above discussion it should be apparent that relative density measurements using Eq. (5) (I_M constant) can be carried out to complement the results of absolute measurements using Eq. (7) with the same three-coil arrangement. In performing measurements using Eq. (7) for which the main coil current is varied over a considerable range, it is experimentally difficult to fix or determine the position of the main coil from vacuum to liquid measurements within the desired precision. This problem does not arise when making relative density measurements for which the main coil current is held constant. In principle, both procedures should give identical density ratios for the same fluids at constant temperature. In practice, the relative density measurements can be carried out to deduce the systematic error in the absolute density measurements that depends on the magnitude of the main coil current. These tests have been performed in the present work and will be discussed in a later section.

III. APPARATUS

A. General considerations and cryostat

An assembly drawing (approximately to scale) of the major components of the apparatus is shown in Fig. 1. The general dimensions and configuration of the cryostat and equilibrium cell were determined by the dimensions and configuration of the main coil and the two gradient coils. (See Table I for coil dimensions.)

Criteria considered essential, and which have been satisfied, in the design of the apparatus are as follows: (a) all materials of construction in close proximity to the magnetic suspension assembly are nonmagnetic; (b) the entire assembly is rigidly supported so that the relative position of the buoy, microscope, and support coils can be maintained; (c) the magnetic buoy and the liquid level are visible within a windowed cell capable of withstanding working pressures up to 5 MPa; (d) the volume occupied by the liquid sample within the cell is sufficiently large to render the unavoidable vapor volume of the access tubing, etc., insignificant within the accuracy goals of experiments involving liquid mixtures; (e) temperature gradients along the length of the working space of the cell are monitored and reduced to a practical minimum, i.e., less than a total of 10 mK; (f) the rate of refrigeration of the equilibrium cell is adjustable and continuous; and (g) the temperature of the cell can be controlled at any temperature between 90 and 300 K.

TABLE I. Parameters of support coils.

	Main coil	Gradient coils
Length	6.0 cm	6.2 cm
Inside diameter	7.4 cm	25.4 cm
Outside diameter	20.24 cm	38.6 cm
Number of turns	5000	5000

A concrete block structure provides a stable support for the cryostat, the coils, and the microscope. The cryostat assembly is suspended from an aluminum plate that spans the top of the concrete structure. The stainless steel central support tube of the cryostat is attached to this aluminum plate with a brass collar (not shown in Fig. 1). The lower end of the stainless steel tube is soldered to a copper tube to which a heat exchanger is soldered.

Refrigeration is provided by continuous transfer of liquid nitrogen from the cryostat reservoir through the heat exchanger. Regulation of the refrigeration rate is accomplished by controlling the nitrogen vent rate to the atmosphere.

Refrigeration is supplied to the bottom of the equilibrium cell through the copper radiation shield and to the top of the cell through two copper braided straps. The radiation shield, which contains a slit aperture in a position corresponding to the cell window, is attached to a copper plate at the top of the shield with Wood's metal to facilitate removal of the shield and alignment of the shield within the glass tail section. The glass tail is connected to the stainless steel vacuum jacket through a stainless steel-to-glass transition joint.

B. Equilibrium cell

The equilibrium cell, made of electrolytic tough pitch copper, has an overall length of approximately 30 cm, including the copper-plated bellows at the bottom. The cell closure is a compression fitting with a silver-plated, solid copper O-ring. The closure plug, threaded backing ring, and compression screws are stainless steel. The top of the cell is held in alignment by a stainless steel tube, which is brazed to the closure plug and extends through the uppermost cryostat plate. The upper end of the cell support tube

is threaded through a nut and bearing assembly to allow small adjustments in the vertical position of the cell and thus the vertical position of the magnetic buoy. The bottom of the cell is thermally anchored to the radiation shield by mechanical attachment of a flanged bellows section. A thin coat of commercially available conducting grease is used to enhance thermal contact between the bellows flange and the shield. Two thermal links of copper braid are also mechanically attached to the top of the cell from the top plate of the radiation shield using thin coats of conducting grease between the contact surfaces.

The outside diameter of the main part of the cell is 4.13 cm and that of the closure section is 7.60 cm. The internal working space is 1.99 cm in diameter and approximately 20 cm long. More than half of the internal volume, however, is occupied by the magnetic buoy–sensor coils assembly (~10 cm^3) and the vapor bulb (~35 cm^3). The vapor bulb is a slip fit in the top section of the cell and is attached directly to the closure plug. The internal free volume of the cell is approximately 20.5 cm^3. Anticipating measurements on mixtures, the volume (~0.3 cm^3) in the annulus between the vapor bulb and the cell wall has been made as small as possible, since this is normally part of the vapor volume.

The electrical lead-throughs for the sensor coils consist of three No. 32 coated copper wires encapsulated with an epoxy adhesive in a copper capillary tube. This tube extends through the closure plug to the bottom of the vapor bulb. The epoxy adhesive, an alumina-filled resin with elevated temperature curing agent, was selected based on an earlier study[3] of low temperature properties of epoxy adhesives. By pressurizing with helium gas while the adhesive was hot, the entire length of the capillary tube was filled with adhesive to minimize the available vapor volume in the equilibrium cell.

The cell window was designed to allow viewing the liquid sample from the base of the vapor bulb down to 2 cm from the bottom of the liquid space. The viewing slit is 0.6 cm wide × 7.5 cm long. The window consists of a piece of tempered Pyrex[4] glass of 0.32-cm thickness with semicircular ends and chamfered edges. The seal between the glass and the cell is made with indium wire compressed in a racetrack groove machined in a flat surface on the cell. The glass is compressed against the indium seal with a hardened beryllium copper plate secured by stainless steel screws. A rubber asbestos pad is placed between the beryllium copper plate and the glass to relieve thermal and mechanical strains. The maximum working pressure of the equilibrium cell is limited by the maximum working pressure of the window.

C. Magnetic buoy

The buoy is a barium ferrite ($BaFe_{12}O_{19}$) magnet in the shape of a right circular cylinder magnetized along its cylindrical axis. Its length and diameter are approximately 0.64 and 0.51 cm, respectively.

Barium ferrite is a magnetically hard, ceramic material with a density of approximately 5×10^3 kg/m^3. It is somewhat porous and has a high electrical resistivity. The buoy used in the present work has been permanently magnetized in a saturation field of 1 T. After initial cycling over maximum ranges of temperature (90–300 K) and magnetic field intensity ($0–1.3 \times 10^4$ A/m) the barium ferrite magnet exhibited no hysteresis over the ranges of currents and temperatures needed in the density measurements. The magnet is operating in a very small segment ($5–13 \times 10^3$ A/m) of a broad hysteresis loop. The slope of the B-vs-H curve is small and constant. The change in the magnetic moment of the float with temperature varies from 0.2%/K at 300 K to 0.1%/K at 100 K, as determined from the present measurements in vacuum. This variation in the magnetic moment with temperature results in a random error in the density of approximately 0.002% at 100 K, increasing to 0.004% at 300 K. This estimate is based on a reproducibility in the temperature of 2 mK from vacuum to liquid measurements.

Since the barium ferrite magnet is porous, it must be coated with a material which does not allow fluid to penetrate into the buoy. Copper was found suitable for this purpose. After a piece of barium ferrite was ground into the shape of a right circular cylinder with chamfered edges (0.25 mm deep), a conducting layer of copper was uniformly plated onto the ceramic magnet by chemical reduction. On top of this conducting layer, copper was electroplated to a thickness of approximately 0.25–0.50 mm; a much thicker coating resulted at the edges. Then most of the copper was removed with a diamond tool until the copper-plated barium ferrite magnet was in the shape of a right circular cylinder without chamfered edges. The final buoy had a minimum of 0.06 mm of copper over the cylindrical surface and the end faces and at least 0.25 mm on the edges where the magnet had been chamfered. The edges were built up to a thicker coating since the plating strength would be weakest at these locations. (For density measurements it is not necessary that the plating be symmetric about the center of mass of the buoy.) Gold was flashed (10^{-3} mm) over the entire copper surface as a protective coating.

D. Electromagnetic support coils

Each of the coils is composed of two separate coils of 2500 turns of epoxy-coated aluminum foil of approximately 0.025-mm thickness. The foil for the main coil has a width of 2.5 cm while that for the gradient coils is 3.0 cm. Selected coil parameters are given in Table I.

Each of the gradient coils is rigidly supported by three aluminum rods resting on the concrete structure. The gradient coils have a separation distance of approximately 23 cm. No effort has been made to control the

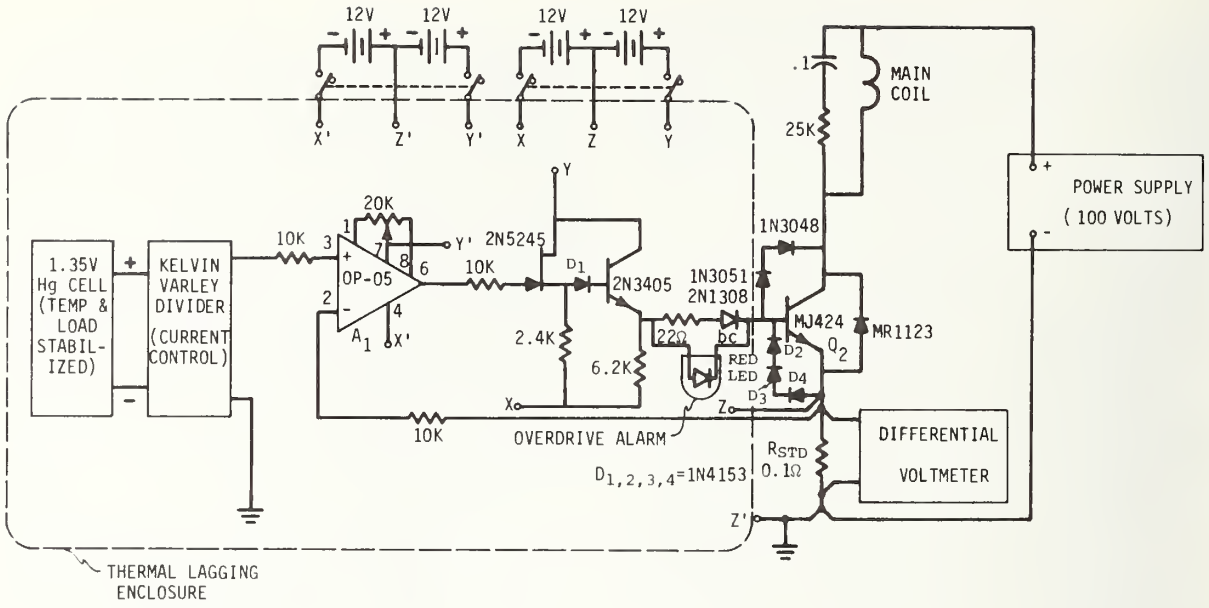

FIG. 2. Current control circuit for main coil.

position of the gradient coils except through the control of the laboratory temperature. The dH/dZ of the gradient coils changes very slowly (2.5×10^{-4}/cm) from a maximum at the float position. Since the change in dH/dZ with position for the main coil is two orders of magnitude larger than that for the gradient coils, special care has been taken to minimize changes in the position of the main coil.

First, the main coil is supported at its midplane so that thermal expansion effects inside the coil are minimized. A circular copper plate has been soldered to the brass tube on which the main coil is wound. A coil of aluminum foil (2500 turns) is clamped tightly to each side of the copper plate with a thin layer of vacuum grease between the aluminum foil and copper for maximum thermal contact. The copper plate (and thus the coil) is supported by quartz rods extending to the concrete structure. Thus, any changes in the position of the midplane of the coil due to room temperature changes would be negligible. Copper plates with cooling water have been placed on the outside faces of each section of the main coil such that the average temperature of the main coil is below room temperature for maximum current (1 A). However, for absolute density measurements, the temperature of the main coil changes from vacuum to liquid measurements (1.2 K for nitrogen at 100 K) since a larger current is required to support the float in vacuum than in the liquid for a given gradient coil current.

E. Support system electronics

The current in the main coil, which contributes the major portion of the magnetic force necessary to lift the buoy, is provided by the circuit of Fig. 2. The circuit functions as follows: The main coil current flows through a stable resistor R_{STD} (0.1 Ω) in the emitter of Q_2 (the current-controlling transistor). The voltage developed across R_{STD} is compared with a reference voltage from a Kelvin–Varley voltage divider by amplifier A_1. The output of A_1 drives the base of Q_2 and controls the current through R_{STD} and the main coil. Since the loop gain of this circuit is exceedingly high ($>10^6$) and the thermal drifts are very low, the long-term stability of the main coil current is of the order of 0.001%. This current controller has a temperature coefficient of the order of 5 ppm/K and a sensitivity to power supply variations of less than 2×10^{-6} A/V. A slow drift of the coil current of 2.5×10^{-6} A/h has negligible effect on the density measurements since the main coil current is measured each time that the gradient coil current is determined. (It should be noted that the precision and accuracy of the density results depend on the short-term stability and not the absolute accuracy of the standard resistor.)

The gradient coils are included in a control circuit (Figs. 3 and 4) that senses and maintains the vertical position of the buoy. The requirements for stability of a magnetic support or levitation system are discussed in detail in Refs. 5 and 6 and will not be repeated here. Suffice it to say that the characteristic equation for a magnetic levitation system has a root with a positive real part, and for system stability the plot of the frequency response of the characteristic equation (the Nyquist plot) must encircle the origin once in the counterclockwise sense. This is accomplished by the dual-lead network composed of R_1, R_2, C_1, and C_2 in Fig. 4. A dual-lead network is required for this system since minimization of the steady state offset or buoy position change requires at least a first-order integrator

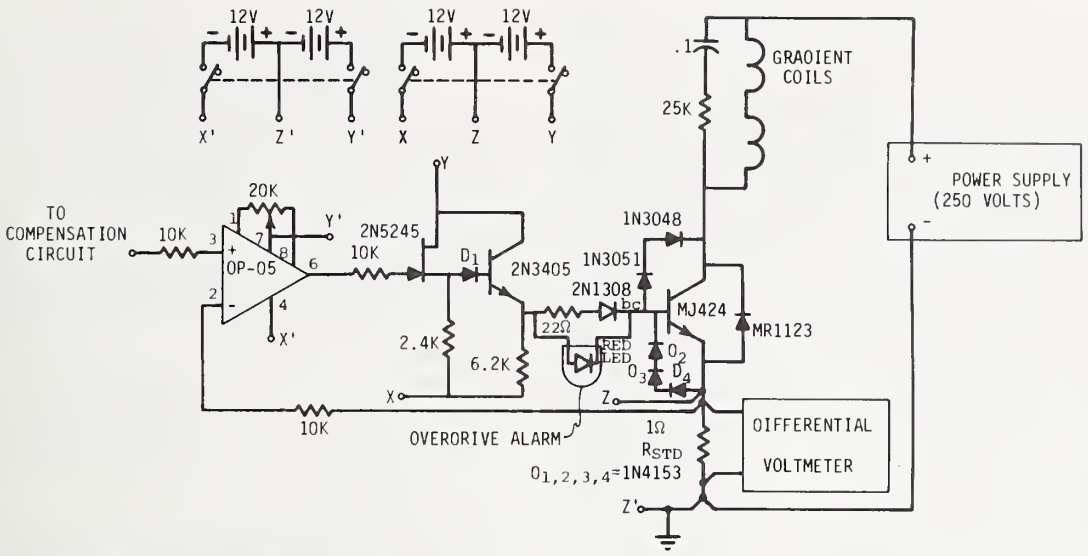

FIG. 3. Current control circuit for gradient coils.

in the control loop. This integrator consists of amplifier A_2 and R_1 and C_2. The additional resistor R_3 is required to stabilize the combined integrator and dual-lead network. A block diagram of the electronics is presented in Fig. 5 to complement the detailed circuit diagrams in Figs. 2–4. The circuit diagrams are presented in detail since this circuit is considerably different from any found in the literature. It should be noted that the

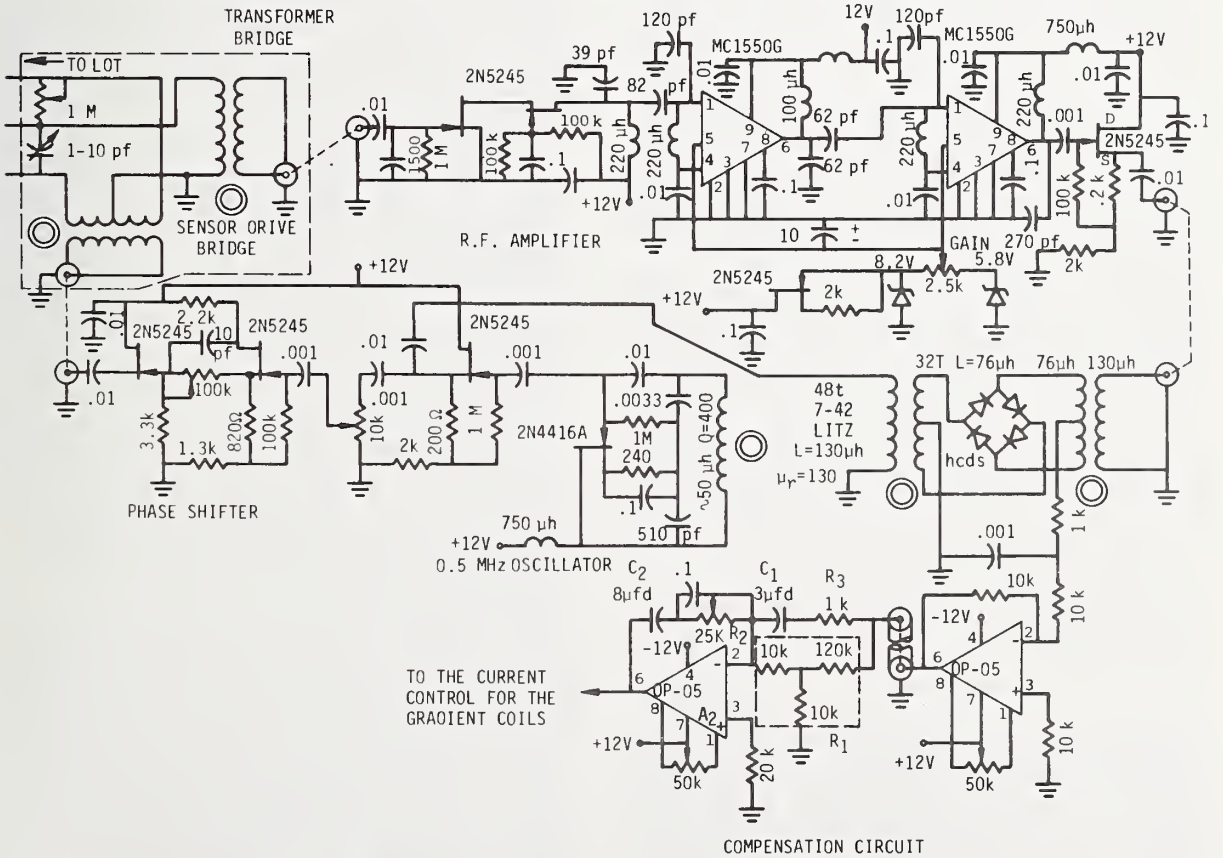

FIG. 4. Position sensor electronics and compensation circuit.

current control amplifier for the main-coil constant-current source is the same as that for the gradient coils.

Perhaps the most interesting part of the support system is the position sensor. In the past, position sensing has been accomplished by either optical[7,8] (light beam–photomultiplier tube arrangement) or electronic[1,9–12] (inductance pickup coil or differential transformer) means. The requirements of small size, low power dissipation, high sensitivity, the ability to withstand high pressure and low temperatures, and exceptional dimensional integrity resulted in the use of a linear differential transformer (LDT) wound on a machinable glass ceramic form. The LDT consists of a pair of coils equally spaced about a transverse rectangular opening in the ceramic form inside which the buoy is suspended. Each coil is wound with 34 turns of double silk-wrapped 50/44 Litz wire in circumferential grooves of 2.8-mm width and 6.1-mm depth. The outside diameter of the coils and the ceramic holder is 17.3 mm. The complete transformer assembly has been potted with a low-viscosity epoxy resin to prevent intrusion of the pressurized fluid into the windings.

The sensitivity of the LDT as measured at the phase-sensitive detector (synchronous detector) is of the order of 1 V/mm. The noise voltage at the sensor amplifier input is less than 10^{-6} V/Hz$^{1/2}$. The operational amplifiers in the compensation circuit have very low offset drifts and are thermally lagged to a large copper block in the amplifier chassis. Consequently, the vertical movement of the buoy due to operational amplifier drifts and rf amplifier noise is less than 10^{-5} mm.

The LDT is the major component of a ratio-transformer-type bridge. Part of the bridge is located at the top of the cryostat and is connected to the LDT through long coaxial lines. The bridge is constructed so as to remove proximity effects of the outer conductors of the coaxial lines. The neutral position of the buoy is controlled by a small variable capacitor between the center lead and one side of the LDT. Conductance balance is achieved with a resistor connected across the capacitor. Unbalance in the LDT due to the inductance of the long leads is minimized by tuning the two halves of the LDT to resonance with matched capacitors (as large as possible for the 0.5-MHz exciting signal). These capacitors are connected near the LDT outside the sample cell but inside the vacuum space.

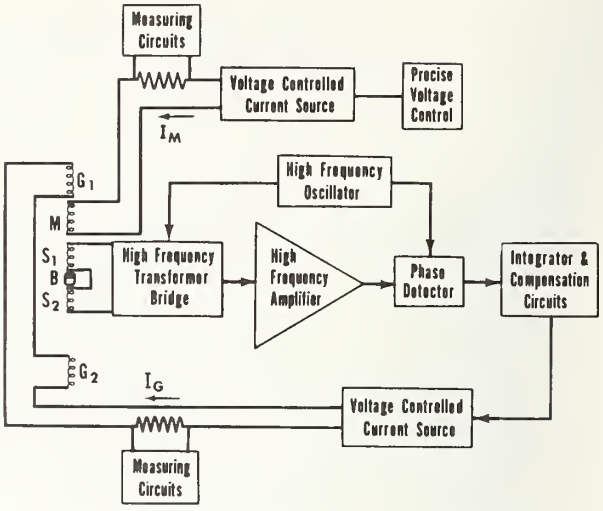

FIG. 5. Block diagram of a magnetic suspension densimeter: G_1, G_2—gradient coils; M—main coil; S_1, S_2—sensing coils; B—magnetic buoy.

IV. EXPERIMENTAL MEASUREMENTS AND PROCEDURES

A. Temperature and pressure

The techniques and instrumentation for the measurement and control of the temperature and pressure are standard. The primary temperature sensor, calibrated on the IPTS 1968, is a platinum resistance thermometer secured in a well at the base of the equilibrium cell with Wood's metal. The calibration of the thermometer has been checked against vapor pressure measurements on liquid methane and nitrogen.

The uncertainty of the calibration is approximately 0.002 K. Due to the specifications of the potentiometric measuring system, uncertainties in the temperature amount to a maximum of 0.010 K at 110 K, increasing to 0.030 K at 300 K. The temperature of the sample holder is controlled to better than 0.005 K, approximately the same as the reproducibility of the temperature measurements.

A current of 1 mA for the thermometer is supplied by an electronic constant current source. The voltage drop across a 100 Ω calibrated standard resistor in series with the thermometer is monitored continuously with a six-digit differential voltmeter. With this setup the uncertainty and repeatability of the current is approximately 0.002%. The voltmeter is checked periodically against a microvolt potentiometer using a calibrated standard cell.

The total uncertainty in the reported temperatures in Sec. VI is believed to be less than 0.03 K. (At room temperature it would be less than 0.04 K.) The 0.03-K total uncertainty consists of approximately 0.025-K systematic error and 0.005-K random error. The systematic error was determined from the uncertainties in the calibration of the thermometer and in the potentiometric measuring system.

The temperature of the cell is regulated by balancing coarsely variable cooling with precisely controlled electric heating. A control heater near the bottom of the cell is connected to a dc power regulator, which is part of a measuring/regulation system that also includes a six-dial microvolt potentiometer and a microvolt amplifier. A second heater at the top of the cell is connected to a manual power supply. Independent heaters at the top and bottom of the cell are used to minimize temperature gradients along the length of the cell.

Temperature gradients are detected by monitoring the vapor pressure of the liquid in the vapor bulb.

Pressures below 7 bars are measured with a 0- to 7-bar spiral quartz Bourdon gauge. This gauge has a resolution of less than 3.5×10^{-4} bar. It has been calibrated against an air dead-weight gauge giving an uncertainty of approximately 0.1% over the full range. For pressures above 7 bars, a double-revolution 0- to 20-bar Bourdon gauge is used. It has also been calibrated against the air dead-weight gauge and can be read to the nearest 0.005 bar.

Vapor pressure measurements have been used in the present work primarily as a means of monitoring temperature gradients. They have also been used as a check against the calibration of the platinum resistance thermometer. In general, the vapor pressures for methane have been consistently lower than those of Prydz and Goodwin.[13] This pressure difference corresponds to a temperature difference of 0.01–0.02 K. The discrepancies between the nitrogen vapor pressures of the present work and those of Wagner[14] correspond to an average temperature difference of less than 0.015 K, with no particular trend observed.

B. Position of buoy

The accuracy and precision of the density measurements depend on being able to suspend the float at the same position relative to the support coils in vacuum and in the test liquid at the same temperature. A 125× filar micrometer microscope is used to determine the position of the float. It has a resolution of approximately 5×10^{-4} mm. The maximum error in the position determination is 2×10^{-3} mm, which corresponds to an error in density of less than 0.03%.

This error includes approximately equal contributions from the alignment of the microscope, so that the "apparent" position of the float is independent of the index of refraction of the fluid inside the sample cell, and from the repositioning of the float for vacuum and liquid measurements. The first contribution would be a systematic error while the second is random. The precision of the density measurements depends primarily on the reproducibility of the position of the buoy from vacuum to liquid measurements.

As mentioned above, the microscope must be aligned so that the "apparent" position of the float does not depend on the index of refraction of the fluid inside the sample cell. In viewing the float inside the cell one must look through the glass tail of the cryostat and the sample holder window. The "apparent" position of the float would be dependent on the refractive index of the fluid inside the cell unless the light rays are perpendicular to the interface between the test liquid and the inside surface of the sample holder window.

The procedure for adjusting or aligning the microscope is as follows. First, the float is positioned at rest on the ceramic holder at the same horizontal position as when in support. Then a fiducial mark on the float is observed under two experimental conditions, i.e., with the float first immersed in gas and then immersed in liquid. Both methane and nitrogen were used to carry out this procedure. During this procedure the microscope tilt is adjusted so that the "apparent" position of the float does not depend on the refractive index of the fluid inside the cell within the resolution of the microscope. The temperature of the cell is controlled to better than 0.01 K during these observations. Care is taken to ascertain that the float is observed through the same parts of the windows as during the density measurements. Necessarily a different part of the float is observed. This presents no special problem since there are diamond tool marks the entire length of the float that can be used as reference lines. This procedure has been repeated frequently during the course of the reported measurements. It has been found that a readjustment of the microscope tilt is necessary only if the apparatus is perturbed by disassembly.

C. Volume of buoy

Absolute density measurements [Eq. (7)] with a magnetic suspension densimeter require a determination of the volume of the magnetic buoy. In the past this has been accomplished either by using distilled water as a reference fluid of known density[15] or by making direct length and diameter measurements on a uniformly constructed float.[1] Here the volume has been determined by the first method.

The volume (0.13485 cm^3 at 300 K) of the magnetic buoy was determined within 0.02%. The distilled water was vacuum distilled to remove air. Any problems with bubbles inside the cell were rectified by pressurizing the water with helium gas. The volume of the buoy has been measured three times at 300 K and once at 290 K. These four measurements gave a standard deviation of 0.005% using thermal expansion data for barium ferrite to calculate the volume change from 290 to 300 K. This resulted in a 99% confidence interval of ±0.015%. The systematic error in the volume determination depends on the uncertainty in the density of water. This should be less than 0.005%.[16]

The present paper reports density data for cryogenic fluids. Thermal expansion data for barium ferrite were used to calculate the volume of the float at low temperatures. Recently the linear thermal expansion of polycrystalline barium ferrite was measured at this laboratory at temperatures from 76 to 293 K with a quartz tube dilatometer.[17] The volume of the float at 100 K is approximately 0.4% less than the room temperature value.

Barium ferrite is somewhat anisotropic and its thermal expansion was measured both parallel and perpendicular to the magnetization direction. An anisotropy of 15–20% was observed. The estimated overall uncertainty of the thermal expansion measurements would correspond to an error of 6% in the adjustment to the volume. This would produce an uncertainty of approximately

0.02% in the volume at 120 K. The uncertainty in the adjustment to the volume due to the contraction of the copper plating is negligible.

The effect of pressure on the volume of the float is negligible at the highest pressures encountered in the present work. The bulk modulus for barium ferrite should be less than that for copper, which is 1.35×10^{11} Pa.[18] This value would correspond to a volume correction of approximately 0.001% at 2.5 MPa, the vapor pressure of nitrogen at 120 K.

D. Mass of buoy

The mass of the magnetic buoy was determined with a 10-g capacity equal-arm microbalance. A calibrated class M weight set was used in the weighings. Precautions were taken to assure that the copper plating and gold protective coating provided an impervious barrier to liquids under pressure. The buoy was rapidly cycled between room temperature and 76 K. It was then immersed in liquid ethanol at 5-atm pressure and room temperature for 4 h. The buoy was weighed twice after removal from the ethanol bath. The average of these weighings was 9 μg higher than the mean of the initial four weighings. A significantly larger increase in the mass was expected if the plating on the float contained a pinhole that allowed ethanol to penetrate into the porous ceramic. Thus, at room temperature, the metallic coating appeared to be impervious after thermal cycling. The reproducibility of liquid methane density measurements (see experimental results) after many cycles between room temperature and 100–140 K is further evidence of the resistance of the metallic coatings to damage from thermal cycling.

The final mass of the magnetic buoy (0.73706 g) was taken as the mean of all weighings, including the weighings after immersion in ethanol, corrected for air buoyancy. A 99% confidence interval for the six weighings, based on a standard deviation of 6 μg, was ± 10 μg. The systematic error in the mass determination, resulting primarily from the weight set calibration, is believed to be less than 5 μg.

V. EVALUATION OF PERFORMANCE OF MAGNETIC SUSPENSION DENSIMETER

A. Performance tests

The use of Eq. (7) for obtaining absolute densities has again been verified experimentally[1]. The gradient coil current has been measured as a function of the main coil current over a range of approximately 20% of the maximum main coil current. These measurements were carried out while supporting the float in a given fluid (including vacuum) at constant height at a fixed temperature. The various pairs of I_M and I_G were fitted by the method of least squares to Eq. (7). The residual standard deviation, with the gradient coil current as the dependent variable, was less than 10^{-5} A. Examination of the residuals showed that they were random and well approximated by a normal probability distribution. These results demonstrated that within the precision of the current measurements the magnetic moment of the barium ferrite float is independent of the magnetic field intensity over the range of fields (0.006–0.016 T) considered in the present work.

Other coil configurations have been tried that gave results that substantiated the observations given above. First the bottom gradient coil was disconnected resulting in a two-coil system. The values of the constant (C) in Eq. (7) for the two- and three-coil arrangements under otherwise identical experimental conditions were in agreement within the experimental uncertainty. In other words, the magnetic moment of the float (contained in C) remains constant for significantly different magnetic field intensities.

Next the pair of approximately identical (gradient) coils were connected to the constant current source in a Helmholtz arrangement. The main coil was connected into the servosystem. The float was first supported at a constant height at fixed temperature by the force supplied by only the main coil. The float was located at the midpoint of the Helmholtz coils while the current in the Helmholtz coils was increased to 0.6 A. There was an insignificant change in the main coil current (10^{-4} A) for this relatively enormous change in the magnetic field intensity (about an order of magnitude more than for the typical data point). The results of these tests demonstrated that this technique could be used for absolute density measurements.

In carrying out density measurements with this technique, the position of the main coil must remain fixed over a wide range of currents for the vacuum and liquid measurements. This means that the "constant" k' in Eq. (4) and the constants, C and D, in Eq. (7) must be independent of the current in the coil. It was hoped that the measures exercised in controlling the temperature and position of the main coil (see Sec. III D) would result in such behavior. It was experimentally impracticable to determine if k' was a constant by monitoring the position of the coil. However, the effect of a change in the current in the main coil on the density measurements could be obtained in another manner. As shown in Sec. II the fluid density is linearly proportional to the current in the gradient coils if the main coil current is held constant. Not only is the position of the main coil fixed, but also the magnetic field intensity at the midpoint of the gradient coils (float position) is constant. Relative measurements [Eq. (5)] carried out with vacuum, nitrogen, methane, and propane at 110 K were not consistent with the density ratios computed from absolute measurements [Eq. (7)] for the same fluids. These results showed that the "constants" (k', C, and D) vary slightly with the main coil current. This variation produces a density error relative to the difference between main coil currents for vacuum and liquid measurements (constant I_G) of approximately 1.4%/A. This corresponds to a density adjustment of 0.1–0.2%/(g/cm^3) to the results from Eq.

TABLE II. Estimated uncertainties in density measurements.

Systematic errors	Percent error in density					
	Methane		Nitrogen		Normal butane	
	105 K	160 K	95 K	120 K	135 K	300 K
Mass of float (Sec. IV D)	±0.002	±0.002	±0.002	±0.002	±0.002	±0.002
Volume of float at 300 K (Sec. IV C)	±0.02	±0.02	±0.02	±0.02	±0.02	±0.02
Thermal expansion coefficient of barium ferrite (Sec. IV C)	±0.022	±0.017	±0.023	±0.021	±0.020	±0.001
Position of float (Sec. IV B)	±0.015	±0.018	±0.010	±0.012	±0.009	±0.009
Position of main coil, determined from relative measurements, Eq. (5) (Sec. V A)	±0.02	±0.02	±0.02	±0.02	±0.02	±0.02
Temperature of sample fluid (Sec. IV A)	±0.010	±0.021	±0.023	±0.076	±0.004	±0.008
Three times standard deviation	±0.045	±0.054	±0.030	±0.036	±0.027	±0.027
Total uncertainty[a]	±0.09	±0.10	±0.07	±0.12	±0.06	±0.06

[a] The total uncertainty was determined from the square root of the sum of the squares of the systematic errors added to three times the standard deviation.

(7). Since all measurements are based on the volume determination using distilled water as a reference fluid of known density, the adjustment must be applied relative to this point.

A further check on this density-dependent adjustment was accomplished by measuring the densities of two other fluids of known density at room temperature. The densities of liquid samples of normal pentane and ethanol were determined by the Mass and Volume Section of the Mechanics Division of the National Bureau of Standards in Washington, DC, to an estimated inaccuracy of less than 0.01%. Measurements on these fluids at 300 K with the present apparatus using Eq. (7), combined with the adjustment based on the relative density measurements at low temperature, gave densities that agreed with the reference values to better than 0.02%. Thus, the densities presented in this paper based on absolute measurements [Eq. (7)] have been adjusted slightly to be consistent with the results of relative measurements [Eq. (5)]. The density difference between the relative and absolute measurements, expressed in terms of the difference in main coil currents between the vacuum and liquid points ($I_v - I_f$) for a constant gradient coil current, is independent of temperature. The temperature dependence of the magnetic moment of the float must be included if the difference is expressed in terms of density.

The relative measurements were carried out using the same experimental setup and parameters (mass, volume, and position) as the absolute measurements. Thus the total uncertainty in the adjustment determination should only include the random error in the measurement process. Thus an estimated uncertainty of ±0.02% in the adjustment is based on the comparisons with the reference fluids since this density difference was larger than a 99% confidence interval from a fit of the differences between relative and absolute measurements.

TABLE III. Experimental results for saturated liquid nitrogen (molecular weight = 28.0134).

T (K)	ρ_{exp} (mol/l)	ρ_{calc} (mol/l)	$\frac{100(\rho_{exp} - \rho_{calc})}{\rho_{calc}}$
95.000	25.6731	25.6755	−0.009
100.000	24.6400	24.6391	0.004
105.000	23.4998	23.4988	0.005
110.000	22.2079	22.2071	0.004
115.000	20.6719	20.6748	−0.014
120.000	18.6818	18.6856	−0.020
100.000	24.6361	24.6391	−0.012
105.000	23.4963	23.4988	−0.011
110.000	22.2044	22.2071	−0.012
115.000	20.6787	20.6748	0.019
120.010	18.6800	18.6808	−0.004
95.075	25.6624	25.6605	0.007
100.075	24.6207	24.6229	−0.009
100.075	24.6279	24.6229	0.020
105.075	23.4841	23.4807	0.015
110.075	22.1840	22.1862	−0.010
115.075	20.6490	20.6492	−0.001
117.575	19.7356	19.7326	0.015
120.075	18.6525	18.6497	0.015

B. Error analysis

Evaluation of the experimental parameters involved in the present work showed that the uncertainty in the density measurements depends primarily on the uncertainties in the determination of the volume of the float, the relative position of the float and the main coil, and the temperature of the sample fluid. The precision of the density measurements is inversely proportional to the difference between the density of the fluid and the density of the float. This variation with density cannot be observed for the measurements reported in this paper because of the density range covered. The precision also varies with temperature, corresponding to the change in the magnetic moment of the float with temperature.

Table II summarizes the uncertainties in the density measurements for the nitrogen and methane results presented in this paper. Normal butane is also included in this table, primarily to show the performance of the instrument at higher temperatures. Normal butane densities, determined with this instrument at tempera-

tures between 135 and 300 K, will be presented in a forthcoming paper.

The standard deviation given in the table for methane at 105 K was based on twelve measurements. The other standard deviations were computed relative to the density and temperature of this point. Standard deviations at the other temperatures and densities could not be estimated from statistical analysis since sufficient repetitive measurements were not taken for these points. Measurements on more dense fluids, such as argon and krypton, have demonstrated the expected variation of the precision with density. Measurements near room temperature, especially those on distilled water, have exhibited the expected improvement in the precision as the temperature is increased.

The total uncertainty of a single density measurement was taken as the square root of the sum of the squares of the systematic errors plus an allowance of three times the standard deviation for random error.

VI. EXPERIMENTAL RESULTS

A. Nitrogen

The experimental saturated liquid densities for nitrogen are presented as a function of temperature (IPTS 1968) in Table III. The explanation for some of the nitrogen points not being at integral temperatures involves the presence of a temperature gradient along the length of the cell in some of the initial measurements with this apparatus. Each of the data points was taken from a new charge of nitrogen. For each datum point the vacuum measurements were carried out immediately before or after the liquid measurements. The same procedure was used for methane. The three data sets for nitrogen over the temperature range of 95– or 100–120 K were obtained at approximately six-month intervals. Of the two data sets at integral temperatures, one was taken with methane, and the other with nitrogen, in the vapor bulb. The third set was taken with no liquid in the vapor bulb. (For the 120.010-K point a slight temperature gradient was applied to remove bubbles from the sample liquid inside the cell.)

The nitrogen samples were taken from commercially available, research grade gas. A purity specification of 99.99 mol% was given by the supplier. The gas has been analyzed chromatographically with a thermal conductivity detector and found to be within the specified purity. The nitrogen gas was passed through a room temperature molecular sieve trap, primarily for removal of water.

The saturated liquid densities (ρ) of nitrogen have been fitted as a function of temperature (T) by the method of least squares to an equation of the following form:

$$\rho - \rho_c = a\left(1 - \frac{T}{T_c}\right)^{0.35} + \sum_{i=1}^{3} b_i \left(1 - \frac{T}{T_c}\right)^{1+(i-1)/3}. \quad (9)$$

TABLE IV. Parameters of Eq. (9) for nitrogen.

a =	19.39217[a] (0.11)[b]	b_3 =	23.32977 (4.8)	ρ_c =	11.21 mol/l
b_1 =	26.01408 (2.5)	T_c =	126.20 K	σ =	0.016%
b_2 =	−39.49759 (6.5)				

[a] These coefficients (a, b_1, b_2, b_3) and those in Table VI were obtained from a least-squares program in which the experimental densities in g/cm³ to five digits were converted to molar densities within the program.

[b] Standard errors of coefficients in parentheses.

ρ_c and T_c are selected values of the critical density and temperature and a, b_i are coefficients determined by least squares. Equation (9) consists of a scaling law modification[19] to a generalized Guggenheim equation.[20] The parameters of Eq. (9) for nitrogen, along with the residual standard deviation (σ) of the fit and the standard errors of the coefficients, are given in Table IV. The standard errors of the calculated densities in Table III are not presented since they are significantly smaller than the standard deviation. The main purpose of the above expression is to facilitate comparisons with independent measurements. The choice of the critical point parameters is arbitrary in the sense that the critical point density can be varied by as much as 5% and the critical point temperature by 0.2% without changing the fit of the data within the estimated precision of the present measurements. For nitrogen the critical point values were obtained from the PVT data compilation of Jacobsen[21].

In Fig. 6 independent experimental data available in the literature are compared with the expression representing the present nitrogen data over the temperature range of the present measurements. The present data are also shown. The experimental temperatures

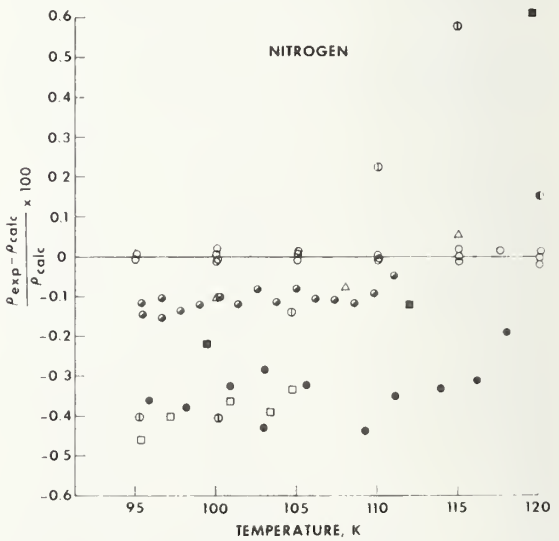

FIG. 6. Deviation plot of experimental densities of saturated liquid nitrogen compared with values calculated from Eq. (9) using parameters from Table IV: ○ present data, ◕ Brauns,[22] ◐ Weber,[23] △ Rodosevich and Miller,[24] ● Goldman and Scrase,[25] □ Terry *et al.*,[26] ⊕ Streett and Staveley,[27] ■ Mathias *et al.*[28]

TABLE V. Results for saturated liquid methane (molecular weight = 16.04303).

Temperature (K)	Mean density (mol/l)	Standard deviation (%)	Number of data points
105.000	26.9458	0.015	12
110.000	26.4985	0.019	11
115.000	26.0443	0.014	12
120.000	25.5721	0.016	17
125.000	25.0845	0.016	18
130.000	24.5775	0.017	16
135.000	24.0540	0.016	23
140.000	23.5067	0.018	5
145.000	22.9312	0.014	5
150.000	22.3218	—	2
160.000	20.9876	—	2

of other measurements have not been adjusted to the temperature scale of the present results.

The data of Brauns,[22] Weber,[23] and Rodosevich and Miller,[24] each obtained with a technique different from that used here, fall within 0.15% of the present results. The densities of Goldman and Scrase[25] and Terry *et al.*[26] are consistently lower than the present results by approximately 0.3–0.4%. This pattern is also followed for methane by Terry *et al.*, and preliminary analysis of recent results for argon and krypton obtained with the magnetic suspension densimeter indicate comparisons with Terry *et al.*, for these fluids exhibit the same behavior.

B. Methane

Methane has been used as a control fluid throughout the entirety of a project that has included density measurements on six pure fluids and, at least, thirty mixtures of these components. As a result, well over one hundred data points have been accumulated for saturated liquid methane, primarily in the temperature range 105–150 K. Although these experimental data are not presented in this paper, the results of an analysis of the methane data are helpful in evaluating the performance of the magnetic suspension densimeter used in the present work. More than ten data points were obtained at each 5-K interval between 105 and 135 K. The mean of the experimental densities, along with the standard deviation and the number of points at each temperature, are given in Table V. (The standard deviations are not given at 150 and 160 K since there are only two data points at each of these temperatures.) Each of the data points represents a new methane sample. The vapor bulb contained liquid methane for all points.

TABLE VI. Parameters of Eq. (9) for methane.

a =	18.65812 (0.035)[a]	T_c =	190.555 K
b_1 =	6.712030 (0.21)	ρ_c =	10.16 mol/l
b_2 =	−0.9472020 (0.20)	σ =	0.016%

[a] Standard errors of coefficients in parentheses.

The liquid samples were obtained from either of two cylinders of different batches of commercial, research grade methane. The purity for each cylinder as specified by the supplier is 99.99 mol% minimum. Analyses in this laboratory substantiated these specifications. As with nitrogen the methane gas was passed through a room temperature molecular sieve trap to remove moisture and any heavy contaminants not detected by analysis.

The 123 experimental data points have been fitted by the method of least squares to Eq. (9). Only three coefficients were needed to fit the methane data within the precision of the measurements. The fourth term in the equation was not statistically significant. The coefficients of Eq. (9), the standard errors of the coefficients, the residual standard deviation (σ) of the fit, and a selected critical density[29] and temperature[30] are given in Table VI for methane. Equation (9), with the coefficients for methane, has been used to compare the present results with experimental data from independent investigators. The methane data from the present work are not shown on the deviation plot because of the large number of points. All of the experimental densities of methane obtained in the present work will be presented in tabular form in a future publication.

For saturated liquid methane there have been considerably more measurements than for saturated liquid nitrogen. All of the other measurements were obtained with techniques different from that of the present work. Some of the older, less precise data have been included in Fig. 7 for the sake of completeness. It is satisfying that the relatively recent data of Orrit and Olives,[31] McClune,[32] Goodwin and Prydz,[33] and Shana'a and

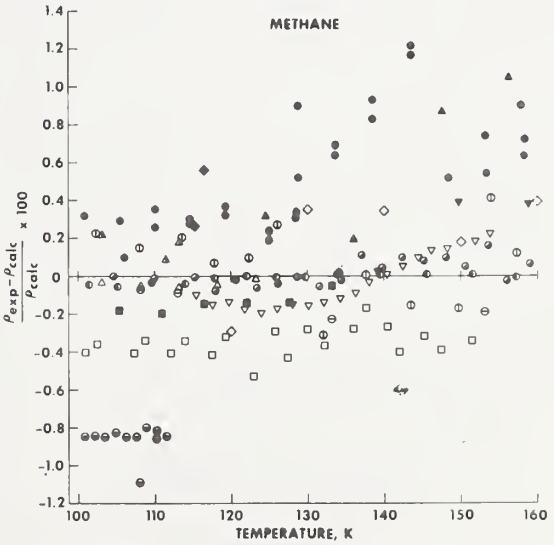

FIG. 7. Deviation plot of experimental densities of saturated liquid methane compared with values calculated from Eq. (9) using parameters from Table VI: □ Terry *et al.*,[26] ◕ Orrit and Olives.[31] △ McClune,[32] ◐ Goodwin and Prydz,[33] ⊗ Shana'a and Canfield,[34] ▼ Vennix,[35] ⓘ Grigor,[36] ▽ Davenport *et al.*,[37] ■ Klosek and McKinley,[38] ⊖ Sinor and Kurata,[39] ▲ Jensen and Kurata,[40] ▲ Bloomer and Parent,[41] ◒ Fuks *et al.*,[42] ● Keyes *et al.*,[43] ◆ Moran,[44] ◇ Van Itterbeek *et al.*[45]

Canfield[34] agree with the present results within 0.1%. However, as mentioned earlier, the densities of Terry *et al.*[26] are systematically lower than the present results by 0.3–0.4%. The extrapolated densities of Vennix[35] at approximately 150 and 160 K are 0.4% larger than the present results although the discrepancy at 140 K is approximately 0.01%.

C. Other fluids

To demonstrate the performance of the magnetic suspension densimeter at low temperature, this paper presents only a representative cross section of the data that have been taken in the present work. Data have recently been obtained for other pure fluids (ethane, propane, isobutane, normal butane, argon, and krypton) over a density range extending to 2.3 g/cm^3 (krypton) and over a temperature range extending to 300 K (isobutane and normal butane). These data will be published in the near future.

ACKNOWLEDGMENTS

The authors would like to express their appreciation to the following individuals who have made significant contributions to the development of this apparatus. M. R. Cines of Phillips Petroleum Co., Chairman of the LNG Density Project Steering Committee, was instrumental in the development of support for this project. W. G. Layne, D. L. Smith, and A. N. DiSalvo assisted in the design and fabrication of the apparatus. J. E. Cruz designed some of the electronics associated with the refrigeration and temperature control systems. J. R. Whetstone determined the densities of liquid samples of normal pentane and ethanol, which were used as reference fluids. P. V. Tryon assisted with the statistical analysis of the data.

This work was carried out at the National Bureau of Standards under the sponsorship of British Gas Corp., Chicago Bridge and Iron Co., Columbia Gas Service Corp., Distrigas Corp., Easco Gas LNG, Inc., El Paso Natural Gas, Gaz de France, Marathon Oil Co., Mobil R and D Corp., Natural Gas Pipeline Co., Phillips Petroleum Co., Shell International Gas, Ltd., Sonatrach, Southern California Gas Co., Tennessee Gas Pipeline, Texas Eastern Transmission Co., Tokyo Gas Co., Ltd., and Transcontinental Gas Pipe Line Corp., through a grant administered by the American Gas Association, Inc.

[1] W. M. Haynes and J. W. Stewart, Rev. Sci. Instrum. **42,** 1142 (1971).
[2] J. W. Beams, Rev. Sci. Instrum. **40,** 167 (1969).
[3] R. M. McClintock and M. J. Hiza, Mod. Plast. **35,** 172 (1958).
[4] The use of a trade name for clarity and completeness does not signify an endorsement or recommendation by the National Bureau of Standards.
[5] J. B. Breazeale, Ph.D. thesis, University of Virginia (1955).
[6] H. S. Morton, Jr., Ph.D. thesis, University of Virginia (1953).
[7] J. P. Senter, Rev. Sci. Instrum. **40,** 334 (1969).
[8] J. W. Beams, C. W. Hulburt, W. E. Lotz, Jr., and R. M. Montague, Jr., Rev. Sci. Instrum. **26,** 1181 (1955).
[9] S. P. Almeida and T. H. Crouch, Rev. Sci. Instrum. **42,** 1344 (1971).
[10] M. G. Hodgins and J. W. Beams, Rev. Sci. Instrum. **42,** 1455 (1971).
[11] J. L. Hales, J. Phys. E **3,** 855 (1970).
[12] S. C. Greer, M. R. Moldover, and R. Hocken, Rev. Sci. Instrum. **45,** 1462 (1974).
[13] R. Prydz and R. D. Goodwin, J. Chem. Thermodyn. **4,** 127 (1972).
[14] W. Wagner, Cryogenics **13,** 470 (1973).
[15] J. W. Beams and A. M. Clarke, Rev. Sci. Instrum. **33,** 750 (1962).
[16] M. Menaché and G. Girard, Metrologia **9,** 62 (1973).
[17] A. F. Clark, W. M. Haynes, V. A. Deason, and R. J. Trapani, Cryogenics **16,** 267 (1976).
[18] G. Simmons and H. Wang, *Single Crystal Elastic Constants and Calculated Aggregate Properties: A Handbook* (MIT Press, Cambridge, MA, 1971), p. 181.
[19] R. D. McCarty, Natl. Bur. Stand. (U.S.) Intern. Rept. 74-357 (1974).
[20] Y. C. Hou and J. J. Martin, AIChE J. **5,** 125 (1959).
[21] R. T. Jacobsen, Ph.D. thesis, Washington State University (1972).
[22] P. Brauns (private communication, 1973).
[23] L. A. Weber, J. Chem. Thermodyn. **2,** 839 (1970).
[24] J. B. Rodosevich and R. C. Miller, AIChE J. **19,** 729 (1973).
[25] K. Goldman and N. G. Scrase, Physica **44,** 555 (1969).
[26] M. J. Terry, J. T. Lynch, M. Bunclark, K. R. Mancell, and L. A. K. Staveley, J. Chem. Thermodyn. **1,** 413 (1969).
[27] W. B. Streett and L. A. K. Staveley, Adv. Cryog. Eng. **13,** 363 (1968).
[28] E. Mathias, H. K. Onnes, and C. A. Crommelin, Commun. Leiden **145C,** 19 (1914).
[29] J. D. Olson, J. Chem. Phys. **63,** 474 (1975).
[30] R. D. Goodwin, Natl. Bur. Stand. (U.S.) Tech. Note No. 653 (1974).
[31] J. Orrit and J. Olives, distributed at 4th International Conference on Liquefied Natural Gas, Algeria (1974).
[32] C. R. McClune, Cryogenics **16,** 289 (1976).
[33] R. D. Goodwin and R. Prydz, J. Res. Natl. Bur. Std. (U.S.) **76A,** 81 (1972).
[34] M. Y. Shana'a and F. B. Canfield, Trans. Faraday Soc. **64,** 2281 (1968).
[35] A. J. Vennix, Ph.D. thesis, Rice University (1965).
[36] A. F. Grigor, Ph.D. thesis, Pennsylvania State University (1966).
[37] A. J. Davenport, J. S. Rowlinson, and G. Saville, Trans. Faraday Soc. **62,** 322 (1966).
[38] J. Klosek and C. McKinley, Proceedings of the First International Conference on LNG, Chicago (1968), Paper 22.
[39] J. E. Sinor and F. Kurata, J. Chem. Eng. Data **11,** 1 (1966).
[40] R. H. Jensen and F. Kurata, J. Petrol. Technol. **21,** 683 (1969).
[41] O. T. Bloomer and J. D. Parent, Chem. Eng. Progr. Symp. Ser. **49,** 11 (1952).
[42] S. Fuks, J. C. Legros, and A. Bellemans, Physica **31,** 606 (1965).
[43] F. G. Keyes, R. S. Taylor, and L. B. Smith, J. Math. Phys. **1,** 211 (1922).
[44] D. W. Moran, Ph.D. thesis, Imperial College, University of London (1959).
[45] A. Van Itterbeek, O. Verbeke, and K. Staes, Physica **29,** 742 (1963).

Simplified magnetic suspension densimeter for absolute density measurements*

W. M. Haynes

National Bureau of Standards, Institute for Basic Standards, Boulder, Colorado 80302

(Received 24 September 1976)

A magnetic suspension densimeter, incorporating three support coils, has been reduced to a system using only one coil. This simplifies considerably the design of the apparatus and the procedures involved in the measurements. This instrument can be used for absolute density measurements; i.e., it does not have to be calibrated with reference fluids of known density.

During the past two decades the magnetic suspension densimeter[1-17] has evolved into a versatile research instrument that has been used routinely for liquid density measurements to a precision of ten parts per million. (Reference 14 presents a detailed review of the principles, applications, and development of the magnetic densimeter.) In the original design (Fig. 1) of the instrument a piece of soft ferromagnetic material is suspended in a fluid of unknown density by the magnetic force produced by a single solenoid. The magnetic force on the buoy is given by the relation

$$F_{\text{mag}} = M \frac{dH}{dZ}, \tag{1}$$

where M is the magnetic moment of the buoy, H is the axial magnetic field intensity of the air core solenoid, and Z is the distance along the vertical. The density (ρ) of the fluid is related to the current (I) in the support coil by

$$\rho = A + BI^2, \tag{2}$$

where A and B are constants to be determined by calibration of the instrument with reference fluids of known density. The above relation is based on the assumption that the magnetic moment of the buoy is linearly proportional to the magnetic field intensity.

It is not unusual for the magnetic susceptibility of the magnetically soft material of the buoy to vary slowly with H. Thus a relatively large number of reference fluids are required to calibrate a one-coil instrument to maintain a given precision over its entire operating range. The precision is inversely proportional to the difference between the density of the fluid and the density of the buoy. To cover an extended density range it is necessary to construct and calibrate buoys of different densities. The calibration of the instrument must be checked periodically to test the buoy material for hysteresis.

These procedural tasks were reduced considerably with the development of a three-coil support system[5] (Fig. 2) which allows variations in dH/dZ while H is held constant. The three-coil arrangement consists of a main coil, which supplies the major part of the force necessary to support the buoy, and a pair of gradient coils connected in such a way that at the buoy position their magnetic fields cancel and their magnetic field gradients add. The magnetic moment of the buoy is held constant; it depends only on the stability of the constant current source that supplies the main coil current. In the first applications of the three-coil arrangement (with a magnetically soft buoy) the instrument still had to be calibrated but now the density range for a given buoy was increased significantly over that for a single-coil system. Also the calibration was simplified since the density was linearly proportional to the current in the gradient coils for a constant main coil current. The buoy may be either magnetically soft or hard for the three-coil system.

Recently, in the adaptation of the magnetic suspension densimeter for use at low temperatures,[11,17] the same three-coil arrangement (Fig. 2) was employed to determine the force on a magnetic material in a nonuniform field; i.e., it was used to determine the variation of the magnetic susceptibility of the buoy material with H over the range of magnetic fields needed for the density measurements. It was found that the magnetic force on a barium ferrite buoy could be represented by the expression

$$F_{\text{mag}} = M\left(\frac{dH_M}{dZ} + \frac{dH_G}{dZ}\right) = CI_M + DI_G, \tag{3}$$

where the subscripts denote the main and gradient coils.

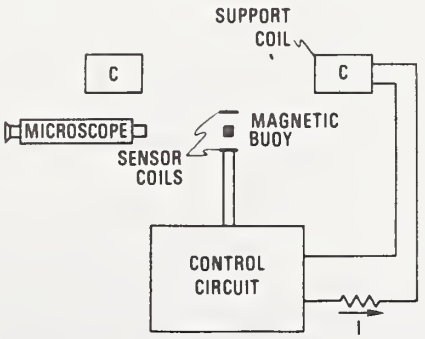

FIG. 1. Schematic diagram of a magnetic suspension densimeter with one support coil.

This result demonstrated that, over the range of magnetic fields considered (0.006–0.016 T), there was no induced moment in the barium ferrite buoy (a magnetically hard material with a permanent moment). Therefore, it was possible to determine fluid densities without the use of calibration fluids. The instrument constants [C, D in Eq. (3)] could be determined from measurements of the gradient coil current as a function of the main coil current while the buoy was supported at a fixed position at constant temperature in vacuum. The mass and volume of the buoy must be determined from independent measurements.

Now that it had been determined with the three-coil arrangement (Fig. 2) that the magnetic moment of the barium ferrite buoy was independent of the magnetic field strength over the range of magnetic fields needed for the desired density measurements, the instrument could be simplified considerably by reducing to a one-coil system (Fig. 1). The magnetic force on the buoy depended only on the magnetic field gradient (dH/dZ) and not on the magnetic field intensity (H). Thus the single (main) coil was connected into the servosystem and the gradient coils were eliminated.

It should be noted that a one-coil system can be used for absolute density measurements as long as the variation in the magnetic moment of the buoy with magnetic field intensity is known. This information could be obtained by techniques other than that used in the present work, e.g., a vibrating sample magnetometer. This is mentioned to emphasize that, with a knowledge of $M(H)$ of the magnetic buoy material, the initial apparatus design could be simplified significantly with the use of only one coil.

To carry out density measurements with the one-coil system with a barium ferrite buoy, first the current necessary to support the buoy in vacuum (I_V) at a given position and temperature must be determined. Then the current necessary to support the buoy in a liquid (I_f) of unknown density at the same position and temperature is measured. The density of the fluid is related to this current ratio by

$$\rho = \frac{m}{V}\left(1 - \frac{I_f}{I_v}\right), \tag{4}$$

where m and V are the mass and volume of the buoy. It should be emphasized that no reference fluids are required for calibration of the one-coil system (or the three-coil system) used in the present work. However, the volume of the float may best be determined near room temperature using distilled water as a reference fluid of known density and, in fact, this procedure was used in the present work.[17]

There are several obvious advantages of the one-coil system over one using three coils; most are involved with the experimental design and procedures. With elimination of the two gradient coils and the alignment problems associated with them, the design and construction of the apparatus are much simpler. The constant current source is no longer needed. The

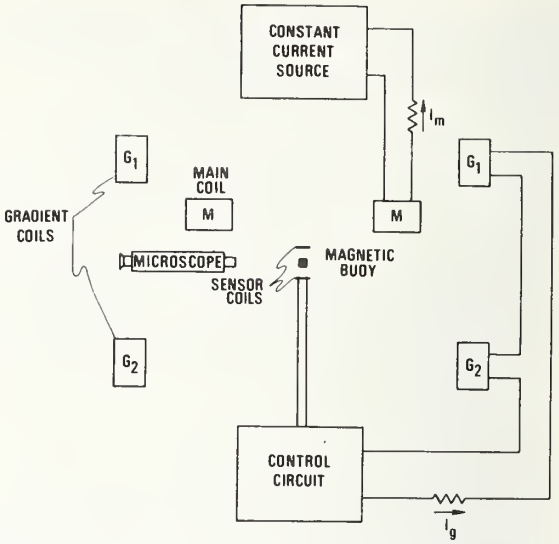

FIG. 2. Schematic diagram of a magnetic suspension densimeter with three support coils.

vacuum points for a single-coil system require only a single current measurement, while those for a three-coil system require a series of measurements of I_M and I_G while holding the buoy at a fixed position. Then the currents must be fitted by the method of least squares to Eq. (3) to obtain the instrument constants. Also the error analysis is less complicated with a one-coil system.

There is one inherent disadvantage in the method for obtaining absolute densities with either the one-coil or three-coil systems where the magnetic force depends only on dH/dZ. The change in dH/dZ with position is significantly larger than the change in the product of H and dH/dZ with position. Thus a very precise determination (10^{-3} mm) of the separation distance of the main coil and buoy was required in the present work and has been described in Ref. 17.

Experimental densities have been determined for saturated liquid argon and methane at temperatures between 100 and 120 K with both the three-coil and one-coil systems. The results agreed within the imprecision of the measurements, which was approximately 0.015% for methane and 0.005% for argon. Thus the simpler one-coil system is now utilized for all density measurements with the present instrument.

The servosystem that is used with the single coil was originally connected to the gradient coils in the three-coil system. No modifications to the servosystem as described in Ref. 17 were required for its use with the single coil.

The present series of density measurements in this laboratory with the magnetic suspension densimeter represented a nontypical use of the instrument. In the past the instrument has been used for highly precise (usually less than 0.001%) measurements over a short density range at a single temperature. Here a relatively modest precision (less than 0.02%) was the result of

measurements over large density (0.3–2.3 g/cm^3) and temperature (95–300 K) ranges with a single buoy. The total uncertainty of the present measurements was approximately 0.1%.

In order to obtain the highest precision and accuracy with the present instrument it was necessary to perform vacuum measurements immediately before or after the liquid measurements. The possible use of the instrument without repeating the vacuum measurements for each datum point has been investigated. In other words the precision and accuracy of the instrument has been estimated, based on a single series of vacuum measurements as a function of temperature at the beginning (and/or end) of a set of density measurements without regard to the temperature and magnetic field cycling of the buoy. The separation distance of the coil and the buoy must be maintained throughout the set of measurements.

In the present setup the position of the main coil was fixed as described in Ref. 17. The position of the float was determined with a 125× microscope and the buoy could be returned to a desired position either electronically or mechanically. Over a period of several months during the course of density measurements at low temperatures on several different fluids, the sample cell was cycled between approximately 100 to 130 K and 300 K more than twenty times. The standard deviation of the vacuum measurements at low temperatures was of the order of 0.05% with no systematic trend observed. This was a measure of the thermal hysteresis of the magnetic moment of the barium ferrite buoy over rather large temperature cycles. This result demonstrated that densities with a total uncertainty of approximately 0.2% could be expected without repeating vacuum measurements for each datum point. Thus, for density data in which the highest precision and accuracy are not required, the use of a one-coil system and a barium ferrite buoy would result in a relatively simple and efficient measurement process that requires few vacuum measurements.

* This work was carried out at the National Bureau of Standards under the sponsorship of British Gas Corp., Chicago Bridge and Iron Co., Columbia Gas Service Corp., Distrigas Corp., Easco Gas LNG, Inc., El Paso Natural Gas, Gaz de France, Marathon Oil Co., Mobil R and D Corp., Natural Gas Pipeline Co., Phillips Petroleum Co., Shell International Gas, Ltd., Sonatrach, Southern California Gas Co., Tennessee Gas Pipeline, Texas Eastern Transmission Co., Tokyo Gas Co., Ltd., and Transcontinental Gas Pipe Line Corp., through a grant administered by the American Gas Association, Inc.

[1] J. W. Beams, C. W. Hulburt, W. E. Lotz, Jr., and R. M. Montague, Jr., Rev. Sci. Instrum. **26**, 1181 (1955).
[2] J. W. Beams and A. M. Clarke, Rev. Sci. Instrum. **33**, 750 (1962).
[3] A. M. Clarke, D. W. Kupke, and J. W. Beams, J. Phys. Chem. **67**, 929 (1963).
[4] D. V. Ulrich, D. W. Kupke, and J. W. Beams, Proc. Nat. Acad. Sci. U.S.A. **52**, 349 (1964).
[5] J. W. Beams, Rev. Sci. Instrum. **40**, 167 (1969).
[6] J. P. Senter, Rev. Sci. Instrum. **40**, 334 (1969).
[7] P. F. Fahey, D. W. Kupke, and J. W. Beams, Proc. Nat. Acad. Sci. U.S.A. **63**, 548 (1969).
[8] A. M. Wims, D. McIntyre, and F. Hynne, J. Chem. Phys. **50**, 616 (1969).
[9] R. Goodrich, D. F. Swinehart, M. J. Kelly, and F. J. Reithel, Anal. Biochem. **28**, 25 (1969).
[10] J. L. Hales, J. Phys. E **3**, 855 (1970).
[11] W. M. Haynes and J. W. Stewart, Rev. Sci. Instrum. **42**, 1142 (1971).
[12] S. P. Almeida and T. H. Crouch, Rev. Sci. Instrum. **42**, 1344 (1971).
[13] M. G. Hodgins and J. W. Beams, Rev. Sci. Instrum. **42**, 1455 (1971).
[14] D. W. Kupke and J. W. Beams, Methods Enzymol. **26**, 74 (1973).
[15] S. C. Greer. M. R. Moldover, and R. Hocken, Rev. Sci. Instrum. **45**, 1462 (1974).
[16] S. C. Greer, T. E. Block, and C. M. Knobler, Phys. Rev. Lett. **34**, 250 (1975).
[17] W. M. Haynes, M. J. Hiza, and N. V. Frederick, Rev. Sci. Instrum. **47**, 1237 (1976).

MEASUREMENTS OF THE ORTHOBARIC LIQUID DENSITIES OF METHANE, ETHANE, PROPANE, ISOBUTANE, AND NORMAL BUTANE[a]

by

W. M. Haynes and M. J. Hiza

Cryogenics Division
National Bureau of Standards
Institute for Basic Standards
Boulder, Colorado 80302

Send proofs to: W. M. Haynes
Cryogenics Division, 275.02
National Bureau of Standards
Boulder, Colorado 80302

Short Title: Liquid Densities of CH_4, C_2H_6, C_3H_8, iC_4H_{10}, and nC_4H_{10}

[a]This work was carried out at the National Bureau of Standards under the sponsorhip of British Gas Corp., Chicago Bridge and Iron Co., Columbia Gas Service Corp., Distrigas Corp., Easco Gas LNG, Inc., El Paso Natural Gas., Gaz de France, Marathon Oil Co., Mobil R&D Corp., Natural Gas Pipeline Co., Phillips Petroleum Co., Shell International Gas, Ltd., Sonatrach, Southern California Gas Co., Tennessee Gas Pipeline, Texas Eastern Transmission Co., Tokyo Gas Co., Ltd., and Transcontinental Gas Pipe Line Corp., through a grant administered by the American Gas Association, Inc.

ABSTRACT

The orthobaric liquid densities of the major components of natural gas have been determined with a magnetic suspension densimeter. This paper reports results for methane (105 to 160 K), ethane (100 to 270 K), propane (100 to 288 K), isobutane (115 to 300 K), and normal butane (135 to 300 K). The imprecision of the measured densities is approximately 0.015 percent; the estimated overall uncertainty is 0.1 percent at low temperatures and decreases to 0.06 percent at 300 K. A simple expression has been used to represent the densities as a function of temperature. Comprehensive comparisons with the experimental results of other investigators are presented.

1. Introduction

Liquefied natural gas (LNG) is expected to become an increasingly important commodity on the world energy market. The basis for sale of LNG is its total heating value, which requires a knowledge of both density and composition. A project was initiated at this laboratory to provide orthobaric (saturated) liquid densities for the major components of LNG, and for mixtures of these components. The density data will be used to develop a mathematical model or correlation that predicts the density of LNG type mixtures with an inaccuracy of 0.1 percent, given a knowledge of the composition and temperature of the liquid. In the development of an accurate mathematical model (correlation), it is important to have both an accurate and an internally consistent set of density data.

Before this project was started there were significant temperature ranges for which saturated (orthobaric) liquid density data did not exist for some of the major components of LNG. For nitrogen and methane there were discrepancies as large as 0.5 per cent between different sets of data. Not only was it important to fill in gaps, but also to provide new independent measurements of sufficient accuracy to help resolve inconsistencies.

In this paper orthobaric liquid densities for methane, ethane, propane, isobutane, and normal butane are reported. Data for nitrogen were presented in an earlier paper[1]. Major emphasis has been placed on the low temperature region of 105 to 140 K; however, measurements have been carried out to 160 K for methane, to 270 K

for ethane, to 288.7 K for propane, and to 300 K for isobutane and normal butane. The densities have been represented as a function of temperature with an expression that is used to facilitate comparisons with other measurements.

The present measurements were carried out with a magnetic suspension densimeter.[1] In this method a magnetic buoy is freely suspended in the liquid of interest by the force generated from the axial magnetic fields of air-core solenoids. The motion of the buoy is controlled by the automatic regulation of a servo-circuit. The magnetic force necessary to maintain the buoy at a given position is inversely proportional to the buoyant force on the buoy. Thus, using Archemedes' principle, along with measurements of the mass and volume of the buoy, the density of the liquid is obtained.

2. Experimental

The experimental apparatus and its operation have been described in detail elsewhere[1]. At low temperatures the experimental procedures for the measurements on the hydrocarbons other than methane differed significantly from those for nitrogen and methane. The density of a given fluid is determined from measurements of the magnetic force necessary to support a barium ferrite buoy in a vacuum and in the fluid at the same position and temperature. For nitrogen and methane the vacuum measurements were performed immediately before or after the liquid measurements. At low temperatures it has been found impossible to evacuate the sample cell within a reasonable length of time after it has been filled with one of the heavier hydrocarbons. Most of the liquid can be

removed by pressurizing with helium gas; however, a liquid film is left on the surfaces, including those of the buoy, inside the cell. The buoy cannot be brought into suport until the film is removed. Thus, for the heavy hydrocarbons at low temperatures, the vacuum points must be obtained before the liquid measurements.

So that more than one data point could be obtained in a given day for a heavy hydrocarbon at low temperatures, vacuum points were obtained at two temperatures separated by 5 K before liquid was condensed into the cell. Then the liquid measurements were performed at each of these temperatures. Performance tests had demonstrated that the barium ferrite buoy does not exhibit any detectable hysteresis at low temperatures within the precision of the current measurements for a temperature range of, at least, 20 K. After the vacuum and liquid measurements were performed for one of the heavy hydrocarbons at low temperatures the cell was warmed to a temperature above the normal boiling point of the test fluid for evacuation.

Methane was used as a control fluid during the heavy hydrocarbon measurements at low temperatures. Each day a new methane data point was taken to insure that the warm-up and cool-down of the apparatus did not affect the apparent position of the buoy from liquid-to-vacuum measurements. The position of the buoy was determined with a high-powered microscope that had been adjusted initially so that the apparent position of the buoy did not depend on the index of refraction of the fluid inside the cell. It was found that the temperature cycling of the cell had no detectable effect on the apparent buoy position.

Some of the data presented in this paper were taken with a one-coil system instead of the three-coil arrangement described in the apparatus paper[1]. The evolution to the use of only one coil is discussed in reference 2.

All of the gases were of research grade quality. The minimum purities as specified by the suppliers were 99.9 mol percent for isobutane and normal butane and 99.99 mol percent for methane, ethane, and propane. The gases were analyzed chromatographically with a thermal conductivity detector and found to be within the specified purities except for isobutane. It was found that the isobutane contained approximately 0.15 percent normal butane. This relatively large amount of normal butane impurity has a negligible effect (< 0.01 percent) on the density results.

The methane gas was passed through a room temperature molecular sieve trap to remove moisture and any heavy contaminants not detected by analysis. The other hydrocarbon gases were normally not passed through a molecular sieve trap.

3. Results

The experimental orthobaric liquid densities of methane, ethane, propane, isobutane, and normal butane are presented as a function of temperature (International Practical Temperature Scale-1968) in tables 1-5. The relatively large number of data points for methane at any given temperature resulted from the use of methane as a control fluid throughout the entirety of this project. Although the mean experimental densities of methane have been given in an earlier paper[1] they are presented again here, along with other information

(calculated densities, etc.), so that the orthobaric liquid densities of all the low molecular weight alkanes investigated in the present work are included in a single paper. All of the experimental points for methane will be presented in a future report[3]. Each methane point was taken from a new filling of the cell. For the other hydrocarbons no more than two data points were taken from a single filling.

The experimental densities (ρ) have been fitted as a function of temperature (T) to the following expression,

$$\rho - \rho_c = a\left(1 - \frac{T}{T_c}\right)^{0.35} + \sum_{i=1}^{3} b_i \left(1 - \frac{T}{T_c}\right)^{\left(1 + \frac{i-1}{3}\right)} \qquad (1)$$

which incorporates a scaling law modification[4] to a generalized Guggenheim equation[5]. The coefficients (a, b_i), determined by least squares, and selected values of the critical temperature (T_c) and density (ρ_c) for each fluid are given in table 6[6-11]. Only three coefficients were needed to fit the methane data, which covered a relatively small temperature range compared to that for the other fluids.

The residual standard deviations of the fit to equation (1) for each fluid are given in table 6. These values substantiate the estimate of the imprecision of the density measurements, which is approximately 0.015 percent. The estimated inaccuracy in the densities is 0.1 percent at low temperatures and decreases to 0.06 percent at 300 K. The total uncertainty in the reported

temperatures is estimated to be less than 30 mK at 100 K and less than 40 mK at 300 K. These uncertainty limits in the temperature correspond to a maximum uncertainty of 0.02% in the density for the data reported in this paper. A detailed error analysis of the magnetic suspension densimeter used in the present work has been given elsewhere[1].

Equation (1), along with the parameters given in table 6, has been used for comparisons of the present results with independent experimental data[8, 12-25]. Deviation plots for ethane, propane, isobutane, and normal butane are presented in figures 1 through 4. The deviation plot for methane was presented in an earlier paper[1]; thus, it is not included here.

In comparing the results of other investigators with equation (1) some general trends are observed. Below 140 K the densities of Shana'a and Canfield[12], Chui and Canfield[13], Orrit and Olives[14], Rodosevich and Miller[15], McClune[16], and Klosek and McKinley[17] are generally lower than the present results by 0.05 to 0.1 percent. Exceptions to this trend are as follows: for isobutane the densities of Rodosevich and Miller[15] between 114 and 120 K are larger (maximum of 0.1 percent) than the present results and exhibit a significantly different temperature dependence; and for ethane the change in density with temperature reported by Klosek and McKinley[17] is appreciably larger than that observed in the present work.

Above 140 K the data of Chui and Canfield[13], Orrit and Olives[14], and McClune[16] differ from the present results by less than 0.05 percent. At higher temperatures (above 280 K) the data of

Sliwinski[8] for propane, isobutane, and normal butane generally differ from the present results by less than 0.05 percent. The orthobaric liquid densities reported by Douslin and Harrison[18] for ethane at temperatures between 248 and 263 K were systematically larger than the present results by 0.3 to 0.35 percent. Some of the older, less precise (but frequently used) data have been included on the deviation plots for the sake of completeness.

Although Klosek and McKinley[17] give densities for isobutane and normal butane at temperatures between 105 and 133 K, these densities are not experimental, and therefore, are not plotted on figures 3 and 4. A few comments on the reliability of the omitted values are appropriate. Their densities were obtained from the Francis equation[26]. For normal butane at temperatures below its triple point temperature, their results were systematically higher by less than 0.2 percent than the densities obtained through extrapolation of the present data[27]. However, their isobutane densities at temperatures between 116 and 133 K were 1.5 percent higher than those of the present work.

4. Summary

This research has provided accurate and self-consistent measurements of the orthobaric liquid densities of methane, ethane, propane, isobutane, and normal butane at temperatures down to 100 K. Most of the measurements recently reported by other workers differ from the present data by less than 0.1 percent. In subsequent papers, density measurements on liquefied mixtures of the major components of liquefied natural gas will be reported.

Acknowledgment

The authors would like to acknowledge R. D. McCarty and M. J. Brown for assistance with the correlation and reduction of the data.

References

1. Haynes, W. M.; Hiza, M. J.; Frederick, N. V. Rev. Sci. Instrum. (to be published).
2. Haynes, W. M. Rev. Sci. Instrum. (submitted for publication).
3. Methane data are available from authors upon request and will be published in a Nat. Bur. Stand. (U.S.) report.
4. McCarty, R. D. Nat. Bur. Stand. (U.S.), Internal Rept. 74-357, 1974.
5. Hou, Y.C.; Martin, J. J. A.I.Ch.E. J. 1959, 5, 125.
6. Goodwin, R. D. Nat. Bur. Stand. (U.S.), Tech. Note 653, 1974.
7. Olson, J. D. J. Chem. Phys. 1975, 63, 474.
8. Sliwinski, P. Z. Phys. Chem. (Frankfurt) 1969, 63, 263.
9. Das, T. R.; Eubank, P. T. Advances in Cryogenic Engineering 1973, 1, 208.
10. Das, T. R.; Reed, Jr., C. O.; Eubank, P. T. J. Chem. Eng. Data 1973, 18, 253.
11. Das, T. R.; Reed, Jr., C. O.; Eubank, P. T. J. Chem. Eng. Data 1973, 18, 244.
12. Shana'a, M. Y.; Canfield, F. B. Trans. Faraday Soc. 1968, 64, 2281.
13. Chui, C. H.; Canfield, F. B. Trans. Faraday Soc. 1971, 67, 2933.
14. Orrit, J.; Olives, J. distributed at 4th International Conference on Liquefied Natural Gas, Algeria, 1974.

15. Rodosevich, J. B.; Miller, R. C. A.I.Ch.E. J. 1973, 19, 729.

16. McClune, C. R. Cryogenics 1976, 16, 289.

17. Klosek, J.; McKinley, C. Proc. First International Conference on LNG, Paper 22, Chicago, 1968.

18. Douslin, D. R.; Harrison, R. H. J. Chem. Thermodynamics 1973, 5, 491.

19. Maass, O.; Wright, C. H. J. Am. Chem. Soc. 1921, 43, 1098.

20. Jensen, R. H.; Kurata, F. J. Petrol. Technol. 1969, 21, 683.

21. Kahre, L. C. J. Chem. Eng. Data 1973, 18, 267.

22. Tomlinson, J. R. Natural Gas Processors Assoc. Tech. Publ. TP-1, Tulsa, Oklahoma, 1971.

23. Seeman, F.-W.; Urban, M. Erdöl und Kohle Erdgas Petrochemie 1963, 16, 117.

24. Tech. Comm., Natl. Gas. Assoc. Am. Ind. Eng. Chem. 1942, 34, 1240.

25. Van der Vet, A. P. Congress Modial du Petrol., Paris, Vol. II, p. 515, 1937.

26. Francis, A. W. Ind. Eng. Chem. 1957, 49, 1779.

27. Haynes, W. M.; Hiza, M. J. Advances in Cryogenic Engineering, Vol. 21. Timmerhaus, K. D. and Weitzel, D. H., editors. Plenum Press, New York, 1976, p. 516.

Table 1. Orthobaric liquid densities of methane, where T is the temperature (IPTS-1968), ρ_{exp} is the mean experimental density for n observations at a given temperature, and ρ_{calc} is the density calculated from equation (1).

T/K	ρ_{exp}/mol ℓ^{-1}	n	ρ_{calc}/mol ℓ^{-1}	Maximum value of $100(\rho_{exp}-\rho_{calc})/\rho_{calc}$
105.000	26.9458	12	26.9456	0.030
110.000	26.4985	11	26.5005	0.035
115.000	26.0443	12	26.0429	0.028
120.000	25.5721	17	25.5712	0.036
125.000	25.0845	18	25.0839	0.037
130.000	24.5775	16	24.5790	0.036
135.000	24.0540	23	24.0540	0.031
140.000	23.5067	5	23.5060	0.024
145.000	22.9312	5	22.9311	0.024
150.000	22.3218	2	22.3243	0.014
160.000	20.9876	2	20.9857	0.037

Table 2. Orthobaric liquid densities of ethane, where T is the temperature (IPTS-1968), ρ_{exp} is the experimental density, and ρ_{calc} is the density calculated from equation (1).

T/K	ρ_{exp}/mol ℓ^{-1}	ρ_{calc}/mol ℓ^{-1}	$\frac{100(\rho_{exp}-\rho_{calc})}{\rho_{calc}}$
100.000	21.3408	21.3388	0.009
105.000	21.1585	21.1568	0.008
110.000	20.9746	20.9742	0.002
115.000	20.7927	20.7907	0.010
120.000	20.6022	20.6063	-0.020
125.000	20.4186	20.4208	-0.011
130.000	20.2317	20.2343	-0.013
135.000	20.0461	20.0466	-0.002
140.000	19.8566	19.8575	-0.005
150.000	19.4751	19.4748	0.002
160.000	19.0857	19.0850	0.004
170.000	18.6867	18.6869	-0.001
180.000	18.2793	18.2787	0.003
190.000	17.8612	17.8586	0.015
200.000	17.4289	17.4240	0.028
210.000	16.9713	16.9720	-0.004
220.000	16.4988	16.4989	-0.001
230.000	15.9973	15.9994	-0.013
240.000	15.4642	15.4670	-0.018
250.000	14.8899	14.8919	-0.013
260.000	14.2610	14.2598	0.008
270.000	13.5493	13.5477	0.012

Table 3. Orthobaric liquid densities of propane, where T is the temperature (IPTS-1968), ρ_{exp} is the experimental density, and ρ_{calc} is the density calculated from equation (1).

T/K	ρ_{exp}/mol ℓ^{-1}	ρ_{calc}/mol ℓ^{-1}	$\frac{100(\rho_{exp}-\rho_{calc})}{\rho_{calc}}$
100.075	16.3065	16.3048	0.011
105.075	16.1872	16.1885	-0.008
110.075	16.0718	16.0723	-0.003
115.075	15.9557	15.9562	-0.003
120.075	15.8411	15.8401	0.006
125.075	15.7250	15.7241	0.006
130.075	15.6085	15.6080	0.003
135.075	15.4910	15.4918	-0.005
140.075	15.3751	15.3755	-0.002
145.075	15.2588	15.2590	-0.002
150.075	15.1400	15.1424	-0.016
200.000	13.9560	13.9524	0.026
240.000	12.9271	12.9285	-0.010
270.000	12.0733	12.0742	-0.008
280.000	11.7622	11.7631	-0.008
288.706	11.4790	11.4775	0.013

Table 4. Orthobaric liquid densities of isobutane, where T is the temperature (IPTS-1968), ρ_{exp} is the experimental density, and ρ_{calc} is the density calculated from equation (1).

T/K	ρ_{exp}/mol ℓ^{-1}	ρ_{calc}/mol ℓ^{-1}	$\frac{100(\rho_{exp}-\rho_{calc})}{\rho_{calc}}$
115.075	12.7305	12.7313	-0.006
120.075	12.6489	12.6491	-0.001
125.075	12.5687	12.5669	0.015
130.075	12.4850	12.4846	0.003
135.075	12.4015	12.4022	-0.005
140.075	12.3215	12.3197	0.014
145.075	12.2353	12.2372	-0.015
150.075	12.1534	12.1544	-0.008
228.000	10.8273	10.8263	0.009
288.706	9.6676	9.6687	-0.012
290.000	9.6411	9.6417	-0.007
300.000	9.4300	9.4287	0.014

Table 5. Orthobaric liquid densities of normal butane, where T is the temperature (IPTS-1968), ρ_{exp} is the experimental density, and ρ_{calc} is the density calculated from equation (1).

T/K	ρ_{exp}/mol ℓ^{-1}	ρ_{calc}/mol ℓ^{-1}	$\frac{100(\rho_{exp}-\rho_{calc})}{\rho_{calc}}$
135.075	12.6517	12.6524	-0.005
140.075	12.5706	12.5714	-0.006
145.075	12.4920	12.4904	0.013
150.075	12.4089	12.4093	-0.003
155.075	12.3299	12.3283	0.014
160.075	12.2484	12.2471	0.010
165.075	12.1634	12.1659	-0.020
170.075	12.0839	12.0846	-0.005
230.000	11.0911	11.0905	0.005
288.706	10.0325	10.0324	0.001
290.000	10.0067	10.0073	-0.007
300.000	9.8103	9.8099	0.004

Table 6. Parameters of equation (1), $\rho - \rho_c = a(1 - \frac{T}{T_c})^{0.35} + \sum_{i=1}^{3} b_i(1 - \frac{T}{T_c})^{(1 + \frac{i+1}{3})}$, where T_c and ρ_c are the critical temperature and density. The coefficients (a, b_1, b_2, b_3) were obtained from a least squares program in which the experimental densities in g/cm^3 to five digits were converted to molar densities within the program.

	Methane	Ethane	Propane	Isobutane	Normal Butane
a	18.65812	12.55205	8.684459	7.657535	7.286063
b_1	6.712030	13.43284	18.04086	8.145251	11.96308
b_2	-0.9472020	-19.00461	-29.46261	-13.10582	-19.87592
b_3		11.07716	16.43559	8.145894	11.60211
T_c/K.	190.555[5]	305.33[7]	369.82[8]	408.13[9]	425.16[10]
ρ_c/mol ℓ^{-1}	10.16[6]	6.86[7]	5.00[8]	3.80[9]	3.92[10]
Standard Deviation	0.016%	0.012%	0.011%	0.013%	0.012%
Molecular Weight	16.04303	30.07012	44.09721	58.1243	58.1243

List of Figure Legends

Figure 1. Deviation plot of experimental orthobaric liquid densities of ethane compared with values calculated from equation (1) using parameters from table 6; ○ present data, ● Shana'a and Canfield[12], ◇ Chui and Canfield[13], ⦶ Orrit and Olives[14], △ Rodosevich and Miller[15], □ McClune[16], ■ Klosek and McKinley[17], ▲ Douslin and Harrison[18], ⊖ Maass and Wright[19], ▽ Jensen and Kurata[20], ▼ Kahre[21].

Figure 2. Deviation plot of experimental orthobaric liquid densities of propane compared with values calculated from equation (1) using parameters from table 6; ○ present data, ✱ Sliwinski[8], ● Shana'a and Canfield[12], ⦶ Orrit and Olives[14], △ Rodosevich and Miller[15], □ McClune[16], ■ Klosek and McKinley[17], ⊖ Maass and Wright[19], ▽ Jensen and Kurata[20], ▼ Kahre[21], ◒ Tomlinson[22], ◆ Seeman and Urban[23], ⊗ NGAA[24], ◐ Van der Vet[25].

Figure 3. Deviation plot of experimental orthobaric liquid densities of isobutane compared with values calculated from equation (1) using parameters from table 6; ○ present data, ✱ Sliwinski[8], ⦶ Orrit and Olives[14], △ Rodosevich and Miller[15], □ McClune[16], ▼ Kahre[21], ⊗ NGAA[24], ◐ Van der Vet[25].

Figure 4. Deviation plot of experimental orthobaric liquid densities of normal butane compared with values calculated from equation (1) using parameters from table 6; ○ present data, ✱ Sliwinski[8], ⦶ Orrit and Olives[14], □ McClune[16], ▼ Kahre[21], ⊗ NGAA[24], ◐ Van der Vet[25].

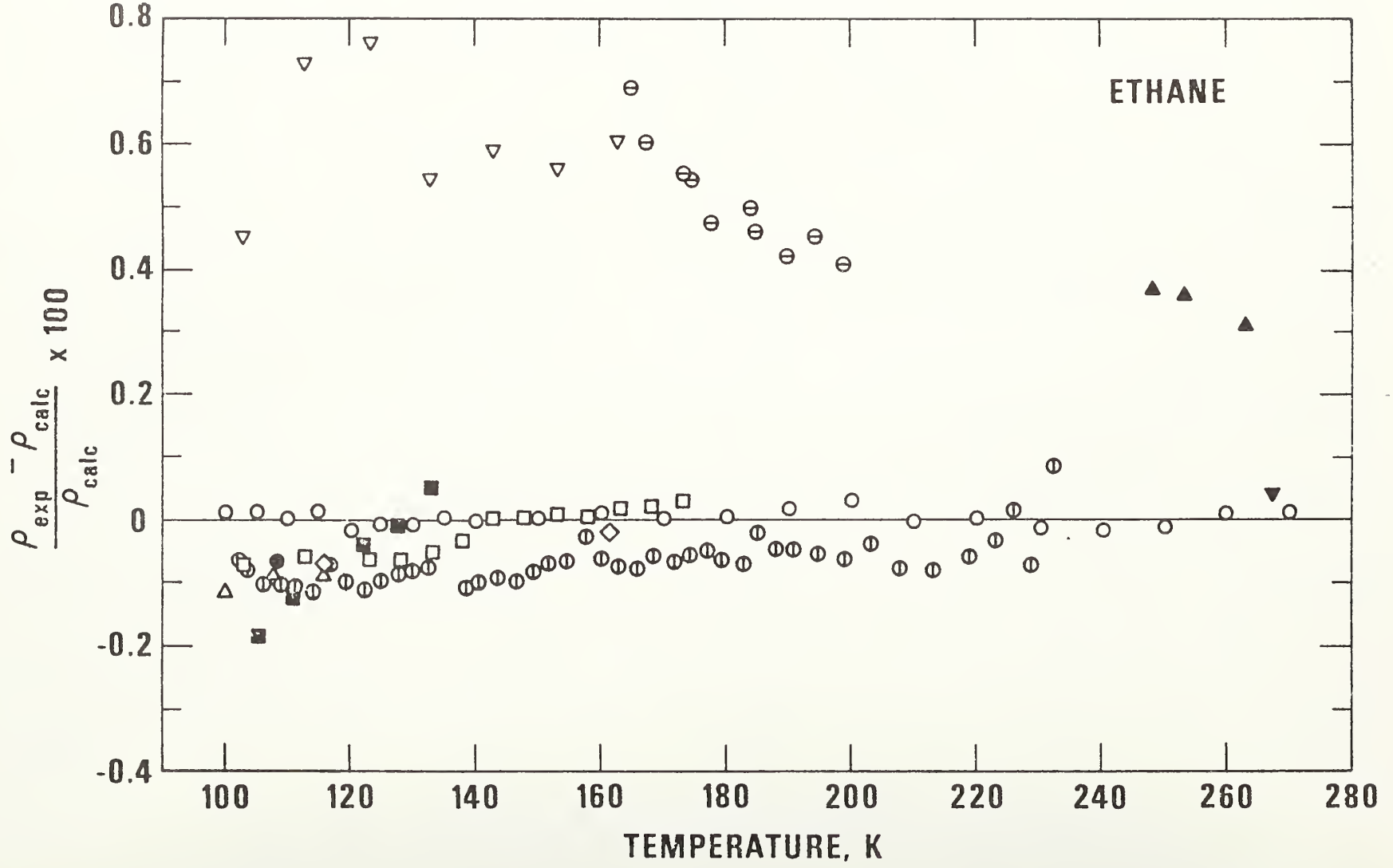
ETHANE
$\frac{\rho_{exp} - \rho_{calc}}{\rho_{calc}} \times 100$
0.8
0.6
0.4
0.2
0
-0.2
-0.4
100
120
140
160
180
200
220
240
260
280
TEMPERATURE, K

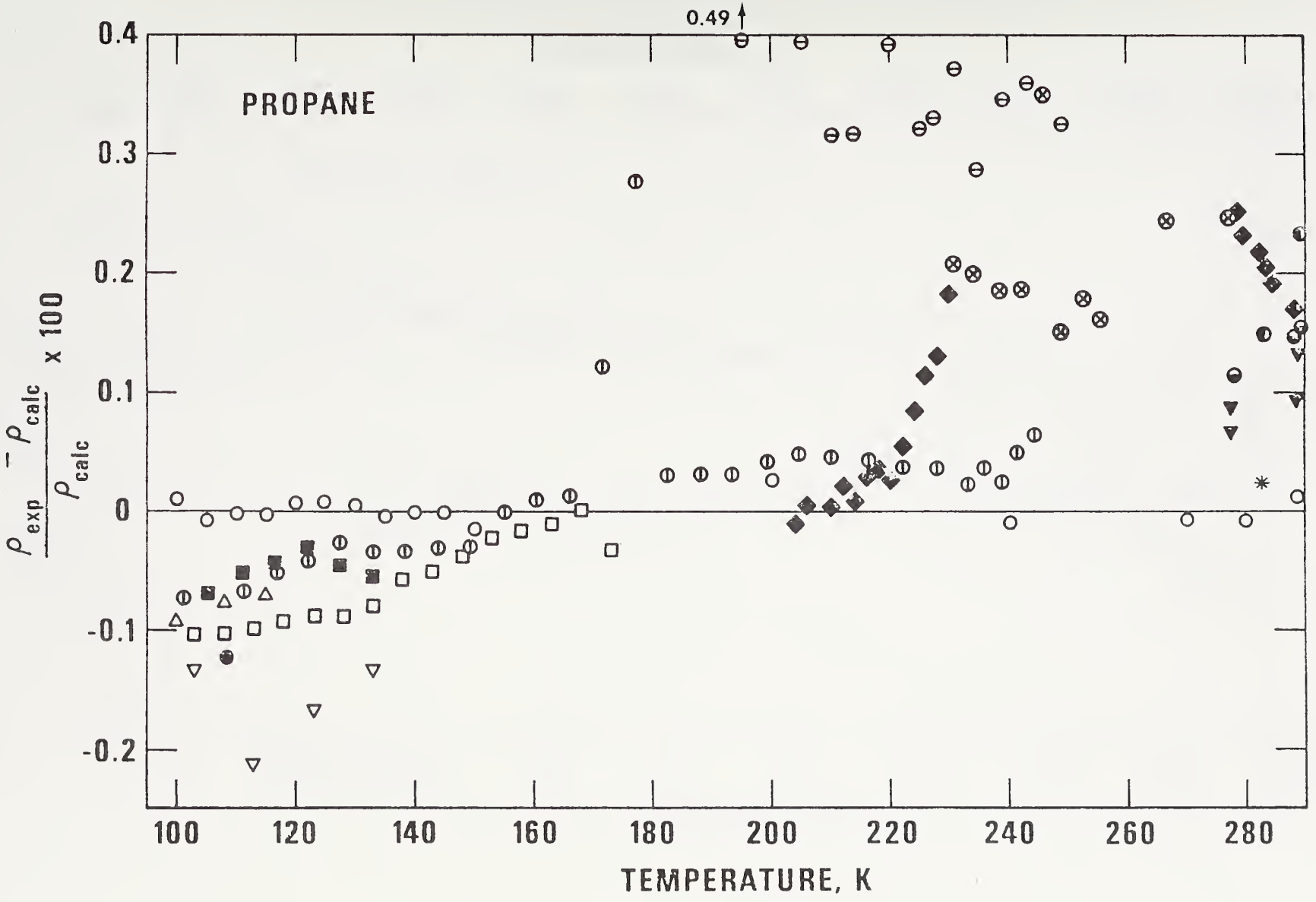
PROPANE
0.49
0.4
0.3
0.2
0.1
0
-0.1
-0.2
100
120
140
160
180
200
220
240
260
280
TEMPERATURE, K
$\frac{\rho_{exp} - \rho_{calc}}{\rho_{calc}} \times 100$

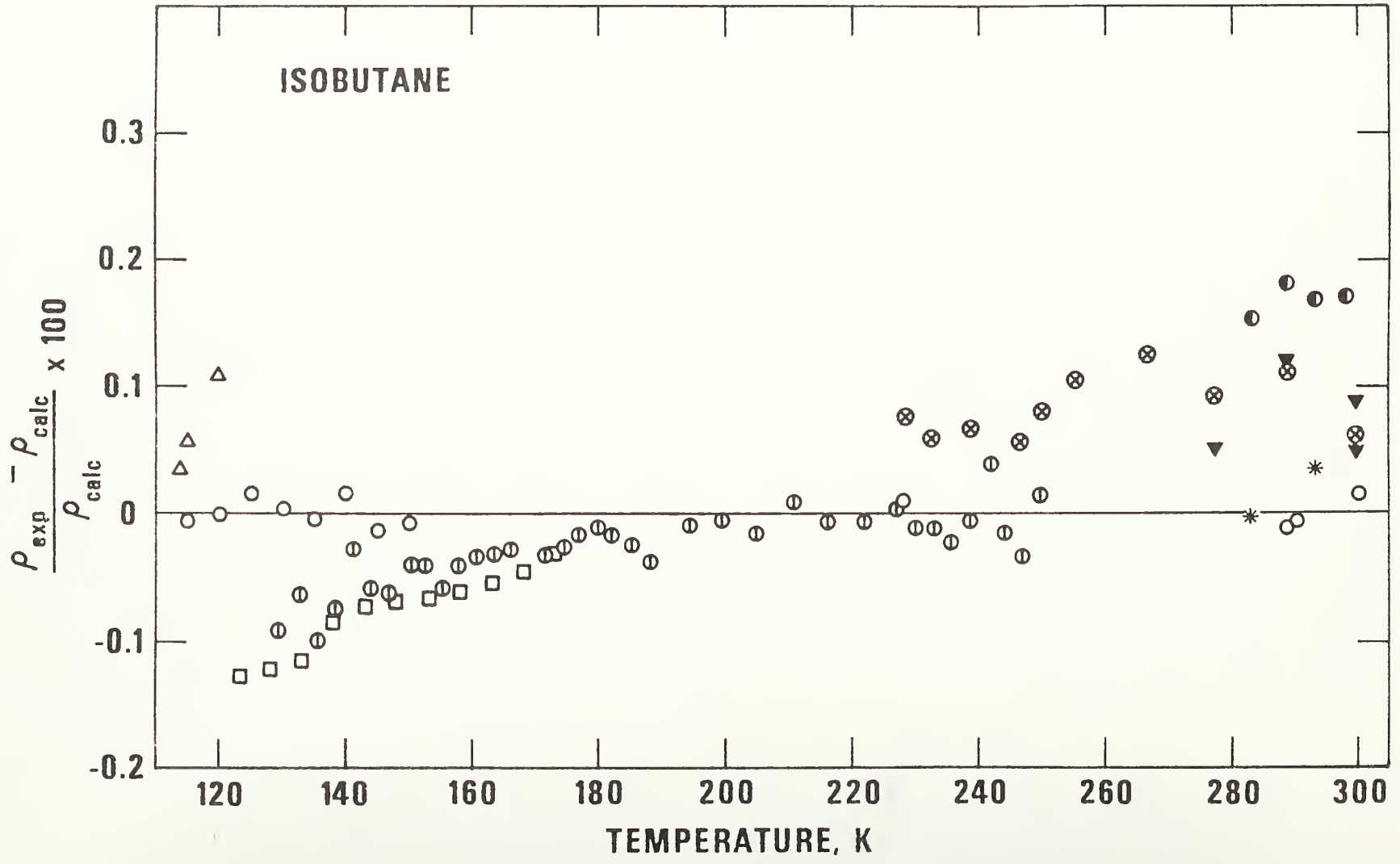
ISOBUTANE
0.3
0.2
0.1
0
-0.1
-0.2
120
140
160
180
200
220
240
260
280
300
TEMPERATURE, K
$\frac{\rho_{exp} - \rho_{calc}}{\rho_{calc}} \times 100$

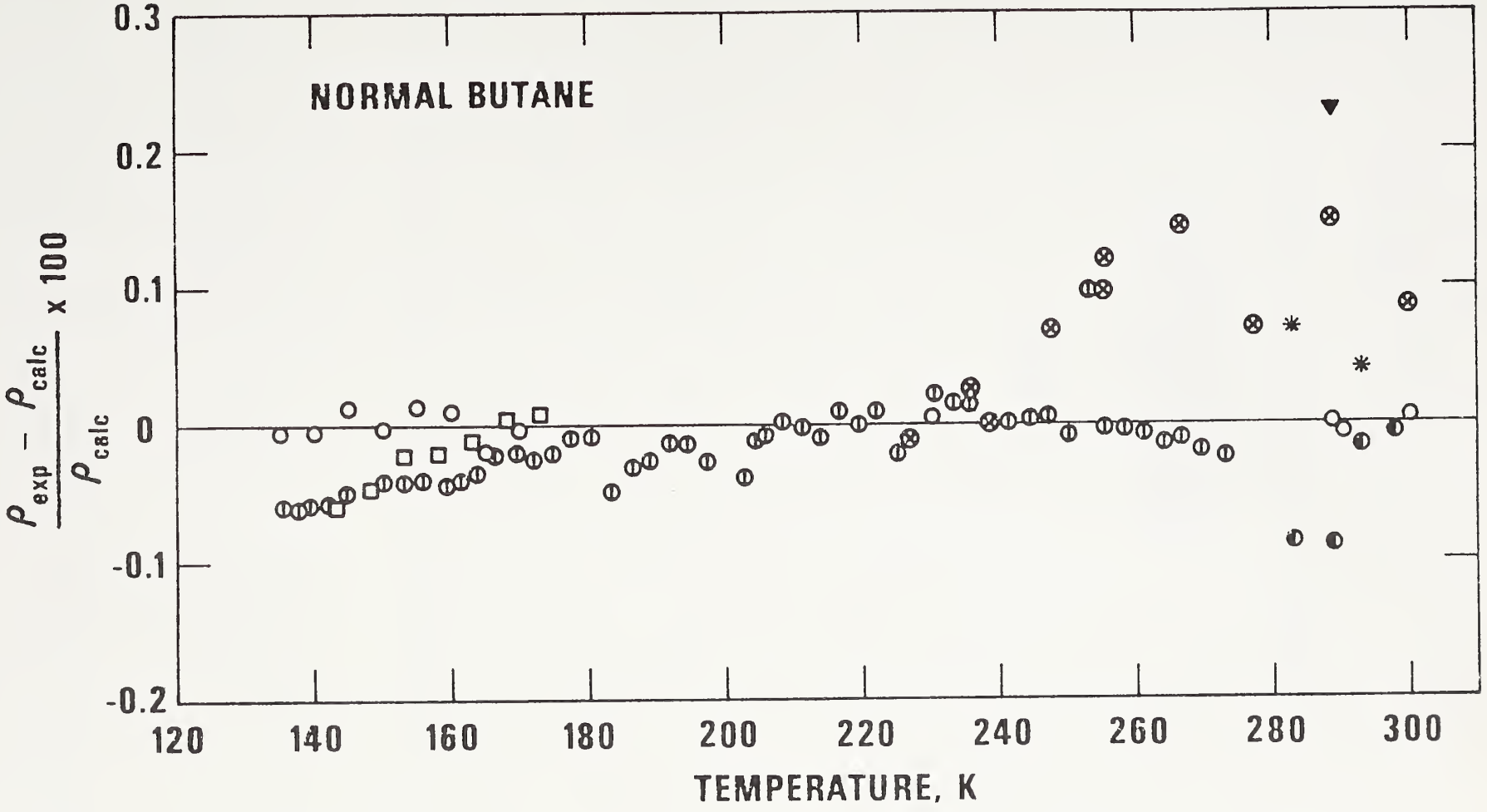
NORMAL BUTANE
0.3
0.2
0.1
0
-0.1
-0.2
120
140
160
180
200
220
240
260
280
300
TEMPERATURE, K
$\frac{\rho_{exp} - \rho_{calc}}{\rho_{calc}} \times 100$

THE VISCOSITY AND THERMAL CONDUCTIVITY COEFFICIENTS FOR DENSE GASEOUS AND LIQUID METHANE*

H. J. M. Hanley, W. M. Haynes and R. D. McCarty

Cryogenics Division
Institute for Basic Standards
National Bureau of Standards
Boulder, Colorado 80302

ABSTRACT

Data for the viscosity and thermal conductivity coefficients of dense gaseous and liquid methane have been evaluated. Selected data were fitted to a function derived in our previous work and tables of values were generated for temperatures from 95 to 500 K and for pressures up to 50 MPa (∿ 500 atm). The uncertainties of the tabular values are estimated to be approximately 3% and 5% for the viscosity and thermal conductivity coefficients, respectively. The contribution for the thermal conductivity enhancement in the critical region is included in the tables. Care has been taken to ensure that the calculated values are consistent with reliable equation-of-state data and also with dilute gas transport coefficients determined previously.

Key words: Correlation; critical point anomaly; methane; tables; thermal conductivity coefficient; viscosity coefficient.

---

1. INTRODUCTION

The viscosity coefficient (η) and the thermal conductivity coefficient ( ) of several fluids — argon, krypton, xenon, oxygen and nitrogen — have been correlated over a wide range of experimental conditions [1]*. The correlation was recently extended to methane [2]. The object of this paper is to expand on reference [2] by presenting tables and to give some further details of the correlation. We will follow closely the outline of reference [1] in which criteria for evaluating systematically literature data were discussed and in which an equation for the viscosity and thermal conductivity coefficients was proposed. The criteria and equations will be used here with only minimal comments.

2. CORRELATING EQUATIONS

The correlations are based on the behavior of the transport coefficients with respect to temperature (T) and density (ρ) according to the equations

$$\eta(\rho,T) = \eta_o(T) + \eta_1(T)\rho + \Delta\eta'(\rho,T) \tag{1}$$

$$\lambda(\rho,T) = \lambda_o(T) + \lambda_1(T)\rho + \Delta\lambda'(\rho,T) + \Delta\lambda_c(\rho,T) \tag{2}$$

for the viscosity and thermal conductivity coefficients, respectively. In these equations, $\eta_o(T)$ and $\lambda_o(T)$ are the dilute gas values, $\eta_1(T)$ and $\lambda_1(T)$ represent

---

* Numbers in brackets refer to references.

density corrections for the moderately dense gas, while $\Delta\eta'(\rho,T)$ and $\Delta\lambda'(\rho,T)$ are remainders. The term $\eta_1(T)$ is given by the empirical expression

$$\eta_1(T) = A + B\,[C - \ell n\ (T/F)]^2 \tag{3}$$

and similarly for $\lambda_1(T)$. The coefficients A, B, C and F can be found from a fit of data but we set $F = \varepsilon/k$ where ε is the energy parameter of the methane pair potential function and k is Boltzmann's constant. See section 3.

The terms $\Delta\eta'(\rho,T)$ and $\Delta\lambda'(\rho,T)$ are expressed empirically by the relations

$$\Delta\eta'(\rho,T) = E\left\{\exp\,[j_1 + j_4/T] \quad \exp\left[\rho^{0.1}\left(j_2 + j_3/T^{3/2}\right) + \theta\rho^{0.5}\left(j_5 + j_6/T + j_7/T^2\right)\right] - 1.0\right\} \tag{4}$$

and

$$\Delta\lambda'(\rho,T) = D\left\{\exp\,[k_1 + k_4/T] \quad \exp\left[\rho^{0.1}\left(k_2 + k_3/T^{3/2}\right) + \theta\rho^{0.5}\left(k_5 + k_6/T + k_7/T^2\right)\right] - 1.0\right\} \tag{5}$$

The parameter θ is included to account specifically for the high density behavior of the transport coefficients and is a function of the density with respect to the critical density, ρ_c:

$$\theta = (\rho - \rho_c)/\rho_c \tag{6}$$

The coefficients, E, D, $j_1 \ldots j_7$, $k_1 \ldots k_7$, are all to be determined from experimental data.

One sees that equation (1) and (2) are of the same structure* except that equation (2) includes the term $\Delta\lambda_c(\rho,T)$. This is included to take into account the known enhancement of the thermal conductivity coefficient in the neighborhood of the critical point [3]. [The viscosity coefficient also shows anomalous behavior close to the critical point [4]. The anomaly is small, however, and is not included in the calculated values.]

We have remarked in reference [1] that the form of equations (4) and (5) was independent of the nature of the fluids considered. The behavior of methane [2] is consistent with this characteristic. This apparent generality is a useful feature of the equations but, since they are empirical, each fluid should be treated on its merits without prior prejudice.

Equation of State. The majority of transport coefficient data in the literature is reported in temperature-pressure coordinates but we emphasized [1] that a correlation of the coefficients should be preferably in terms of density rather than pressure. An accurate equation of state is, therefore, essential to our procedure. The equation of state used here for methane is a modified Benedict-Webb-Rubin (BWR), which was introduced and discussed in reference [5]. The equation is, in turn, based on the methane correlation of Goodwin [6]. The form of the BWR and values for its parameters are given in the Appendix of the present paper.

---

* Equation (5) here includes a contribution proportional to θ, unlike the corresponding equation [equation (9)] in reference [1]. In our earlier work with oxygen, nitrogen, and the rare gases, however, the data were either not sufficiently precise, or extensive to justify seven k coefficients.

3. THE DILUTE GAS

The dilute gas coefficients appear separately in equations (1) and (2). We have discussed the calculation of these quantities from statistical mechanics [7,8,9] and have shown, in particular, that statistical mechanics can give a consistent representation of the transport properties and the thermodynamic properties for a given simple gas.

Dilute gas transport coefficient data for methane have been listed and evaluated in reference [10]. Calculated values were obtained via the standard kinetic theory equations [9] using the m-6-8 pair potential function of Klein and Hanley [10]. This potential has the form

$$\phi(r) = \frac{\varepsilon}{m-6}\,[6 + 2\gamma']\left(\frac{r_m}{r}\right)^m - \frac{\varepsilon}{m-6}\,[m - \gamma'(m-8)]\left(\frac{r_m}{r}\right)^6 - \gamma'\left(\frac{r_m}{r}\right)^8 \qquad (7)$$

where r is the intermolecular separation, ε the maximum well-depth of the potential, and r_m is defined according to the relation $\phi(r_m) = -\varepsilon$. Repulsive forces between molecules are represented by a $1/r^m$ contribution, while attractive forces are represented by $-1/r^6$ and $-1/r^8$ contributions; γ' depicts the strength of the latter. Since we have discussed the application of kinetic theory to methane in reference [10], details of the calculation procedure are omitted here. m-6-8 methane parameters are given in table 1. The dilute gas data were fitted to within their estimated accuracy (approximately $\pm$ 2% for the viscosity coefficient and approximately $\pm$ 5% for the thermal conductivity coefficient). Recent work [53] has suggested, however, that the m-6-8 potential can lead to small systematic differences between theory and experiment at very low temperatures [$T/(\varepsilon/k) \lesssim 0.8$] and at very high temperatures [$T/(\varepsilon/k) \gtrsim 20$]. Accordingly we revise our estimate of accuracy for the dilute gas transport coefficients of methane for temperatures

less than 150 K to 3% and 6% for the viscosity and thermal conductivity coefficient, respectively. Ely and Hanley have further discussed [9] the approximations introduced when a nonspherical molecule, such as methane, is regarded as spherical from the viewpoint of the pair potential. For methane, we have verified that this assumption does not effect the correlation of a single property (e.g., the viscosity) but effects slightly the consistency between calculated values of different properties.

For computational convenience we fitted the calculated η_o and λ_o to a polynomial in temperature

$$\eta_o = GV(1)T^{-1} + GV(2)T^{-2/3} + GV(3)T^{-1/3} + GV(4) + GV(5)T^{1/3} + GV(6)T^{2/3} + GV(7)T + GV(8)T^{4/3} + GV(9)T^{5/3} , \quad (8)$$

and similarly for λ_o, but with coefficients GT(i)(i = 1...9) replacing GV(i) in equation (8). Values of the coefficients are listed in table 2.

4. CALCULATION OF THE THERMAL CONDUCTIVITY COEFFICIENT IN THE CRITICAL REGION

The quantity $\Delta\lambda_c$ appears as a separate term in equation (2) and represents the anomalous behavior of the thermal conductivity coefficient in the neighborhood of the critical point [3]. There is no doubt that $\Delta\lambda_c$ can contribute significantly to the value of the thermal conductivity coefficient and has to be included in a correlation [1]. Conductivity data, however, in the critical region for methane are scarce and we prefer to obtain $\Delta\lambda_c$ by calculation.

The calculation follows a procedure suggested by Sengers [3] and expanded by Hanley, Sengers and McCarty [11]. Details are given in reference [11], in

section 3.2 of reference [1], and in reference [2]. Our application to methane is given in appendix C of reference [2].

5. DATA SELECTION AND CORRELATION

Since the dilute gas coefficients, η_o and λ_o, have been calculated previously [10], we considered here data for the dense gas and liquid regions only. A comprehensive search of the world's literature through 1975 turned up references [12] - [37] for the viscosity coefficient and references [38] - [49] for the thermal conductivity. Much of the data prior to 1970 are summarized in references [50] - [52]. The data reported in these papers were examined according to the criteria set out in section 2 of reference [1]. The data used for correlation purposes were chosen on the basis of the procedure described in section 2.3 of reference [1] and table 3 gives the final choices with our accuracy assessments.

We have shown that it is essential to have reliable data close to the saturated liquid boundary and for at least one high temperature (about 2 T_c) isotherm if equations (1) to (5) are to give a reliable correlation. Such data are available for methane. [Conversely, if data are available for the saturated liquid boundary and for one high temperature isotherm only, equations (1) to (5) are excellent interpolation functions.]

The experimental coverage for the thermal conductivity coefficient of methane is perhaps the most extensive of any fluid due to the measurements of Mani [39], using a transient hot wire technique, and to those of Le Neindre [38], using a concentric cylinder apparatus. In the region of overlap, data from these two authors differ systematically by about two percent, which is within their estimated uncertainties.

5.1 Parameters for Equations (3)-(5)

The parameters for equations (3)-(5) were estimated by the least squares procedure outlined in section 3.1 of reference [1], using the selected data from table 3, and are given in table 4. As remarked, however, thermal conductivity data close to the critical point (from references [39] and [40]) were excluded from the fit; rather $\Delta\lambda_c$ was obtained by calculation [2].

5.2 Deviation Curves

Representative deviation curves are shown as figures 1-4. In every example the percent deviation has been defined as

$$\text{percent deviation} = \frac{(\text{expt.}-\text{calc.})}{\text{expt.}} \times 100 \qquad (9)$$

The figures are self-explanatory and show that we have been able to fit the data to within the estimated experimental uncertainties with one possible exception: namely, the calculated viscosity coefficient appears too low close to the critical point, see figure 1. Although it is possible that experimental error and/or incorrect density values contribute to the deviation, it is more likely that the deviation is the result of a small enhancement in the viscosity close to the critical point [4], which is excluded in the correlating equation. This feature was also observed in our previous work [1].

6. CONSTRUCTION OF TABLES

We constructed tables of values for the viscosity coefficient (table 5) and the thermal conductivity coefficient (table 6) from equations (1)-(5) with the parameters of table 4 using the equation of state in the appendix. The temperature range is 95 to 500 K. The pressures extend to 50 MPa for temperatures less than

.75 K, and to 75 MPa for temperatures between 205 and 500 K. These ranges sometimes correspond to a slight extrapolation of the data. The correlations, however, are based on the temperature-density behavior of the transport coefficients. Density is the limiting variable. We therefore assured that a P-T entry in the table did not correspond to a density exceeding 0.445 g/cm^3 [27.8 mole/ℓ], which was the upper experimental limit.

For convenience we constructed table 7 which presents values for the saturated liquid.

6.1 Uncertainty of the Tables and Extrapolation

Our assessment of the correlating procedure of reference [1] led to the conclusion that the correlation does not give rise to significant systematic deviations between calculated and experimental values of the transport coefficients. This conclusion is reinforced from this work with methane. Hence, an estimate of the uncertainty of the tabulated values is essentially the estimate of the uncertainty of the input data. [We note that the percentage of uncertainty given in table 3 and mentioned here is an assessment of inaccuracy.] For temperatures below 200 K, we assign an uncertainty of ± 3% to the tabulated viscosity values, ± 5% to the tabulated thermal conductivity values. For temperatures above 200 K, the uncertainties are felt to be slightly less: ± 2% and ± 4%, respectively. Close to the critical point, our viscosity values are probably too low by about 5% and our values for the thermal conductivity have an uncertainty of 15%. Extrapolation of the tables is not recommended.

7. CONCLUSION

A general equation, identical in form for both transport coefficients (excluding the critical point enhancement for the thermal conductivity coefficient), has been used to represent selected viscosity and thermal conductivity data of

methane from the dilute gas to the dense liquid. Parameters for the equation were determined by fitting experimental data. Comprehensive tables of the transport coefficients are presented.

8. ACKNOWLEDGEMENTS

We are most grateful for the information given us by many of the authors of the experimental papers. We are also grateful to D. E. Diller, H. M. Roder and J. V. Sengers for comments on the data in the literature. The work was supported in part by the Office of Standard Reference Data.

REFERENCES

1. Hanley, H. J. M., McCarty, R. D., and Haynes, W. M., J. Phys. Chem. Ref. Data 3, 979 (1974).
2. Hanley, H. J. M., McCarty, R. D., and Haynes, W. M., Cryogenics 15, 413 (1975).
3. Sengers, J. V., in Transport Phenomena - 1973 (AIP, New York) Kestin, J., Ed. (1973) p. 229.
4. Strumpf, H. J., Collings, A. F., and Pings, C. J., J. Chem. Phys. 60, 3109 (1974).
5. McCarty, R. D., Cryogenics 14, 276 (1974).
6. Goodwin, R. D., Nat. Bur. Stand. (U.S.), Tech. Note 653 (1974).
7. Hanley, H. J. M., J. Phys. Chem. Ref. Data 2, 619 (1973).
8. Hanley, H. J. M., and Ely, J. F., J. Phys. Chem. Ref. Data 2, 735 (1973).
9. Ely, J. F., and Hanley, H. J. M., Mol. Phys. 30, 565 (1975).
10. Hanley, H. J. M., and Klein, Max, J. Phys. Chem. 76, 1743 (1972).
11. Hanley, H. J. M., Sengers, J. V., and Ely, J. F., Proc. 14th Int. Conference Therm. Cond. (Pergammon Press, 1976).
12. Haynes, W. M., Physica 70, 410 (1973).
13. Giddings, J. G., Kao, J. T. F., and Kobayashi, R., J. Chem. Phys. 45, 578 (1966).
14. Barua, A. K., Afzal, M., Flynn, G., and Ross, J., J. Chem. Phys. 41, 374 (1964).

15. Kestin, J., and Leidenfrost, W., Thermodynamics and Transport Properties of Gases, Liquids and Solids, ASME Heat Transfer Division, Publ. by McGraw-Hill, N. Y. (1959), p. 321-38.

16. Boon, J. P., and Thomaes, G., Physica 29, 208 (1963); Boon, J. P., Legros, J. C., and Thomaes, G., Physica 33, 547 (1967).

17. Carmichael, L. T., Berry, V., and Sage, B. H., J. Chem. Eng. Data 10, 57 (1965).

18. Sage, B. H., and Lacey, W., Trans. Am. Inst. Mining. Met. Eng. 127, 118 (1938).

19. Bicher, L., and Katz, D., Ind. Eng. Chem. 35, 754 (1943).

20. Baron, J. D., Roof, J. G., and Wells, F. W., J. Chem. Eng. Data 4, 283 (1959).

21. Ross, J. F., and Brown, G. M., Ind. Eng. Chem. 49, 2026 (1957).

22. Hellemans, J., Zink, H., and Van Paemel, O., Physica 46, 395 (1970); 47, 45 (1970).

23. Galkov, G. I., and Gerf, S. F., Zhur. Tekh. Fiz. 11, 613 (1941).

24. Gerf, S. F., and Galkov, G. I., Zhur. Tekh. Fiz. 10, 725 (1940).

25. Rudenko, N. S., and Shubnikov, L. N., Physik. Z. Sowjetunion 6, 470 (1934).

26. Rudenko, N. S., Soviet-Physics-JETP 9, 1078 (1939).

27. Huang, E. T. S., Swift, G. W., and Kurata, F., AIChE J. 12, 932 (1966).

28. Swift, G. W., Lohrenz, J., and Kurata, F., AIChE J. 6, 415 (1960).

29. Carr, N. L., Inst. Gas Tech. Res. Bull. 23 (1953).

30. Comings, E. W., Mayland, R. J., and Egly, R. S., Univ. Illinois, Eng. Exp. Sta. Bull. Serial 354 (1944).

31. Gnezdidov, N. E., and Golubev, I. F., Gazov. Prom. 13, 46 (1968).

32. Iwasaki, H., J. Chem. Soc. Japan 62, 918 (1959).

33. Makita, T., J. Chem. Soc. Japan 23, 367 (1959).

34. Pavlovich, N. V. and Timrot, D. L., Teploenergetika 5, 61 (1958).

35. Kuss, E., Z. Agnew. Phys. 4, 203 (1952).

36. Meshcheryakov, N. V., and Golubev, I. F., Trudy GIAP 4 (1954).

37. Timrot, D. L., Serednitskaya, M. A., and Bespalov, M. S., Soviet Physis-Dokl. 20, 107 (1975).

38. Le Neindre, B., "Contribution a I'etude Experimentale de la Conductivite Thermique de Quelques Fluides a haute Temperature et a haute Pression," Ph.D. Thesis, Univ. of Paris (1969); Le Neindre,B., Tufeu, R., and Bury, P., Proc. 8th Conf. Thermal Conductivity, Plenum Press, New York, 1969, Eds. Ho, C. Y., et al., page 75; Le Neindre, B., Int. J. Heat Mass Transfer 15, 1 (1972).

39. Mani, N., Ph.D. Thesis, University of Calgary (1971).

40. Ikenberry, L., and Rice, S. A., J. Chem. Phys. 39, 1561 (1963).

41. Pavlovich, N. V., Gaz. Prom. 5, (1959).

42. Sokalova, V., and Golubev, I., Tephoenergetika 4 (1967).

43. Lenoir, J., Junk, W., and Comings, E., Chem. Eng. Progr. 49, 539 (1953); Lenoir, J. M., Ph.D. Thesis, Univ. of Illinois (1943); Lenoir, J. M., and Comings, E. W., Chem. Eng. Prog. 47, 223 (1951).

44. Misic, D., and Thodos, G., Physica 32, 885 (1966).

45. Keys, F. G., Trans. Am. Soc. Mech. Eng. 76, 809 (1954); 77, 1395 (1955).

46. Golubev, I. F., Teploenergetika 10, 78 (1963).

47. Carmichael, L. T., Reamer, H. H., and Sage, B. H., J. Chem. Eng. Data 11, 52 (1966).

48. Borovick, E. S., Manveev, A., and Panina, Y. E., Zhur. Tekh. Fiz. 10, 988 (1940).

49. Stoliarov, E. A., Ipatev, V. V., and Teodorovich, V. P., Zhur. Fiz. Khim. 24, 166 (1950).

50. Golubev, I. F., Viscosity of Gases and Gas Mixtures, Israel Program for Scientific Translations, Jerusalem, 1970. Available from the U. S. Department of Commerce.

51. Zagoruchenko, V. A., and Zhuravlev, A. M., Thermophysical Properties of Gaseous and Liquid Methane, Israel Program for Scientific Translations, Jersulem, 1970. Available from the U. S. Department of Commerce.

52. Vargaftik, N. B., Filippov, L. P., Tarzimanov, A. A., and Yuchak, R. P., Thermal Conductivity of Gases and Liquids (Moscow, 1970).

53. Kestin, J. and Mason, E. A., Reference [3], p 137.

FIGURE CAPTIONS

Figure 1. Deviations between experiment and calculation for the viscosity of saturated liquid methane.

Figure 2. Viscosity deviations at several representive temperatures.

Figure 3. Thermal conductivity deviations at low temperature.

Figure 4. Thermal conductivity deviations at representive temperatures above 300 K.

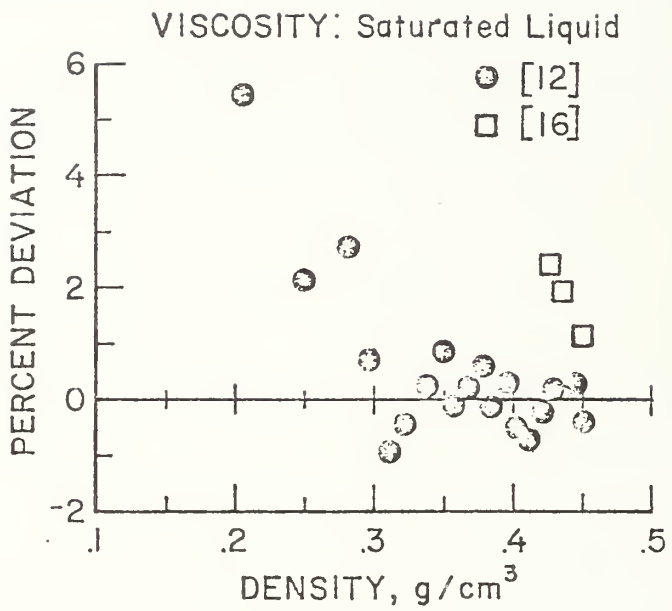
VISCOSITY: Saturated Liquid
[12]
[16]
PERCENT DEVIATION
6
4
2
0
-2
.1
.2
.3
.4
.5
DENSITY, g/cm³

Fig 1

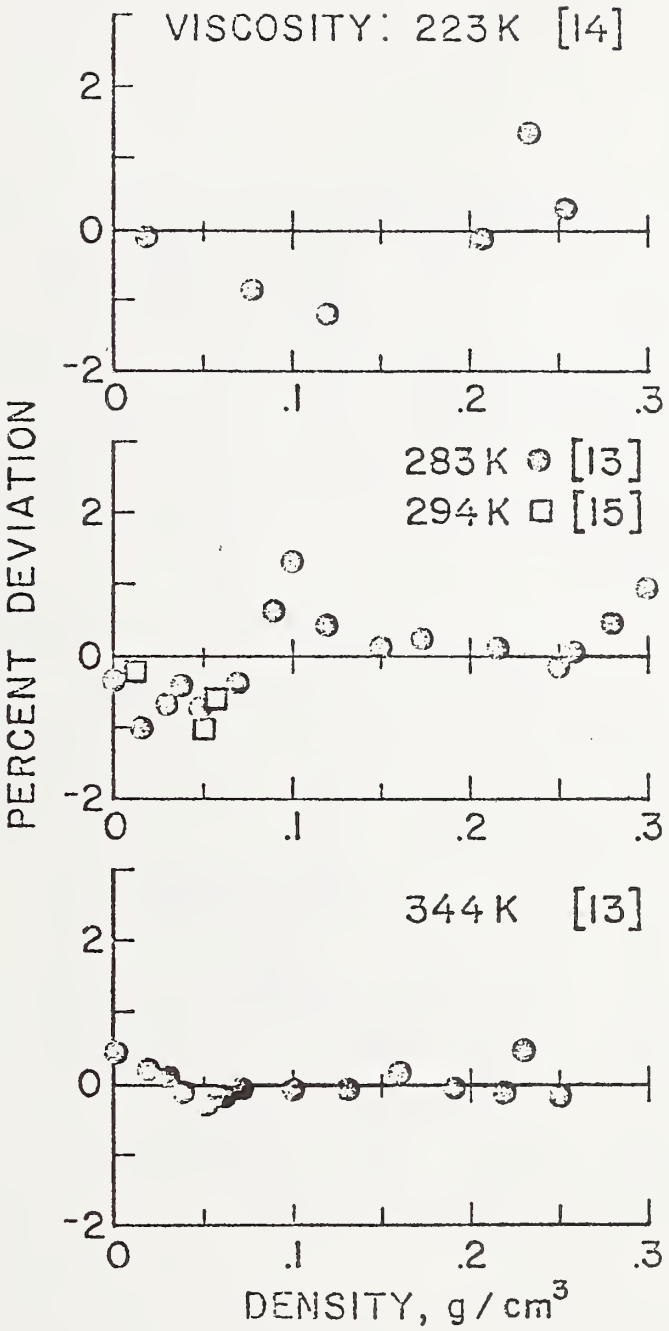
VISCOSITY: 223 K [14]
283 K ○ [13]
294 K □ [15]
344 K [13]
PERCENT DEVIATION
DENSITY, g / cm³
2
0
-2
0
.1
.2
.3

Fig 2

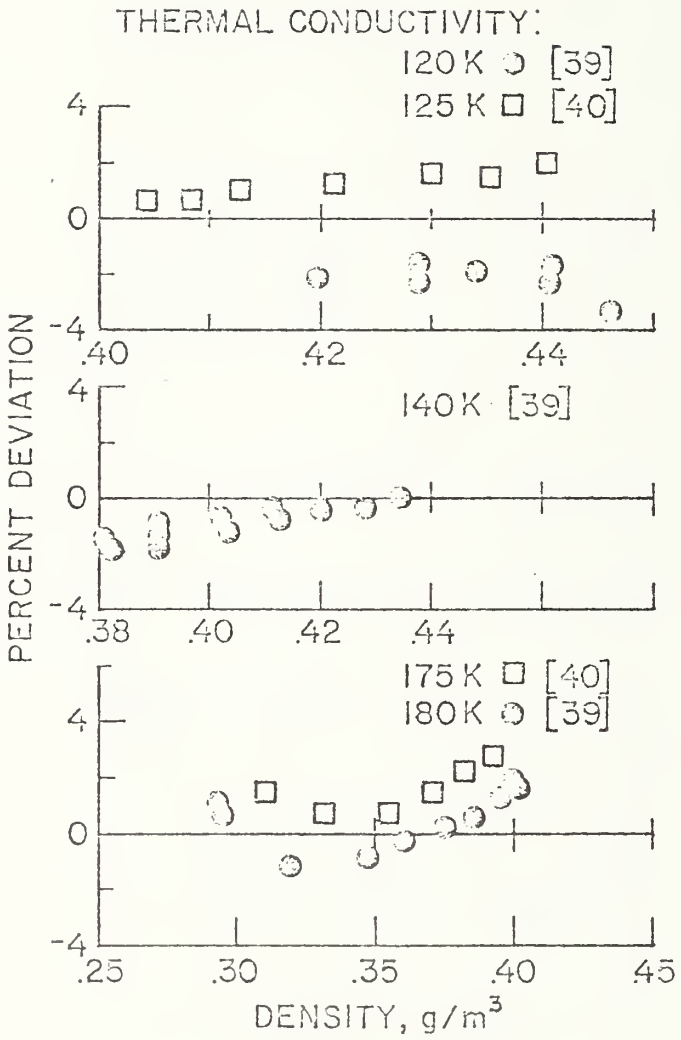
THERMAL CONDUCTIVITY:
120 K [39]
125 K [40]
140 K [39]
175 K [40]
180 K [39]
PERCENT DEVIATION
4
0
-4
.40
.42
.44
.38
.25
.30
.35
.45
DENSITY, g/m³

Fig. 3

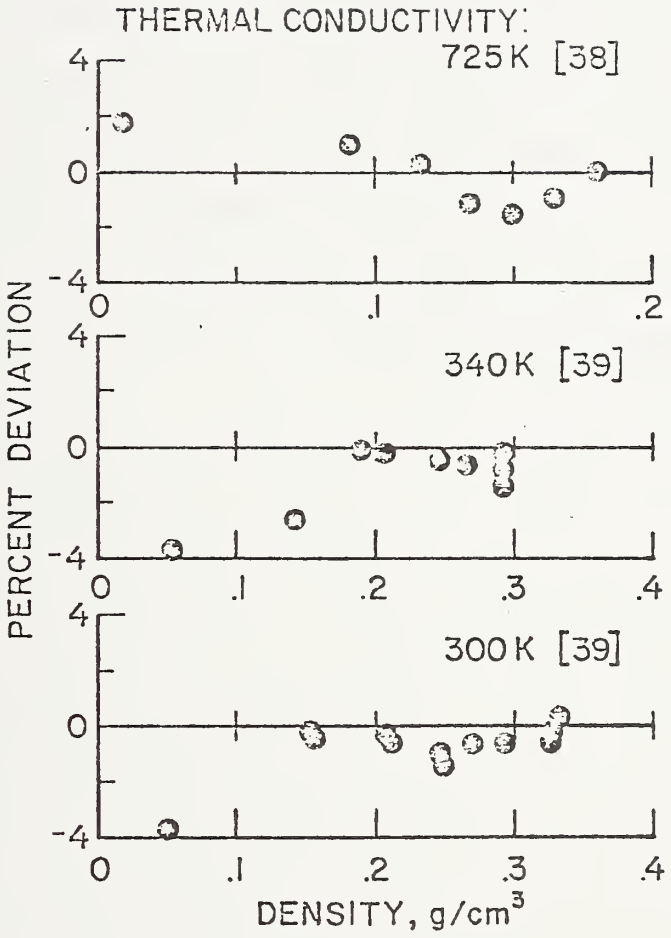
THERMAL CONDUCTIVITY:
725 K [38]
340 K [39]
300 K [39]
PERCENT DEVIATION
4
0
-4
0
.1
.2
.3
.4
DENSITY, g/cm³

Fig 4

TABLE 1. Potential Function Parameters [Equation (7)] and Critical Point Parameters for Methane

$m = 11$

$\gamma' = 3.0$

$r_m = 4.101 \times 10^{-10}$ m ($\sigma = 3.68 \times 10^{-10}$ m)

$\varepsilon/k = 168.0$ K

$T_c = 190.55$ K

$P_c = 4.5988$ MPa (45.387 atm)

$\rho_c = 0.1628$ g/cm^3 (10.15 mole/ℓ)

molecular weight = 16.043

TABLE 2. Parameters for the Dilute Gas Equation (8). The units are: Temperature in K, viscosity in μg/(cm·s), and thermal conductivity in mW/(m·K).

GV(1)	-2.090975×10^{5}	GT(1)	-2.147621×10^{5}
GV(2)	2.647269×10^{5}	GT(2)	2.190461×10^{5}
GV(3)	-1.472818×10^{5}	GT(3)	-8.618097×10^{4}
GV(4)	4.716740×10^{4}	GT(4)	1.496099×10^{4}
GV(5)	-9.491872×10^{3}	GT(5)	-4.730660×10^{2}
GV(6)	1.219979×10^{3}	GT(6)	-2.331178×10^{2}
GV(7)	-9.627993×10^{1}	GT(7)	3.778439×10^{1}
GV(8)	4.274152	GT(8)	-2.320481
GV(9)	-8.141531×10^{-2}	GT(9)	5.311764×10^{-2}

TABLE 3. Selected References for Methane

Authors	Approximate experimental range	Estimated accuracy ± %
Viscosity		
Haynes [12]	Saturated liquid 95-190 K	2%
Giddings, et al. [13]	283-410 K Pressures to 54 MPa	2%
Barua, et al. [14]	223-423 K Pressures to 17 MPa	2%
Kestin and Leidenfrost [15]	∿296 K Pressures to 15 MPa	1%
Boon and Thomaes [16]	Saturated liquid 91-114 K	3%
Thermal conductivity		
Le Neindre [38]	298-723 K Pressures to 100 MPa	4%
Mani [39]	139-400 K Pressures to 60 MPa	3.5%
Ikenberry and Rice [40]	98-235 K Pressures to 50 MPa	5%

TABLE 4. Parameters for Equations (3) - (5). The units are: Density in g/cm^3, temperature in K, viscosity in $\mu g/(cm \cdot s)$, thermal conductivity in $mW/(m \cdot K)$.

Viscosity			
Equation (3)	A	=	1.696985927
	B	=	-0.133372346
	C	=	1.4
	F	=	168.0
Equation (4)	E	=	1.0
	j_1	=	$-1.035060586 \times 10^{1}$
	j_2	=	$1.7571599671 \times 10^{1}$
	j_3	=	$-3.0193918656 \times 10^{3}$
	j_4	=	$1.8873011594 \times 10^{2}$
	j_5	=	$4.2903609488 \times 10^{-2}$
	j_6	=	$1.4529023444 \times 10^{2}$
	j_7	=	$6.1276818706 \times 10^{3}$
Thermal conductivity			
Equation (3)	A	=	-0.25276292
	B	=	0.33432859
	C	=	1.12
	F	=	168.0
Equation (5)	D	=	1.0
	k_1	=	-7.0403639907
	k_2	=	12.319512908
	k_3	=	$-8.8525979933 \times 10^{2}$
	k_4	=	72.835897919
	k_5	=	0.74421462902
	k_6	=	-2.9706914540
	k_7	=	$2.2209758501 \times 10^{3}$

TABLE 5. Tabulated values for the viscosity coefficient of methane. The units for the viscosity are μg/(cm•s).

TABLE 6. Tabulated values for the thermal conductivity coefficient of methane. The units are mW/(m•K).

T, K	P, MPa									
	0.1	0.5	1.0	1.5	2.0	2.5	3.0	3.5	4.0	5.0
95	1793.2									
100	1563.7	1570.3	1578.4	1586.6	1594.8	1603.0	1611.2	1619.4	1627.6	1644.1
105	1377.2	1383.2	1390.6	1398.1	1405.6	1413.1	1420.6	1428.0	1435.5	1450.5
110	1222.9	1228.4	1235.4	1242.3	1249.2	1256.1	1263.0	1269.9	1276.8	1290.5
115	46.0	1098.4	1104.9	1111.4	1117.9	1124.3	1130.8	1137.2	1143.6	1156.4
120	47.9	987.7	993.8	1000.0	1006.1	1012.2	1018.3	1024.4	1030.5	1042.5
125	49.8	892.0	897.9	903.8	909.7	915.6	921.4	927.3	933.1	944.6
130	51.8	808.3	814.1	819.9	825.6	831.3	837.0	842.6	848.3	859.4
135	53.7	734.1	739.9	745.6	751.3	756.9	762.5	768.1	773.6	784.5
140	55.6	56.9	673.3	679.1	684.8	690.5	696.1	701.6	707.1	717.9
145	57.5	58.8	612.9	618.8	624.7	630.4	636.1	641.7	647.2	658.1
150	59.4	60.7	62.6	563.4	569.5	575.5	581.4	587.1	592.8	603.9
155	61.3	62.6	64.4	511.7	518.2	524.5	530.7	536.7	542.7	554.1
160	63.2	64.4	66.2	68.5	469.5	476.4	483.1	489.5	495.9	508.0
165	65.1	66.3	68.0	70.1	422.0	429.9	437.4	444.6	451.5	464.5
170	67.0	68.2	69.8	71.7	74.4	383.4	392.3	400.6	408.4	423.0
175	68.9	70.0	71.6	73.4	75.8	79.2	345.5	355.9	365.4	382.4
180	70.8	71.9	73.3	75.1	77.3	80.2	84.5	306.6	319.8	341.3
185	72.6	73.7	75.1	76.8	78.9	81.5	84.9	90.3	263.0	297.2
190	74.5	75.5	76.9	78.6	80.5	82.8	85.8	89.9	96.5	240.9
195	76.3	77.3	78.7	80.3	82.1	84.3	87.0	90.4	95.1	121.0
200	78.2	79.2	80.5	82.0	83.7	85.8	88.2	91.2	95.0	108.2

	P, MPa									
T, K	6.0	7.0	8.0	9.0	10.0	15.0	20.0	30.0	40.0	50.0
95										
100	1660.5	1677.0	1693.5	1710.0						
105	1465.4	1480.4	1495.3	1510.3	1525.2	1599.7				
110	1304.3	1318.0	1331.7	1345.4	1359.1	1427.0	1494.4			
115	1169.2	1182.0	1194.7	1207.3	1220.0	1282.7	1344.4	1465.2		
120	1054.6	1066.5	1078.5	1090.3	1102.1	1160.5	1217.7	1329.1	1436.1	
125	956.0	967.4	978.7	989.9	1001.1	1056.0	1109.5	1213.1	1312.2	1407.1
130	870.4	881.4	892.2	903.0	913.6	965.8	1016.3	1113.3	1205.7	1294.0
135	795.2	805.9	816.4	826.8	837.1	887.1	935.2	1026.8	1113.6	1196.2
140	728.5	739.0	749.3	759.5	769.5	818.0	864.1	951.3	1033.2	1111.0
145	668.8	679.2	689.4	699.5	709.3	756.7	801.3	884.8	962.7	1036.3
150	614.7	625.2	635.4	645.5	655.3	702.0	745.5	826.0	900.4	970.4
155	565.2	576.0	586.4	596.5	606.4	652.8	695.5	773.6	845.1	912.0
160	519.5	530.7	541.4	551.7	561.7	608.3	650.5	726.6	795.7	859.9
165	476.9	488.5	499.7	510.4	520.7	567.8	609.7	684.4	751.3	813.2
170	436.4	448.9	460.7	471.9	482.6	530.6	572.6	646.1	711.3	771.2
175	397.5	411.2	423.9	435.7	447.0	496.3	538.6	611.4	675.1	733.2
180	359.1	374.6	388.6	401.4	413.4	464.6	507.3	579.6	642.1	698.7
185	320.0	338.5	354.3	368.5	381.4	435.0	478.4	550.5	612.0	667.3
190	277.9	301.6	323.4	336.5	350.7	407.3	451.6	523.8	584.5	638.6
195	226.3	262.3	286.1	304.9	320.9	381.3	426.7	499.1	559.1	612.2
200	157.2	218.1	250.5	273.4	291.8	356.8	403.5	476.2	535.7	588.0

T, K	P, MPa									
	0.1	0.5	1.0	1.5	2.0	2.5	3.0	3.5	4.0	5.0
200	78.2	79.2	80.5	82.0	83.7	85.8	88.2	91.2	95.0	108.2
205	80.0	81.0	82.2	83.7	85.4	87.3	89.5	92.2	95.5	105.2
210	81.8	82.7	84.0	85.4	87.0	88.8	90.9	93.4	96.3	104.2
215	83.6	84.5	85.7	87.1	88.6	90.4	92.3	94.6	97.2	104.1
220	85.4	86.3	87.5	88.8	90.3	91.9	93.8	95.9	98.3	104.4
225	87.2	88.1	89.2	90.5	91.9	93.5	95.3	97.3	99.5	105.0
230	89.0	89.8	90.9	92.2	93.6	95.1	96.8	98.7	100.8	105.8
235	90.7	91.6	92.7	93.9	95.2	96.7	98.3	100.1	102.0	106.7
240	92.5	93.3	94.4	95.5	96.8	98.2	99.8	101.5	103.4	107.7
245	94.2	95.0	96.1	97.2	98.5	99.8	101.3	102.9	104.7	108.8
250	95.9	96.7	97.7	98.9	100.1	101.4	102.8	104.4	106.1	109.9
255	97.7	98.4	99.4	100.5	101.7	103.0	104.4	105.9	107.5	111.1
260	99.4	100.1	101.1	102.1	103.3	104.5	105.9	107.3	108.9	112.4
265	101.1	101.8	102.7	103.8	104.9	106.1	107.4	108.8	110.3	113.6
270	102.7	103.5	104.4	105.4	106.5	107.7	108.9	110.3	111.7	114.9
275	104.4	105.1	105.0	107.0	108.1	109.2	110.4	111.7	113.1	116.2
280	106.1	106.8	107.6	108.6	109.7	110.8	111.9	113.2	114.6	117.5
285	107.7	108.4	109.3	110.2	111.2	112.3	113.5	114.7	116.0	118.8
290	109.4	110.0	110.9	111.8	112.8	113.8	115.0	116.2	117.4	120.2
295	111.0	111.6	112.5	113.4	114.3	115.4	116.5	117.6	118.9	121.5
300	112.6	113.2	114.1	114.9	115.9	116.9	118.0	119.1	120.3	122.9
310	115.8	116.4	117.2	118.1	119.0	119.9	120.9	122.0	123.1	125.6
320	119.0	119.5	120.3	121.1	122.0	122.9	123.9	124.9	126.0	128.3
330	122.1	122.6	123.4	124.2	125.0	125.9	126.8	127.8	128.8	131.0
340	125.1	125.7	126.4	127.2	128.0	128.8	129.7	130.6	131.6	133.7
350	128.2	128.7	129.4	130.1	130.9	131.7	132.6	133.5	134.4	136.4
360	131.2	131.7	132.4	133.1	133.8	134.6	135.4	136.3	137.2	139.1
370	134.1	134.7	135.3	136.0	136.7	137.5	138.2	139.1	139.9	141.7
380	137.1	137.6	138.2	138.8	139.5	140.3	141.0	141.8	142.6	144.4
390	140.0	140.4	141.0	141.7	142.4	143.1	143.8	144.6	145.3	147.0
400	142.8	143.3	143.9	144.5	145.1	145.8	146.5	147.3	148.0	149.6
410	145.6	146.1	146.7	147.3	147.9	148.6	149.2	150.0	150.7	152.2
420	148.4	148.9	149.4	150.0	150.6	151.3	151.9	152.6	153.3	154.8
430	151.2	151.6	152.2	152.7	153.3	153.9	154.6	155.3	155.9	157.4
440	153.9	154.3	154.9	155.4	156.0	156.6	157.2	157.9	158.5	159.9
450	156.6	157.0	157.5	158.1	158.6	159.2	159.8	160.5	161.1	162.5
460	159.3	159.7	160.2	160.7	161.3	161.8	162.4	163.0	163.7	165.0
470	161.9	162.3	162.8	163.3	163.9	164.4	165.0	165.6	166.2	167.5
480	164.6	164.9	165.4	165.9	166.4	167.0	167.5	168.1	168.7	169.9
490	167.1	167.5	168.0	168.5	169.0	169.5	170.0	170.6	171.2	172.4
500	169.7	170.1	170.5	171.0	171.5	172.0	172.5	173.1	173.6	174.8

	P, MPa									
T, K	6.0	7.0	8.0	9.0	10.0	15.0	20.0	30.0	50.0	75.0
200	157.2	210.1	250.5	273.4	291.8	356.8				
205	126.1	172.5	213.9	241.9	263.3	333.6				
210	117.7	143.9	180.5	211.8	235.9	311.8	361.5			
215	114.3	131.1	157.1	185.8	210.9	291.4	342.5			
220	112.8	125.2	143.5	166.6	189.9	272.4	324.8			
225	112.2	122.1	135.9	153.8	173.8	255.1	308.3			
230	112.2	120.5	131.6	145.7	162.2	239.5	293.1	369.1		
235	112.5	119.7	129.0	140.5	154.2	225.8	279.2	355.2		
240	113.0	119.5	127.5	137.2	148.7	213.9	266.5	342.3		
245	113.7	119.6	126.6	135.0	144.9	203.9	255.0	330.3		
250	114.5	119.9	126.2	133.7	142.3	195.5	244.8	319.2		
255	115.4	120.4	126.2	132.9	140.5	188.6	235.7	308.9		
260	116.4	121.0	126.4	132.5	139.4	182.9	227.7	299.4		
265	117.4	121.8	126.8	132.4	138.7	178.3	220.7	290.7		
270	118.5	122.7	127.3	132.5	138.3	174.6	214.5	282.6	382.5	
275	119.7	123.6	127.9	132.8	138.1	171.6	209.2	275.3	373.8	
280	120.8	124.5	128.7	133.2	138.2	169.2	204.6	268.6	365.6	
285	122.0	125.6	129.5	133.8	138.5	167.3	200.7	262.5	358.0	
290	123.2	126.6	130.3	134.4	138.8	165.8	197.3	256.9	350.8	
295	124.5	127.7	131.3	135.1	139.3	164.6	194.4	251.9	344.0	
300	125.7	128.8	132.2	135.9	139.9	163.8	191.9	247.3	337.7	
310	128.2	131.1	134.2	137.6	141.3	162.7	188.0	239.4	326.2	
320	130.8	133.5	136.4	139.5	142.8	162.3	185.3	233.0	316.1	
330	133.3	135.9	138.6	141.5	144.6	162.5	183.5	227.8	307.3	388.3
340	135.9	138.3	140.9	143.6	146.5	163.0	182.3	223.6	299.5	378.4
350	138.5	140.8	143.2	145.7	148.4	163.9	181.7	220.3	292.8	369.5
360	141.1	143.2	145.5	147.9	150.5	164.9	181.5	217.7	286.9	361.5
370	143.7	145.7	147.9	150.2	152.6	166.1	181.7	215.7	281.8	354.2
380	146.2	148.2	150.3	152.5	154.7	167.5	182.2	214.1	277.4	347.7
390	148.8	150.7	152.7	154.7	156.9	169.0	182.8	213.1	273.6	341.8
400	151.3	153.1	155.0	157.0	159.1	170.6	183.7	212.3	270.3	336.5
410	153.9	155.6	157.4	159.3	161.3	172.3	184.7	211.9	267.5	331.7
420	156.4	158.1	159.8	161.7	163.6	174.1	185.9	211.8	265.1	327.4
430	158.9	160.5	162.2	164.0	165.8	175.9	187.1	211.9	263.1	323.5
440	161.4	163.0	164.6	166.3	168.0	177.7	188.5	212.1	261.4	320.1
450	163.9	165.4	167.0	168.6	170.3	179.6	189.9	212.6	260.0	317.0
460	166.3	167.8	169.3	170.9	172.5	181.5	191.4	213.2	258.9	314.2
470	168.8	170.2	171.7	173.2	174.8	183.4	193.0	213.9	258.0	311.8
480	171.2	172.6	174.0	175.5	177.0	185.3	194.6	214.7	257.3	309.6
490	173.6	175.0	176.3	177.8	179.2	187.3	196.2	215.6	256.9	307.7
500	176.0	177.3	178.7	180.0	181.5	189.3	197.9	216.7	256.5	306.0

T, K	P, MPa									
	0.1	0.5	1.0	1.5	2.0	2.5	3.0	3.5	4.0	5.0
95	215.51									
100	206.19	206.62	207.16	207.69	208.23	208.76	209.29	209.82	210.35	211.41
105	197.31	197.75	198.30	198.86	199.40	199.95	200.50	201.04	201.59	202.67
110	188.80	189.25	189.82	190.39	190.95	191.52	192.08	192.64	193.19	194.30
115	13.58	181.06	181.64	182.23	182.81	183.40	183.97	184.55	185.12	186.26
120	14.14	173.11	173.72	174.33	174.94	175.54	176.14	176.74	177.33	178.51
125	14.70	165.36	166.01	166.65	167.28	167.91	168.53	169.16	169.77	170.99
130	15.26	157.77	158.45	159.13	159.80	160.46	161.12	161.77	162.41	163.69
135	15.82	150.29	151.02	151.74	152.45	153.15	153.85	154.54	155.22	156.56
140	16.38	17.66	143.65	144.43	145.19	145.95	146.69	147.43	148.15	149.58
145	16.94	18.17	136.29	137.14	137.98	138.80	139.60	140.40	141.18	142.70
150	17.49	18.68	20.10	129.83	130.75	131.65	132.54	133.40	134.25	135.90
155	18.05	19.20	20.54	122.38	123.43	124.45	125.43	126.39	127.33	129.14
160	18.60	19.72	21.00	22.51	115.92	117.09	118.21	119.30	120.35	122.36
165	19.15	20.24	21.46	22.85	108.07	109.46	110.78	112.03	113.24	115.52
170	19.70	20.76	21.94	23.23	24.91	101.42	103.02	104.52	105.93	108.56
175	20.25	21.28	22.41	23.63	25.13	27.38	94.92	96.74	98.43	101.48
180	20.80	21.81	22.90	24.05	25.42	27.28	30.47	88.92	90.91	94.44
185	21.35	22.33	23.39	24.49	25.75	27.36	29.73	34.24	84.04	87.80
190	21.90	22.86	23.88	24.93	26.11	27.54	29.47	32.47	38.29	82.03
195	22.45	23.39	24.38	25.39	26.49	27.78	29.43	31.72	35.28	59.45
200	23.01	23.92	24.88	25.85	26.88	28.07	29.51	31.38	33.98	44.24

T, K	P, MPa									
	6.0	7.0	8.0	9.0	10.0	15.0	20.0	30.0	40.0	50.0
95										
100	212.46	213.51	214.56	215.59						
105	203.74	204.81	205.88	206.94	207.99	213.16				
110	195.40	196.50	197.58	198.66	199.74	205.00	210.09			
115	187.39	188.51	189.63	190.73	191.83	197.18	202.34	212.10		
120	179.67	180.83	181.97	183.10	184.22	189.68	194.91	204.78	213.92	
125	172.20	173.39	174.57	175.74	176.89	182.47	187.79	197.77	206.99	215.52
130	164.95	166.19	167.41	168.61	169.80	175.53	180.96	191.07	200.35	208.94
135	157.88	159.17	160.45	161.70	162.93	168.84	174.38	184.64	194.01	202.66
140	150.97	152.33	153.66	154.97	156.26	162.37	168.05	178.48	187.94	196.65
145	144.18	145.63	147.03	148.41	149.76	155.11	161.96	172.57	182.14	190.91
150	137.49	139.04	140.53	141.99	143.41	150.04	156.07	166.90	176.58	185.42
155	130.87	132.53	134.13	135.69	137.19	144.14	150.39	161.46	171.27	180.18
160	124.26	126.08	127.81	129.48	131.09	138.41	144.89	156.23	166.17	175.16
165	117.64	119.64	121.53	123.34	125.07	132.83	139.57	151.21	161.30	170.37
170	110.96	113.19	115.28	117.25	119.12	127.38	134.41	146.37	156.62	165.78
175	104.23	106.73	109.04	111.21	113.24	122.06	129.42	141.72	152.14	161.40
180	97.53	100.32	102.87	105.24	107.45	116.87	124.57	137.25	147.85	157.20
185	91.17	94.18	96.92	99.45	101.82	111.82	119.88	132.94	143.73	153.18
190	85.43	88.58	91.42	94.05	96.50	106.94	115.34	128.79	139.78	149.34
195	79.82	83.48	86.50	89.18	91.66	102.31	110.98	124.81	135.99	145.65
200	68.45	77.54	81.66	84.69	87.28	97.99	106.82	120.98	132.36	142.13

T, K	P, MPa 0.1	0.5	1.0	1.5	2.0	2.5	3.0	3.5	4.0	5.0
200	23.01	23.92	24.88	25.85	26.88	28.07	29.51	31.38	33.98	44.24
205	23.56	24.46	25.39	26.32	27.30	28.40	29.68	31.27	33.32	40.01
210	24.12	25.00	25.91	26.80	27.73	28.75	29.91	31.29	32.99	37.94
215	24.69	25.54	26.42	27.28	28.17	29.12	30.19	31.41	32.86	36.78
220	25.25	26.09	26.95	27.78	28.62	29.52	30.51	31.61	32.87	36.10
225	25.82	26.64	27.48	28.28	29.09	29.94	30.86	31.86	32.98	35.73
230	26.40	27.20	28.02	28.79	29.57	30.38	31.24	32.16	33.17	35.56
235	26.98	27.77	28.56	29.32	30.07	30.84	31.64	32.50	33.43	35.55
240	27.56	28.33	29.11	29.85	30.57	31.31	32.08	32.88	33.74	35.65
245	28.15	28.91	29.67	30.38	31.09	31.80	32.53	33.29	34.09	35.84
250	28.75	29.49	30.24	30.93	31.61	32.30	33.00	33.72	34.48	36.10
255	29.35	30.08	30.81	31.49	32.15	32.82	33.49	34.18	34.89	36.42
260	29.96	30.68	31.39	32.06	32.70	33.34	33.99	34.66	35.34	36.78
265	30.57	31.28	31.98	32.63	33.26	33.88	34.51	35.15	35.81	37.17
270	31.19	31.89	32.58	33.21	33.83	34.44	35.05	35.66	36.29	37.60
275	31.82	32.50	33.18	33.80	34.40	35.00	35.59	36.19	36.80	38.06
280	32.45	33.13	33.79	34.40	34.99	35.57	36.15	36.73	37.32	38.53
285	33.09	33.76	34.41	35.01	35.59	36.15	36.72	37.28	37.86	39.03
290	33.74	34.40	35.04	35.63	36.19	36.75	37.30	37.85	38.41	39.54
295	34.40	35.04	35.68	36.25	36.81	37.35	37.89	38.43	38.97	40.07
300	35.06	35.69	36.32	36.89	37.43	37.96	38.49	39.01	39.54	40.61
310	36.40	37.02	37.63	38.18	38.70	39.21	39.72	40.22	40.72	41.74
320	37.78	38.38	38.97	39.50	40.01	40.50	40.98	41.47	41.95	42.92
330	39.18	39.77	40.34	40.85	41.34	41.82	42.29	42.75	43.22	44.14
340	40.61	41.18	41.74	42.24	42.72	43.18	43.63	44.08	44.52	45.41
350	42.07	42.63	43.17	43.66	44.12	44.57	45.00	45.44	45.87	46.72
360	43.55	44.10	44.63	45.11	45.56	45.99	46.41	46.83	47.25	48.07
370	45.07	45.61	46.12	46.58	47.02	47.44	47.85	48.26	48.66	49.46
380	46.61	47.14	47.64	48.09	48.52	48.93	49.33	49.72	50.11	50.88
390	48.18	48.70	49.19	49.63	50.04	50.44	50.83	51.21	51.59	52.34
400	49.78	50.28	50.76	51.19	51.60	51.99	52.36	52.74	53.10	53.83
410	51.40	51.89	52.36	52.78	53.18	53.56	53.93	54.29	54.64	55.35
420	53.04	53.52	53.99	54.40	54.78	55.15	55.51	55.87	56.22	56.90
430	54.71	55.18	55.64	56.04	56.42	56.78	57.13	57.47	57.81	58.48
440	56.40	56.87	57.31	57.70	58.07	58.43	58.77	59.11	59.44	60.09
450	58.11	58.57	59.01	59.39	59.75	60.10	60.44	60.77	61.09	61.72
460	59.85	60.30	60.72	61.10	61.46	61.80	62.13	62.45	62.76	63.38
470	61.60	62.04	62.46	62.84	63.18	63.52	63.84	64.15	64.46	65.07
480	63.37	63.81	64.22	64.59	64.93	65.26	65.57	65.88	66.18	66.77
490	65.17	65.60	66.00	66.36	66.70	67.02	67.32	67.63	67.92	68.50
500	66.98	67.40	67.80	68.15	68.48	68.79	69.10	69.39	69.68	70.25

T, K	P, MPa									
	6.0	7.0	8.0	9.0	10.0	15.0	20.0	30.0	50.0	75.0
200	68.45	77.54	81.66	84.69	87.28	97.99				
205	53.48	63.06	75.53	79.85	82.93	94.02				
210	46.33	58.03	67.51	73.82	78.09	90.33	99.22			
215	42.72	51.03	59.78	66.94	72.36	86.75	95.78			
220	40.64	46.73	53.81	60.57	66.38	83.09	92.51			
225	39.36	44.06	49.63	55.48	60.99	79.27	89.34			
230	38.58	42.34	46.80	51.67	56.59	75.35	86.20	101.42		
235	38.12	41.24	44.89	48.94	53.20	71.53	83.08	98.69		
240	37.90	40.55	43.61	47.02	50.68	68.00	80.02	96.08		
245	37.85	40.16	42.78	45.70	48.86	64.90	77.08	93.58		
250	37.92	39.97	42.27	44.82	47.57	62.27	74.36	91.19		
255	38.09	39.95	42.00	44.25	46.69	60.11	71.90	88.92		
260	38.33	40.04	41.90	43.93	46.11	58.37	69.74	86.78		
265	38.64	40.22	41.93	43.78	45.76	56.99	67.87	84.79		
270	38.99	40.47	42.06	43.77	45.58	55.92	66.28	82.96	106.47	
275	39.38	40.78	42.27	43.86	45.54	55.11	64.94	81.29	104.75	
280	39.80	41.13	42.54	44.03	45.60	54.50	63.83	79.79	103.14	
285	40.24	41.52	42.86	44.27	45.75	54.07	62.91	78.44	101.62	
290	40.71	41.94	43.21	44.55	45.95	53.78	62.16	77.24	100.19	
295	41.20	42.38	43.61	44.88	46.21	53.60	61.56	76.18	98.86	
300	41.71	42.85	44.02	45.25	46.52	53.52	61.09	75.24	97.62	
310	42.78	43.84	44.94	46.07	47.23	53.59	60.47	73.71	95.41	
320	43.90	44.90	45.93	46.99	48.07	53.90	60.20	72.58	93.53	
330	45.08	46.03	47.00	47.99	49.00	54.40	60.20	71.79	91.96	112.50
340	46.30	47.21	48.13	49.06	50.02	55.05	60.44	71.30	90.67	110.83
350	47.58	48.44	49.31	50.20	51.10	55.83	60.85	71.06	89.66	109.39
360	48.89	49.72	50.56	51.40	52.26	56.72	61.43	71.04	88.88	108.17
370	50.25	51.04	51.84	52.65	53.47	57.70	62.13	71.22	88.32	107.14
380	51.64	52.41	53.18	53.95	54.73	58.76	62.96	71.56	87.97	106.31
390	53.08	53.81	54.56	55.30	56.05	59.89	63.88	72.05	87.80	105.66
400	54.54	55.26	55.97	56.69	57.41	61.09	64.89	72.66	87.79	105.17
410	56.04	56.73	57.43	58.12	58.81	62.34	65.97	73.40	87.94	104.84
420	57.57	58.25	58.91	59.58	60.26	63.65	67.13	74.24	88.23	104.66
430	59.14	59.79	60.44	61.09	61.73	65.01	68.35	75.16	88.64	104.62
440	60.73	61.36	61.99	62.62	63.25	66.42	69.63	76.18	89.17	104.71
450	62.35	62.96	63.58	64.19	64.80	67.86	70.97	77.26	89.80	104.91
460	63.99	64.59	65.19	65.78	66.38	69.35	72.35	78.42	90.53	105.23
470	65.66	66.25	66.83	67.41	67.98	70.87	73.77	79.64	91.35	105.65
480	67.35	67.93	68.49	69.06	69.62	72.42	75.24	80.91	92.26	106.17
490	69.07	69.63	70.18	70.73	71.28	74.01	76.74	82.24	93.23	106.78
500	70.81	71.35	71.90	72.43	72.97	75.63	78.28	83.61	94.28	107.47

TABLE 7. Transport Coefficients of Saturated Liquid Methane

Temperature, K	Density, mol/ℓ	Viscosity, μg/(cm·s)	Thermal conductivity, mW/(m·K)
95	27.789	1792	215
100	27.367	1563	206
105	26.934	1377	197
110	26.491	1223	189
115	26.035	1094	181
120	25.566	984	173
125	25.081	889	165
130	24.578	807	158
135	24.055	734	150
140	23.508	669	143
145	22.932	611	136
150	22.322	558	129
155	21.672	509	122
160	20.971	464	115
165	20.206	421	108
170	19.356	380	101
175	18.386	340	94
180	17.226	300	88
185	15.690	256	84
190	12.485	187	89

APPENDIX

METHANE EQUATION OF STATE

The equation of state used in the work is that reported by McCarty in reference [5]. The form of the equation, and its parameters are reproduced in this appendix.

The equation of state is given by the following functional form:

$$
\begin{aligned}
P = \rho RT &+ \rho^2 (N_1 T + N_2 T^{1/2} + N_3 + N_4/T + N_5/T^2) \\
&+ \rho^3 (N_6 T + N_7 + N_8/T + N_9/T^2) \\
&+ \rho^4 (N_{10} T + N_{11} + N_{12}/T) + \rho^5 (N_{13}) \\
&+ \rho^6 (N_{14}/T + N_{15}/T^2) + \rho^7 (N_{16}/T) \\
&+ \rho^8 (N_{17}/T + N_{18}/T^2) + \rho^9 (N_{19}/T^2) \\
&+ \rho^3 (N_{20}/T^2 + N_{21}/T^3) \exp(-\gamma\rho^2) \\
&+ \rho^5 (N_{22}/T^2 + N_{23}/T^4) \exp(-\gamma\rho^2) \\
&+ \rho^7 (N_{24}/T^2 + N_{25}/T^3) \exp(-\gamma\rho^2) \\
&+ \rho^9 (N_{26}/T^2 + N_{27}/T^4) \exp(-\gamma\rho^2) \\
&+ \rho^{11} (N_{28}/T^2 + N_{29}/T^3) \exp(-\gamma\rho^2) \\
&+ \rho^{13} (N_{30}/T^2 + N_{31}/T^3 + N_{32}/T^4) \exp(-\gamma\rho^2)
\end{aligned}
$$

where, to be consistent with reference [5], P is in atmospheres, ρ is in mol/ℓ, and T is in kelvins.

The coefficients (N_j, γ and R) are

$$N_1 = -1.8439486666 \times 10^{-2}$$
$$N_2 = 1.0510162064$$
$$N_3 = -1.6057820303 \times 10$$
$$N_4 = 8.4844027562 \times 10^{2}$$
$$N_5 = -4.2738409106 \times 10^{4}$$
$$N_6 = 7.6565285254 \times 10^{-4}$$
$$N_7 = -4.8360724197 \times 10^{-1}$$
$$N_8 = 8.5195473835 \times 10$$
$$N_9 = -1.6607434721 \times 10^{4}$$
$$N_{10} = -3.7521074532 \times 10^{-5}$$
$$N_{11} = 2.8616309259 \times 10^{-2}$$
$$N_{12} = -2.8685285973$$
$$N_{13} = 1.1906973942 \times 10^{-4}$$
$$N_{14} = -8.5315715699 \times 10^{-3}$$
$$N_{15} = 3.8365063841$$
$$N_{16} = 2.4986828379 \times 10^{-5}$$
$$N_{17} = 5.7974531455 \times 10^{-6}$$
$$N_{18} = -7.1648329297 \times 10^{-3}$$
$$N_{19} = 1.2577853784 \times 10^{-4}$$
$$N_{20} = 2.2240102466 \times 10^{4}$$
$$N_{21} = -1.4800512328 \times 10^{6}$$
$$N_{22} = 5.0498054887 \times 10$$
$$N_{23} = 1.6428375992 \times 10^{6}$$
$$N_{24} = 2.1325387196 \times 10^{-1}$$
$$N_{25} = 3.7791273422 \times 10$$
$$N_{26} = -1.1857016815 \times 10^{-5}$$
$$N_{27} = -3.1630780767 \times 10$$
$$N_{28} = -4.1006782941 \times 10^{-6}$$
$$N_{29} = 1.4870043284 \times 10^{-3}$$
$$N_{30} = 3.1512261532 \times 10^{-9}$$
$$N_{31} = -2.1670774745 \times 10^{-6}$$
$$N_{32} = 2.4000551079 \times 10^{-5}$$
$$\gamma = -0.0096$$
$$R = 0.08205616$$

A corresponding states procedure to predict the viscosity and thermal conductivity coefficients of a pure fluid or mixture is discussed. We show the transport properties of a fluid or mixture can be calculated to within experimental error given only corresponding values for a reference fluid and equation of state data. With methane, as the reference fluid, we consider nitrogen, ethane, propane, butane, carbon dioxide, and mixtures of these fluids. LNG is also included. It is shown that the conventional corresponding states approach is not sufficient to predict correctly the transport properties. The effect of internal degrees of freedom on the thermal conductivity coefficient and the enhancement in the critical region for this coefficient is discussed briefly.

Prediction of the viscosity and thermal conductivity coefficients of mixtures

H.J.M. Hanley

The task of measuring the transport properties for all mixtures of possible practical interest is out of the question, even for simple fluids. Any method, then, which could predict the properties to within the experimental error would be both interesting and useful. Unfortunately, the lack of suitable data, on the one hand, and the theoretical problems that can be encountered in the study of transport phenomena in general, on the other hand, are obstacles which have only been overcome for special cases.

Similar problems come up when one considers the thermodynamic (or *PVT*) properties of mixtures. In this case, however, the principle of corresponding states has been used widely as a prediction tool and, in particular, the principle has been extended systematically to multicomponent mixtures of polyatomic molecules. It is thus logical to investigate how the corresponding states approach can be broadened to include transport properties and the object of this paper is to do this. Specifically, we discuss an *ad hoc* procedure, based on the principle of corresponding states, to predict the viscosity coefficient (η) and the thermal conductivity coefficient (λ) of fluid mixtures given thermodynamic data. We will show that the procedure appears to work (data for comparison are scarce) for a variety of mixtures over a wide range of experimental conditions.

Background

Some introductory material is summarized in this section.

Simple two-parameter corresponding states

The basic criterion for two pure fluids to obey the principle of corresponding states, or to 'conform' or 'correspond' is that a given intermolecular potential form, such as

$$\phi = \epsilon f\left(\frac{r}{\sigma}\right) \tag{1}$$

(where r is the intermolecular separation) is appropriate for both. Each fluid can thus be characterized by an energy parameter, ϵ, and a distance parameter, σ. If the two fluids do correspond, then the transport coefficients of the one fluid, α, at a particular temperature (T) and density (ρ) can be expressed in terms of the coefficients of the other fluid, o. For example, for the viscosity and thermal conductivity coefficients we have[1]

$$\eta_\alpha[\rho, T] = \eta_0\left[\rho\left(\frac{\sigma_\alpha}{\sigma_0}\right)^3, T\left(\frac{\epsilon_0}{\epsilon_\alpha}\right)\right]\left(\frac{M_\alpha}{M_0}\right)^{1/2}\left(\frac{\sigma_0}{\sigma_\alpha}\right)^2\left(\frac{\epsilon_\alpha}{\epsilon_0}\right)^{1/2} \tag{2}$$

and

$$\lambda_\alpha[\rho, T] = \lambda_0\left[\rho\left(\frac{\sigma_\alpha}{\sigma_0}\right)^3, T\left(\frac{\epsilon_0}{\epsilon_\alpha}\right)\right]\left(\frac{M_0}{M_\alpha}\right)^{1/2}\left(\frac{\alpha_0}{\sigma_\alpha}\right)^2\left(\frac{\epsilon_\alpha}{\epsilon_0}\right)^{1/2} \tag{3}$$

The coefficients, η_0 and λ_0, which can be taken as reference values, have to be evaluated at the proper density and temperature as indicated. M is the molecular weight.

Since one can write $T^c \sim \epsilon/k$, $\rho^c \sim \sigma^{-3}$, where the superscript, c, refers to the critical point value and k is Boltzmann's constant, alternative expressions for η_α and λ_α are

$$\eta_\alpha(\rho, T) = \eta_0\left[\rho\left(\frac{\rho_0^c}{\rho_\alpha^c}\right), T\left(\frac{T_0^c}{T_\alpha^c}\right)\right]\left(\frac{M_\alpha}{M_0}\right)^{1/2}\left(\frac{\rho_\alpha^c}{\rho_0^c}\right)^{2/3}\left(\frac{T_\alpha^c}{T_0^c}\right)^{1/2} \tag{4}$$

$$\lambda_\alpha(\rho, T) = \lambda_0\left[\rho\left(\frac{\rho_0^c}{\rho_\alpha^c}\right), T\left(\frac{T_0^c}{T_\alpha^c}\right)\right]\left(\frac{M_0}{M_\alpha}\right)^{1/2}\left(\frac{\rho_\alpha^c}{\rho_0^c}\right)^{2/3}\left(\frac{T_\alpha^c}{T_0^c}\right)^{1/2} \tag{5}$$

Equations (4) and (5) are the basis for many of the correlation techniques of transport properties discussed in the literature,[2] both for pure fluids and for mixtures. However, results can be very inconsistent if the equations are used as predictive tools, and clear-cut procedures have not been proposed. This is particularly true for mixtures for which one needs mixing rules (for the critical parameters, for

The author is with the National Bureau of Standards, Cryogenics Division, Boulder, Colorado 80302, USA. Received 7 July 1976.

example). Several mixing rules have been suggested, but on essentially intuitive grounds.[3]

Recently, however, the relationship between corresponding states and transport properties of mixtures has been clarified considerably by Mo and Gubbins.[4] These authors considered a conformal fluid mixture [that is, a mixture[5] in which each component obeys the universal potential of equation (1)] in the Van der Waals one-fluid approximation. The one-fluid approximation allows the mixture to be equated to an equivalent pure fluid so (4), for example, becomes for mixture x,

$$\eta_x(\rho, T) = \eta_0\left[\rho\left(\frac{\rho_0^c}{\rho_x^c}\right), T\left(\frac{T_0^c}{T_x^c}\right)\right]\left(\frac{M_x}{M_0}\right)^{1/2}\left(\frac{\rho_x^c}{\rho_0^c}\right)^{2/3}\left(\frac{T_x^c}{T_0^c}\right)^{1/2} \tag{6}$$

with a similar expression for the thermal conductivity coefficient. Mo and Gubbins derive (6) under well-defined assumptions and show that one possible set of mixing rules for the density and temperature of a binary mixture are (using the notation of Gubbins et al)

$$(\rho_x^c)^{-1} = \sum_\alpha \sum_\beta x_\alpha x_\beta (\rho_{\alpha\beta}^c)^{-1} \tag{7}$$

and

$$T_x^c(\rho_x^c)^{-1} = \sum_\alpha \sum_\beta x_\alpha x_\beta T_{\alpha\beta}^c(\rho_{\alpha\beta}^c)^{-1} \tag{8}$$

where x_α is the mole fraction of α. It is also argued that a mixing rule is needed for the molecular mass, namely for η_x

$$M_x^{1/2}(T_x^c)^{1/2}(\rho_x^c)^{2/3} = \sum_\alpha \sum_\beta x_\alpha x_\beta M_{\alpha\beta}^{1/2}(T_{\alpha\beta}^c)^{1/2}(\rho_{\alpha\beta}^c)^{2/3} \tag{9}$$

and for λ_x

$$M_x^{-1/2}(T_x^c)^{1/2}(\rho_x^c)^{2/3} = \sum_\alpha \sum_\beta x_\alpha x_\beta M_{\alpha\beta}^{-1/2}(T_{\alpha\beta}^c)^{1/2}(\rho_{\alpha\beta}^c)^{2/3} \tag{10}$$

The cross parameters of (9) and (10) can be estimated from the relations

$$T_{\alpha\beta}^c = \xi_{\alpha\beta}(T_{\alpha\alpha}^c T_{\beta\beta}^c)^{1/2} \tag{11}$$

$$(\rho_{\alpha\beta}^c)^{-1} = \psi_{\alpha\beta}[\tfrac{1}{2}(\rho_{\alpha\alpha}^c)^{-1/3} + \tfrac{1}{2}(\rho_{\beta\beta}^c)^{-1/3}]^3 \tag{12}$$

and

$$M_{\alpha\beta} = \frac{1}{2}\left(\frac{1}{M_\alpha} + \frac{1}{M_\beta}\right)^{-1} \tag{13}$$

where $\xi_{\alpha\beta}$ and $\psi_{\alpha\beta}$ are binary interaction parameters, which are best obtained from experiment.

The mixing rules, (7) and (8), are consistent with the mixing rules derived for thermodynamic properties using the one-fluid approximation. If, therefore, the binary interaction parameters *are assumed to be those valid for thermodynamic properties*, one has a procedure to predict the viscosity and thermal conductivity coefficients of mixture x, given the equivalent coefficients of the reference fluid.

Extension to polyatomic fluids and non-conformal mixtures

Equations (2)–(6) are not general since the assumption of the simple two-parameter corresponding states theory are not valid for polyatomic fluids, or for mixtures containing polyatomic molecules. The situation is, of course, paralleled with respect to the thermodynamic properties and has been discussed extensively in this context. A particularly convenient extension of corresponding states has been developed by Leland[6] and Rowlinson[7] and appears relevant to the transport properties of interest here.

According to the Leland approach, a third parameter, ω, which can be taken as the Pitzer acentric factor,[8] is introduced, but the framework of simple corresponding states is preserved, if one works with the relations

$$f_{\alpha\alpha,o} = \left(\frac{T_{\alpha\alpha}^c}{T_o^c}\right)\theta_{\alpha\alpha,o}; \quad h_{\alpha\alpha,o} = \left(\frac{\rho_o^c}{\rho_{\alpha\alpha}^c}\right)\phi_{\alpha\alpha,o} \tag{14}$$

for fluid α with respect to o. The terms $\theta_{\alpha\alpha,o}$ and $\phi_{\alpha\alpha,o}$ are called shape factors and are weakly varying functions of temperature and density

$$\theta_{\alpha\alpha,o} = 1 + (\omega_{\alpha\alpha} - \omega_o)f(T, \rho)$$

$$\phi_{\alpha\alpha,o} = 1 + (\omega_{\alpha\alpha} - \omega_o)g(T, \rho) \tag{15}$$

where $\omega_{\alpha\alpha}$ and ω_o are acentric factors for fluids α and o, respectively. [The form of the functions $f(T, \rho)$ and $g(T, \rho)$ are given in reference 6. A set of numerical values for the parameters of f and g, and for ω, are also given. However these parameters are subject to revision depending on the state-of-the-art of the appropriate equation of state data. The set used by us are preliminary but are available from the Cryogenics Division.] Using the shape factors, the compressibility factor (for example) of α would be given by the relation $Z_\alpha(\rho, T) = Z_o(\rho h_{\alpha\alpha,o}, T/f_{\alpha\alpha,o})$. With the appropriate[7] expression for the Helmholtz free energy, the thermodynamic properties of α are completely defined in terms of the properties of o.

Let us introduce shape factors into the expressions for the viscosity and thermal conductivity coefficients.[9] We then obtain for fluid α

$$\eta_\alpha(\rho, T) = \eta_o[\rho h_{\alpha\alpha,o}, T/f_{\alpha\alpha,o}]\left(\frac{M_\alpha}{M_o}\right)^{1/2} h_{\alpha\alpha,o}^{-2/3} f_{\alpha\alpha,o}^{1/2} \tag{16}$$

$$\lambda_\alpha(\rho, T) = \lambda_o[\rho h_{\alpha\alpha,o}, T/f_{\alpha\alpha,o}]\left(\frac{M_o}{M_\alpha}\right)^{1/2} h_{\alpha\alpha,o}^{-2/3} f_{\alpha\alpha,o}^{1/2} \tag{17}$$

and for the transport properties of the mixture x,

$$\eta_x(\rho, T) = \eta_o[\rho h_{x,o}, T/f_{x,o}]\left(\frac{M_x}{M_o}\right)^{1/2} h_{x,o}^{-2/3} f_{x,o}^{1/2} \tag{18}$$

$$\lambda_x(\rho, T) = \lambda_o[\rho h_{x,o}, T/f_{x,o}]\left(\frac{M_o}{M_x}\right)^{1/2} h_{x,o}^{-2/3} f_{x,o}^{1/2} \tag{19}$$

where mixing rules for x are

$$h_{x,o} = \sum_\alpha \sum_\beta x_\alpha x_\beta h_{\alpha\beta,o} \tag{20}$$

$$f_{x,o}h_{x,o} = \sum_\alpha \sum_\beta x_\alpha x_\beta f_{\alpha\beta,o} h_{\alpha\beta,o} \tag{21}$$

with

$$f_{\alpha\beta,o} = \xi_{\alpha\beta}(f_{\alpha\alpha,o}f_{\beta\beta,o})^{1/2} \tag{22}$$

and

$$h_{\alpha\beta,\,o} = \psi_{\alpha\beta}(\tfrac{1}{2}h_{\alpha\alpha,\,o}^{1/3} + \tfrac{1}{2}h_{\beta\beta,\,o}^{1/3})^3 \qquad (23)$$

Following Gubbins.[9] a mixing rule for M_x is

$$M_x^{1/2} f_{x,\,o}^{1/2} h_x^{-2/3} = \sum_{\alpha}\sum_{\beta} M_{\alpha\beta}^{1/2} f_{\alpha\beta,\,o}^{1/2} h_{\alpha\beta,\,o}^{-2/3} \qquad (24)$$

for the viscosity coefficient, and an equivalent rule for the thermal conductivity coefficient follows from (10).

Evaluation of the extended corresponding states equations

One might hope that (16)-(24), which we designate as the extended corresponding state equations, could predict the transport properties of non-conformal fluids given a reference transport property and appropriate thermodynamic data. It was decided to test this assumption. Initially we considered the calculation of the viscosity coefficient for the pure fluids (α) nitrogen, ethane, propane, and carbon dioxide. Methane was chosen as the reference fluid (o): methane viscosity data have been analysed and correlated as a function of temperature and density,[10] and the methane equation of state of Goodwin[11] was used[12] as the basis for the shape factor calculations.

Results for nitrogen are shown in Fig. 1 in which the ratio η(exp)/η(calc) has been plotted as a function of temperature for several reduced densities (ρ/ρ_c): η(calc) refers to values from (16), while values for η(exp) were obtained from our previous correlation of the transport properties of nitrogen.[13]

It is seen that (16) gives a reasonable prediction if $\rho/\rho^c \lesssim 1$ (that is, the viscosity ratio is close to unity) but there is a strong density dependence in the deviation pattern above the critical density. As a contrast, the temperature dependence is relatively weak for all densities.

As a matter of interest we include Fig. 2 which illustrates the variation of the shape factors θ and ϕ used to obtain η(calc). The density dependence of these variables is very weak.

Results similar to those shown in Fig. 1 were observed for the other fluids. Thus it appears that (16), with shape factors obtained from thermodynamic data, cannot represent adequately at high densities the viscosity coefficients of fluids which do not correspond with methane. These results for the pure fluids further suggest that (18) will also be unsatisfactory for non-conformal mixtures – with the added complication of mixing rules and binary interaction parameters – and, in fact, this turned out to be the case.

Modified equation for the viscosity coefficient

The relationship between the experimental viscosity coefficient and values calculated from (16) for the fluids studied in this work suggests that an equation of the form

$$\eta_\alpha(\rho, T) = \eta_o(\rho', T')FH_{\alpha\alpha,\,o}^{\eta}\, X(\rho, T) \qquad (25)$$

might be successful where (16) is re-written as

$$\eta_\alpha(\rho, T) = \eta_o(\rho', T')FH_{\alpha\alpha,\,o}^{\eta} \qquad (16a)$$

where

$$\rho' = \rho h_{\alpha\alpha,\,o};\ T' = T/f_{\alpha\alpha,\,o} \qquad (26)$$

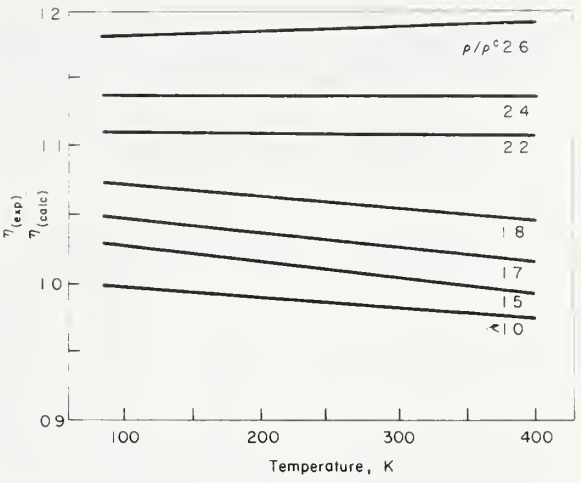

Fig. 1 Ratio of η(exp)/η(calc) for nitrogen plotted schematically as a function of temperature at several densities. Values of η(exp) were extracted from reference 13 while values of η(calc) were obtained from the extended corresponding states equation (16). The figure indicates (16) is not satisfactory if $\rho/\rho^c \gtrsim 1$. ρ^c is the critical density

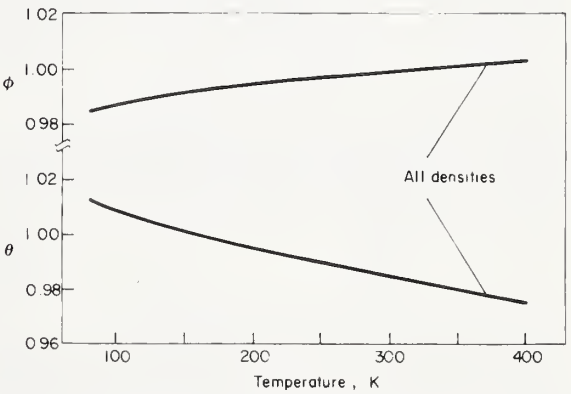

Fig. 2 Plot of the shape factors for nitrogen with respect to methane, θ and ϕ, [(14) and (15)] based on a fit of thermodynamic data. The density dependence is small and can essentially be ignored

and

$$FH_{\alpha\alpha,\,o}^{\eta} = \left(\frac{M_\alpha}{M_o}\right)^{1/2} h_{\alpha\alpha,\,o}^{-2/3} f_{\alpha\alpha,\,o}^{1/2} \qquad (27)$$

The correction factor, $X(\rho, T)$, should be unity if fluids α and o follow simple corresponding states, but should be a strong function of density and a weak function of temperature otherwise. However, X should approach unity as the density approaches zero in this latter example (see Fig. 1). Furthermore, if X can be expressed in terms of thermodynamic (PVT) data alone, (25) would have the predictive capability of (5) for fluids in addition to those which obey simple corresponding states.

A suggestion for a convenient form for $X(\rho, T)$ is now discussed.

The modified Enskog theory

We have shown in references 14, 15, and 16 that an *ad hoc* modification of the Enskog theory for the hard sphere fluid,

called the modified Enskog theory (MET), can represent the transport properties of real fluids given only *PVT* data. The MET expressions for the viscosity and thermal conductivity coefficients of fluid α, are,

$$\eta_\alpha^E = \eta_\alpha(o) b\rho \left(\frac{1}{b\rho\chi} + 0.8 + 0.716\, b\rho\chi \right) \tag{28}$$

and

$$\lambda_\alpha^E = \lambda'_\alpha(o) b\rho \left(\frac{1}{b\rho\chi} + 1.2 + 0.755 b\rho\chi \right) + \lambda''_\alpha(o) \tag{29}$$

where

$$\lambda''_\alpha(o) = \rho D_\alpha(o) c''_v(o) \tag{30}$$

In the above equations, $\eta_\alpha(o)$ is the dilute gas viscosity of fluid α, which can be obtained from experiment or calculated from kinetic theory; $\lambda'_\alpha(o)$ and $\lambda''_\alpha(o)$ are contributions to the dilute gas thermal conductivity due to translational and internal degrees of freedom, respectively; $D_\alpha(o)$ is the dilute gas self-diffusion coefficient; $c''_v(o)$ is the constant volume dilute gas specific heat per unit mass due to internal degrees of freedom.

The term $b\rho\chi$ is obtained from the equation of state written in the form

$$\frac{V}{R}\left(\frac{\partial P}{\partial T}\right)_v = 1 + b\rho\chi \tag{31}$$

which introduces the thermal pressure, $T(\partial P/\partial T)_v$, of the fluid α. b is a second virial term. A particular choice for b, selected to ensure that (28) and (29) approach the dilute gas limit as the density tends to zero is

$$b = B + T\frac{dB}{dT} \tag{32}$$

where B is the second virial coefficient of fluid α.

The MET is discussed at length in reference 14–16 so details are unnecessary here but, generally, the MET can predict and represent the transport properties of simple fluids to within about 10–15% for densities not exceeding about twice the critical density.

One particular feature of the MET can be deduced from our previous work, viz, that a pair of fluids (say α and o) do not necessarily correspond if η^E and λ^E are reduced according to simple corresponding states. In other words, in the context of this paper, suppose we calculate the MET viscosity for fluid α, η_α^E, at a given density and temperature, but also calculate the MET viscosity for o, η_o^E, at the equivalent density and temperature: $\rho(\rho_o^c/\rho_\alpha^c)$ and $T(T_o^c/T_\alpha^c)$, respectively. According to simple corresponding states one then has,

$$\eta_\alpha^E(1) = \eta_o^E\left[\rho\left(\frac{\rho_o^c}{\rho^c}\right),\ T\left(\frac{T_o^c}{T_\alpha^c}\right)\right]\left(\frac{M_\alpha}{M_o}\right)^{1/2}\left(\frac{\rho_\alpha^c}{\rho_o^c}\right)^{2/3}\left(\frac{T_\alpha^c}{T_o^c}\right)^{1/2} \tag{33}$$

and

$$\eta_\alpha^E = \eta_\alpha^E(1) \tag{34}$$

But the results of references 14 to 16 show that (34) is not always upheld and, moreover, we showed that the lack of correspondence according to the MET arose from the lack of correspondence in the *PVT* terms of (28), that is, in $b\rho$ and $[1/b\rho\chi + 0.8 + 0.755\, b\rho\chi]$. This being the case, a relationship

$$\eta_\alpha^E = \eta_\alpha^E(2) \tag{35}$$

cannot be expected to hold, where $\eta_\alpha^E(2)$ is calculated from extended corresponding states, that is, from the relation

$$\eta_\alpha^E(2) = \eta_o^E(\rho', T') F H^\eta_{\alpha\alpha,o} \tag{36}$$

That η_α^E was not equal to $\eta_\alpha^E(2)$ was in fact, verified. However, as a matter of interest, we repeated, with the MET viscosity coefficients, the procedure which led to the conclusions depicted in Fig. 1 for nitrogen, and to similar conclusions for the other fluids. Hence, the ratio $\eta_\alpha^E/\eta_\alpha^E(2)$ was examined as a function of temperature and density for the fluids of interest.

The results turned out to be significant. We observed that the temperature and density behaviour of the MET ratio was very similar to the corresponding ratio $\eta_\alpha(\text{exp})/\eta_\alpha(\text{calc})$, and actually indicated a relationship, namely

$$\frac{\eta_\alpha^E}{\eta_\alpha^E(2)} \approx \frac{\eta_\alpha(\text{exp})}{\eta_\alpha(\text{calc})} \tag{37}$$

Here $\eta_\alpha(\text{exp})$ is the experimental viscosity and $\eta_\alpha(\text{calc})$ is the value from (16) as before.

The significance of (37) is that it leads to an expression for the correction factor $X(\rho, T)$ of (25) since, if one accepts (37) as an apparently empirical fact

$$\eta_\alpha(\text{exp}) \approx \eta_\alpha(\text{calc})\, q_{\alpha\alpha,o} G^\eta_{\alpha\alpha,o} \tag{38}$$

where we have used that $\eta_\alpha(o) = \eta_o(o) F H^\eta_{\alpha\alpha,o}$ for the dilute gas. $q_{\alpha\alpha,o}$ is the ratio $(b\rho)_\alpha/(b\rho)_o$ and $G^\eta_{\alpha\alpha,o}$ is the ratio $[\,]_\alpha/[\,]_o$ where $[\,] = [1/b\rho\chi + 0.8 + 0.755 b\rho\chi]$ from (28). Note that both $(b\rho)_\alpha$ and $[\,]_\alpha$ for fluid α can be determined from the equivalent terms for fluid o using the shape factor approach. For example, for $b_\alpha(T)$

$$b_\alpha(T) = h_{\alpha\alpha,o} B_o + T\frac{d(h_{\alpha\alpha,o} B_o)}{dT} \tag{39}$$

[The shape factors do not necessarily cancel if one takes the ratio of $b\rho$ since θ and ϕ are, in general, functions of temperature and density.]

Since $\eta_\alpha(\text{calc})$ is given by (16) or (16a), $\eta_\alpha(\rho, T)$ can be redefined from (38)

$$\eta_\alpha(\rho, T) = \eta_o(\rho', T') F H^\eta_{\alpha\alpha,o}\, q_{\alpha\alpha,o} G^\eta_{\alpha\alpha,o} \tag{40}$$

Comparison with (25) indicates that

$$X(\rho, T) \equiv q_{\alpha\alpha,o} G^\eta_{\alpha\alpha,o} \tag{41}$$

We examined the experimental behaviour of $X(\rho,T)$. The result was that X turned out to be a strong function of temperature and density if fluid α did not correspond with o. However, it was observed that the temperature dependence was due largely to $q_{\alpha\alpha,o}$, that is, the ratio of the $b\rho$ terms. This feature suggested a refinement to (41) according to the following reasoning. In the MET, b is defined in a way to ensure that the viscosity coefficient approach the correct zero density limit. Further, $q_{\alpha\alpha,o} G^\eta_{\alpha\alpha,o} \approx 1$ in this dilute gas limit. We thus argue that $q_{\alpha\alpha,o}$ imposes an incorrect temperature dependence to the product $q_{\alpha\alpha,o} G^\eta_{\alpha\alpha,o}$ for the dense gas and liquid. Since it is not clear how to redefine b,

we replace $q_{\alpha\alpha,o}$ by $Q_{\alpha\alpha,o}$ where

$$Q_{\alpha\alpha,o} = q_{\alpha\alpha,o}^{[1-1/\exp(\rho^c/\rho)^3]} \quad (42)$$

In this way $Q_{\alpha\alpha,o} \to q_{\alpha\alpha,o}$ at low densities and the MET format is preserved, but the temperature dependence of $q_{\alpha\alpha,o}$ becomes insignificant at high densities since $Q_{\alpha\alpha,o} \to 1$.

Our modified equation for the viscosity coefficient of fluid α is thus

$$\eta_\alpha(\rho, T) = \eta_o(\rho', T')FH^\eta_{\alpha\alpha,o}Q_{\alpha\alpha,o}G^\eta_{\alpha\alpha,o} \quad (43)$$

This equation predicts η_α from η_o and PVT information.

Test of (43)

Initially we tested (43) for nitrogen (a) given, as before, the viscosity of methane (o) as a reference. The procedure is summarized as follows: from a fit of the thermodynamic properties of nitrogen using the equation of state for methane, one determines the shape factors and $h_{\alpha\alpha,o}$ and $f_{\alpha\alpha,o}$ and $f_{\alpha\alpha,o}$ defined by (14). Hence one has ρ', T' and $FH^\eta_{\alpha\alpha,o}$ and $\eta_o(\rho', T')$. $(b\rho)_\alpha$ and $[\ ]_\alpha Q_{\alpha\alpha,o}$ and $G_{\alpha\alpha,o}$ follow from (30) and (31).

Selected results for nitrogen are given in Tables 1 and 2. Results predicted from (16) are included for comparison. The improvement of (43) over (16) as a representation of the data is significant. Since both the experimental nitrogen viscosities and the reference methane viscosities are judged accurate to about 2%, the agreement between experimental and calculated nitrogen values is considered satisfactory.

Similar agreement between calculation and experiment was observed for the other fluids of interest here; ethane, propane, and carbon dioxide.

Viscosity equation for mixtures

For mixtures, one modifies (43) to become

$$\eta_x(\rho, T) = \eta_o(\rho', T')FH^\eta_{x,o}Q_{x,o}G^\eta_{x,o} \quad (44)$$

If (44) is to have the predictive capability of the equation for pure fluids, then the shape factor terms and mixing rules $h_{x,o}$ and $f_{x,o}$, have to be defined by (20) and (21) which, in turn, incorporate the *equilibrium* binary interaction parameters. $\xi_{\alpha\beta}$ and $\psi_{\alpha\beta}$ of (22) and (23). Thus $\phi_{x,o}$, $\theta_{x,o}$, $\xi_{\alpha\beta}$, and $\psi_{\alpha\beta}$ can be found from thermodynamic data alone. [It is not clear what mixing rule to use for the molecular weight. Although (24) has been proposed, the mixing rule that arises naturally from thermodynamics is

$$M_x = \sum_\alpha x_\alpha M_\alpha,$$

We prefer this rule because we have modified (16) on the basis of the PVT behaviour of the mixtures.]

Comparison between experiments and the viscosity equation for mixtures

Viscosity data for non-conforming mixtures, apart from the dilute gas, are scarce and their reliability are often difficult to assess. Further, the choice of mixture data suitable for comparisons is somewhat restricted by our previous work on the equation of state. In principle, the shape factors and binary interaction parameters can be estimated for many fluids and their mixtures but, in practice at this time, our work is limited to methane, ethane, propane, n-butane, i-butane, pentane, nitrogen, carbon dioxide, nitrous oxide, and mixtures thereof. Equation (44), however, was checked with data for several representative mixtures over a wide range of experimental conditions.

Table 1. Nitrogen viscosity: saturated liquid

Deviations between the experimental viscosity coefficients[13] and values calculated from (43) for saturated liquid nitrogen. Deviations between experiment and the extended corresponding states equation, (16) are also given.

T, K	ρ/ρ^c	η(exp), $\mu g\ cm^{-1}\ s^{-1}$	$\frac{\eta_{exp}-\eta_{calc}}{\eta_{calc}} \times 100$ (43)	(16)
75	2.61	1658	−8.1	20.1
80	2.54	1377	−3.5	18.4
85	2.46	1160	3.0	17.1
90	2.38	988	3.0	16.2
95	2.29	846	4.6	15.3
100	2.19	726	5.0	14.4
115	1.84	447	2.6	10.6
120	1.67	365	2.0	8.6
125	1.37	259	1.5	8.0

Table 2. Nitrogen viscosity: 220 K isotherm

Deviations between the experimental viscosity coefficients[13] for nitrogen at 220 K and values calculated from (43) as a function of reduced density. Deviations between experiment and values from (16) are also given.

ρ/ρ^c	$\frac{\eta_{exp}-\eta_{calc}}{\eta_{calc}} \times 100$ (43)	(16)
0.1	0.5	0.8
0.3	−2.8	−1.1
1.0	−7.0	−4.3
1.6	−4.0	4.0
1.9	−4.8	12.0
2.1	−5.8	18.6
2.5	−6.9	24.0

Table 3 gives typical and representative results for the methane-propane system. The data, perhaps the most extensive and reliable viscosity mixture data available, are those of Huang, Swift, and Kurata.[17] Approximate critical temperatures and densities of the given mixture[18] are included in the tables as a measure of the reduced temperature and density involved. Values from extended corresponding states are given in parentheses. The data are judged accurate to within about 3% so our equation (44) is very satisfactory.

Table 4 illustrates typical results for the methane-n-butane system. The data are those from reference 19. Agreement is excellent between the predicted values from (44) and experiment. The experimental accuracy is about 6%.

Data for liquid mixtures which contain components other than hydrocarbons are scarce and the majority are reproduced in the monograph by Gobubev.[20] We investigated

Table 3a. Methane-propane viscosity

Comparison between viscosity data[17] for a methane (22.1%)-propane (77.9%) mixture at 193.15 K and the results predicted from (44): $T^c \approx 350$ K, $\rho^c \approx 6.25$ mole l^{-1}.

ρ, mole l^{-1}	η(exp), $\mu g\ cm^{-1}s^{-1}$	η(calc), $\mu g\ cm^{-1}s^{-1}$	
15.39	2390	2412	(2086)*
15.63	2676	2610	(2300)
15.79	2846	2750	(2441)
15.92	3020	2900	(2580)
16.06	3184	3040	(2717)

* Values obtained from extended corresponding states.

Table 3b. Methane-propane viscosity

Comparison between viscosity data[17] for a methane (50%)-propane (50%) mixture at 153.15 K and the results predicted for (44): $T^c \approx 319$ K, $\rho^c \approx 7.7$ mole l^{-1}.

ρ mole l^{-1}	η(exp), $\mu g\ cm^{-1}s^{-1}$	η(calc), $\mu g\ cm^{-1}s^{-1}$	
18.69	2780	2614	(2286)*
18.78	2860	2710	(2360)
18.96	3030	2878	(2509)
19.12	32000	3002	(2659)
19.28	3380	3232	(2807)
19.42	3550	3407	(2952)

* Values obtained from extended corresponding states.

Table 3c. Methane-propane viscosity

Comparison between viscosity data[17] for a methane (75.3%)-propane (24.7%) mixture at 173.15 K and the results predicted from (44): $T^c \approx 276$ K, $\rho^c \approx 9.8$ mole l^{-1}.

ρ, mole l^{-1}	η(exp), $\mu g\ cm^{-1}s^{-1}$	η(calc), $\mu g\ cm^{-1}s^{-1}$	
19.52	975	943	(889)*
19.76	1020	988	(933)
20.17	1090	1075	(1013)
20.53	1170	1156	(1090)
20.84	1250	1233	(1162)
21.12	1320	1308	(1232)

* Values obtained from extended corresponding states.

the N_2/CH_4 system discussed in that work and Fig. 3 illustrates our prediction from (44) for the equimolar mixture. The data are those of Gerf and Galkov[21] for the saturated liquid. Our values are generally lower than experiment; the discrepancy increases as the temperature increases. Superficially the prediction appears poor but we can argue that the data are unreliable on the following

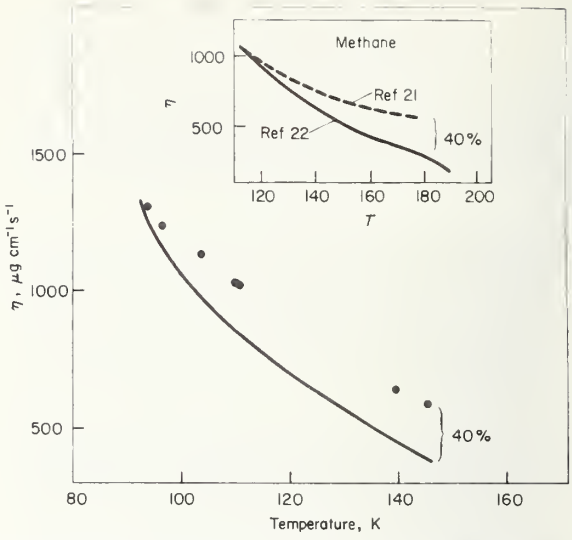

Fig. 3 Saturated liquid viscosity of a N_2/CH_4 equimolar mixture. Data (filled circles) from reference 21, curve from (44). The insert gives a plot of the saturated liquid viscosity of *pure methane*. It can be argued that the data from reference 21 are unreliable (see text)

Table 4. Methane-n-butane viscosity

Comparison between viscosity data[19] for a methane (50%)-n-butane (50%) mixture at 311 K and the results predicted from equation (44): $T^c \approx 375$ K, $\rho^c \approx 7.1$ mole l^{-1}.

ρ, mole l^{-1}	η(exp), $\mu g\ cm^{-1}s^{-1}$	η(calc), $\mu g\ cm^{-1}s^{-1}$	
11.58	645	675	(730)*
12.21	772	730	(836)
12.66	835	854	(922)
13.03	920	927	(1000)
13.34	993	995	(1070)
13.61	1070	1056	(1136)
13.85	1115	1144	(1200)
14.07	1230	1172	(1258)

* Values obtained from extended corresponding states.

grounds. First, it is surprising that the discrepancy increases with temperature since the density decreases. The evidence from pure fluids indicates that the extended corresponding states treatment is reasonable if $\rho/\rho^c \lesssim 1$, and the factor $Q_{x,o}G^{\eta}_{x,o}$ approaches unity as the density approaches the critical density. Second, the insert in Fig. 3 gives a schematic plot of pure methane saturated liquid viscosity. The lower curve is based on the data of Haynes,[22] which we believe to be accurate to within ± 2%, while the upper curve is based on the data of Gerf and Galkov;[21] the authors of the N_2/CH_4 data. The similarity between the methane and nitrogen/methane plots is obvious. We suggest, therefore, that the mixture data of reference 21 are systematically in error.

Table 5 compares our prediction with Golubev and Petrov's data[20] for a 62% N_2-38% CO_2 gaseous mixture at 289 K. Note that the mixture does not contain the reference fluid (methane) as a component.

Finally we include Table 6 which gives a comparison between predicted and experimental values for an LNG gaseous mixture[20] at 273 K. The mixtures have the following composition: CH_4 – 91.5%; C_2H_6 – 1.8%; C_3H_8 – 0.8%; C_4H_{10} – 0.6%; N_2 – 5%; others – 0.3%. We cannot evaluate the accuracy of the data but the prediction appears reasonable. Although, in fact, the viscosity values for this mixture are very close to those for pure methane under equivalent conditions, Table 6 does illustrate that our procedure can adapt to a six-component mixture without difficulty.

Thermal conductivity equation for mixtures

We have investigated the prediction of the thermal conductivity coefficient for a pure fluid and for a nonconformal mixture. At this stage our results are to be considered preliminary. There are two principle reasons for this caution: it is not clear how to treat the contribution of internal degrees of freedom to the conductivity (these contributions are known not to follow the corresponding states principle), and the data for thermal conductivity of liquid mixtures are very limited.

Based on the procedure discussed for the viscosity coefficient, we considered the equations [see (17) and (19)];

$$\lambda_\alpha(\rho, T) = \lambda_o(\rho', T')\frac{\lambda_\alpha^E}{\lambda_o^E} \tag{45}$$

and

$$\lambda_x(\rho, T) = \lambda_o(\rho', T')\frac{\lambda_\alpha^E}{\lambda_o^E} \tag{46}$$

for a pure fluid and mixture, respectively. λ_α^E, etc, are the MET expressions from (29). If we substitute from (29) we obtain from (45)

$$\lambda_\alpha(\rho, T) = \lambda_o(\rho', T')FH_{\alpha\alpha,o}^{\lambda} q_{\alpha\alpha,o}G_{\alpha\alpha,o}^{\lambda} \times \left\{1 + x[(\lambda_\alpha''(o), \lambda_o''(o)]\right\} \tag{47}$$

where the terms $\lambda_\alpha''(o)/\chi$ and $\lambda_o''(o)/\chi$ are assumed to give only small contributions to λ_α^E and λ_o^E, respectively. This has been verified experimentally.[14] $FH_{\alpha\alpha,o}^{\lambda}$, analogous to $FH_{\alpha\alpha,o}^{\eta}$, is defined from (17)

$$FH_{\alpha\alpha,o}^{\lambda} = \left(\frac{M_o}{M_\alpha}\right)^{1/2} h_{\alpha\alpha,o}^{-2/3} f_{\alpha\alpha,o}^{1/2} \tag{48}$$

We introduced $FH_{\alpha\alpha,o}^{\lambda}$ into (46) by assuming that $\lambda_\alpha'(o) = \lambda_o'(o)FH_{\alpha\alpha,o}^{\lambda}$ is valid for the translational contributions in the dilute gas. $G_{\alpha\alpha,o}^{\lambda}$ is the ratio of the MET terms

$$G_{\alpha\alpha,o}^{\lambda} = \frac{[1/b\rho\chi + 1.2 + 0.755b\rho\chi]_\alpha}{[1/b\rho\chi + 1.2 + 0.755b\rho\chi]_o} \tag{49}$$

Ignoring the function, $\chi[\lambda_\alpha''(o), \lambda_o''(o)]$, and introducing the correction for the $b\rho$ ratio, $q_{\alpha\alpha,o}$, (47) becomes

$$\lambda_\alpha(\rho, T) = \lambda_o(\rho', T')FH_{\alpha\alpha,o}^{\lambda}Q_{\alpha\alpha,o}G_{\alpha\alpha,o}^{\lambda} \tag{50}$$

Similarly for a mixture

$$\lambda_x(\rho, T) = \lambda_o(\rho', T')FH_{x,o}^{\lambda}Q_{x,o}G_{x,o}^{\lambda} \tag{51}$$

Internal degrees of freedom enter into (50) and (51) through $\lambda_o(\rho', T')$.

Table 5. Nitrogen-carbon dioxide viscosity

Comparison between predicted viscosity coefficients for a nitrogen (62%)-carbon dioxide (38%) mixture at 289 K. Data from Golubev.[20]

P, atm	ρ, mole l^{-1}	η(exp), μg cm^{-1} s^{-1}	η(calc), μg cm^{-1} s^{-1}
20	0.9	167.0	167.0
60	2.8	179.5	186.5
100	4.9	200.5	213.6
120	7.0	212.5	229.1

Table 6. Viscosity of LNG

Comparison between predicted viscosity coefficients of an LNG mixture at 273 K. Data from Golubev.[20]

P, atm	ρ, mole l^{-1}	η(exp), μg cm^{-1} s^{-1}	η(calc), μg cm^{-1} s^{-1}
20	0.9	109.3	110.0
60	3.1	132.2	123.6
100	5.8	160.2	145.8
200	11.8	244.5	227.7
300	15.0	313.7	298.8
400	17.0	372.3	345.0

Table 7. Nitrogen thermal conductivity: saturated liquid

Comparison between experimental data[13] and values predicted from (50) for the thermal conductivity of nitrogen at the saturated liquid.

T, K	λ(exp), mW m^{-1} K^{-1}	λ(calc), mW m^{-1} K^{-1}	
75	137.0	142.1	(122.2)*
80	129.9	128.1	(114.2)
85	122.3	116.4	(106.5)
90	114.4	106.4	(99.1)
100	98.1	89.9	(84.9)
115	72.5	67.2	(63.7)
120	64.6	60.1	(56.3)

* Values from extended corresponding states.

Comparison between experiment and the thermal conductivity equations

As remarked earlier, limited data restricts a comparison of (50) and (51) with experiment, but we followed the procedure discussed with respect to the viscosity coefficient as far as possible. That is, (50) was first used to predict values for the pure fluid, (51) was then used to predict values for a mixture.

Results for nitrogen are reported in Tables 7 and 8 for the saturated liquid boundary and for the 220 K isotherm; data from reference 13. Also included in parentheses are the results from the extended corresponding states equation (17), that is, without an MET correction. We estimate[13]

Table 8. Nitrogen thermal conductivity: 220 K isotherm

Comparison between experimental data[13] and values predicted from (50) for the thermal conductivity of nitrogen at 220 K.

ρ, mole l^{-1}	ρ/ρ^c	λ(exp), mW m^{-1} K^{-1}	λ(calc), mW m^{-1} K^{-1}	
1.0	0.09	21.47	22.00	(27.90)*
5.0	0.45	28.01	28.72	(33.5)
9.1	0.82	35.74	36.90	(40.14)
12.1	1.09	43.17	44.06	(46.4)
18.37	1.65	65.89	64.00	(65.52)
22.6	2.04	90.33	88.66	(92.37)
25.7	2.32	115.8	118.2	(106.9)
27.7	2.50	137.1	145.2	(124.0)

* Values from extended corresponding states.

Table 9. Ethane thermal conductivity: 310 K isotherm

Comparison between experimental data[23] and values predicted from (50) for the thermal conductivity of ethane at 310 K.

ρ, mole l^{-1}	ρ/ρ^c	λ(exp), mW m^{-1} K^{-1}	λ(calc), mW m^{-1} K^{-1}	
1.0	0.15	29.37	27.36	(19.08)*
4.0	0.60	49.94	48.90	(35.69)
7.0†	1.05	79.26	74.61	(60.6)
10.0	1.49	77.90	71.03	(58.4)
14.0	2.09	105.5	93.8	(83.8)
17.0	2.53	145.4	137.8	(125.7)

* Values from extended corresponding states.

† Note the anomalously large value of λ. This arises from the critical point enhancement.[24]

the nitrogen data to be accurate to within about ± 4 and our predictions are generally within this error band.

Table 9 displays the results for ethane. The data are from a recent correlation[23] and are accurate to within about ± 10% only, which is the agreement between experiment and prediction.

There are two remarks on the results in Tables 8 and 9. The first is that the predictions at low densities are surprisingly good since, as remarked, the internal degrees of freedom enter the calculation through λ_o only: the internal degrees of freedom are known to contribute up to 50% of the value of the dilute gas thermal conductivity. The second remark is that Table 9 indicates, for the $\rho/\rho^c = 1.05$ data point, the critical point enhancement in the thermal conductivity coefficient.[24] Our prediction will also include the enhancement through the reference thermal conductivity for methane.[10] The topic is under further investigation, however, and will be discussed in detail separately.

Results similar to those of Tables 7-9 were observed for propane and carbon dioxide.

Two mixtures were selected for study: a liquid methane (39.4%)-n-butane (60.6%) mixture discussed by Carmichael, Jacobs and Sage[25] and a gaseous nitrogen-ethane mixture discussed by Gilmore and Comings.[26] Tables 10 and 11 give typical comparisons between the data and our predictions from (51). The mixing rules and binary interaction parameters were again determined from thermodynamic information, as for the viscosity.

We estimate the data to be accurate to 5–10%. The agreement, therefore, between experiment and prediction is excellent.

Discussion and conclusions

A corresponding states procedure to predict the viscosity and thermal conductivity coefficients of a pure fluid or mixture has been presented.

In developing our procedure, we first considered modifying the two-parameter (T^c and ρ^c in this work) conformal fluid corresponding states equations to include non-conformal fluids by introducing the concepts of the extended corresponding state approach of Leland and Rowlinson. We had, however, only, partial success with this approach, which is essentially a technique to include a third parameter, if the necessary parameters were obtained from thermodynamic (PVT) data. We observed, in particular, that deviations between calculated and experimental transport coefficients for the *pure* fluid could be as much as 20% at high densities (see Fig. 1, for example). The deviations did suggest, however, a possible modification of the basic corresponding states relationships, (15)–(16), by the inclusion of a term $X(\rho, T)$. The form of X was deduced by observing the behaviour of the transport coefficients according to the modified Enskog theory (MET). Our final equations for a pure fluid, α, and for a mixture, x, are (43) and (44), and (50) and (51) for the viscosity coefficient and thermal conductivity coefficient, respectively. Note that the calculation of the transport coefficients for a given fluid require corresponding values for a reference fluid and thermodynamic data only. Hence out method is predictive in the sense that transport data of the given fluid are *not* needed.

With methane as a reference fluid, we calculated the viscosity and thermal conductivity coefficients of nitrogen, ethane, propane, butane, and carbon dioxide and for mixtures of these fluids. Typical results are given in Tables 3–11. Although transport data for mixtures are limited, the results show we have tested our method over a wide range of experimental conditions, including the dense liquid, and we have predicted consistently the data to within the experimental error.

We are very grateful to R.D. McCarty for his considerable help with the equation of state calculations needed in this study. The work was supported by the Office of Standard Reference Data.

References

1 **Hirschfelder, J.O., Curtiss, C.F., Bird, R.B.** Molecular Theory of Gases and Liquids, 2nd edn (Wiley, NY, 1964) 617

2 See, for example, **Reid, R.C., Sherwood, T.K.** The Properties of Gases and Liquids (McGraw-Hill, NY, 1966) Ch 9 and 10, and references therein

Table 10. Thermal conductivity of a methane–n-butane mixture

Comparisons between thermal conductivity data from reference 25 and the predictions from (51) for a CH_4 (39.4%)-n-C_4H_{10}(60.6%) mixture at 277.6 K. For this mixture[18] $T^c \approx 390$ K, $\rho^c \approx 6.25$ mole l^{-1}.

ρ, mole l^{-1}	λ(exp), mW m^{-1} K^{-1}	λ(calc), mW m^{-1} K^{-1}	
12.26	99.00	95.33	(92.50)*
12.49	101.46	99.63	(96.61)
13.01	113.39	109.99	(106.5)
13.25	114.90	115.05	(111.3)

* From extended corresponding states.

Table 11. Thermal conductivity of a nitrogen-ethane mixture

Comparison between thermal conductivity data from reference 26 and the predictions from (51) for a nitrogen (59.8%)—ethane (40.2%) mixture at 348.16 K. For this mixture,[18] $T^c \approx 260$ K, $\rho^c \approx 12.0$ mole l^{-1}.

ρ mole l^{-1}	λ(exp), mW m^{-1} K^{-1}	λ(calc), mW m^{-1} K^{-1}	
7.34	46.0	46.11	(61.5)*
10.16	55.2	54.69	(72.65)
13.75	70.3	69.47	(92.4)
16.43	85.4	84.44	(113.0)

* From extended corresponding states.

3 Preston, G.T., Chapman, T.W., Prausnitz, J.M. *Cryogenics* 7 (1967) 274
4 Mo, K.C., Gubbins, K.E. *Chem Eng Commun* 1 (1974) 281; Molecular Physics (forthcoming)
5 Longuet-Higgins, H.C. *Proc Roy Soc (London)* A205 (1951) 247
6 Leland, T.W., Chappelear, P.S., Gamson, B.W. *AIChE J* 8 (1962) 482; Leach, J.W., Chappelear, P.S., Leland, T.W. *Proc Am Petrol Inst* 46 (1966) 223
7 Mollerup, J., Rowlinson, J.S. *Chem Eng Sc* 29 (1974) 1373
8 Pitzer, K.S., Curl, R.F. Thermodynamic and Transport Properties of Fluids, (Inst of Mech Eng, London, 1958) 1
9 Haile, J.M., Mo, K.C., Gubbins, K.E. Cryogenic Eng Conf (1975); Gubbins, K.E. private communication
10 Hanley, H.J.M., McCarty, R.D., Haynes, W.M. *Cryogenics* 15 (1975) 413
11 Goodwin, R.D. NBS Tech Note (US) No 653 (1974)
12 Mollerup, J. *Advances in Cryogenic Engineering* 20 (Plenum Press, NY) 172
13 Hanley, H.J.M., McCarty, R.D., Haynes, W.M. *J Phys Chem Ref Data* 3 (1974) 979
14 Hanley, H.J.M., McCarty, R.D., Cohen, E.G.D. *Physica* 60 (1972) 322
15 Hanley, H.J.M., Prydz, R. *J Chem Ref Data* 1 (1972) 1101
16 Hanley, H.J.M., Cohen, E.G.D. *Physica* 83A (1976) 215
17 Huang, E.T.S., Swift, G.W., Kurata, F. *AIChE J* 13 (1967) 846
18 Hicks, C.P., Young, C.L. *Chem Rev* 75 (1975) 119
19 Dolan, J.P., Ellington, R.T., Lee, A.L. *J Chem Eng Data* 9 (1964) 484; 'Monograph on API Research Project 65, Viscosity of light hydrocarbons', [Lee, A.L. (ed)]
20 Golubev, I.F. Viscosity of Gases and Gas Mixtures, (Israel Programme for Scientific Translations, Jerusalem, 1970)
21 Gerf, S.F., Galkov, G.I. *Zhur Tekh Fiz* 11 (1941) 801
22 Haynes, W.M. *Physica* 70 (1973) 410
23 Hanley, H.J.M., Gubbins, K.E. (forthcoming); data available from the Cryogenics Division, NBS, Boulder
24 Sengers, J.V., Hanley, H.J.M., Ely, J.F. Proc 14th Int Conf Thermal Conductivity (Pergamon Press, NY, 1976)
25 Carmichael, L.T., Jacobs, J., Sage, B.H. *J Chem Eng Data* 13 (1968) 489
26 Gilmore, T.F., Comings, W.E. *AIChE J* 12 (1966) 1172

FRACTURE MECHANICS PARAMETERS FOR A 5083-O ALUMINUM ALLOY AT LOW TEMPERATURES†

R. L. Tobler and R. P. Reed

Cryogenics Division
Institute for Basic Standards
National Bureau of Standards
Boulder, Colorado 80302

ABSTRACT

The fatigue crack growth and fracture resistance of a 5083-O aluminum alloy plate were investigated at four temperatures in the ambient-to-cryogenic range -- 295, 111, 76, and 4 K. J-integral test methods were applied using compact specimens 3.17 cm thick, and the value of J required to initiate crack extension (J_{Ic}) is reported as an index of fracture toughness. The fracture toughness was orientation dependent, with anisotropy accounting for J_{Ic} variations of up to a factor of 2. For specimens having fracture planes parallel to the rolling direction, J_{Ic} increases progressively from 9 to 25 kJm^{-2} as temperature decreases between 295 and 4 K. In contrast, the fatigue crack growth rates (da/dN) are insensitive to specimen orientation. The fatigue crack growth rates at cryogenic temperatures are up to 10 times lower than in air at room temperature, but are virtually constant between 111 and 4 K. These results should be useful in fracture mechanics analyses of cryogenic structures, including liquified natural gas tankers.

Key words: Aluminum alloys; cryogenics; crack propagation; fatigue; fracture; low temperature tests; mechanical properties.

INTRODUCTION

The aluminum alloy designated 5083-O is strengthened by solid solution additions of magnesium and used in the annealed condition. Excellent formability, weldability, toughness, and relatively low cost are some advantages that make this alloy an attractive low temperature structural material. Applications include storage and transport tanks for cryogenic fluids. Currently, thousands of tons of 5083-O alloy are destined for use in liquefied natural gas (LNG) tankers at service temperatures as low as 111 K. Emerging applications may include structural components for superconducting machinery. These structures are costly, and in the case of LNG tankers, the transported cryogen is flammable. Design engineers and regulatory agencies therefore require efficient and fail-safe design.

Extensive mechanical property data exist for 5083-O aluminum [1-7]. Between room and liquid helium temperatures (295 to 4 K), the yield and ultimate strengths increase by 25% and 70%, respectively, with most of the improvement occurring at lower temperatures [2]. Ductility also improves at low temperatures, and precracked specimens retain the ability to deform prior to fracture. Nevertheless, quantitative fracture toughness data for this alloy are lacking. Several attempts to measure the critical stress intensity factor, K_{Ic}, have been unsuccessful. As defined by the ASTM testing method for plane strain fracture toughness of metallic materials (ASTM E 399-74), the parameter K_{Ic} applies to linear-elastic loading behavior. Kaufman, Nelson, and Wygonik [3] showed that 5083-O alloys in section thicknesses up 20 cm remain sufficiently plastic to invalidate direct K_{Ic} measurements.

This study employs an alternative approach to fracture toughness characterization. The method is based on Rice's formulation of the J-integral [8], which is the rate of change of potential energy with respect to crack area. In applications of the J-integral, Begley and Landes identify a parameter denoted J_{Ic} which, unlike K_{Ic}, can be measured under nonlinear-elastic conditions [9,10]. Since experimental results for aluminum alloys support the hypothesis that J_{Ic} is a material constant [11,12], the J-resistance curve test method [10] was applied here to a 5083-0 aluminum plate. The J_{Ic} values and fatigue crack growth rates reported in this study should assist fracture mechanics analyses of 5083-0 structures at temperatures in the ambient-to-cryogenic range.

PROCEDURES

Material and Specimens

A 4.32 cm thick 5083-0 aluminum alloy plate was obtained from a commercial source and tested in the as-received condition. The microstructure is shown in Figure 1. The ASTM specification B 209-66 gives the chemical composition of this alloy in wt% as: 4.0-4.9 Mg, 0.3-1.0 Mn, 0.05-0.25 Cr, 0.4 max. Si, 0.4 max. Fe, 0.10 max. Cu, 0.25 max. Zn, 0.15 max. Ti, and 0.15 max. of other impurities.

After machining 0.44 cm of metal from each surface of the stock plate, 3.17 cm thick compact specimens were fabricated with the geometry shown in Figure 2. The specimen width, W, was 7.62 cm. The width-to-thickness ratio, W/B, was 2.4. Knife edges were machined integral to the notch to enable clip gage attachment and deflection measurements at the loadline. Most of the specimens were machined in the TL orientation (fracture plane normal to the long transverse direction), but

several specimens of the LT orientation (fracture plane normal to the longitudinal or rolling direction) were also tested.

Tensile tests of unnotched, longitudinally-oriented specimens were performed at room and liquid nitrogen temperatures, following ASTM Method E 8-69. Two tests were performed at each temperature. The yield and ultimate strengths, elongation, and reduction of area results, shown in Table 1, agree with other data for similar 5083-0 products [13].

Fatigue Crack Growth

A 100 kN servo-hydraulic test machine adaptable for cryogenic service was used in all fatigue and fracture tests. Room temperature tests were conducted in unconditioned air at a relative humidity, H, of approximately 30%. Low temperatures were achieved by enclosing the load frame, specimen, and clip gage in a dewar of liquid helium (4 K), liquid nitrogen (76 K), or nitrogen gas (111 $\pm$ 4 K). The low temperature apparatus and techniques were previously described [14,15]. The clip gage satisfied ASTM Method E 399-74 linearity requirements, and its sensitivity changed by no more than 5% over the temperature range investigated.

The compact specimens were precracked at their test temperatures using maximum fatigue stress intensity factors of from 10 to 22 $MPa \cdot m^{1/2}$. The minimum-to-maximum load ratio, R, was 0.1. Some fatigue crack growth rates were measured during precracking, but additional rates at relatively high stress intensity factors or R values were measured using specimens not intended for J-tests. All precracking and fatigue crack growth tests used sinusoidally-varying loads at a frequency of 20 Hz.

A correlation between crack length (a) and specimen compliance

(deflection per unit load, δ/P) was established using measurements from fractured specimens. Crack length was defined as the average of three measurements at the middle and quarter points of specimen thickness. The fatigue tests were then interrupted periodically to record compliance, and the inferred crack length was plotted as a function of load cycles, N. The fatigue crack growth rates, da/dN, were calculated by graphical differentiation of a-versus-N curves, while the corresponding stress intensity factor ranges, ΔK, were calculated from the maximum and minimum fatigue loads:

$$\Delta K = (P_{max} - P_{min})B^{-1}W^{-1/2}[f(a/W)], \quad (1)$$

According to ASTM Method E 399-74,

$$f(a/W)=29.6(a/W)^{1/2}-185.5(a/W)^{3/2}+655.7(a/W)^{5/2}-1017.0(a/W)^{7/2}+638.9(a/W)^{9/2}. \quad (2)$$

The uncertainty in crack growth rates is estimated at less than $\pm$ 25%.

Fracture Toughness

At each test temperature, a series of specimens having similar precrack lengths were loaded to selected deflections at the stroke rate of 0.05 mms^{-1}. These loadings were sufficient to cause stable crack extensions of up to 0.25 cm. Each specimen was then unloaded and refatigued using cyclic loads no greater than 70% of the maximum static load. After the refatigue crack was propagated several millimeters, the specimens were fractured into halves by a single loading.

The fracture surfaces showed, in succession: (1) a precrack zone, (2) a crack extension increment due to static loading, and (3) a refatigue

crack zone. The relatively coarse and less reflective increment of static crack extension was measured to the nearest 0.003 cm with a traveling microscope at the center and quarter points of specimen thickness, the three-point average being defined as Δa. The corresponding values of J were calculated for each test, using the approximate solution for deeply cracked compact specimens [16]:

$$J = 2A/Bb. \tag{3}$$

Here, A is the total area (energy) under the test record up to the point of unloading, and b is the original ligament depth ($b = W - a$). The uncertainty in J measurements was not greater than $\pm$ 2%.

To obtain critical J values, the resistance curves of J-versus-Δa were back-extrapolated to Δa = 0.005 cm. In tests of a 2219-T6 aluminum alloy, Read and Reed [12] suggested that defining J_{Ic} at 0.005 cm crack extension leads to reproducible results. The uncertainty in the J_{Ic} values obtained in this way for 5083-O aluminum is estimated at $\pm$ 15%.

RESULTS AND DISCUSSION

Fatigue Crack Growth

Fatigue crack growth data at 4, 76, 111, and 295 K for 5083-O aluminum specimens of the TL orientation at R = 0.1 are shown in Figure 3. The results span two orders of magnitude from 5 X 10^{-6} mm/cycle to 2.5 X 10^{-3} mm/cycle. For a given ΔK value, the rates of crack growth at 111, 76, and 4 K are equivalent within the degree of scatter among replicate tests. However, the rates at room temperature are up to 10 times faster than the rates at cryogenic temperatures.

As plotted on logarithmic coordinates, the low temperature fatigue crack growth data describe an approximately linear trend over the entire ΔK range, whereas the room temperature data do not. The linear approximation to the data at 111, 76 and 4 K, shown in Figure 3, is consistent with a Paris equation of the form:

$$\frac{da}{dN} = C(\Delta K)^n. \tag{4}$$

Here da/dN (mm/cycle) is a power law function of ΔK (MPa$\cdot m^{1/2}$). The constants C and n correspond to the ordinate intercept at $\Delta K = 1$, and the slope, respectively. A graphical solution for the equation of the line drawn through the 111, 76 and 4 K data yields:

$$\frac{da}{dN} = 1.3 \times 10^{-10}(\Delta K)^{5.2}. \tag{5}$$

The room temperature data fail to conform to a single power-law equation, due to the appearance of a "shoulder" on the da/dN-versus-ΔK plot at ΔK values between 10 and 15 MPa$\cdot m^{1/2}$. This shoulder brings the room and low temperature crack growth rates into closer agreement at higher ΔK values. Consequently, the room temperature fatigue crack growth resistance is only slightly inferior at stress intensity factor ranges greater than 15 MPa$\cdot m^{1/2}$.

Figure 4 shows additional crack growth data for the TL orientation at 295 and 111 K (R = 0.3), as well as data on specimens of the LT orientation at 111 K (R = 0.1). Scatterbands representing the data of Figure 3 are superimposed on Figure 4 for comparison. This comparison indicates that the change in R from 0.1 to 0.3 had no effect on the

room temperature fatigue crack growth rates, whereas, at 111 K, this change increased the rates by nearly a factor of 2. Also the data obtained for specimens of the LT orientation at 111 K fall within the band for TL orientations for the same stress ratio, R = 0.1. Thus, specimen orientation has no measureable effect on fatigue crack growth rates. Kaufman and Kelsey [17] also noted relatively isotropic fatigue crack growth in their tests of a 5083-0 aluminum alloy.

Comparisons of fatigue crack growth data reported in the literature for compact specimens of 5083-0 aluminum are shown in Figures 5 and 6. Although these data show considerable variance, most results can be rationalized in terms of the different test variables and procedures. Usually, higher R values lead to increased fatigue crack growth rates. Other significant factors to be considered include the procedure used to obtain a-versus-N data, and the relative humidity at room temperature.

In reference to Figures 5 and 6 note first that the present study yielded somewhat lower rates at a given ΔK value as compared with other investigations [4,17-19]. In our study, the crack length was defined as an average of measurements at the center and quarter points of thickness. Other studies used measurements of the crack at specimen edges. In our study the edge crack lengths were typically 5 to 8% shorter than the average crack lengths. If edge crack lengths had been used, the f(a/W) values of Eq. (1) would have been reduced, and the ΔK value for a given growth rate would have been 10 to 17% lower than actually reported. This would shift the bands of Figures 5 and 6 into good agreement with the bulk of previously published results.

As shown in Figure 5, at least three other laboratories report a shoulder in room temperature fatigue crack growth rates [17-19]. This

shoulder occurs at rates near 3 X 10^{-4} mm/cycle, for tests conducted in air with appreciable moisture contents. Kelsey, Nordmark and Clark's [4] room temperature results at 90% relative humidity and R = 0.33 are nearly in agreement with Argy, Paris, and Shaw's [18] results at ∿ 50% relative humidity and R = 0.4. However, as the relative humidity is decreased to less than 10%, the shoulder is eliminated and fatigue crack propagation resistance at low ΔK is improved. Note in Figure 5 that the overall agreement of data is better at high ΔK values where differences in relative humidity are less influential.

Deleterious effects on the fatigue crack growth resistance of this alloy due to moisture are not surprising in view of the trends exhibited by other aluminum alloys [20]. Hartman and Schijve's [21] data for a 7075-T6 alloy demonstrate trends analogous to the behavior indicated in Figure 5. In dry air, their logarithmic plots of da/dN-versus-ΔK display a linear trend for growth rates in the range 10^{-5} to 10^{-3} mm/cycle; in moist air (relative humidity = 45%), a shoulder appears in the data at $\Delta K \simeq 15$ MPa$\cdot m^{1/2}$, and the rates at lower ΔK are accelerated by up to a factor of 10. Again, the rates at high ΔK are not sensitive to moisture.

Thus, the effects of moisture on the room temperature fatigue crack growth behavior of 5083-0 and 7075-T6 alloys are remarkably similar. The trend of the Kelsey et al. [4] data for 5083-0 aluminum in a dry air environment probably represents the true trend of room temperature results when moisture effects are practically eliminated. Note from Figures 5 and 6 that the rates reported by Kelsey et al. [18] for tests in dry air at 295 K are nearly equivalent to but slightly faster than their rates at 76 K. Based on these observations, it may be concluded

that moisture effects at 295 K are predominant, and temperature variations between 295 K and 4 K intrinsically have little effect on the fatigue crack propagation resistance of 5083-0 aluminum. This is consistent with results for other face-centered cubic alloys which show only modest improvements of fatigue crack growth resistance at low temperatures [22].

Fracture Toughness

Plasticity and stable crack extension caused nonlinearity in the fracture test records at all temperatures, and unstable cracking was never observed. As expected, the linearity requirements of sections 9.1.2 and 9.1.5 of ASTM Method E 399-74 could not be satisfied using our specimens of aluminum alloy 5083-0, so it was appropriate to conduct J-integral tests. Table 2 lists the J-integral test results for both the LT and TL specimen orientations.

Resistance curves (J-versus-Δa graphs) for the TL orientation are shown in Figure 7. The results at 295, 111, 76, and 4 K show that higher J values are required for a given crack extension as temperature decreases. The J_{Ic} values obtained at Δa = 0.005 cm progressively increase from 9 to 25 kJm^{-2} between 295 and 4 K. Moreover, the rate of increase of J with respect to Δa is greater at 111, 76, and 4 K than at room temperature. Thus, greater energy is expended in fracture initiation and propagation at cryogenic temperatures. Kahn-type tear and dynamic tear tests render a similar conclusion [5-7, 23].

Figure 8 compares the J-resistance curves for the TL and LT orientations at 111 K, demonstrating the anisotropy of fracture toughness for this alloy. Based on these curves, J_{Ic} for the LT orientation is approximately 39 kJm^{-2} at 111 K, or twice the value for the TL orientation. The superiority of the LT orientation in comparison with the TL

orientation is typical of many alloys, and the tear test results and projected K_{Ic} values reported by Kaufman et al. [3,5,6] indicate a similar orientation dependence for 5083-O aluminum.

The fracture anisotropy is also evident in Figure 9, which shows TL and LT specimens that were tested at 111 K. The LT specimen was fatigue cracked and fractured in a single loading. The TL specimen was used in a J-test, and it shows an increment of crack extension, Δa, located between two fatigue cracks. The LT specimen displays shear fracture portions amounting to 30% of specimen thickness; delaminations are also visible at mid-thickness. In comparison, the TL specimen exhibits a flat fracture mode requiring less energy for crack extension. The fracture surface appearance of the TL orientation was not significantly influenced by test temperature.

The J_{Ic} data listed in Table 2 can be used to estimate K_{Ic} values by using the equation:

$$K_{Ic}^2 = \frac{EJ_{Ic}}{1 - \nu^2} \tag{6}$$

In this equation, E is Young's modulus of elasticity and ν is Poisson's ratio. The values of E and ν at temperatures between 295 and 4 K are known from Naimon, Weston, and Ledbetter's study [24]. The K_{Ic} estimates based on these data at 295, 111, 76 and 4 K are plotted in Figure 10, along with the corresponding J_{Ic} values.

As shown in Figure 10, the K_{Ic} estimates converted from J_{Ic} data range from 27.0 to 60.2 $MPa \cdot m^{1/2}$, depending on temperature and specimen orientation. For the TL orientation, the K_{Ic} estimates at 295 and 76 K are 27.0 and 43.4 $MPa \cdot m^{1/2}$, respectively. These are lower than Kaufman

and Kelsey's [17] projected K_{Ic} estimates of 49.5 MPa·$m^{1/2}$ at 295 K and 55 MPa·$m^{1/2}$ at 77 K. Kaufman and Kelsey's K_{Ic} estimates also pertain to specimens of the TL orientation, but their K calculations are based on the maximum load observed in fracture tests. Their procedure does not account for the fact that crack extension occurs prior to maximum load.

Finally, it should be noted that Merkle and Corten's method [25] of J calculation could have been used in this study. When applied to the 5083-O aluminum experiments described in the text, that method amounts to replacing the coefficient 2 in Eq. (3) by higher factors from 2.2 to 2.3. The J_{Ic} values would have been increased by about 10%; the K_{Ic} estimates, by 5%. Read and Reed [12] found from measuring both K_{Ic} and J_{Ic} at 76 K for the aluminum alloy 2219-T87 that J_{Ic} as calculated from the measured K_{Ic} was about 40% greater than the measured J_{Ic}. Thus, the J_{Ic} data and K_{Ic} estimates reported here for 5083-O may be considered conservative.

SUMMARY AND CONCLUSIONS

The fatigue crack growth behavior and J-integral fracture toughness of a 5083-O aluminum alloy have been investigated at 295, 111, 76 and 4 K, a wider range of temperatures than previously studied. Specifically:

1. Fatigue crack growth resistance at 111 K was insensitive to specimen orientation, but improves at decreasing R ratios.

2. Although the fatigue crack growth rates in ambient air at room temperature exceed the rates at cryogenic temperatures by up to a factor of 10, the rates between 111 and 4 K are nearly equivalent. The high rates in ambient air can be attributed to the presence of moisture, rather than temperature effects per se.

3. Results for the TL orientation at decreasing temperatures between 295 K and 4 K indicate nearly a three-fold increase of J_{Ic} from 9 to 25 kJm^{-2}.

4. Anisotropy in rolled plate caused a J_{Ic} variation of a least 2:1 at the LNG temperature of 111 K.

5. In view of the favorable low temperature effects on tensile, fatigue, and fracture properties, it is apparent that the structural reliability of flawed or unflawed 5083-O alloy components will not be decreased by cryogenic temperatures.

ACKNOWLEDGMENTS

This work was sponsored by the Maritime Administration and the Advanced Research Projects Agency of the U.S. Department of Defense. The authors gratefully acknowledge the assistance of R. L. Durcholz and Dr. R. P. Mikesell in conducting the tensile tests. We also wish to thank Dr. R. A. Kelsey of the Alcoa Technical Center for reviewing the manuscript.

REFERENCES

1. Properties of Materials for Liquefied Natural Gas Tankage, ASTM STP 579, Amer. Soc. Test. Mater., Philadelphia, 1975, pp. 1-204.
2. Rice, L. P., Campbell, J. E., and Simmons, W. F., in Advances in Cryogenic Engineering, Vol. 8, 1963, pp. 671-677.
3. Kaufman, J. G., Nelson, F. G., and Wygonik, R. H., in Fatigue and Fracture Toughness -- Cryogenic Behavior, ASTM STP 556, Amer. Soc. Test. Mater., 1974, pp. 125-158.
4. Kelsey, R. A., Nordmark, G. E., and Clark, J. W., in Fatigue and Fracture Toughness -- Cryogenic Behavior, ASTM STP 556, Amer. Soc. Test. Mater., 1974, pp. 159-185.
5. Kaufman, J. G., Nelson, F. G., and Wanderer, E. T., Mechanical Properties and Fracture Characteristics of 5083-O Products and 5183 Welds in 5083 Products, Proceedings of the International Congress of Refrigeration, Washington, D.C., Vol. 1, 1971, pp. 651-658.
6. Nelson, F. G., Kaufman, J. G., and Wanderer, E. T., Tear Tests of 5083 Plate and of 5183 Welds in 5083 Plate and Extrusions, Paper D-1 in Adv. in Cryo. Eng., K. D. Timmerhaus, Ed., pp. 91-101.
7. Judy, R. J., Jr., and Goode, R. J., Fracture Resistance of Thick Plate 5083-O Alloy, Report of NRL Progress, December 1974, pp. 36-38.
8. Rice, J. R., J. Appl. Mechs., Trans. ASME, Vol. 35, 1968, pp. 379-386.
9. Begley, J. A. and Landes, J. D., in Fracture Toughness, ASTM STP 514, Amer. Soc. Test. Mater., 1972, pp. 1-39.
10. Landes, J. D. and Begley, J. A., in Fracture Analysis, ASTM STP 560, Amer. Soc. Test. Mater., 1975, pp. 170-186.

11. Griffis, C. A. and Yoder, G. R., Application of the J-Integral to Crack Initiation in a 2024-T351 Aluminum Alloy, Naval Research Report 7676, 1974, pp. 1-25.

12. Read, D. T. and Reed, R. P., Effects of Specimen Thickness on Fracture Toughness of Some Aluminum Alloys, submitted to Int. J. Fract. (1976).

13. Bogardus, K. O. and Malcolm, R. C., in Ref. 1, pp. 190-204.

14. Fowlkes, C. W. and Tobler, R. L., Fracture Testing and Results for a Ti-6Al-4V Alloy, Eng. Fract. Mechs., to be published.

15. Tobler, R. L., Mikesell, R. P., Durcholz, R. L., and Reed, R. P., in Ref. 1, pp. 261-287.

16. Rice, J. R., Paris, P. C., and Merkle, J. G., in Progress in Flaw Growth and Fracture Toughness Testing, ASTM STP 536, Amer. Soc. Test. Mater., 1973, pp. 231-244.

17. Kaufman, J. G. and Kelsey, R. A., in Ref. 1, pp. 138-158.

18. Argy, R., Paris, P. C., and Shaw, F., in Ref. 1, pp. 96-137.

19. Person, N. L. and Wolfer, G. C., in Ref. 1, pp. 80-95.

20. Wei, R. P., Eng. Fract. Mechs., Vol. 4, 1970, pp. 633-651.

21. Hartman, A. and Schijve, NLR Tech Note No. MP 68001 U, 1968; see also Fig. 11 of Reference 17.

22. Materials Research in Support of Superconducting Machinery, Vols. III, IV, and V, Reed, R. P., Clark, A. F., and van Reuth, E. C., Eds., National Bureau of Standards, Boulder, CO.

23. Zinkham, R. E. and Ashton, R. F., in ASTM STP 579, Ref. 1, pp. 159-175.

24. Weston, W. F., Naimon, E. R., and Ledbetter, H. M., in Ref. 1, pp. 397-420.

25. Merkle, J. G. and Corten, H. T., "A J-Integral Analysis for the Compact Specimen, Considering Axial Force as Well as Bending Effects," presented at the Pressure Vessels and Piping Conference with Nuclear Engineering and Mechanical Divisions, American Society of Mechanical Engineers, Paper No. 74-PVP-33, 1974.

Table 1. Tensile property results for 5083-0 aluminum alloy specimens in the longitudinal orientation (average values for two tests per temperature).

Temperature K	Temperature (°F)	0.2% Yield Strength MPa	0.2% Yield Strength (ksi)	Ultimate Strength MPa	Ultimate Strength (ksi)	Elongation (2.54 cm gage) %	Reduction of Area %
295	(70)	142	(20.6)	305	(44.2)	23.4	36.9
76	(-323)	150	(21.7)	404	(58.6)	34.1	36.7
4	(-452)	186	(27.0)	472	(68.5)	23.2	11.6

Table 2. J-integral test results.

Temperature K	Specimen	Orientation	K_{fmax} MPa•m$^{1/2}$	a/W cm	Δa cm	J kJm^{-2}	J_{Ic} kJm^{-2}
295	13	TL	14	.642	.010	10.3	
	28	TL	21	.647	.020	15.8	
	9	TL	15	.647	.029	20.1	
	8	TL	21	.620	.036	22.9	9
	31	TL	13	.641	.059	27.5	
	7	TL	15	.644	.070	30.5	
	14	TL	22	.611	.109	41.6	
111	2	LT	16	.622	.033	65.6	
	3	LT	18	.612	.019	54.2	41
	4	LT	18	.622	.033	60.8	
	5	LT	18	.619	.053	76.0	
111	30	TL	19	.622	.010	23.6	
	20	TL	13	.630	.023	36.4	
	22	TL	14	.617	.056	59.1	19
	10	TL	20	.629	.103	78.5	
	11	TL	20	.617	.253	122.4	
76	20	TL	15	.629	.010	27.9	
	17	TL	14	.623	.019	31.2	
	19	TL	16	.631	.026	40.5	
	16	TL	14	.633	.039	54.7	21
	14	TL	17	.628	.083	72.5	
	9	TL	21	.632	.093	77.3	
4	15	TL	19	.602	.003	13.7	
	11	TL	18	.597	.003	17.6	
	10	TL	20	.608	.010	30.2	
	17	TL	19	.602	.019	38.3	25
	16	TL	18	.602	.030	47.3	
	18	TL	18	.597	.056	61.4	

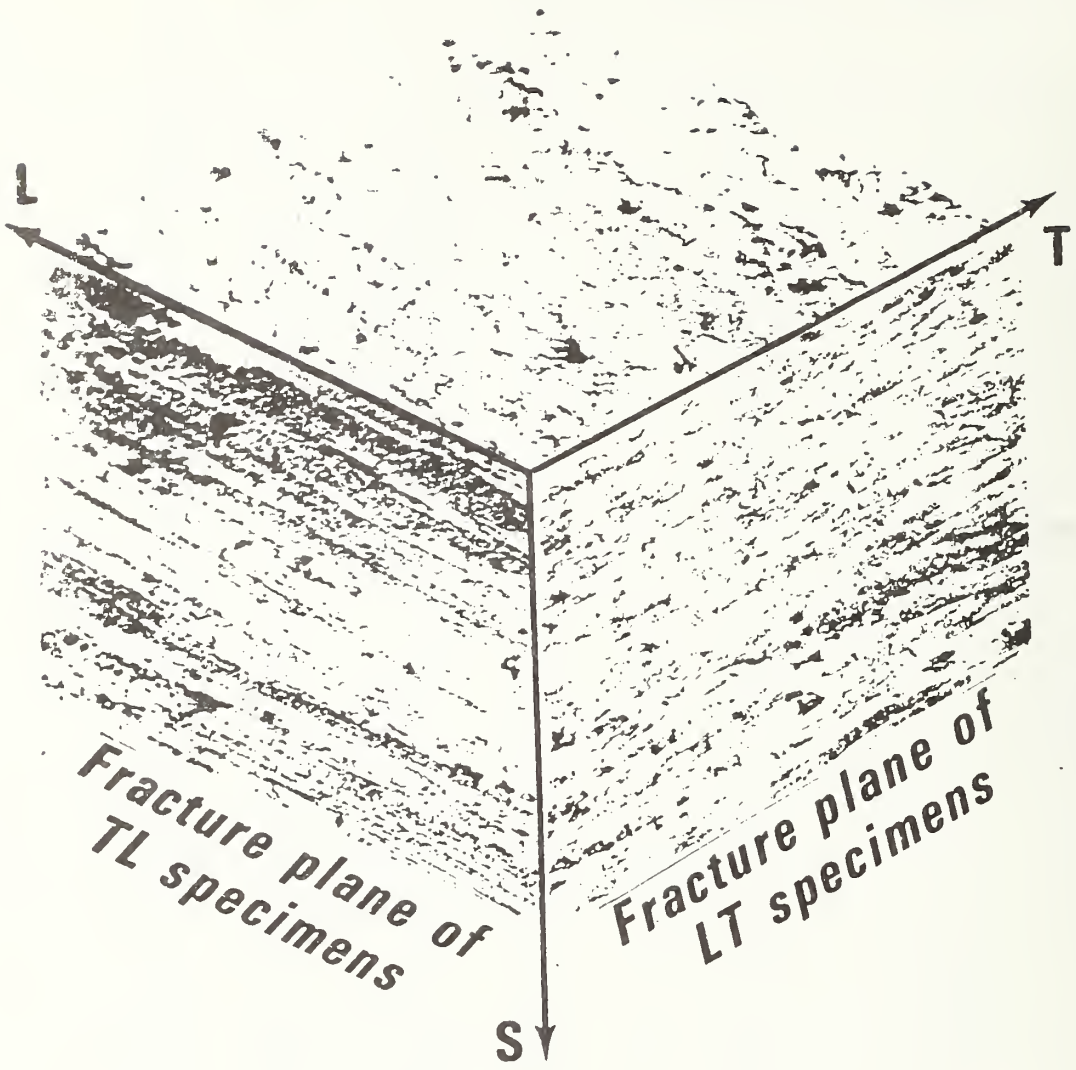

L—longitudinal or rolling direction
T—long transverse direction
S—short transverse or plate thickness direction

Figure 1. Microstructure of 5083-O after rolling and annealing, 100X.

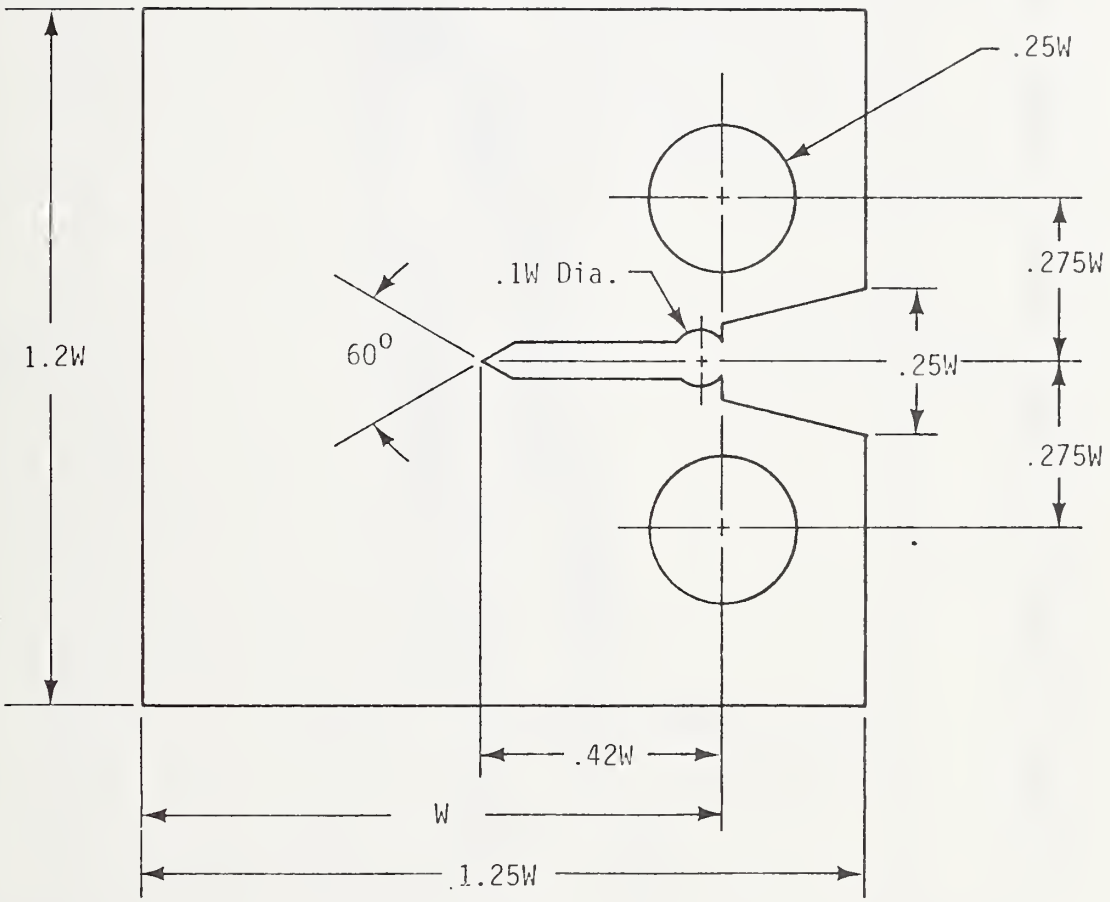

Figure 2. Compact specimen used in fatigue and fracture tests (thickness, B = 3.17 cm; dimensions are in cm).

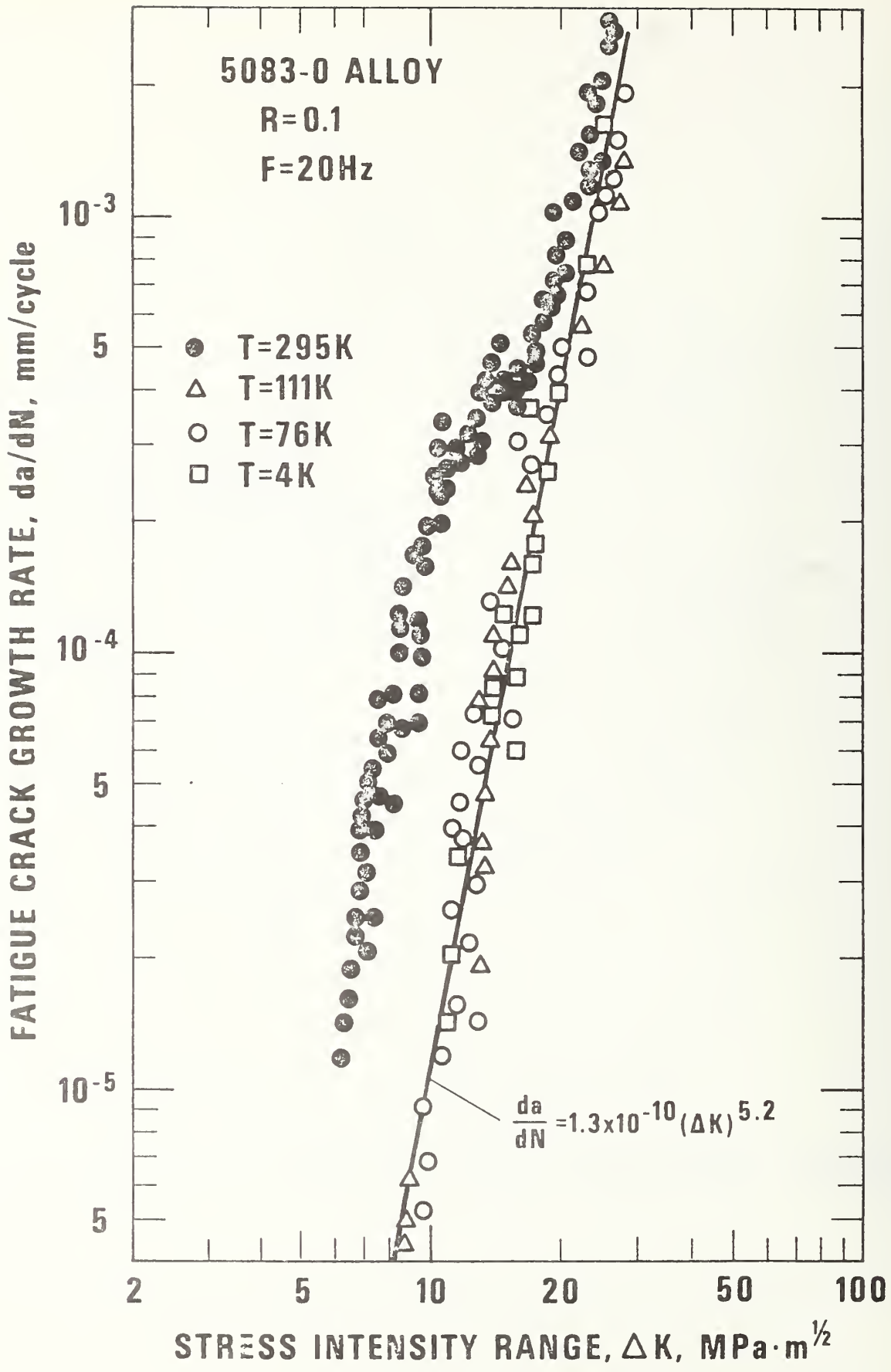

Figure 3. Fatigue crack growth rate results for TL orientations at 295, 111, 76 and 4 K.

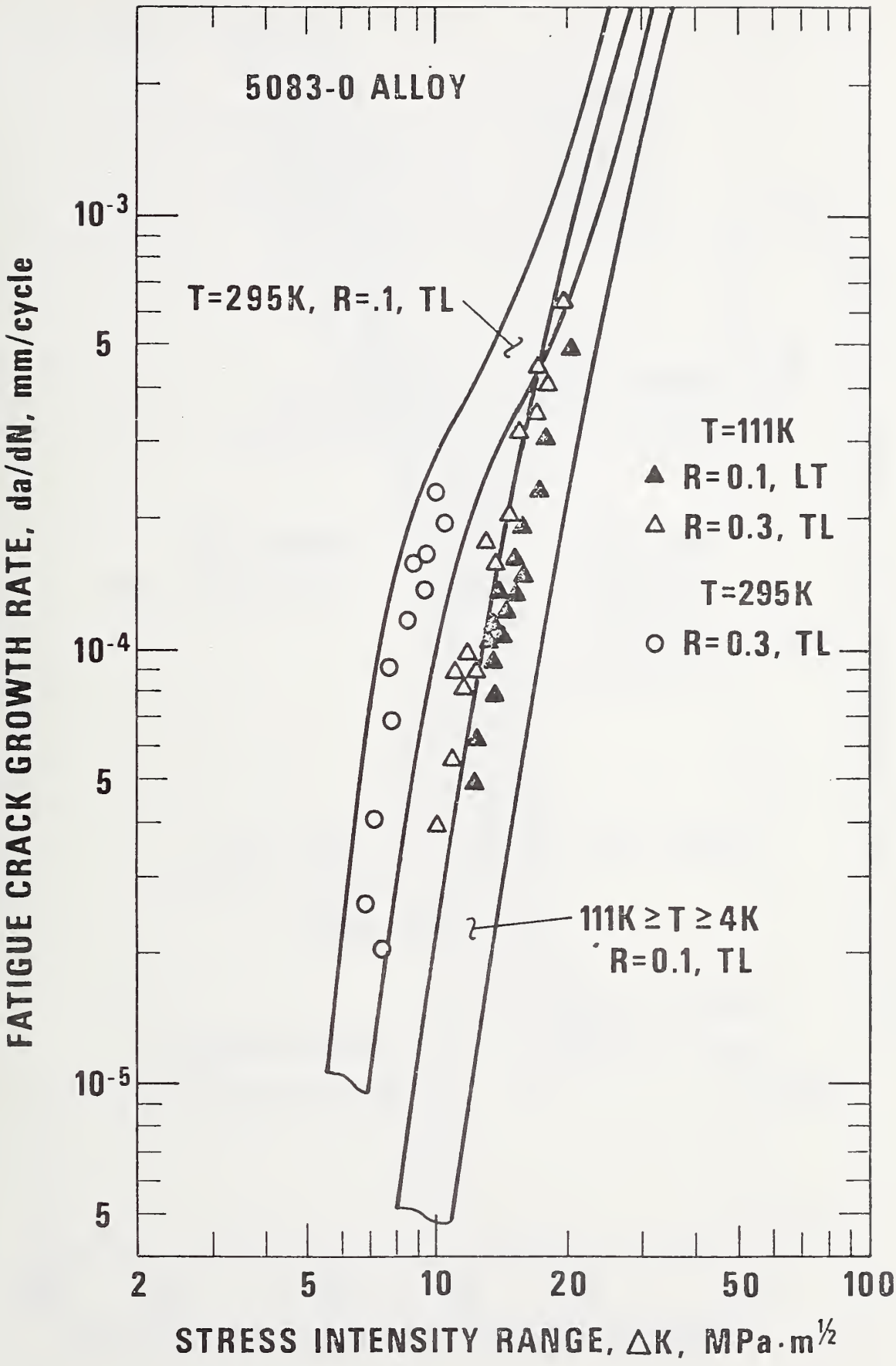

Figure 4. Fatigue crack growth rate results at 295 and 111 K, showing the effects of orientation and R ratio variations.

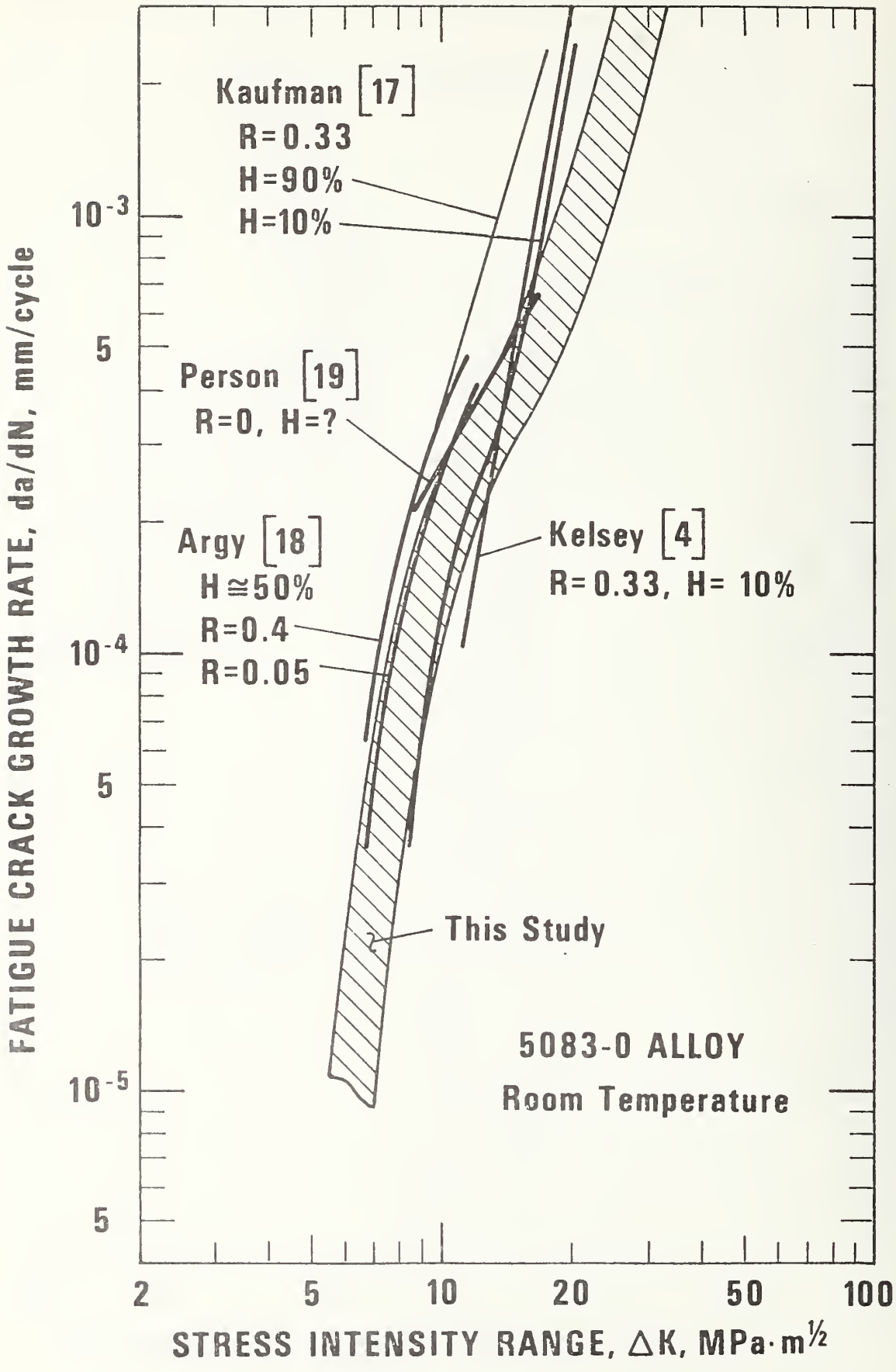

Figure 5. Comparison of fatigue crack growth data at 295 K.

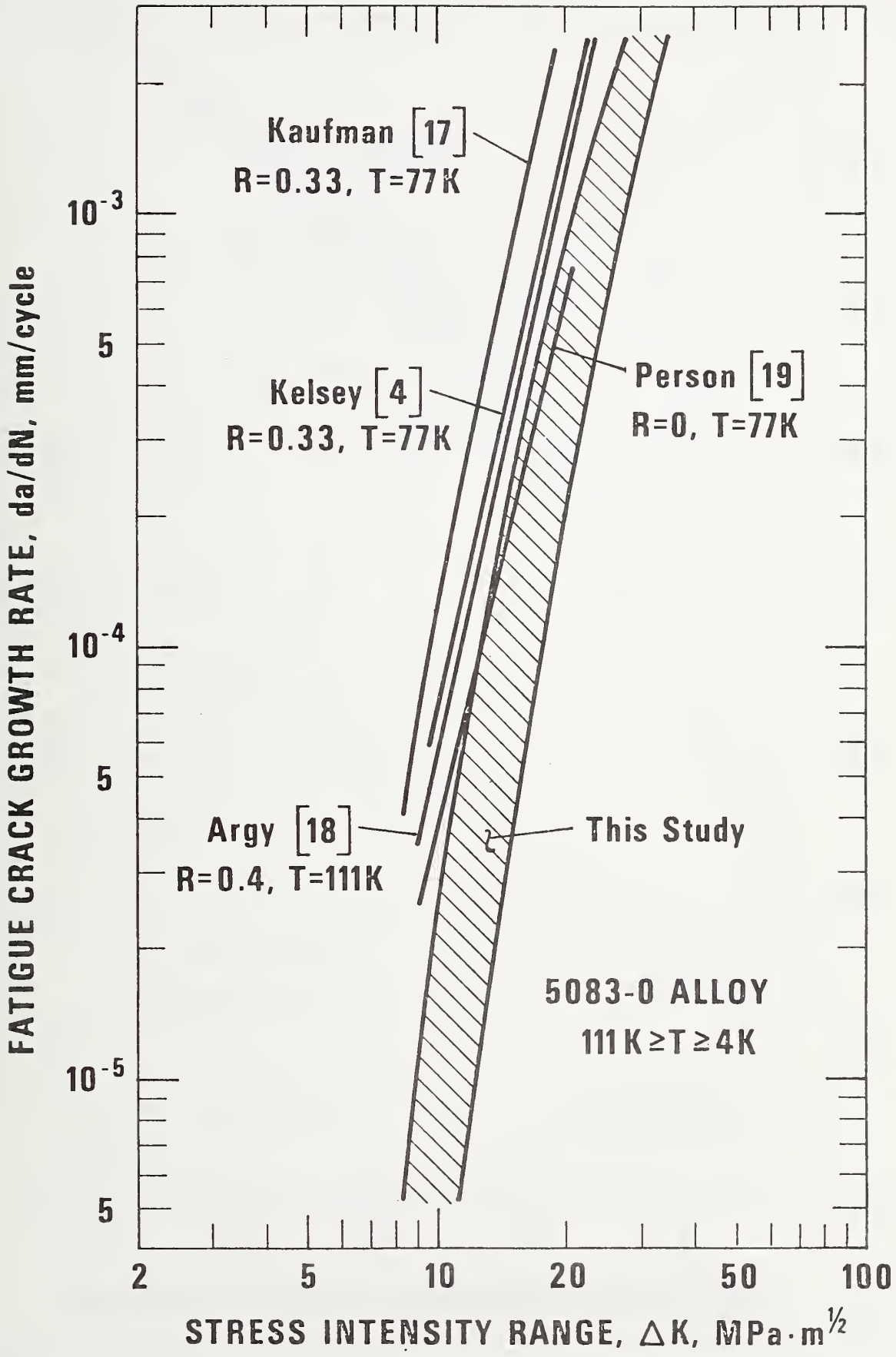

Figure 6. Comparison of fatigue crack growth data at low temperatures.

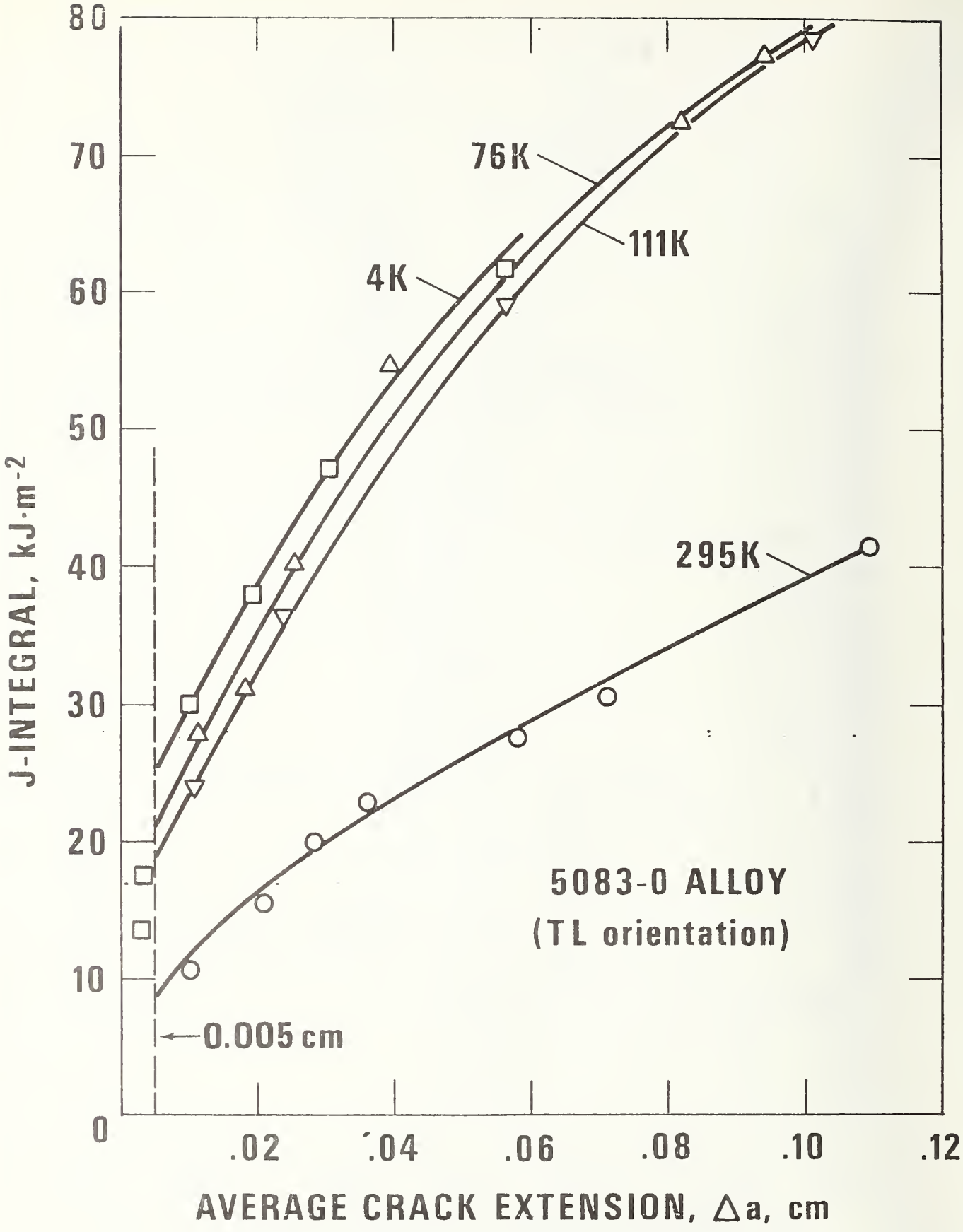

Figure 7. J-integral resistance curves for 5083-0 aluminum, showing the effect of temperature.

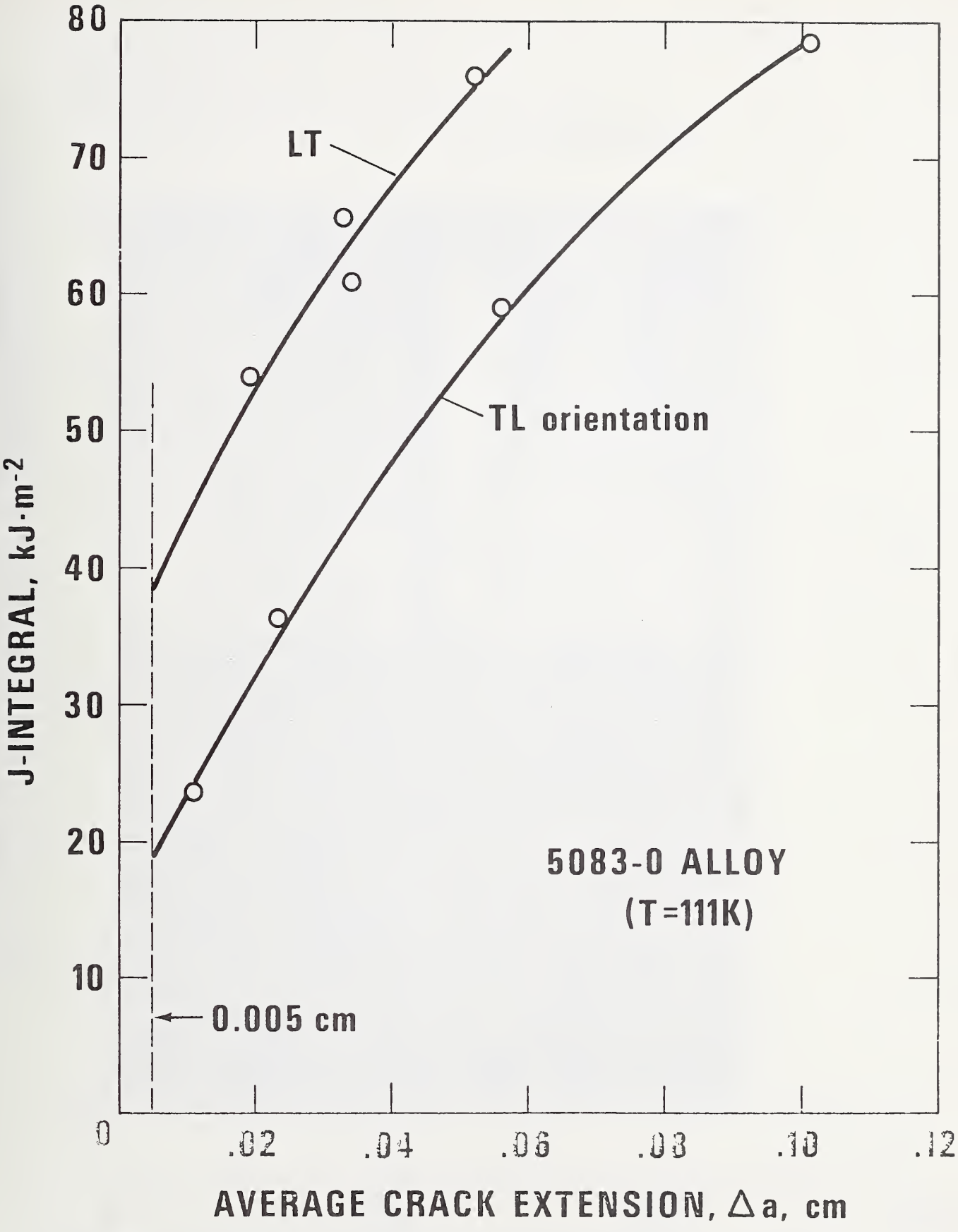

Figure 8. J-integral resistance curves for 5083-0 aluminum at 111 K, showing the effect of orientation.

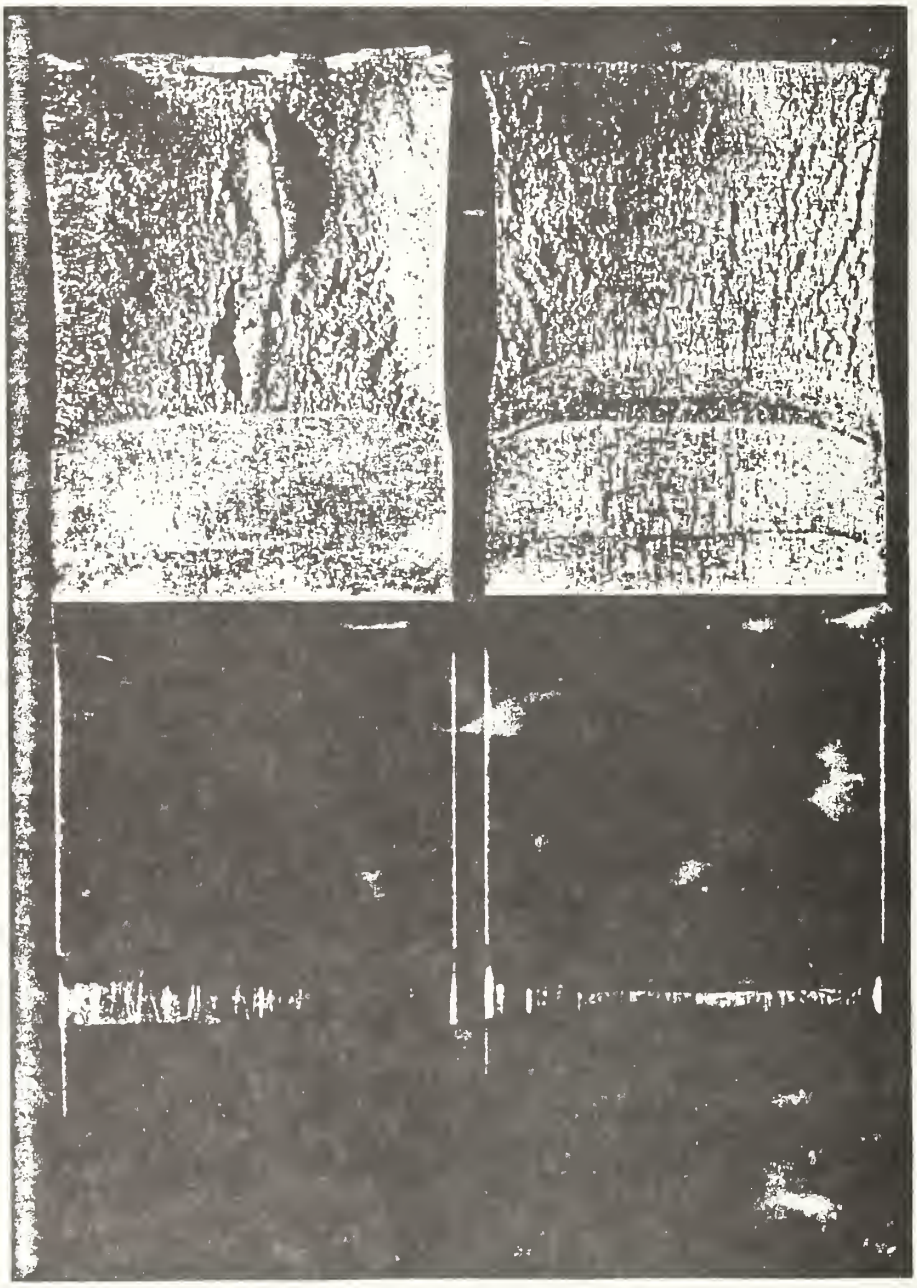

Figure 9. Fracture appearance of LT (left) and TL (right) specimens tested at 111 K.

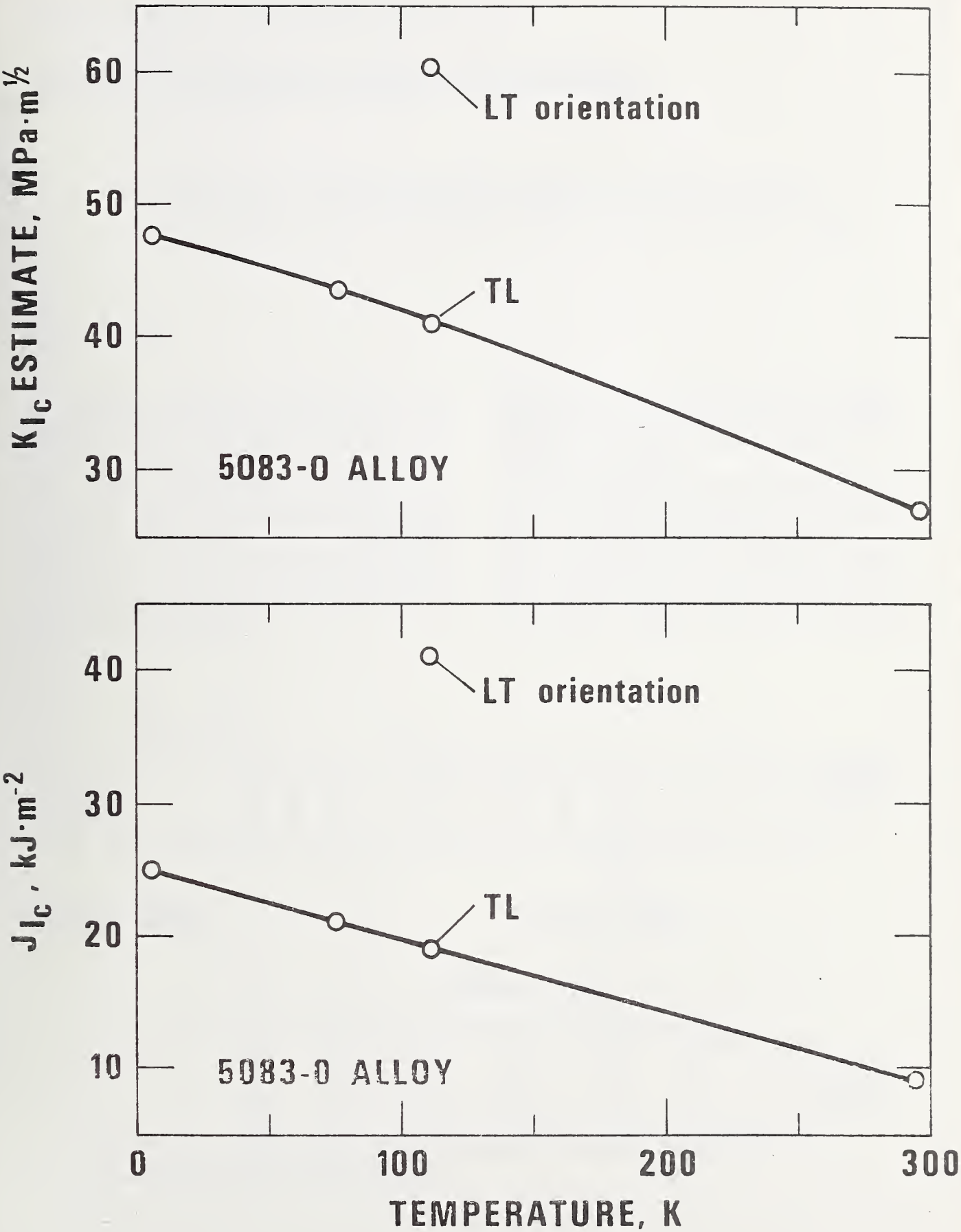

Figure 10. Temperature dependences of J_{Ic} data and K_{Ic} estimates.

Ship Steel Weldments for
Low Temperature Service

Cooperation among shipyards, regulatory agencies and steelmakers may lead the way to higher welding productivity

BY H. I. MCHENRY

A large fleet of tankers is under construction for the marine transport of liquefied natural gas (LNG). In LNG ships, significant portions of the hull are cooled by the cryogenic cargo to temperatures ranging from 0 to −46 C. At these temperatures many ship steels exhibit brittle behavior. Consequently, the U.S. Coast Guard (Ref. 1), the American Bureau of Shipping (Ref. 2) and comparable regulatory agencies around the world have established strict requirements on the ship steels and weld procedure qualifications for weldments subjected to low temperatures. To meet these requirements, shipyards generally employ low heat input, multipass welding practices. As a result, welding productivity is being limited to a level far below the capability of the equipment and facilities.

The Maritime Administration (MarAd) was advised of the increased costs of welding LNG ship hulls by the Welding Panel of the Ship Production Committee, a group of industry experts organized by the Society of Naval Architects and Marine Engineers to advise MarAd on how to improve shipyard productivity. In their efforts to reduce the cost of ship construction, MarAd requested the National Bureau of Standards to conduct a survey to establish the feasibility of improving

H. I. MCHENRY is associated with the Cryogenics Division, National Bureau of Standards, U.S. Department of Commerce, Boulder Colorado 80302.

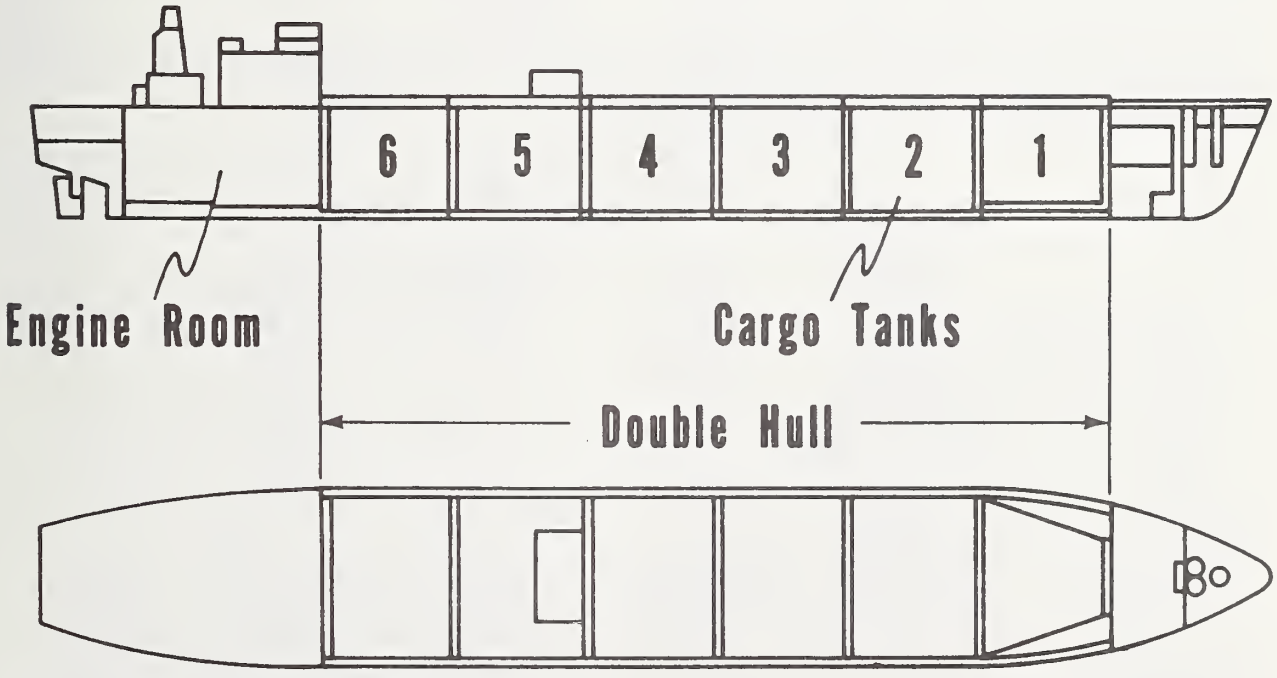

Fig. 1 — Structural arrangement of an LNG ship hull (Ref. 3)

Reprinted from WELDING JOURNAL, *May 1976*

the efficiency of welding ship steels for low temperature service. The survey included visits to the shipyards involved in LNG construction, to the appropriate regulatory agencies, to the steel plate producers and to other companies engaged in fabricating structures for low temperature service. These visits clarified the problem and the rules, and provided a review of the technology available for improving welding efficiency. The survey has been completed and the results are presented herein.

Shipyard Practice

The LNG ships under construction in the United States are approximately 280 m long, 42 m wide and 30 m deep and have a cargo capacity of 125,000 cubic meters. The ships are double-hull vessels with transverse bulkheads dividing the ship into several cargo bays as shown in Fig. 1 (Ref. 3). The cryogenic containment system fitted within each cargo bay consists of the cargo tank, the insulation and generally a secondary barrier to contain the LNG in case of tank failure. Thomas and Schwendtner (Ref. 4) have described eight types of containment systems in use or under consideration worldwide. In the U.S., three designs are under construction: The Conch free-standing prismatic tank, the Gazocean membrane prismatic tank and the Kvaerner-Moss free-standing spherical tank. For each system, the insulation is sufficient to permit transport of the LNG at approximately −162 C and atmospheric pressure with boil-off rates less than 0.25% per day.

The temperature environment within the hull is a function of the ambient air and water conditions, the effectiveness of the insulation system and the proximity of the cargo. For North Atlantic routes, the USCG specifies that the design temperatures be based on assumed ambient conditions of −18 C air, a 5 mph (2.33 m/s) wind and still water at 0 C. The inner hull, the transverse bulkheads and the tank support structure are the principal areas cooled by proximity to the cargo. Minimum design temperatures in these areas range from 0 C to −46 C. The coldest locations are the inner side-shell above waterline and parts of the tank support structure.

Steel Selection

The chemistry, processing and testing requirements of steels used in LNG ships being made in the U.S. are summarized in Table 1. These steel selections are generally in accordance with the proposed (1975) regulations of the International Maritime Consultive Organization (IMCO) as outlined in Tables 2 and 3. For temperatures below −10 C, fully killed, aluminum treated, fine grain, C-Mn-Si steels are used. For temperatures below −25 C, the steel must also be either normalized or quenched and tempered. The most commonly used steels are the ABS ordinary strength grades; CN is used for temperatures to −23 C, CS for temperatures to −34 C and V-051 for temperatures to −46 C. For high strength applications, ABS grade EH steel is commonly used for temperatures to −34 C and ASTM grade A537 Modified is used for temperatures to −46 C.

Approximately 28,000 metric tons of steel are required for the hull of a 125,000 cubic meters LNG ship. The tonnage requirements for all grades of hull steel and for low temperature steels are summarized in Table 4. These data are indicative of the total usage of low temperature steels and include significant tonnage selected for improved toughness and used in parts of the ship not exposed to temperatures below 0 C.

Table 1 — Specifications for Steel Plates Used in LNG Ship Hulls[a]

	Ordinary strength grades			Higher strength grades	
	CN	CS	V-051	EH-36	A537-A, Mod.
Min. design temp, C	−23	−34	−46	−34	−46
Composition, %	ABS 1972 Rules	ABS 1974 Rules		ABS 1974 Rules	ASTM 1970 Std
C, max	0.23	0.16	0.16	0.18	0.16
Mn	0.6-0.9	1.00-1.35	1.15-1.50	0.90-1.60	1.15-1.50
Si	0.1-0.35	0.10-0.35	0.10-0.35	0.10-0.50	0.15-0.50
P, max	0.05	0.04	0.04	0.04	0.04
S, max	0.05	0.04	0.04	0.04	0.04
Al	0.02-0.06	0.02-0.06	—	0.06 max	—
Ni, max				0.40	0.25
Cr, max				0.25	0.25
Mo, max				0.08	0.08
Cu, max				0.35	0.35
Cb, max				0.05	—
V, max				0.10	0.08
Mech. properties:					
Tensile, MPa (ksi)	402-490 (58-71)	402-490 (58-71)	402 (58), min	490-618 (71-90)	451 (65), min
Yield, MPa (ksi)	—	235 (34), min	245 (35), min	353 (51), min	314 (47), min
Elong. in 50 mm	24%	24%, min	24%, min	22%, min	22%, min
Charpy impact:					
Test temp., C			−51	−40	−51
Energy, min avg. J (ft-lb)			27.5 (20) transv.	34.3 (24) longit.	41.2 (30) longit.
Specimens			3/plate	3/plate	3/plate

(a) Heat Treatment: all grades normalized. Deoxidation: all grades aluminum killed, fine grain practice

Weld Procedure Qualification

For service temperatures less than −18 C, the welding procedures must be qualified in accordance with USCG and ABS requirements. Procedures are specific for each base metal, filler metal and flux combination and must be established for each welding process and position. The joint edge preparation, preheat and interpass temperatures, and other aspects of the procedure must be representative of the procedures used in production. Generally, two qualifications are required to cover the range of plate thicknesses: $9.5 < t \leq 19$ mm and $t > 19$ mm. Test plates for these qualifications are usually 19 mm thick for the lower thickness range and the maximum thickness used in production for thicknesses greater than 19 mm. The test plates are oriented such that the weld axis is parallel to the rolling direction.

The qualification requirements include the room temperature tensile and guided bend tests specified by ABS for all weld procedure qualifications plus a series of Charpy V-notch impact tests. The Charpy tests are conducted at 5.5 C below the minimum service temperature in accordance with ASTM A 370, using type A specimens. The specimens are cut transverse to the weld axis with the notches normal to the plate surface. Three specimens are tested for each of the following notch locations: centered in the weld metal; on the fusion line; and in the heat-affected zone (HAZ) 1, 3 and 5 mm from the fusion line. The impact specimen location requirements are summarized in Fig. 2. The average Charpy value must equal or exceed 27.5 J (20 ft-lb); the minimum value for one specimen is 18.6 J (13.3 ft-lb).

Table 2 — IMCO Requirements for LNG Hull Steels

Minimum design temp., T, C	Plate thickness, t, mm	Approved ABS steel grades
$T \geq 0$	—	Normal Practice
$0 > T \geq -10$	$t \leq 12.5$	B
	$12.5 < t \leq 25.5$	D
	$t > 25.5$	E
$-10 > T \geq -25$	$t \leq 12.5$	D
	$t > 12.5$	E
$-25 > T \geq -55$	—	See table 3

Table 3 — IMCO Requirements for LNG Hull Steels for Design Temperatures of −25 to −55C

Chemical composition

C	Mn	Si	S	P
.16% max	0.70-1.60%	0.10-0.50%	0.035% max	0.035% max

Optional additions:

Ni	Cr	Mo	Cu	Cb	V
0.80% max	0.25% max	0.08% max	0.35% max	0.05% max	0.10% max

Heat Treatment:
normalized or quenched and tempered

Deoxidation:
fully killed, aluminum treated, fine grain practice

Toughness requirements:
Temperature: 5 C below design temperature
Specimens: Charpy V-notch-transverse
Energy, min. avg: 27.5 J (20 ft-lb)
No. of Tests: 3 from each plate

Welding Processes and Consumables

Conventional shipyard welding practices are generally being used to fabricate low temperature steels; however, the heat inputs are restricted in order to meet the Charpy impact requirements. Consequently, the deposition rates are far below the equipment capabilities. The principal welding processes are submerged arc (SA), shielded metal-arc (SMA) and gas metal-arc (GMA) welding. For flat position welds and horizontal fillet welds, SA welding is the most efficient and reliable process, and therefore is widely used on automated panel lines. Both SMA and GMA welding are used for most of the other applications; the selection of one process over the other varies widely from yard to yard. Variations of these processes such as one-side welding, gravity welding, tandem arc and 3 o'clock SA welding are used in specific instances depending on the capabilities of the shipyard. High heat input processes such as the electroslag and electrogas processes are not approved by ABS for use on low temperature steels.

A wide range of electrodes and fluxes are used to weld ship steels for low temperature service. For submerged arc welding, two approaches have been taken: (1) use of a mild steel electrode and an alloy flux, or (2) use of an alloy electrode and a neutral flux. The mild steel electrodes conform to AWS specification A5.17-69 Class EM12K, and the alloy fluxes are of a proprietary nature. The alloy electrodes, which contain 1 to 2% Mn, 0.1 to 0.5% Mo and 0.5 to 2.0% Ni, are welded with a neutral flux suitable for multipass welding. For SMA welding, the most common electrode is AWS E 8018-C3 which contains 1% Ni. In some cases, E 7018 electrodes, which contain 0.5% Mo, are used for moderately low temperatures and E 8018-C1 electrodes, which contain 2 to 2.75% Ni, are used for the lowest temperatures. Both solid and flux-cored electrodes are used for GMA welding. The solid electrodes are alloyed with Mn, Mo and Ni for low temperature toughness and

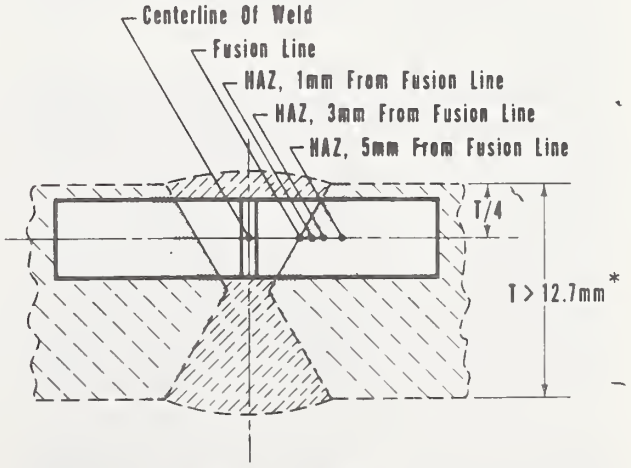

Fig. 2 — Charpy V-notch specimen locations for weld procedure qualification (Ref. 1)

Table 4 — Usage of Low Temperature Steels in LNG Ship Hulls

Ship design	Steel	Weldment test temp., C	Tonnage, long tons	Applications
Gazocean	All grades	—	29,573	Total hull plus scrap and spare
Membrane	ABS CS	−34	9,666	Inner bottom, web frames, gunwale, bilge
Prismatic	ABS V-051	−43	2,695	Inner side shell, transverse deck box
Conch	All grades	—	17,810	Midbody (hull less bow and stern)
Free standing	ABS CN	−23	6,058	Trans. Bulkhead, inner side shell, deck
Prismatic	ABS CS	−21 to −32	4,602	Inner bottom, gunwale, bilge
	ASTM A678-A	−45	418	Roll key
Kvaerner-Moss	All grades	—	17,393	Midbody
Free standing	ABS CN	−23	1,408	Inner hull
Spherical	ABS CS	−33	1,602	Transverse bulkheads
	ABS EH-36	−29	1,515	Deck girders
	ASTM A537 (Mod)	−51	1,185	Cylindrical tank support

the flux cored generally has a mild steel sheath and a proprietary flux.

Low heat input welding practices are necessary to meet the USCG impact requirements in the HAZ of low temperature ship plate weldments. This poses a significant productivity problem to the LNG shipyards because deposition rate is proportional to heat input, and their welding equipment is capable of far greater deposition rates than are possible using the low heat input practices. Consider, for example, the welding procedures that are representative for welding 19 mm plate. For x-ray quality welds in steels such as ABS grade B, the following conditions are recommended (Ref. 5):

Joint preparation: double V-groove with an 8 mm root face

Backing weld: 850 A, 33 V, 16 in./min (6.8 mm/s), 105 kJ/in.

Finishing weld: 1150 A, 35 V, 13 in./min (5.5 mm/s), 186 kJ/in.

In contrast, 19 mm ship plate for low temperature service must be multipass welded with the heat input limits ranging from about 40 to 80 kJ/in. ~~102 to 205 kJ/cm~~ depending on the particular combination of steel grade and service temperature. At heat input levels within this range, anywhere from 4 to 14 passes may be required to weld 19 mm plate.

Two approaches to solving the productivity problem are apparent: either change the weldment toughness requirements or improve the tolerance of the base metal to higher heat input welding practices. Changing the rules is not a viable solution to the problem, because strict requirements are appropriate for hazardous cargo such as LNG. In addition, the requirements have recently been adopted by IMCO as standards acceptable to all major shipping countries. Thus, any change in the existing requirements would probably be contingent upon agreement by both the USCG and IMCO, certainly a long term proposition. The alternative solution would be to make available an economical steel which, when welded using efficient procedures, provides the required level of toughness. This potential solution is attractive because it is based on steelmaking technology and shipyard economics instead of international agreements. The feasibility of this solution is addressed in the next section.

Steelmaking Technology

Current steelmaking technology offers several methods for providing improved toughness at low temperatures. The methods include alloying, rolling practice, sulfide shape control and heat treating. The extent to which the improvements are reflected in HAZ toughness of high heat input welds is not well documented. Nevertheless, there exists reason to believe that one or a combination of the available metallurgical treatments will permit higher heat inputs than currently being used. Whether or not the improvement will be economically justifiable depends on the cost increment added to the price of the steel and the extent of the improvement. Because of the large tonnages involved, the added cost of an improved ship steel will likely be limited to a maximum of $20 to $60 per metric ton (Mg), depending on the specific application.

Alloying

The use of additional alloying to improve ship steels is severely constrained by steel pricing practices. Steel prices are comprised of a base price and extras for the specification, plate dimensions and quantity. There are two base prices; the carbon steel base and the alloy steel base, the latter of which is about 40% higher. The carbon steel base price is applicable to all the steels used in LNG ship hulls. The American Iron and Steel Institute (AISI) considers a steel to be an alloy steel when either (1) the maximum of the range given for the content of alloying elements exceeds one or more of the following limits: Mn, 1.65%; Si, 0.60%; Cu, 0.60%; or (2) a definite range or a definite minimum quantity of any other element is specified to obtain a desired alloyed effect (Ref. 6).

The chemistry specification for ABS EH 36 shown in Table 1 is typical of the degree of alloying permissible in carbon steels. Notice that there are no minimum requirements on alloying elements such as Cr, Mo, Ni, V and Cb. Thus, the steelmaker has flexibility on how best to achieve the required tensile and impact properties. These pricing practices preclude the use of 0.4 to 0.8% Ni additions that are frequently specified for low temperature applications by Japanese and European shipbuilders. However, the transition temperature of

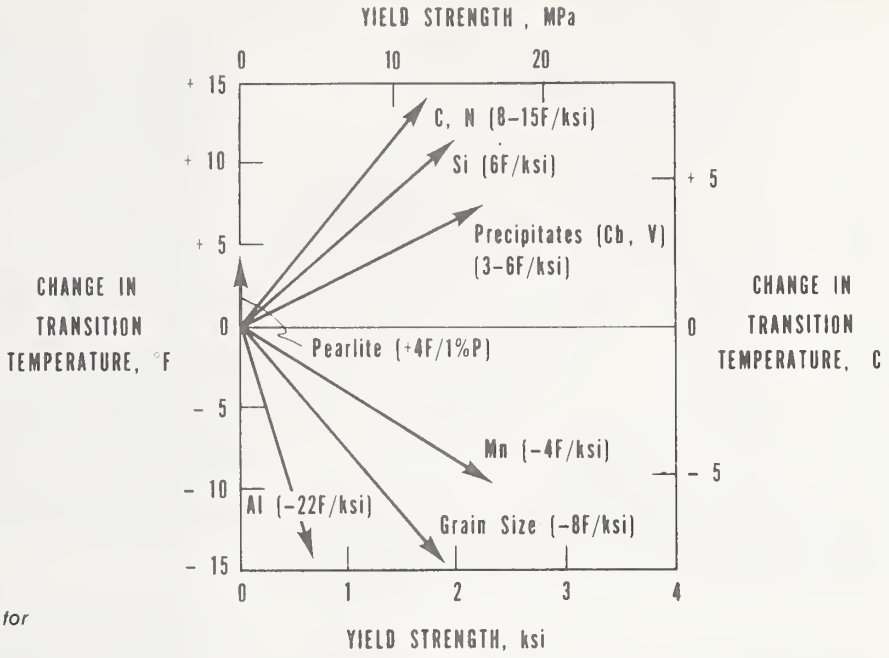

Fig. 3 — Strength toughness vectors for structural steels (Ref. 7)

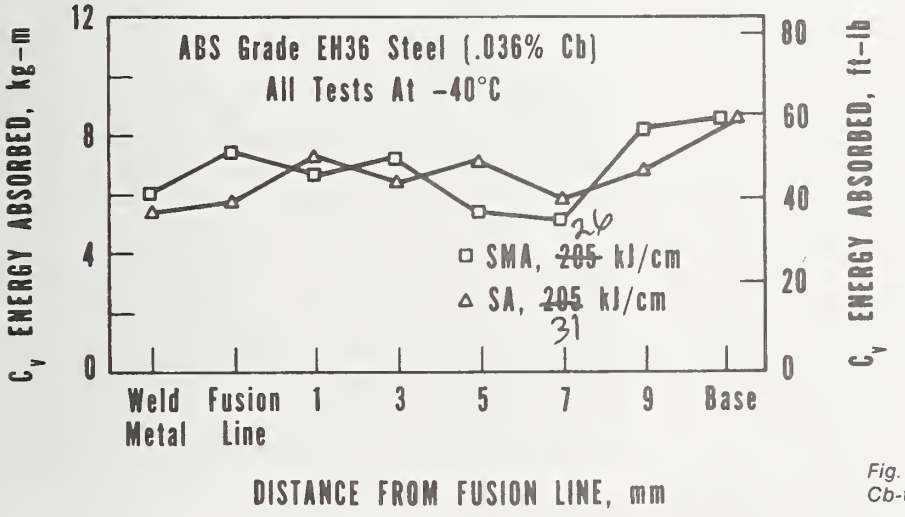

Fig. 4 — Charpy toughness traverse for Cb-treated EH-36 weldment (Ref. 10)

ship steels can be reduced by alloy adjustments within the AISI limits for carbon steels. As shown in Fig. 3, the transition temperature is reduced by increasing the Mn content and by lowering C, Si and N (Ref. 7).

Microalloying with Cb or V is an economical approach to providing strength and good low temperature properties in the base plate, and is currently used in EH 36 and A537 Modified steels. Strengthening is provided by a combination of reduced grain size and precipitation hardening. The low temperature toughness is improved because of the small grain size — an improvement that is only partially offset by the precipitation hardening effect shown in Fig. 3. However, the HAZ toughness near the fusion line is adversely affected by grain coarsening and further reduced by the strengthening effect of carbonitride precipitation (Refs. 8, 9). This embrittlement is almost always observed in simulated HAZ specimens, but is frequently not evident in Charpy specimens taken from weldments. The absence of embrittlement in high heat input weldments such as shown in Fig. 4 suggests that the high toughness material surrounding the embrittled region substantially reduces the embrittlement (Ref. 10). It is not clear at this time whether this can be attributed to an averaging effect, i.e., the Charpy impact specimen samples a composite of high and low toughness material, or to a reduction of constraint provided by the ductile material surrounding the embrittled region. In either case, it appears that the problem of Cb or V embrittlement in the HAZ may not be as significant in real weldments as suggested by some investigators (Refs. 8, 9) on the basis of simulated HAZ studies.

Inclusion Control

Nonmetallic inclusions are an intrinsic constituent of all steels. There are two main types of inclusions: (1) the indigenous inclusions which precipitate in the molten or

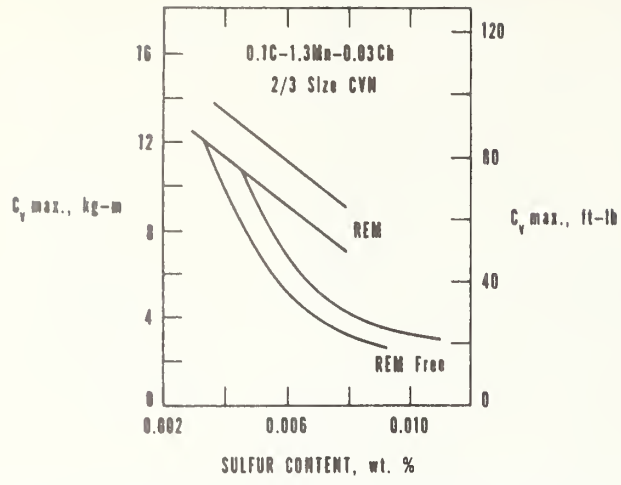

*Fig. 5 — The effect of rare earth metal treatments on the transverse shelf energy of low sulfur C-Mn steel (Ref. 12)**

solidifying metal due to decreased solubility of oxygen and sulfur upon cooling, and (2) the exogenous inclusions which are introduced into the steel from materials such as the refractories which come in contact with the molten steel. The indigenous inclusions are far more numerous and predictable in their behavior than the exogenous types, which occur sporadically. The principal types of indigenous inclusions are oxides and sulfides. In Al killed steels, the dominant oxide is Al_2O_3, which precipitates as small refractory crystals that do not agglomerate and do not change shape appreciably during rolling operations.

The principal sulfide inclusion in C-Mn steels is MnS. In low oxygen steels (e.g., Al killed), the MnS inclusions are quite plastic and tend to elongate during rolling. These stringer shaped inclusions separate readily from the steel matrix, and have a higher surface-to-volume ratio and a shorter interparticle spacing than globular inclusions. Consequently, the MnS stringers serve as initiation sites for low energy fracture when the steel is loaded transverse to the direction of rolling.

Sulfide shape control is rapidly emerging as a practical tool for eliminating stringers and thereby improving the transverse toughness of structural steels (Ref. 11). The process generally consists of lowering the sulfur content of the heat below 0.015% and then adding elements to the melt which form refractory sulfides. The refractory sulfides take on a spherical shape in the liquid steel and tend to retain this shape upon solidification and during the rolling process. Several elements, including Ti, Zr, Ca, Mg and the rare earth metals, form refractory sulfides. Although practices vary widely, sulfide shape control by the ladle addition of rare earth metal (REM) in the form of mischmetal, a mixture of rare earths containing about 50% Ce, appears to be gaining favor. The rare earths are preferred over Ti and Zr because, in addition to shape control, an appreciable reduction in sulfur content occurs due to the solution of rare earth sulfides and oxysulfides in the slag. Calcium and magnesium are effective for both sulfide shape control and sulfur reduction; however, Mg is difficult to introduce into molten steel because of its high vapor pressure; and Ca, which is not soluble in liquid iron, does not mix readily enough to assure complete sulfide shape control. The influences of sulfur content and REM additions on toughness are shown in Fig. 5 (Ref. 12).

**Reprinted with permission of the Metallurgical Society of AIME.*

Rolling Practice

Significant toughness improvements can be obtained by altering the rolling practice. Cross rolling can improve transverse properties at a moderate increase in steel cost; however, substantial improvements require rolling ratios that approach unity. Steel specifications rarely include cross rolling requirements; however, a guaranteed transverse Charpy requirement generally implies that cross rolling will be used. Thus, the principal use for cross rolling is to make moderate improvements in transverse properties to assure conformance to a transverse toughness guarantee.

Controlled rolling can improve strength and low temperature toughness by substantially reducing the austenite grain size and the fineness and nature of the transformation products (Ref. 13). It involves a schedule of reductions at specified temperatures, sometimes coupled with controlled cooling between passes and after the final pass. Most commonly, controlled rolling is limited to performing the final reduction at a specified temperature which is lower than normally employed. As shown in Fig. 6, the reduction below 900 C causes a significant decrease in transition temperature. It is particularly useful for the production of line pipe, where the large tonnage involved permits optimization of the rolling schedules on an economical basis. For ship steels, the large variety of plate sizes, thickness and grades, and the lack of facilities for producing controlled-rolled plates greater than 16 mm thick, limit the practicability of controlled rolling. In addition, the large variety of rolling schedules can lead to more scatter in the material properties than is associated with more easily controlled procedures such as normalizing. Due to these limitations, controlled rolling is not considered practical for improving the toughness of ship plate.

Heat Treatment

Nearly all the ship steels used for low temperature (to −46 C) applications are normalized. The typical normalizing heat treatment involves heating the as-rolled plate to 925 ± 25 C and air cooling to room temperature. As shown in Fig 7, the low temperature toughness of these steels could be improved by a quench and temper (Q and T) heat treatment (Ref. 14). For C-Mn steels such as ship plate, Q and T involves heating to 925 ± 25 C, quenching in water and subsequently tempering at 650 ± 50 C. This heat treatment is nearly twice as expensive as normalizing. Although Q and T improves base plate toughness, it is not clear whether this benefit will be apparent in the heat-affected zone of weldments. It is considered likely that the reheat treatment caused by the weld thermal cycle will impart the same toughness to the heat-affected zone regardless of prior heat treatment. Thus, the extra cost of Q and T over normalizing, $30 to $40/metric ton (Mg), is not considered a cost effective means of improving heat-affected zone toughness.

Work In Progress

On the basis of the shipbuilding and steel industry survey, MarAd requested NBS to conduct a follow-on program in cooperation with the LNG shipbuilders to evaluate improved ship steels for low temperature service. In this program, the major steel companies are providing the LNG shipyards with production heats of ABS steels, modified to possess improved transverse fracture properties at the appropriate test temperatures. The shipyards will evaluate these steels by qualifying optimum weld procedures in accordance with the USCG requirements. A comparison of the optimized procedures with those currently employed will be indicative of the cost reduction possible through the use of improved steels. As a result, each participating shipyard will be in a position to make a rational decision regarding the cost effectiveness of premium quality steels. The program, currently in the formative stages, will be completed in mid-1977, and the results will be published shortly thereafter.

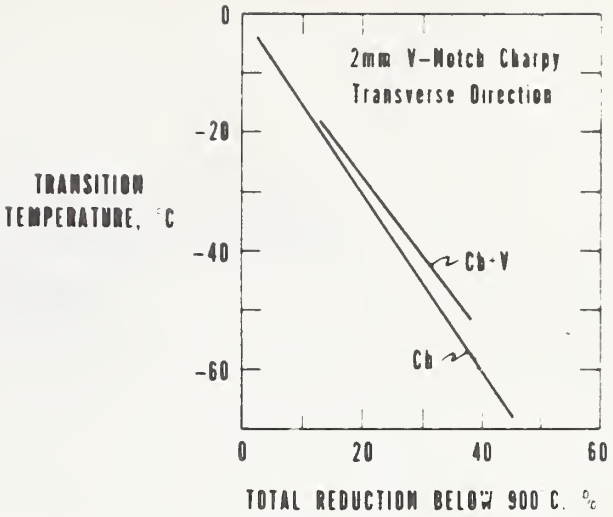

Fig 6 — The effect of rolling reduction below 900 C on the fracture appearance transition temperature (Ref. 13)

Summary

A survey of the U.S. shipyards engaged in LNG ship construction, the major steel plate producers and the maritime regulatory agencies has been conducted to establish the feasibility of improving the efficiency of welding ship steels for low temperature service. The results of this survey suggest that application of state-of-the-art steelmaking technology can substantially improve the low temperature toughness of ship steels. A program is being conducted to determine if steels with improved toughness retain satisfactory toughness in the HAZ when higher heat input welding practices are used.

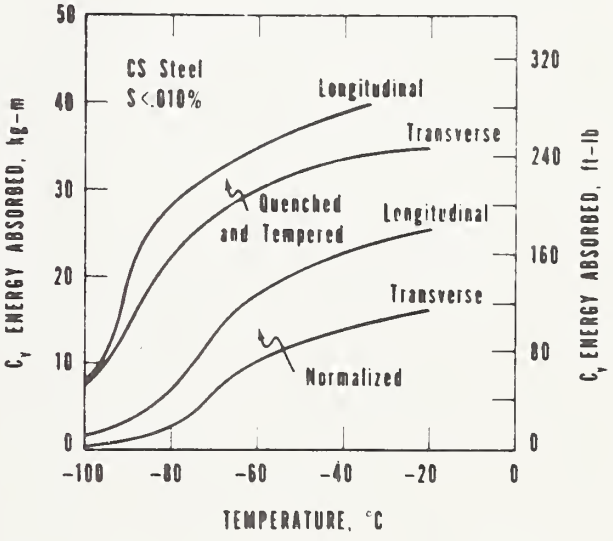

Fig 7 — Charpy impact transition curves for normalized and for quenched and tempered CS steel (Ref. 14)

Acknowledgments

This work was sponsored by the U.S. Maritime Administration. The author wishes to acknowledge the many contributions of M. B. Kasen and R. P. Reed of NBS who collaborated on all aspects of the program described herein. The author also expresses appreciation to R. W. Schaffran of the U.S. Maritime Administration and W. C. Brayton of Bethlehem Steel Corporation who were responsible for initiating the program.

References

1. USCG, *U.S. Coast Guard Marine Engineering Regulations*, Subchapter F, CG-115, July 1970.

2. ABS. *Rules for Building and Classing Steel Vessels*, American Bureau of Shipping, New York, 1974.

3. Emery II, W. B., Sterrett, E. L. and Moore, C. S., "Alaskan Liquefaction Plant to Supply Gas for Japanese Use," *Oil and Gas Journal*, 66(1), 55-59.

4. Thomas, W. D. and Schwendtner, A. H., "LNG Carriers: The Current State of the Art," 1971 Annual New York Meeting, The Society of Naval Architects and Marine Engineers, 1971.

5. Anon, *Submerged Arc Welding Handbook*, Linde Reference Library, Union Carbide Corp., New York, 1974.

6. Anon., "Alloy Steel Plates," American Iron and Steel Institute, New York, April 1970.

7. Cordea, J. N. "Niobium-and Vanadium-Containing Steels for Pressure Vessel Service," *Welding Research Council Bulletin No. 203*, February 1975.

8. Hannerz, N. E., "Effect of Cb on HAZ Ductility in Constructional HT Steels," *Welding Journal*, 54, (5) May 1975, Res. Suppl., pp 162-s to 168-s.

9. Hannerz, N. E. and Jonsson-Holmquist, B. M., "Influence of V on the HAZ Properties of Mild Steel." *Metal Science* 8 (1974) 228-233.

10. Alia, B. L., Stern, I. L. and Null, C., "Toughness Evaluation of Electrogas and Electroslag Weldments." Project Report, The National Shipbuilding Research Program, U.S. Maritime Administration, March 1975.

11. Korchynsky, M., "The Relationships Between Sulfide Composition Morphology and Distribution on Mechanical Properties of HSLA Steels," presented at the International Symposium on Sulfide Inclusions in Steel, American Society for Metals, Port Chester, N.Y., November 1974.

12. Kozasu, I. and Osuka, T., "Processing Conditions and Properties of Control-Rolled Steel Plates," in *Processing and Properties of Low Carbon Steel*, Gray, J. M. (editor). The Metallurgical Society of AIME, New York, 1973.

13. Gray, J. M., "Columbium (Niobium) as a Grain Refiner in Hot Rolled Steels," in *Processing and Properties of Low Carbon Steel*, Gray, J. M. (editor), The Metallurgical Society of AIME, New York, 1973.

14. Anon., "N-Tuf, Low Temperature Steels," Nippon Steel Corp., Tokyo, 1972.

NBSIR 77-852

CRYOGENIC FLUIDS DENSITY REFERENCE SYSTEM: PROVISIONAL ACCURACY STATEMENT

B.A. Younglove
J.D. Siegwarth

Cryogenics Division
Institute for Basic Standards
National Bureau of Standards
Boulder , Colorado 80302

January 1977

Prepared for:

American Gas Association, Inc.
1515 Wilson Boulevard
Arlington, Virginia 22209

U.S. DEPARTMENT OF COMMERCE, Elliot L. Richardson, Secretary

Edward O. Vetter, Under Secretary
Dr. Betsy Ancker-Johnson, Assistant Secretary for Science and Technology

NATIONAL BUREAU OF STANDARDS, Ernest Ambler, Acting Director

CONTENTS

CRYOGENIC FLUIDS DENSITY REFERENCE SYSTEM: PROVISIONAL ACCURACY STATEMENT

B. A. Younglove and J. D. Siegwarth

Cryogenics Division
Institute for Basic Standards
National Bureau of Standards
Boulder, Colorado 80302

The measurement capability of the density reference system (DRS) of the National Bureau of Standards, Cryogenics Division, is described. This system measures density, pressure, and temperature of LNG mixtures for the purpose of testing densimeters which are contained in the liquid sample. Sample composition is determined by weighing the gas samples separately before condensing them into the sample. The DRS measures density by weighing a single-crystal of silicon immersed in the LNG mixture. This process is described and the equations used in the computation of density are discussed.

At this time the estimate of sample standard deviation for a single density measurement made on this system is $\pm$ 0.062% (at 0.4 g/cc). Using three times this standard deviation as a limit for random error and adding $\pm$ 0.026% as an upper bound for known sources of possible systematic error, the uncertainty of a single determination by this system is $\pm$ 0.21%. This statement of accuracy applies for the density range 380 to 430 kg/m^3 and 1200 to 1400 kg/m^3, pressures to 7 bar, and temperatures from 80 K to 140 K. This statement is expected to be correct in the intermediate density range and for all temperatures up to 300 K.

Measurement uncertainties for temperature, pressure, and composition are discussed. Comparison of measurements for liquid argon densities with the results of other laboratories is given.

Key words: Densimeters; density reference system; liquid methane; LNG.

1. INTRODUCTION

The density reference system (DRS) was evolved to determine the uncertainty of measurements made by several field type densimeters capable of operating at cryogenic temperatures in liquefied natural gas (LNG). The project was performed under a grant from the American Gas Association, Inc. (A.G.A.) on behalf of its membership.

This system has the capability at present of operating from room temperature to near the boiling point of liquid nitrogen (300 K to 80 K), and at pressures of 7 bar (100 psi) to vacuum. In this work we covered densities of 390-500 kg/m^3, a range normally found in LNG work. Some additional density measurements were made on liquid argon. Only methane density measurements were used in the determination of the system uncertainty.

At this time the value of the sample standard deviation for a single density measurement made on this system is $\pm$ 0.062% (at 0.4 g/cc), based on measurements made using samples of liquid methane (99.97%). Using three

times the standard deviation as a limit for the random error, and adding 0.026% as an upper bound for known sources of possible systematic error, the uncertainty of a single determination by this system is $\pm$ 0.21%.

Density is determined in the DRS by weighing an extremely pure (semiconductor grade) single-crystal of silicon in the liquid whose density is to be determined. The density of the liquid is calculated from the apparent weight of the silicon submerged in the liquid using Archimedes principle.

It is appropriate that silicon was used in this work as its density has been recommended by Bowman [1] of NBS as the primary standard for solid densities. His work which uses Archimedes principle discusses the several advantages that this type of silicon has for accurate measurements of liquid densities: relatively low density (compared to other solids), high thermal conductivity, reasonably low electrical resistance, and low compressibility. Of course Bowman's work and others [2] provide accurate values for silicon density.

1.1. Symbols

g	acceleration of a freely falling body
k	compressibility factor
L	length
L_{298}	length at reference temperature 298 K
L_T	length at absolute temperature T
M_a	apparent mass
M_{ak}	apparent mass as read by balance during calibration
M_{ao}	apparent mass as read by balance for zero mass load
M_b	buoy mass, silicon crystal + tungsten wire + stainless steel wire immersed in liquid
M_{bg}	apparent mass of buoy in gas
$M_{b\ell}$	apparent mass of buoy in liquid
M_c	counterweight mass
M_{cg}	apparent mass of counterweight in gas
M_h	hanger mass
M_{hg}	apparent mass of hanger in gas
M_k	calibration mass
M_{kg}	apparent mass of calibration mass in gas
M_r	range mass
M_{rg}	apparent mass of range mass in gas

M_s	silicon crystal mass
M_w	replacement mass standard used to evaluate zero of balance
M_{wg}	apparent mass of replacement mass in gas
M_1	hanger mass, brass part
M_2	hanger mass, stainless steel wire part
M_3	hanger mass, stainless steel wire, that part of M_2 located in liquid
M_4	hanger mass,tungsten wire part
P	system pressure
T	system temperature
V	volume of buoy
V_s	volume of silicon
ΔMa	apparent mass less zero mass reading of DRS balance
δ	density difference between DRS density and a reference density
ϵ	density variation in δ from the average value of δ, for a methane sample
η	density variation in δ from a methane sample to an average methane sample
ρ	density of liquid sample
ρ_g	density of gas (vapor phase in equilibrium with sample liquid)
ρ_h	density of reference methane liquid
ρ_s	density of silicon
ρ_1	density of brass
ρ_2	density of stainless steel
ρ_4	density of tungsten
σ	standard deviation
σ_ϵ	standard deviation of ϵ
σ_η	standard deviation of η
μ	density difference bias

2. DESCRIPTION OF THE BASIC MEASUREMENT PROCESS

2.1. Density

The density reference system determines density via the Archimedes principle, which is that a body submerged wholly or partially in a liquid is buoyed by a force equal to the weight of the fluid displaced. The net force on the object is the difference between its weight and the buoyant force.

The basic arrangement of the silicon crystal, the weighing balance, and sample holder can be seen in figure 1. Figures 2 and 3 are photographs of the partially disassembled reference system. A silicon crystal, is weighed immersed in the test liquid. Its apparent weight is the difference in its true weight and the buoyant force exerted by the liquid.

$$M_a g = (M_s - \rho V_s) g. \tag{1}$$

In the following relations we have removed the factor, g, as it is common in all terms. Solving for density

$$\rho = (M_s - M_a) \frac{1}{V_s}. \tag{2}$$

Using the measured value for the silicon mass and the value for single-crystal pure silicon density, ρ_s, we have

$$M_s = \rho_s V_s . \tag{3}$$

Combining equations (2) and (3) to eliminate V_s,

$$\rho = \rho_s (1 - M_a/M_s). \tag{4}$$

This is the basic form of the measurement equation. The one actually used is more elaborate and is developed in the following sections.

Density from actual readings using a balance.

In practice we measure density using an automatic balance. This balance uses magnetic force to achieve balance. It has the advantage of speed and convenience of operation. On one side of the balance we have a movable counterweight M_c which can be initially adjusted to put the system in balance. Ordinarily one would adjust its moment arm to precisely balance the system. Here we leave a slight unbalance so that the automatic system will always react in one direction initially. For purpose of clarity we take the small initial unbalance of the system as being M_c, however this will subtract out subsequently as seen below. The force generated by the magnetic balancing system is considered to be an equivalant mass M_a (or apparent mass), and is the reading of the automatic balance. Here we have

$$M_a + M_{cg} = M_{rg} + M_{hg} + M_{b\ell}. \tag{5}$$

CRYOGENIC FLUIDS DENSITY REFERENCE SYSTEM

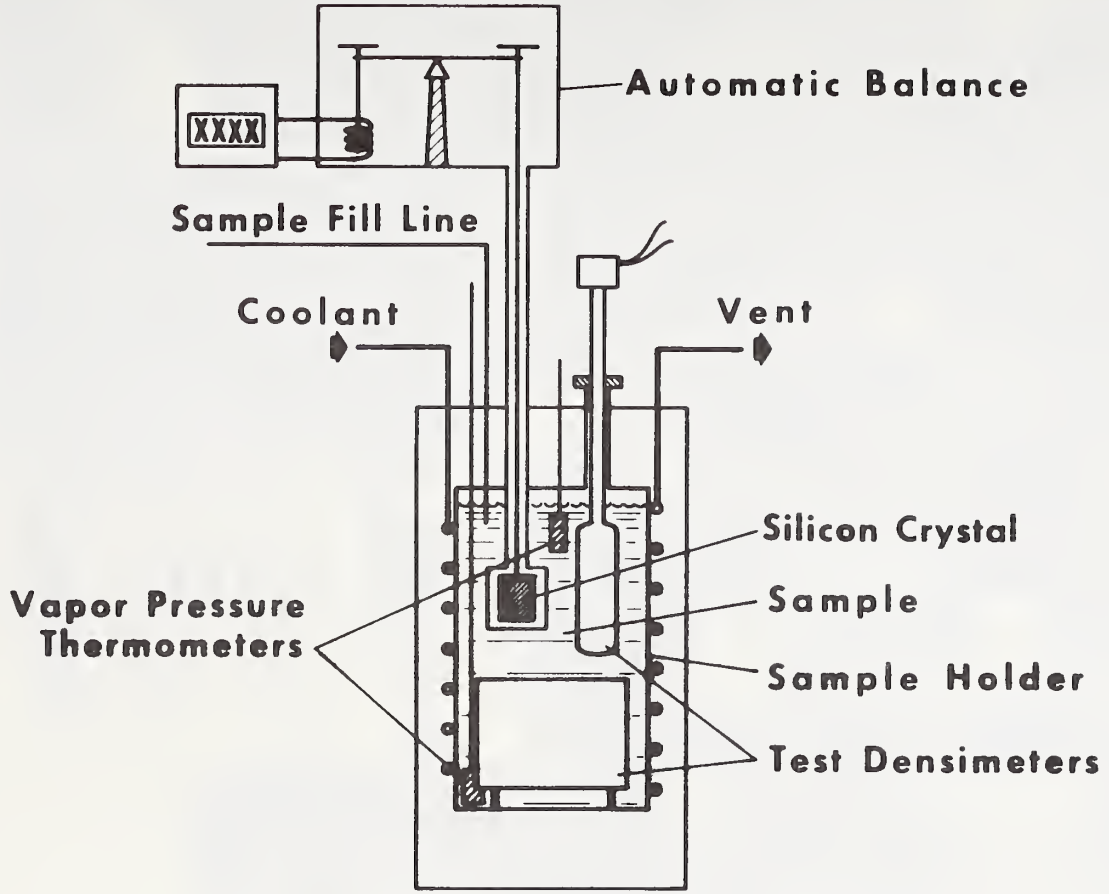

Figure 1.

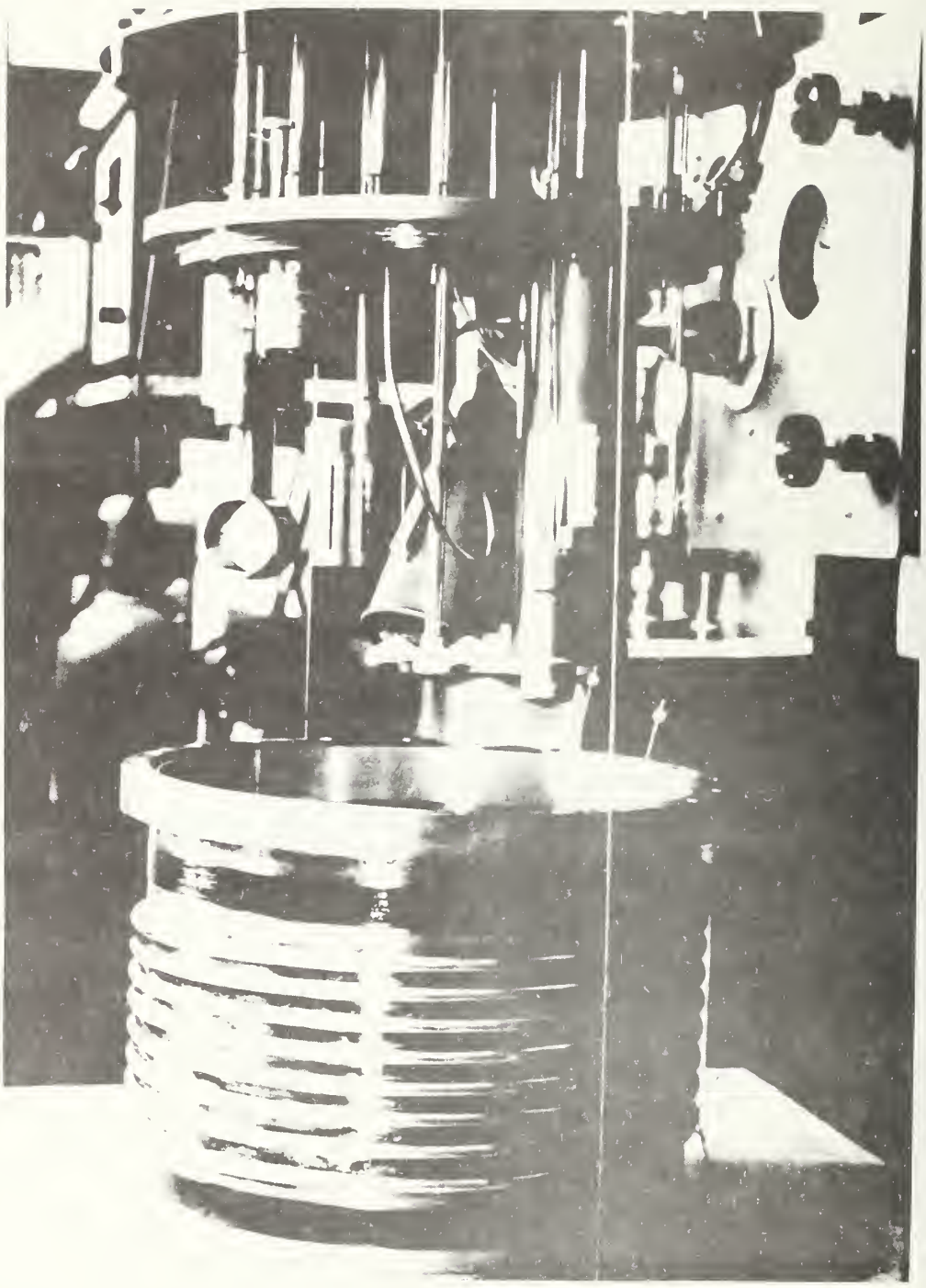

Figure 2. Density Reference System showing small sample holder.

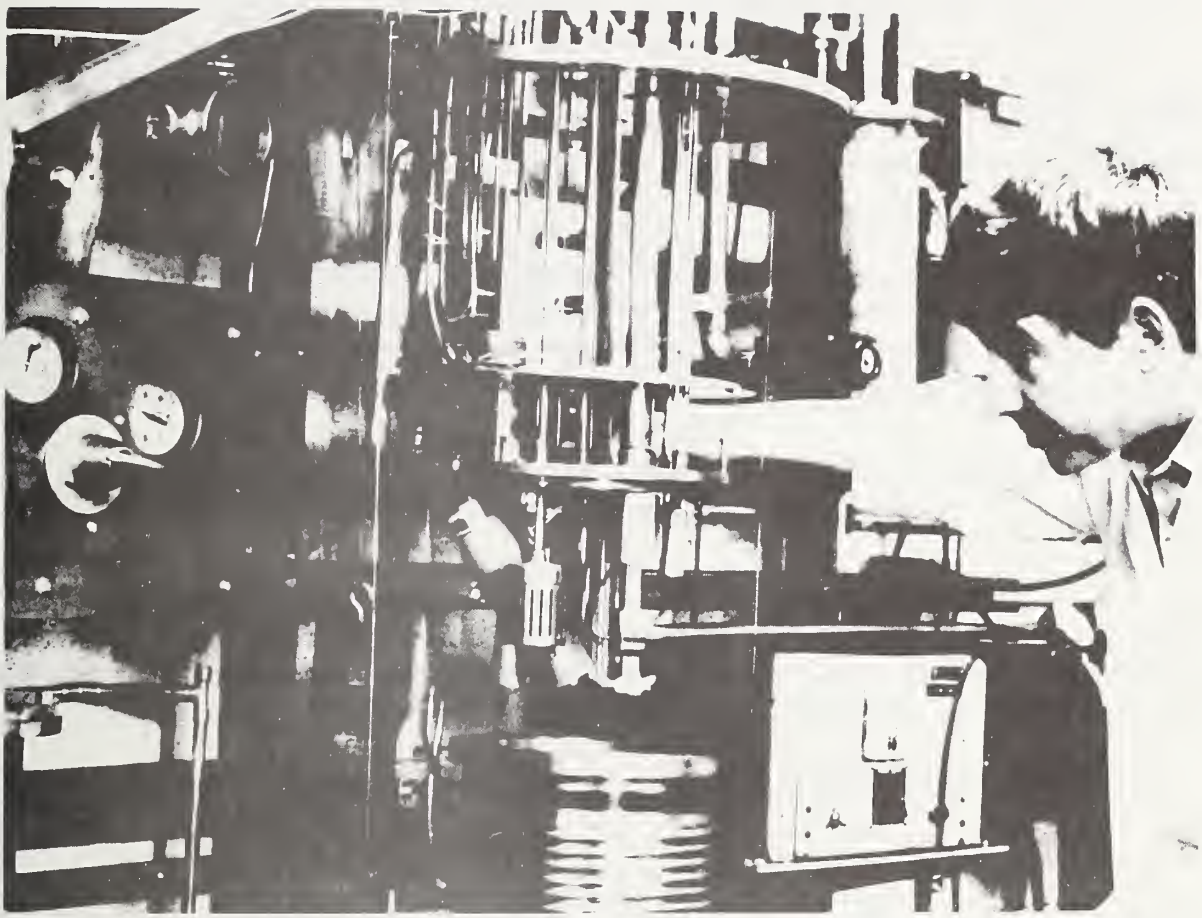

Figure 3. Partially disassembled Density Reference System.

Notice that M_c is now M_{cg}, as we have a buoyant effect of the gas pushing upwards on the masses in the gas.

The value of M_r was chosen for a given M_h and M_s to be large enough to give a reading on-scale (0 to 20 grams) for the automatic balance for the range of densities of LNG under consideration. When more dense liquids were measured, for example liquid argon, a heavier range weight was used.

Zeroing the balance.

Experience with the balance showed that the zero would change although the calibration did not. In order to zero the balance the silicon crystal and its wire hanger and brass support piece were lifted off manually via a mechanical contrivance that could be operated outside the enclosure through a sliding vacuum seal.

This decrease in weight was compensated for by placing the weight M_w on the balance pan, again with a mechanical device such that

$$M_{ao} + M_{cg} = M_{rg} + M_{wg} \tag{6}$$

where M_{ao} is the zero reading of the balance. Here the range weight is still on the pan as before. Since this measurement occurs just before the measurement described by equation (5) then we may subtract out M_{cg} and M_{rg} giving

$$M_a - M_{ao} = M_{hg} + M_{b\ell} - M_{wg}$$

or

$$\Delta M_a = M_{hg} + M_{b\ell} - M_{wg}. \tag{7}$$

Calibration of the balance.

The linearity was verified using a procedure recommmended by the Statistical Engineering Laboratory of NBS. See appendix 8.5. A continual check of the calibration was performed using a 10 gram weight. Provision was made for lowering this calibration weight onto the balance pan by a thermally actuated bi-metallic strip. This allowed a very gentle and precise method of placing this weight onto the balance pan.

The calibration was checked under the zero check procedure. Immediately after checking the zero, as described by equation (6), the calibration weight, M_k, was placed on the balance pan so that the apparent mass (the M_{ao} in equation (6)) is now M_{ak},

$$M_{ak} + M_{cg} = M_{rg} + M_{wg} + M_{kg}. \tag{7a}$$

Subtracting equation (6) from (7a),

$$M_{ak} - M_{ao} = M_{kg}. \tag{7b}$$

As long as equation (7b) holds, no adjustment was needed for the balance. In practice it was found that adjustment of the balance was rarely needed.

The measurement equation.

As in equation (4), the final measurement equation can be put in the form

$$\rho = \rho_s(1 - f(M_1,M_2,\ldots\rho_1,\rho_2\ldots)) \tag{8}$$

where the independent variables are all known. In actual practice the hanger M_h, consisted of a brass part (M_1,ρ_1) and a stainless steel wire suspended from this brass hanger (M_2,ρ_2). However, part of the stainless steel wire was immersed in the liquid. The part in the gas is $M_2 - M_3$ and the part in the liquid is M_3. Therefore,

$$M_h = M_1 + M_2 - M_3 \tag{9}$$

and,

$$M_{hg} = (M_1 + M_2 - M_3) - \rho_g \left(\frac{M_1}{\rho_1} + \frac{M_2 - M_3}{\rho_2}\right) . \tag{10}$$

Also the mass M_b breaks down into

$$M_b = M_s + M_3 + M_4,$$

where M_4 is a short length of tungsten wire (M_4,ρ_4) wrapped around the silicon crystal (M_b,ρ_s) so we have

$$M_{b\ell} = M_s + M_3 + M_4 - \rho \left(\frac{M_s}{\rho_s} + \frac{M_3}{\rho_2} + \frac{M_4}{\rho_4}\right) . \tag{11}$$

Putting these relations into equation (7)

$$\Delta M_a = M_1 + M_2 - M_3 - \rho_g \left(\frac{M_1}{\rho_1} + \frac{M_2 - M_3}{\rho_2}\right)$$

$$+ M_s + M_3 + M_4 - \rho \left(\frac{M_s}{\rho_s} + \frac{M_3}{\rho_2} + \frac{M_4}{\rho_4}\right) - M_w + \rho_g \frac{M_w}{\rho_1} \tag{12}$$

$$\rho = \frac{M_s + M_1 + M_2 + M_4 - M_w - \Delta M_a - \rho_g [(M_1 - M_w)/\rho_1 + (M_2 - M_3)/\rho_2]}{(M_s/\rho_s + M_3/\rho_2 + M_4/\rho_4)} \tag{13}$$

the form of equation (8) may be obtained by factoring out ρ_s and M_b to obtain

$$\rho = \rho_s \frac{1 + \dfrac{M_1 + M_2 + M_4 - M_w - \Delta M_a}{M_s} - \dfrac{\rho_g}{M_s} [(M_1 - M_w)/\rho_1 + (M_2 - M_3)/\rho_2]}{\left(1 + \dfrac{M_3}{M_s}\dfrac{\rho_s}{\rho_2} + \dfrac{M_4}{M_s}\dfrac{\rho_s}{\rho_4}\right)} . \tag{14}$$

The following are the measured values of the masses used in equation (13). Literature values of the densities were used, the possible effect this could have on measurement accuracy is discussed below.

M_s = 127.4330 g, ρ_s = 2.33078 g/cm^3		the silicon crystal.
M_1 = 4.2441 g, ρ_1 = 8.5 g/cm^3		the brass hanger.
M_2 = 0.2121 g, ρ_2 = 7.9 g/cm^3		the stainless steel suspension wire.
M_3 = 0.026 g		stainless steel suspension wire submerged in liquid.
M_4 = 0.055 g, ρ_4 = 18.8 g/cm^3		the tungsten wire tied about the silicon crystal.
M_w = 100.9296 g		the brass replacement weight.

The denominator of equation (13), $M_s/\rho_s + M_3/\rho_2 + M_4/\rho_4$ is the total volume of the submerged material. From the above it is

$$V = 54.674 + 0.00329 + 0.00293 \text{ cm}^3$$

$$V = 54.680 \text{ cm}^3.$$

The total equation (13) becomes

$$\rho = \frac{31.0146 - \Delta M_a + \rho_g(11.351)}{54.6802} \text{ g/cm}^3 .$$

The value for the silicon mass is an average of several weighings in air, corrected to weight in vacuum. (See appendix 8.2, page 23).

The density of silicon of 2.33078 g/cm^3 has been corrected for thermal contraction to LNG temperatures (appendix 8.3) from the literature values (appendix 8.1). Pressure dependence of ρ_s is negligible (appendix 8.1).

2.2. Pressure

The system pressure was measured using a quartz-spiral bourdon tube. During the first series of measurements (data taken before December 1975), the system used a 500 psi* gage, the data after that used a 200 psi gage. The calibration of all pressure gages used was checked at this laboratory using an air-dead weight gage, which is accurate to 0.015%, with the accuracy traceable to NBS. Pressure uncertainty was found to be within the 0.015% of full scale pressure specified by the manufacturer.

2.3. Temperature

Temperature was measured using vapor pressure thermometers. One thermometer bulb was located at the bottom of the sample volume and the other near the top. Each thermometer contains about 5 cm^3 of liquid methane. Pressure

* 1 psi = 6.895 k Pa.

communicates from the thermometers to a quartz-spiral bourdon tube (100 psi maximum) via 1/16" O.D. stainless capillary tubing. The temperature range was 100 K to 140 K. Sensitivity and precision of this device is the same as specified for the gages in section 2.2. This pressure uncertainty is equivalent to 0.03 K at 100 K and 0.003 K at 140 K for the 100 psi gage used to measure vapor pressure.

Temperature gradients as measured by the vapor pressure thermometers were generally 0.030 K and on rare occasions approached 0.3 K. The density difference resulting from this temperature difference can be calculated by using methane properties [3,4]. Here we can use the dimensionless derivative $d\ell n\rho/d\ell nT$ at saturation:

Average System Temperature	$d\ell n\rho/d\ell nT$	$\frac{\Delta\rho}{\rho}$ for $\Delta T = 0.03$ K
110 K	0.38	0.0038%
140 K	0.26	0.0026%

In the worst instance the difference was only 0.04%. The densimeters under test were actually physically closer to the DRS density probe (the silicon crystal) than were the two vapor pressure thermometers, implying a lower density difference.

2.4. Composition

When mixtures were used for the density measurements, the compositions (mole fractions) were determined by accurate measurement of the mass of the separate constituents and subsequently applying corrections for the effect of gas phase to the total system composition to obtain liquid phase compositions.

The samples were weighed in metal cylinders. After transfer to the DRS cryostat, the cylinders were again weighed and the amount transferred computed from the difference.

The balance used for this purpose is a high-resolution and high-capacity balance (resolution better than 0.01 g, with maximum capacity of 20 kg). Class S weights were used (see appendix 8.4).

Upon condensation in the cryostat the sample separates into a liquid and gas phase. The volume of the gas phase was two to four times the volume of the liquid. The large volume of the gas phase was required to house the automatic balance used in weighing the silicon crystal which measured the liquid density.

The composition of the liquid phase was calculated from the total composition by subtracting the amount of the vapor phase. The total composition is that computed from the amounts of sample gas transferred into the system. If the composition of the gas and liquid phase were the same, then the liquid composition would be the same as the total composition.

For mixtures of methane with ethane, propane and butane the vapor phase was assumed to be methane. The vapor phase densities in the balance volume sample chamber and interconnecting tube are computed from a virial equation of state [3] using the system pressure and temperatures. The calculated quantities of methane are then subtracted from the total amount of methane in the system and the result is used to compute the liquid phase composition.

For mixtures with nitrogen, the vapor phase is assumed to be methane and nitrogen. The densities of the vapor phase were computed from a mixture virial equation which included terms to the second virial coefficient. Since this equation used the mixture second virial coefficient, it was computed from the second virial coefficients of the pure components and the interaction second virial coefficient for the mixture, as well as the vapor phase compositions. The vapor phase compositions were estimated from phase-equilibria data for methane-nitrogen of this laboratory [5] using enhancement factors. The resulting computation of vapor densities allows a first estimate of the amount of nitrogen and methane in the vapor phase. From this, a corresponding first estimate of the liquid phase composition is made. The estimate is improved by iterating the computation using the results of the preceding evaluation.

In the instance of a binary mixture the composition could be computed from another approach. Dielectric constant density measurements of the liquid and with the assumption that the polarizability of the methane-nitrogen mixture could be computed from ideal mixing, allows one to compute the mole fraction of the binary mixture. Agreement between the calculation described in the above paragraphs and the dielectric constant calculation was found to be about 0.2 to 0.4 mole percent when the nitrogen composition was less than 2 mole percent.

Because of the additional uncertainties of mixtures discussed above, only pure methane results were used in the random error determination.

3. MEASUREMENT PROCESS PARAMETERS

3.1. Bounds for Systematic Errors

A listing of the primary sources of uncertainty in density measurement can be obtained from examination of the measurement equation. If one has knowledge of the basic uncertainties of the separately measured quantities such as the masses and densities, then these can be combined to give an estimate of the systematic errors in the density as measured by the density reference system.

However, until experimental evidence of the actual effect is obtained by introducing an offset in these factors, both singly and jointly, this analysis is just that, an estimate of undemonstrated validity.

Equation (13), the measurement equation, has the density ρ as a function of several independent variables.

$$\rho = \rho(M_s, M_1, M_2, M_3, M_4, M_w, \Delta M_a, \rho_s, \rho_1, \rho_2, \rho_4) \quad . \tag{15}$$

The uncertainty in ρ, arising from uncertainty in ρ_s, for example, can be evaluated from

$$\delta\rho = \frac{\delta\rho}{\delta\rho_s}\,\delta\rho_s \tag{16}$$

or as a dimensionless ratio,

$$\frac{\delta\rho}{\rho} = \frac{\partial \ell n \rho}{\partial \ell n \rho_s}\,\frac{\delta\rho_s}{\rho_s} \quad , \tag{17}$$

which has the advantage of expressing the independent and dependent variables as dimensionless ratios. The total uncertainty in density is the square root of the sum of the squares of the various contributions.

$$\frac{\delta\rho}{\rho} = \sum \left(\frac{\partial \ell n \rho}{\partial \ell n x_i}\,\frac{\delta x_i}{x_i}\right)^2 \quad ^{1/2} \quad . \tag{18}$$

This is the propagation of error relationship for systematic error [6] when the variables are independent and the magnitudes of the relative errors are small so that second order terms are negligible.

Table 1 is a summary of the most significant contributions to the total systematic uncertainty in density as estimated from the various contributing sources. The first column, labelled x identifies the variable for which the uncertainty is calculated. The second column is the total logarithmic partial derivative of the liquid density with respect to the variable of the first column. The column labelled $\delta x/x$ is the ratio of the estimated worst possible uncertainty of that variable.

The systematic error, $\delta x/x$, due to mass determinations is estimated from the uncertainty generated by the balance and weights used to determine the masses. The estimate of the systematic error of the apparent mass is the uncertainty of the electronic balance reading as specified by the manufacturer. Linearity measurements (appendix 8.5) indicate this number is conservative. The error estimate of the silicon crystal density covers uncertainties due to the temperature and pressure effects (appendix 8.1) as well as uncertainties in published densities (appendix 8.3). The metal density uncertainties of which M_w is the dominant term are estimated from volume and weight. The gas density is required for bouyancy corrections, contains all gas pressure, temperature and composition uncertainties and is the leading systematic error for mixtures containing LN_2. The uncertainties due to temperature gradients is discussed in section 2.3. An additional systematic error results from the uncertainty in the absolute value of T. This is not included in the table since it makes no contribution to the systematic error when densimeters are

being compared. When density measurements are being compared with those of other workers, however, there is an 0.01% maximum contribution to the systematic error at the lowest temperature that decreases to less than 0.001% at the highest temperatures.

Table 1. Systematic errors.

Variable, x	$\partial \ell\rho/\partial \ell nx$	$\delta x/x$	$\delta\rho/\rho$ in %
silicon crystal mass	$(\rho_s - \rho)M_s/\rho\rho_s V$ 3.9	1.6×10^{-5}	$\pm$ 0.0062
brass hanger mass	$(\rho_1 - \rho_g)M_1/\rho\rho_1 V$..1.8 x 10^{-1}	2.4×10^{-4}	$\pm$ 0.0043
steel wire mass	$(\rho_2 - \rho_g)M_2/\rho\rho_2 V$..8.9 x 10^{-4}	4.7×10^{-3}	$\pm$ 0.00042
steel wire mass in liquid	$(\rho - \rho_g)M_3/\rho\rho_2 V$...6.0 x 10^{-5}	3.8×10^{-4}	--
tungsten wire mass	$(\rho_4 - \rho_g)M_4/\rho\rho_4 V$..5.4 x 10^{-5}	1.8×10^{-2}	--
apparent mass	$\Delta M_a/\rho V$.....	1.0×10^{-4}	$\pm$ 0.010
silicon density	$M_s/\rho_s V$.....	1.6×10^{-5}	$\pm$ 0.0016
metal densities	$(M_1 - M_w)\rho_g/\rho_1\rho V$..2.0 x 10^{-3}	2.3×10^{-2}	$\pm$ 0.0046
gas density	$\rho_g((M_1 - M_w)/\rho_1 +$ $(M_2 - M_3)/\rho_2)/\rho V$..2.2 x 10^{-3}	1.0×10^{-1}*	$\pm$ 0.022
temperature gradient	$d\ell n\rho/d\ell nT$.....3.8 x 10^{-1}	1.0×10^{-4}	$\pm$ 0.0038

Total, from equation (18) ... $\pm$ 0.026%.

*The large uncertainty for gas density results from the large uncertainty of the methane-nitrogen vapor densities. The uncertainty due to gas density is only 0.002% for methane and the total from equation (18) is $\pm$ 0.014%.

Some of the systematic errors listed above will be eliminated in future measurements. By moving the point the silicon float disconnects from the balance down into the liquid such that the float disconnects from all suspension hardware, all systematic errors associated with the brass hanger and the steel and tungsten hanger wires will be eliminated. The uncertainty of the silicon mass was determined from the uncertainty of the measuring weights and the density uncertainty comes from literature values of the density. The uncertainty in apparent mass is due to the balance and has been determined experimentally (see appendix 8.2). The temperature gradient was measured to determine that uncertainty. Only the uncertainty due to the density of the replacement weight and the gas density correction has yet to be examined experimentally. This can be done by using a more dense mass for the replacement weight. However, any effect due to changing

this weight should be very small compared to the random error. If any change in the estimated systematic error is warranted after experimentally checking for replacement weight buoyancy effects, this correction will be made in the updated uncertainty statements.

3.2. Random Error from Measurements on Methane

The random error of the density reference system was determined experimentally by measurements on liquid methane.

Density measurements on pure methane were compared to densities computed from the Haynes-Hiza relation for density versus temperature for saturated liquid methane [4]. The vapor pressure measurements were converted to temperature [3] and the resulting temperature converted to densities as described.

The present estimates of the precision for density determinations made using the DRS are based on measurements of the density of eight different samples (fillings) of liquid methane. For the eight samples there was a total of seventy-one density measurements of saturated methane in the temperature range 100 K to 140 K -- for the last four samples the temperatures were 110 K, 125 K, and 140 K.

The model used to analyze the methane data is

$$y_{(T)ij} - H_{(T)} = \mu_{(T)} + \alpha_i + e_{ij}$$

where $y_{(T)ij}$ is the jth density determination by the DRS on the ith methane sample for temperature T; $H_{(T)}$ is the corresponding density value derived from the Haynes-Hiza relationship, $\mu_{(T)}$ represents the long term relative bias, α_i is the random contribution to all measurements made using the ith sample, and e_{ij} is the random contribution to the jth measurement made on the ith sample. The standard deviation (SD) for the α_i is called the between sample SD, and the SD for the e_{ij} is called the within sample SD. The SD of measurements $y_{(T)ij}$ is the square root of the sum of the squares of these two SD.

There were seventy-one least squares estimates of the e_{ij} for the liquid methane measurements. The variability among the estimate samples -- the last twenty-two, e.g. -- is less than among the preceeding forty-nine. The point estimate for the within SD for the first six samples is $\pm$ 0.074% (using 400 kg/m^3 as reference) and that for the last two is $\pm$ 0.034%. The corresponding 99% confidence intervals are (0.057, 0.101) and (0.024, 0.055). This change in variability is attributed to the cleaning of the knife edges on the DRS's balance. The point estimate for the between samples SD for the eight samples is $\pm$ 0.052%, a 99% confidence interval is (0.029, 0.13). The cleaning of the knife edges has not effected this component of the variability. The estimated SD for a single measurement made on the DRS

previous to the cleaning of the balance is ± 0.090%. For measurements made after that time the SD is estimated to be ± 0.062%.

Only the within SD's after the knife edges were cleaned are taken to correctly reflect the precision of the within sample density measurements. A comparison of these data with the Haynes-Hiza densities is shown in Figure 4 as well as a comparison to the work of Goodwin [3].

For the methane data the DRS measurements of density shows a bias with the Haynes-Hiza relationship which is a linear function of density. For a density of 0.38 g/cc the bias is -0.062% with an estimated SD of 0.021%; a 99% confidence interval is (-0.12%, -0.006%). For a density of 0.43 g/cc the bias is -0.11% with an estimated SD of 0.018%; a 99% confidence interval is (-0.16%, -0.062%).

Figure 5 shows a comparison of densities for two samples of liquid argon as measured by the density reference system to those measured by the Haynes-Hiza apparatus, as well as other laboratories as indicated in the caption. As can be seen in this figure, the agreement with Haynes and Hiza is generally within 0.1%.

3.3. Uncertainty Statement

While the use of three times the estimated SD is commonly used in reporting the limits of random error, because of the small number of observations (eight) relating to the sample-to-sample error, the limits using 3 x 0.062% will provide a 98% confidence interval rather than one of 99%. When the samples of liquid methane measured by the DRS exceed fifteen, the use of the factor 3 will give confidence intervals of better than 99%. The limit of possible sources of systematic error has been judged to be ± 0.026% (see section 3). This systematic limit of 0.026% plus 3 x 0.062% gives the present estimated limit of total uncertainty for a single density measurement made on the DRS as ± 0.21%.

4. MEASUREMENT PROCESS CONTROL

As future measurements are made, the random errors will be continually checked and the systematic error estimates will be confirmed experimentally or the error source eliminated where possible as described below.

Each time a set of density reference measurements are made using the system, measurements on at least two separate fillings of pure liquid methane will be included in the tests. Density measurements will be made at temperatures around 110 K, 125 K, 130 K and 140 K. Three measurements will be made at each temperature in random order. The remeasured methane densities can be compared to the Haynes-Hiza results and to the earlier reference system measurements to determine whether the system has shifted. This reliability of the system will be checked only in conjunction with density comparison

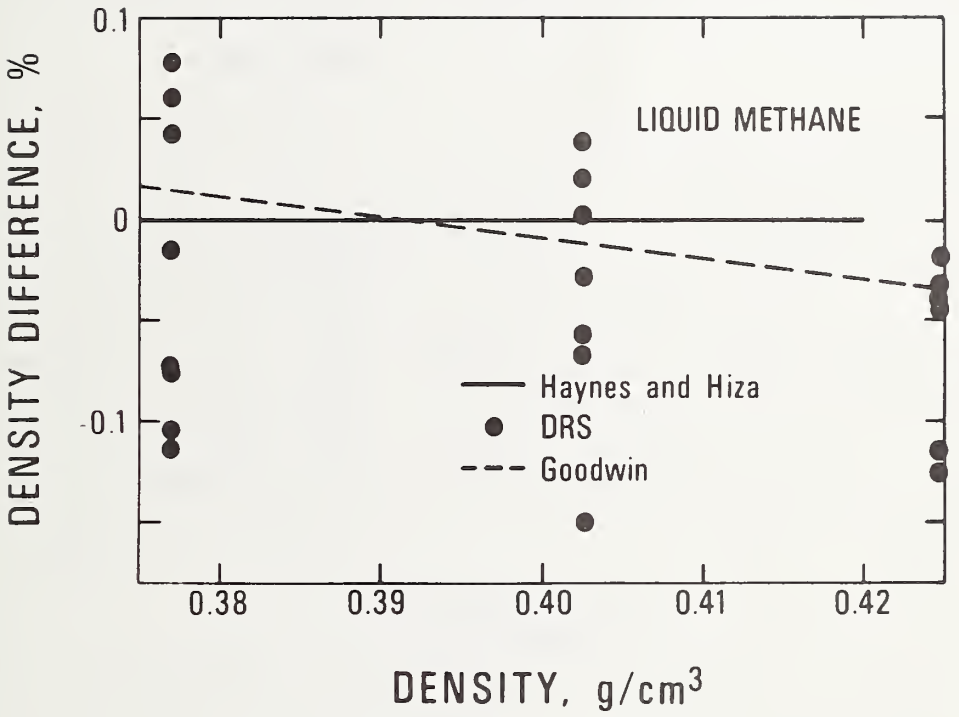

Figure 4. Liquid methane density results of this work relative to the work of Haynes, et al.[4]. The data are the 22 points taken after the knife edges were cleaned.

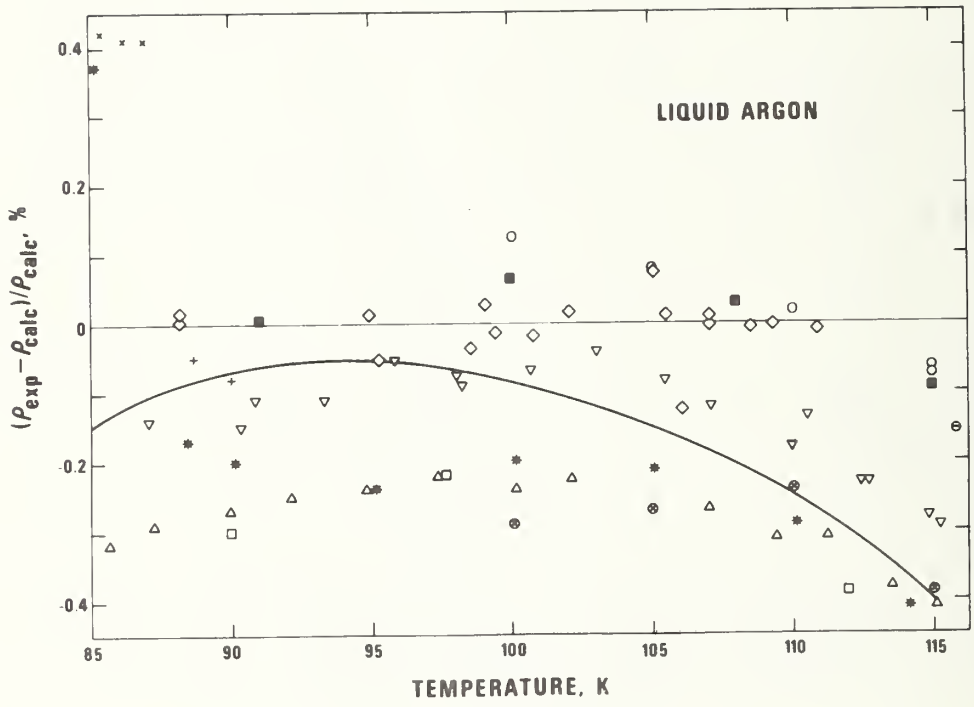

Figure 5. Liquid argon densities of other workers compared to a least squares fit to this work.

- ◇ Younglove, this work.
- ○ Haynes and Hiza [9].
- ⊖ Chui and Canfield [10].
- \+ Van Itterbeek and Verbeke [11].
- △ Terry, et al. [12].
- — Gosman, et al. [13].
- ■ Pan, et al. [14].
- ▽ Goldman and Serase [15].
- × Saji and Kobayashi [16].
- □ Mathias, et al. [17].
- ⊛ Street and Staveley [18].
- ✱ Dobrovolskii and Golubev [19].

work rather than periodically because of the expense of making density measurements.

For these occasions the within SD's will be compared statistically to those of previous occasions for any change in this measure of precision, and the occasion-to-occasion shifts, α_i (see 3.2), will be tested for any change in their variability or for signs of non-random behavior (e.g., drifting). If there is no apparent change, the data from previous occasions will be combined with the new data to obtain updated estimates. Any statistically verifiable changes in the DRS process will call for corrective action with respect to the process. A revised uncertainty statement will be presented as further calibration measurements are completed.

5. SUMMARY

The density reference system of the National Bureau of Standards, Cryogenics Division is described. Since the density determination by the DRS is basically a weighing process, the details of calculation of this process are described in detail. The procedure for determining the density from weighing, zeroing and calibrating the balance is discussed.

The uncertainty of the density reference system is $\pm$ 0.21%. The contribution from the estimated systematic error in density was $\pm$ 0.026%. The estimated uncertainty caused by random error is three times the standard deviation of $\pm$ 0.062% and is based on the measurements of the densities [4] of liquid methane taken on eight samples and on 22 independent measurements. The total density uncertainty was taken to be the sum of the systematic and random errors.

6. ACKNOWLEDGEMENTS

Special acknowledgement is given to John LaBrecque of the NBS Statistical Engineering Laboratory for the considerable help and advice given this project during its various phases. Acknowledgement is also given to Janet Donaldson of the same group for her recommendations on the method of acquiring data from the automatic balance.

Jim Holste contributed very heavily in the construction and start up phase of this project. He designed and built several important features of the DRS.

7. REFERENCES

[1] Bowman, H. A., Schoonover, R. M., and Jones, M. V., Procedure for high precision density determinations by hydrostatic weighing, J. of Research, NBS C, 71C, 178 (1967).

[2] Henins, I., and Bearden, J. A., Silicon crystal determination of the absolute scale of x-ray wavelengths, Phys. Rev. 135, A890 (1964).

[3] Goodwin, R. D., The thermophysical properties of methane, from 90 to 500 K at pressures to 700 bar, NBS Tech. Note 653, Apr. 1974.

[4] Haynes, W. M., Hiza, M. J., and Frederick, N. V., A magnetic suspension densimeter for measurements on fluids of cryogenic interest, to be submitted to Review of Scientific Instruments.

[5] Parrish, W. R. and Hiza, M. J., Liquid-vapor equilibria in the nitrogen-methane system between 95 and 120 K, Advances in Cryogenic Engineering (Proc. 1973 CEC), Vol. 19 (Plenum Press, NY, 1974).

[6] Cook, N. H. and Rabinowicz, E., Physical Measurement and Analysis, Addison-Wesley Publishing Co., Inc., 1963.

[7] McSkimmin, H. J., J. Appl. Phys. 24, 988 (1953).

[8] Corruccini, R. J. and Gniewek, J. J., Thermal expansion of technical solids at low temperatures, Nat. Bur. of Stand. (U.S.) Monograph 27, May 1961.

[9] Private communication.

[10] Chui, C. and Canfield, F. B., Trans. Faraday Soc. 67, 2933 (1971).

[11] Van Itterbeek, A., Verbeke, O., and Staes, K., Physica 29, 742 (1963).

[12] Terry, M. J., Lynch, J. T., Bunclark, M., Mansell, K. R., and Stavely, L. A. K., J. Chem. Thermodyn. 1, 413 (1969).

[13] Gosman, A. L., McCarty, R. D., and Hust, J. G., Thermodynamic properties of argon from the triple point to 300 K at pressures to 1000 atmospheres. NSRDS-NBS 27 (1969).

[14] Pan, W. P., Mady, M. H. and Miller, R. C., AIChE J. 21, 283 (1975).

[15] Goldman, K. and Scrase, N. G., Physica 45, 1 (1969).

[16] Saji, Y. and Kobayashi, S., Cryogenics 4, 136 (1964).

[17] Mathias, E., Onnes, H. K., and Crommelin, C. A., Ann. Phys. 17, 442 (1922).

[18] Street, W. B. and Staveley, L. A. K., J. Chem. Phys. 50, 2302 (1969).

[19] Dobrovolskii, O. A., and Golubev, I. F., Tr. Nauch.-Issled. Proekt. Inst. Azion. Prom. Prod. Org. Sin. 8, 14 (1971).

8. APPENDICES

8.1. The Change in Volume of the Silicon Crystal from Hydrostatic Compression and Temperature

The buoyant force of the liquid on the silicon crystal will be reduced by the effect of its volume being decreased by hydrostatic compression. This is described by

$$V = V_o(1 - kP)$$

where V_o is the volume at the reference pressure, in this case about one atmosphere or one bar. P would be the pressure in excess of this and k the compressibility;

$$k = -\frac{1}{v}\frac{\partial v}{\partial P}\Big)_t .$$

This correction was found to be negligible since $k = 1.01 \times 10^{-6}$ bar^{-1} and at 110 K and $P \simeq 6$ bar, $\frac{\Delta v}{v} = 6 \times 10^{-6}$. In this case k was computed from silicon data on velocity of sound by McSkimmin [7] using the usual relations for bulk modulus and elastic constants as evaluated from sound velocities.

The change in volume was computed from the thermal contraction of silicon values from Corruccini and Gniewek [8]. We have

$$\frac{L_{298} - L_T}{L_{298}} = 25.5 \times 10^{-5}$$

for the change from 298 K to 100 K. This value is essentially unchanged over the temperature interval 100 K to 140 K.

$$\frac{\Delta v}{v} = 3\frac{\Delta L}{L} ,$$

$$\rho_s = 232.90\ (1.000765)\ \text{kg/m}^3$$

$$\rho_s = 233.08\ \text{kg/m}^3.$$

8.2. Silicon Crystal Weighings in Air

Date	Silicon Weight in Air gram	Temperature Celsius	Pressure mm Hg	Silicon Weight in Vacuum gram
01-10-74	127.3947	21	633	127.4335
01-15-74	127.3950	20	631	127.4339
01-27-74	127.3941	20	625	127.4335
02-28-74	127.3945	21	620	127.4334
04-02-74	127.3926	21	628	127.4320
04-05-74	127.3941	20	630	127.4338
10-27-74	127.3930	23	625	127.4319
10-28-75	127.3927	21	620	127.4316
			Average	127.4330 ± 0.0003 std. dev.

8.3. Densities of Single-Crystal Silicon

Densities of Silicon	Temperature	Preparation	Std. Deviation, 1σ
2.328932*	22-27°C	Grown in Vacuum	1 ppm
2.329021*	22-27°C	Grown in Argon	1 ppm
2.32904**	25°C	Not known	± 9 ppm

* Each are average of 12 measurements, Bowman, Schoonover, and Jones [1].

** An average of about 75 measurements, Henins and Bearden [2]. Reference density for silicon was taken to be 2.3290 at 25°C.

A 14 g portion of the same crystal was weighed in water and in air. Using averages of four weighings in air and water the density computed at 30 °C was $\rho = 2.3291\ g/cm^3$, as compared to $\rho = 2.3289$ from the above after correction for thermal expansion. This is a difference of about 0.009%.

8.4 Weight certificate

TROEMNER, Inc.
MANUFACTURERS OF PRECISION BALANCES AND WEIGHTS and LABORATORY APPARATUS
6825 GREENWAY AVENUE, PHILADELPHIA, PA. 19142 PHONE 215 SA 4-0800

TRACEABLE CERTIFICATE

Voland Corporation
27 Centre Ave.
New Rochelle, N. Y. 10802

Attn: Robert C. Luce

Order 1695

This is to certify that the weights furnished on your referenced order have been calibrated to Class S of the National Bureau of Standards tolerances under our N.B.S. Certificate No. as follows:

Weight Set 5 kg - 1 g	N.B.S. Certificate No.
5 Kg. 2 kg. 2 kg. 1 kg	232.09/209275 Set A
500 g, 200 g, 200 g, 100 g	232.09/209275 Set A
50 g, 20 g, 20 g, 10 g	232.09/209275 Set A
5 g, 2 g, 2 g, 1 g	232.09/209275 Set A

Dated: March 28, 1974

By: W. D. Abele
Wilbert D. Abele
Vice President and General Manager

STATE OF COLORADO

COLORADO DEPARTMENT OF AGRICULTURE
406 STATE SERVICES BUILDING
1525 SHERMAN STREET
DENVER, COLORADO 80203

June 9, 1976

REPORT OF TEST

OWNER: National Bureau of Standards
Cryogenic Laboratory
Boulder, Colorado

Certification No. 3087

DESCRIPTION: Seven weights from NBS Kit No. 143922

The standards described below have been tested and compared with the standards of the State of Colorado, and have been found to be within the tolerances as prescribed by the National Bureau of Standards for Class S weights. The effect of air bouyancy has been considered negligible.

ITEM	APPARENT MASS CORRECTION	UNCERTAINTY	CLASS S ADJUSTMENT TOLERANCE
20.gram	-0.0080 mg	.022 mg	0.074 mg
20..	+0.016	.022	0.074
10	+0.009	.020	0.074
5	-0.0403	.0134	0.054
2.	+0.0216	.0134	0.054
2..	+0.0431	.0134	0.054
1	+0.0229	.0093	0.054

The uncertainty figure is an expression of the overall uncertainty using three standard deviations as a limit to the effect of random errors of measurement, the magnitude of systematic errors from known sources being negligible.

F H Brzotick, Metrologist
Test completed June 9, 1976
Colorado Department of Agriculture
Metrology Laboratory
3125 Wyandot Street
Denver, Colorado 80211

Baro. Press. 627.0mm
Temp. 23.4°C
Rel. Hum. 45.5%

THESE CERTIFICATIONS ARE TRACEABLE TO THE NATIONAL BUREAU OF STANDARDS.

ALL CERTIFICATION CERTIFICATES ISSUED BY THE COLORADO DEPARTMENT OF AGRICULTURE-WEIGHTS AND MEASURES-FOR STANDARDS HERE LISTED EXPIRE AS INDICATED BELOW:

(a) PRIMARY STANDARDS - Five Years After Date of Certification
(b) OFFICE (OR SECONDARY) STANDARDS - ONE YEAR AFTER DATE OF CERTIFICATION.
(c) Working (or Field) Standards - One Year After Date of Certification

8.5. Linearity Check of the Balance

The linearity of the balance was verified by weighing 1, 2, 2, 5, 10, and 20 g class S weights (see weight certificate in appendix 8.4) in combinations to produce weights of 1, 2, 3, 4, 5, 6, ... 20 g in a random order. These weighings were analyzed by the Statistical Engineering Laboratory of NBS.

Their interpretation was that the residual standard deviation is 0.0008 g based on 37 degrees of freedom. The linearity coefficient was 0.99960.

A summary of these measurements are shown below.

Independent Variable	Dependent Variable	Predicted Values	Standard Deviation of Predicted Values
4.000	4.000	4.001	.20E-03
15.998	15.998	15.998	.19E-03
10.999	10.997	11.000	.12E-03
2.000	2.001	2.001	.24E-03
6.999	7.000	7.000	.16E-03
1.000	1.002	1.001	.26E-03
8.999	9.000	9.000	.14E-03
17.998	17.998	17.999	.22E-03
8.999	9.000	9.000	.14E-03
18.998	18.999	18.998	.24E-03
10.999	11.000	11.000	.13E-03
11.999	11.999	12.000	.14E-03
14.998	14.999	14.999	.17E-03
19.998	18.998	19.998	.26E-03
4.000	4.000	4.000	.20E-03
12.999	12.997	12.999	.15E-03
4.999	5.000	5.001	.19E-03
12.999	12.999	12.999	.15E-03
1.000	1.002	1.001	.26E-03
11.999	12.000	12.000	.14E-03
18.998	18.999	18.998	.24E-03
13.998	14.000	13.999	.16E-03
19.998	19.999	19.998	.26E-03
17.998	17.999	17.999	.22E-03
7.999	8.000	8.000	.15E-03
15.998	15.999	15.999	.19E-03
1.999	2.002	2.001	.24E-03
5.999	6.001	6.000	.17E-03
9.998	10.000	10.000	.13E-03
14.998	15.000	14.999	.17E-03
6.999	7.001	7.000	.16E-03
3.000	3.001	3.000	.22E-03
16.998	17.000	16.999	.20E-03
5.999	6.002	6.000	.17E-03
3.000	3.001	3.001	.22E-03
9.999	10.000	10.000	.13E-03
16.998	16.999	16.999	.20E-03
7.999	8.001	8.000	.15E-03
13.998	13.998	13.999	.16E-03
4.999	5.000	5.001	.19E-03

NBS-114A (REV. 7-73)

U.S. DEPT. OF COMM. BIBLIOGRAPHIC DATA SHEET	1. PUBLICATION OR REPORT NO. NBSIR 77-852	2. Gov't Accession No.	3. Recipient's Accession No.

4. TITLE AND SUBTITLE

CRYOGENIC FLUIDS DENSITY REFERENCE SYSTEM: PROVISIONAL ACCURACY STATEMENT

5. Publication Date: January 1977

6. Performing Organization Code: 275.08

7. AUTHOR(S)

B. A. Younglove and J. D. Siegwarth

8. Performing Organ. Report No.

9. PERFORMING ORGANIZATION NAME AND ADDRESS

NATIONAL BUREAU OF STANDARDS
DEPARTMENT OF COMMERCE
WASHINGTON, D.C. 20234

10. Project/Task/Work Unit No.: 2750161

11. Contract/Grant No.

12. Sponsoring Organization Name and Complete Address (*Street, City, State, ZIP*)

American Gas Association, Inc.
1515 Wilson Boulevard
Arlington, Virginia 22209

13. Type of Report & Period Covered

14. Sponsoring Agency Code

15. SUPPLEMENTARY NOTES

16. ABSTRACT (*A 200-word or less factual summary of most significant information. If document includes a significant bibliography or literature survey, mention it here.*)

The measurement capability of the density reference system (DRS) of the National Bureau of Standards, Cryogenics Division, is described. This system measures density, pressure, and temperature of LNG mixtures for the purpose of testing densimeters which are contained in the liquid sample. Sample composition is determined by weighing the gas samples separately before condensing them into the sample. The DRS measures density by weighing a single-crystal of silicon immersed in the LNG mixture. This process is described and the equations used in the computation of density are discussed.

At this time the estimate of sample standard deviation for a single density measurement made on this system is $\pm$ 0.062% (at 0.4 g/cc). Using three times this standard deviation as a limit for random error and adding $\pm$ 0.026% as an upper bound for known sources of possible systematic error, the uncertainty of a single determination by this system is $\pm$ 0.21%. This statement of accuracy applies for the density range 380 to 430 kg/m^3 and 1200 to 1400 kg/m^3, pressures to 7 bar, and temperatures from 80K to 140 K. This statement is expected to be correct in the intermediate density range and for all temperatures up to 300 K.

Measurement uncertainties for temperature, pressure, and composition are discussed. Comparison of measurements for liquid argon densities with the results of other laboratories is given.

17. KEY WORDS (*six to twelve entries; alphabetical order; capitalize only the first letter of the first key word unless a proper name; separated by semicolons*)

Densimeters; density reference system; liquid methane; LNG

18. AVAILABILITY

[X] Unlimited

[ ] For Official Distribution. Do Not Release to NTIS

[ ] Order From Sup. of Doc., U.S. Government Printing Office Washington, D.C. 20402, SD Cat. No. C13

[X] Order From National Technical Information Service (NTIS) Springfield, Virginia 22151

19. SECURITY CLASS (THIS REPORT)	21. NO. OF PAGES
UNCLASSIFIED	30
20. SECURITY CLASS (THIS PAGE)	**22. Price**
UNCLASSIFIED	$4.00

USCOMM-DC 29042-P74

USCOMM - ERL

What's new in LNG measurement methods and instrumentation

Industry supported research programs at National Bureau of Standards provide data on cryogenic metering devices

D. B. Mann, Coordinator of LNG Programs, Cryogenics Division, Institute for Basic Standards, National Bureau of Standards, Boulder, Colo.

Characterization, instrumentation and measurement of liquefied natural gas are the primary objectives of the LNG Program at the National Bureau of Standards (NBS).

Characterization involves the determination of accurate PVT, thermodynamic, electromagnetic and transport properties data for multi-component mixtures of liquefied hydrocarbon gases. Instrumentation and measurement are essential to the safe and economic liquefaction, transport storage and custody transfer of this form of fossil fuel.

Although the main purpose of this article is to report on current progress in instrumentation and measurements, it should be emphasized that basic reference quality property data are fundamental to accurate, precise field measurements for pressure, temperature, density, liquid level and flow.

Data development. The NBS approach to development of thermophysical properties data for LNG has been to concentrate initially on providing accurate wide range data and calculation methods for the pure components. These include methane, ethane, propane, iso and normal butane and nitrogen.

The range of interest is from the triple point conditions to temperatures above ambient at pressures to at least 34,500 kPa (5,000 psi). This work is being carried out primarily in the Properties of Cryogenic Fluids Section under the supervision of D. E. Diller.

Accomplishments to date under an American Gas Association (AGA) funded grant include published reports on comprehensive thermophysical properties data for methane, dielectric constant and polarizability of methane, velocity of sound in methane, specific heats of methane, provisional thermodynamic functions for ethane, dielectric constant of ethane, PVT and vapor pressure measurements on ethane, phase transitions of ethane and a comprehensive accurate equation of state for the thermodynamic properties of fluids.

Related accomplishments funded by NBS and other agencies include publications on refractive index data for methane, viscosity and thermal conductivity equations for methane and saturation densities of liquefied normal butane.

Additional publications influenced by the quality of the data are available and are classic illustrations of the diffusion and widespread use of accurate and precise property data generated as a result of an original AGA grant.

Another NBS project is concerned with prediction of densities of LNG, at or near saturation as a function of pressure, temperature and mixture composition. This project is funded by the LNG Density Project Steering Committee, through a grant administered by the AGA.

Objectives of the project are to mea-

TABLE 1—Densities of liquefied natural gas mixtures
Scope of work on project

- Pure Components
  - Methane
  - Ethane
  - Propane
  - Isobutane
  - n-butane
  - Nitrogen
- Binary Mixtures
  - Methane-Ethane
  - Methane-Propane
  - Methane-Isobutane
  - Methane-n-butane
  - Methane-Nitrogen
  - Ethane-Propane
  - Ethane-Isobutane
  - Ethane-n-butane
  - Ethane-Nitrogen
  - Propane-Isobutane
  - Propane-n-butane
  - Ethane-Nitrogen
- Multicomponent Mixtures
  - Methane-Ethane-Propane
  - Methane-Ethane-Nitrogen
  - Methane-Ethane-Propane-n-butane
  - Methane-Ethane-Propane-Nitrogen
  - Methane-Ethane-Propane-n-butane-Nitrogen
  - Typical LNG Mixtures

O-1

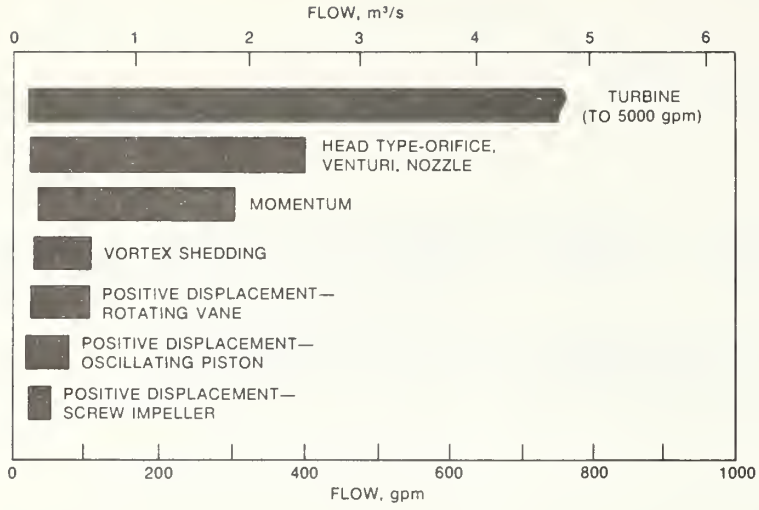

Fig. 1—Flow range of cryogenic flowmeters confirmed by experiment.

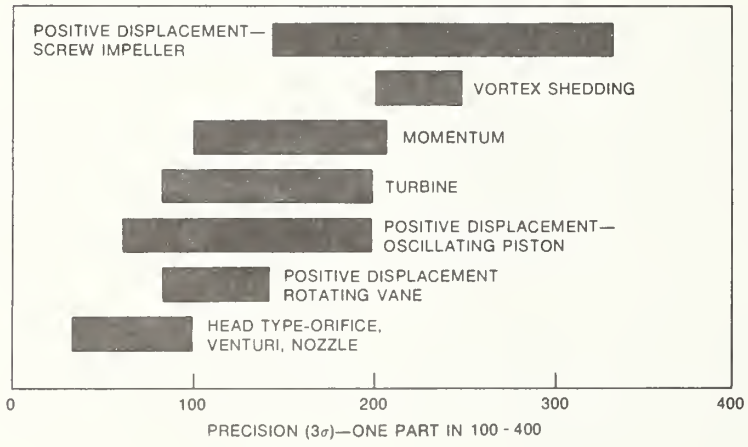

Fig. 2—Precision of flowmeters for cryogenic service based on experimental data.

sure the saturated liquid densities of LNG type mixtures with an inaccuracy and imprecision of less than 0.1 percent and to evaluate and optimize three existing density calculation methods using this experimental data as the measurement base. Table 1 outlines the content and scope of the experimental program.

The approach involves precise measurements of the pure fluid and binary mixture densities throughout a temperature range of 110 to 140 K. Optimization of the correlation methods are then evaluated by comparing calculated densities with precise density measurements for selected multi-component (including LNG type) mixtures. The project is nearing completion, and several reports will be issued describing the methods and results.

The basic properties data required for assessing and proving field-type LNG measurements are becoming available. The following projects dealing with field instruments and measurements are also underway at NBS and rely heavily on these properties data measurements and correlations.

Flow measurements. Within general advances in the state-of-the-art, instrumentation for LNG flow measurements can draw on a well-developed research and field experience of cryogenic industrial gases (liquid nitrogen, argon, oxygen, hydrogen), specifically in the area of small diameter, truck mounted, custody transfer meters. An 8-year joint NBS-industry effort has provided extensive data on the performance of volumetric and mass flow devices, both under well controlled laboratory conditions and in the field.

The program was begun in 1968 as a cooperative effort involving NBS and members of the Compressed Gas Association. Accomplishments include:

- An evaluation of generic classes of flowmetering devices over a broad range of expected operating conditions
- Initial work on establishment of specifications, tolerances and recommended practices for flow devices used in commerce
- Promulgation of transfer standards traceable to NBS for field certification of new meters to be put in service or recertification of in-service meters.

More than 60 meters, based on five different generic types, were included in the program. A summary of experimental cryogenic performance of these meters is shown in Fig. 1. Documented performance for various cryogenic volumetric flow ranges is shown in Fig. 2, which includes experimental results from the literature in addition to that developed under the NBS-CGA program.

Active work under this program is drawing to a close with the development of a model code (NBS, 1972) and conclusion of field tests of transfer standards to be used for field certification. The model code will be submitted to the National Conference on Weights and Measures this year for approval as a permanent code.

Members of the LNG industry, particularly those interested in road trailer operation involving custody transfer, could take advantage of the results of this work. Actual code and recommended practices specifically exclude LNG, primarily because the industrial cryogenic fluids—hydrogen, oxygen, argon and nitrogen—are more adequately characterized than LNG mixtures. As mentioned above, this situation is changing and most other aspects of the flow metering program could prove useful.

Densimeter evaluation. Prediction of LNG densities by using a computer program which relates pressure, temperature and mixture fraction to pre-

cise accurate density measurements is most probably the method which provides the least possibility of error. However, accomplishing this inferred density calculation will require meticulous attention to detail in the sample extraction, gas analysis and temperature and pressure measurments.

These activities, in most cases, can be handled best in a well equipped laboratory environment where all elements are under careful control. If such measurements are made in the field where sampling, gas analysis, etc. are made under varying or severe conditions, then uncertainties associated with sampling and analysis may be unacceptable.

An alternative to this approach would be to use, in the field, a direct reading densimeter evaluated and calibrated under the most accurate and precise laboratory conditions. The densimeter could be placed in the LNG directly, avoiding sampling errors, and the calibration would be based on accurate, precise measurements needed for correlations of density with pressure, temperature and mixture fraction. A direct reading densimeter would also eliminate the need for field gas analysis for density determination.

A program designed to evaluate performance of several different types of commercial densimeters has recently been completed at NBS. This work is being carried out primarily in the Metrology Section under the supervision of R. S. Collier.

Funded under an AGA grant, the program provided a reference system of such size as to allow installation of several densimeters. The measurement of the performance of each densimeter under various pressure, temperature and LNG mixture composition conditions was made with a comparison to an accurate Archimedes principle densimeter and continuously monitored and referenced to precise laboratory density measurements.

Three types. Three generic types of densimeters were investigated. Changes of dielectric properties with density were incorporated in a capacitance densimeter and in a microwave resonant cavity. Changes in damping of a vibrating element with density provided a second generic type densimeter and the changes in the forces acting on an element submerged in LNG provided the third type.

The work at NBS will be reported in two parts. The first will be a detailed description of the density reference system with particular attention to accuracy and precision of the system. The second part will be performance data for the three generic types of densimeters.

A number of summary statements can be made which provide a preview of the program results (in general, the density ranged from 390 to 490 kg/m³ for the densimeters under test):

1) **Dielectric Cell Densimeter.** Analysis of the data for density difference versus density computed from vapor pressure measurements for pure methane, using

$$(\rho_\varepsilon - \rho_{NBS}) = A + B\rho_{NBS}$$

shows an over-all standard deviation of about 1 percent.

From the mixture data other than the butane and nitrogen mixtures, the data *all* lie in a band ±0.24 percent with butane mixture data below the median line by about 0.4 percent. The nitrogen mixtures are outside this range and further work needs to be done on mixtures containing nitrogen.

2) **Vibrating Element Densimeter.** The performance of the two types of densimeters when fitted to the relation in (1) above varied over a range of 0.2 percent to 1.6 percent for pure fluids and mixtures.

3) **Displacement or Archimedes Densimeter.** All of the data taken for this device lie in a band ±0.2 percent wide. From a median line the data have a standard deviation of about ±0.1 percent. The measurements taken on this device are less extensive than for the others but include pure methane, a methane-nitrogen mixture and a five component hydrocarbon mixture.

A detailed analysis of the dielectric constant densimeter will be published. Under this Maritime Administration funded program, densities of LNG type mixtures under saturation and subcooled conditions were calculated by means of the Mollerup [Mollerup, 1975] computer program; the corresponding density-dielectric constant relationship was determined from the Clausius-Mosotti relationship for the mixture using ideal mixing rules for the CM function.

The results show that a nearly unique and linear relationship between saturation density and dielectric constant exists for both constant pressure and constant temperature conditions independent of mixture. Furthermore, it is shown that the linear relationship is not a segment of the Clausius-Mosotti function, but results from the more fundamental thermodynamic properties of the mixture.

Also, the nitrogen composition of the mixture is predicted to have a pronounced effect on the saturation density versus dielectric constant, the increase in nitrogen causes an increase in saturation density for the same dielectric constant. There is also a substantial decrease in the saturation temperature with an increasing nitrogen content. This allows a temperature compensation for the nitrogen content.

For the normal range of LNG type mixtures, it is possible to determine the density to ±0.3 percent independent of a knowledge of the composition from an exact measurement of dielectric constant and temperature. Further improvements can be made if the exact composition of the mixture is known.

Therm meter. A current program for therm meter for flowing LNG, funded by the Pipeline Research Committee of AGA, is an illustration of objectives from one measurement's requirement being met by output from other ongoing measurements and activities. The therm meter program goals are to demonstrate and assess the accuracy and precision of a three-element measurement system for pre-

About the author

DOUGLAS B. MANN *is coordinator of LNG Programs at the Cryogenics Division, NBS Institute for Basic Standards, Boulder, Colo. A mechanical engineer (B.S. and M.S., Colorado University), he has more than 20 years experience in the field of cryogenic engineering. He led the joint NBS-Compressed Gas Association program at NBS which assessed the performance of cryogenic flowmeters in commercial service, developed the model code for their use in commerce and aided in the acceptance of this type of measurement in the U.S. and Europe. His interests are primarily in measurement and instrumentation for determining density, pressure, temperature, liquid level and flow of cryogenic fluids. Since 1968, he has been involved with the application of these cryogenic measurement techniques to liquefied natural gas. He holds three patents on cryogenics devices and has authored or co-authored more than 45 papers on cryogenic subjects.*

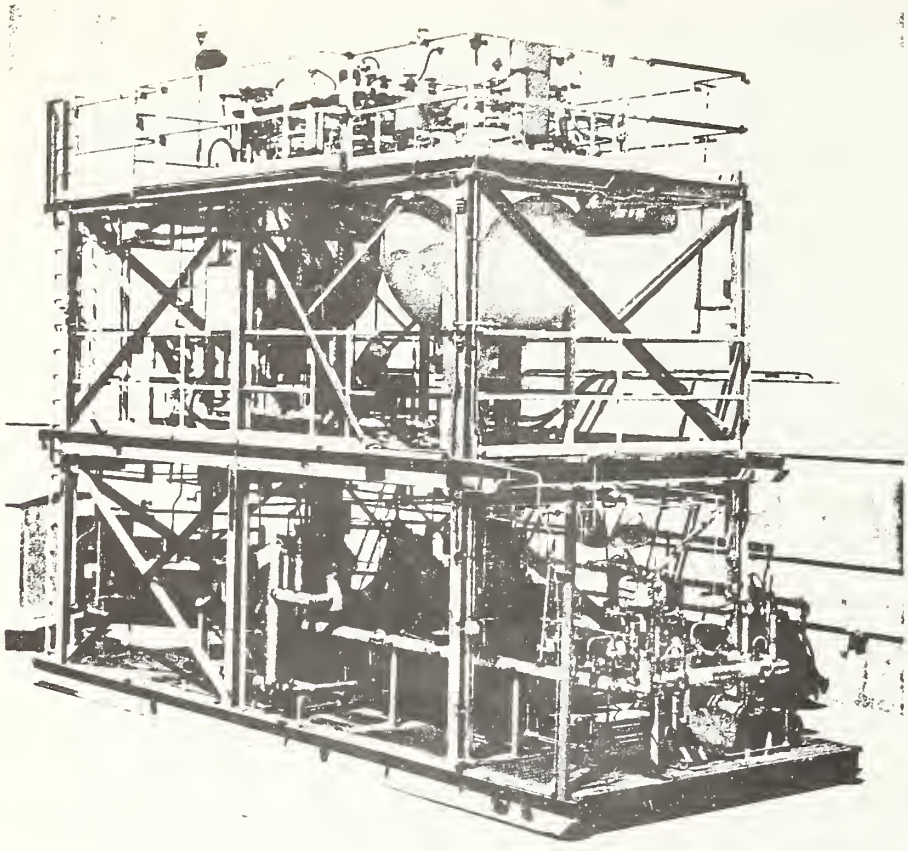

Fig. 3—LNG flow facility at National Bureau of Standards, Boulder, Colo.

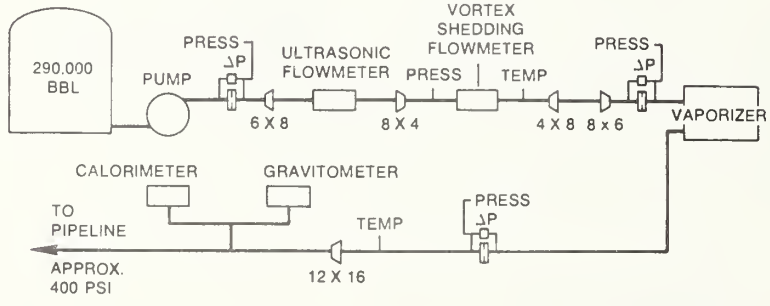

Fig. 4—Flow schematic of Transco field tests in New Jersey.

dicting the gross heating value of LNG flowing in a pipe line.

This is a minimum risk approach combining existing performance data of volumetric flowmeters (NBS-CGA Program), performance and calibration data for a direct reading densitometer (density reference system) and the industry compatible combustion calorimeter.

Therefore the volumetric flow may be measured in cubic meters per hour —combined with measured density and kilograms per cubic meter to give mass flow rates in kilograms per hour. This rate is then combined with the output of the combustion calorimeter (fitted with a gravitometer to provide data in joules per kilogram) to give the required measurement of joules per hour.

Fig. 3 shows the NBS Liquefied Natural Gas Flow Facility at Boulder, Colo. The facility, made available through a grant from PRC, is currently testing the individual measurement components under flow conditions with LNG. Conditions of pressure, temperature, flow and mixture fraction can be controlled, and the recently installed calorimeter with gravitometer provides the complete "breadboard" of the therm flow measurement system.

The wide application and use of this measurement system for LNG must consider scaling to large pipe diameters (0.6 to 0.9 m). It is believed that for single phase fully developed turbulent flow, the densitometer and combustion calorimeter will not be affected by line size.

However, the performance of cryogenic flowmeters is generally documented only at diameters less than about 0.1 m. Therefore, a second goal of the NBS-PRC program is directed at defining the scaling laws when increasing the meter diameters to the 0.6 to 0.9 m size.

Demonstration of the methods used to scale the flowmeters is complicated by not having cryogenic flow reference systems of a size or capacity required. The NBS facility is limited by a maximum line size of 0.1 m and a flow rate of 45 m^3 per hour. Larger capacity LNG flow rates are available at industrial LNG peak shaving plants, and gas flow measurement after LNG vaporization could provide a reference system for the liquid flow.

A three-step program to define the scaling laws was selected. A volumetric vortex flowmeter was chosen based on the performance on this meter type under the NBS-CGA flowmetering program and the potential for scaling to larger sizes. Water and liquid nitrogen calibrations were used for both the LNG and gas flowmeters where applicable.

In this cooperative effort, Transcontinental Gas Pipeline Corp. allowed the installation of a 0.1 and 0.2 m diameter flowmeter (4 and 8-in. diameter) at its New Jersey peak shaving facility and testing of these two meters was conducted last winter. A flow schematic of the installation is shown in Fig. 4.

Data from these tests are currently being analyzed but indicate an agreement of near ± 1.5 percent with the gas flow measurements. Current plans under this program include the selection of a large capacity LNG site for the installation and testing of meters of greater than 0.4 m in diameter. ■

NBS-114A (REV. 7-73)

U.S. DEPT. OF COMM. BIBLIOGRAPHIC DATA SHEET	1. PUBLICATION OR REPORT NO. NBSIR 77-854	2. Gov't Accession No.	3. Recipient's Accession No.

4. TITLE AND SUBTITLE

LIQUEFIED NATURAL GAS RESEARCH AT THE NATIONAL BUREAU OF STANDARDS

5. Publication Date: March 1977

6. Performing Organization Code

7. AUTHOR(S): D. E. Diller, Editor

8. Performing Organ. Report No.

9. PERFORMING ORGANIZATION NAME AND ADDRESS

NATIONAL BUREAU OF STANDARDS
DEPARTMENT OF COMMERCE
WASHINGTON, D.C. 20234

10. Project/Task/Work Unit No.: 2750104

11. Contract/Grant No.

12. Sponsoring Organization Name and Complete Address (*Street, City, State, ZIP*)

Same as Item #9.

13. Type of Report & Period Covered: Semi-Annual -- 1 July-31 December 1976

14. Sponsoring Agency Code

15. SUPPLEMENTARY NOTES

16. ABSTRACT (*A 200-word or less factual summary of most significant information. If document includes a significant bibliography or literature survey, mention it here.*)

Twenty-five cost centers, supported by six other agency sponsors in addition to NBS, provide the basis for liquefied natural gas (LNG) research at NBS. During this six-month reporting period the level of effort was 20 man-years/year with funding expenditures of over $500,000. This integrated progress report to be issued in January and July is designed to:

1) Provide all sponsoring agencies with a semi-annual and annual report on the activities of their individual programs.

2) Inform all sponsoring agencies on related research being conducted at the Cryogenics Division of NBS-IBS.

3) Provide a uniform reporting procedure which should maintain and improve communication while minimizing the time, effort and paperwork at the cost center level.

The contents of this report will augment the quarterly progress meetings of some sponsors, but will not necessarily replace such meetings. Distribution of this document is limited and intended primarily for the supporting agencies. Data or other information must be considered preliminary, subject to change and unpublished; and therefore not for citation in the open literature.

17. KEY WORDS (*six to twelve entries; alphabetical order; capitalize only the first letter of the first key word unless a proper name; separated by semicolons*)

Cryogenics; liquefied natural gas; measurement; methane; properties; research.

18. AVAILABILITY

☐ Unlimited

☒ For Official Distribution. Do Not Release to NTIS

☐ Order From Sup. of Doc., U.S. Government Printing Office Washington, D.C. 20402, SD Cat. No. C13

☐ Order From National Technical Information Service (NTIS) Springfield, Virginia 22151

19. SECURITY CLASS (THIS REPORT)	21. NO. OF PAGES
UNCLASSIFIED	
20. SECURITY CLASS (THIS PAGE)	22. Price
UNCLASSIFIED	